



Universiteit  
Leiden  
The Netherlands

## Quantum liquid crystals

Cvetković, V.

### Citation

Cvetković, V. (2006, March 29). *Quantum liquid crystals*. Retrieved from <https://hdl.handle.net/1887/4456>

Version: Corrected Publisher's Version

License: [Licence agreement concerning inclusion of doctoral thesis in the Institutional Repository of the University of Leiden](#)

Downloaded from: <https://hdl.handle.net/1887/4456>

**Note:** To cite this publication please use the final published version (if applicable).

# Quantum Liquid Crystals

*Vladimir Cvetković*



# Quantum Liquid Crystals

PROEFSCHRIFT

TER VERKRIJGING VAN  
DE GRAAD VAN DOCTOR AAN DE UNIVERSITEIT LEIDEN,  
OP GEZAG VAN DE RECTOR MAGNIFICUS DR. D. D. BREIMER,  
HOGLERAAR IN DE FACULTEIT DER WISKUNDE EN  
NATUURWETENSCHAPPEN EN DIE DER GENEESKUNDE,  
VOLGENS BESLUIT VAN HET COLLEGE VOOR PROMOTIES  
TE VERDEDIGEN OP DONDERDAG 29 MAART 2006  
TE KLOKKE 15.15 UUR

DOOR

Vladimir Cvetković

GEBOREN OP 26 FEBRUARI 1977  
TE JAGODINA, SERVIË

**Promotiecommissie:**

Promotor: Prof. dr. J. Zaanen  
Referent: Prof. dr. ir. W. van Saarloos  
Overige leden: Prof. dr. E. Demler (Harvard University, Verenigde Staten)  
Prof. dr. D. van der Marel (Université de Genève, Zwitserland)  
Prof. dr. ir. H.T.C. Stoof (Universiteit Utrecht)  
Prof. dr. J. van den Brink (Radboud Universiteit Nijmegen)  
Prof. dr. H.W.J. Blöte  
Prof. dr. P.H. Kes

ISBN: 90-8593-011-1

Thesis – Instituut-Lorentz, Universiteit Leiden, 2006  
Casimir Ph.D. series, Delft-Leiden, 2006-04  
Printed by PrintPartners Ipskamp, Enschede

Het onderzoek beschreven in dit proefschrift is onderdeel van het wetenschappelijke programma van de Stichting voor Fundamenteel Onderzoek der Materie (FOM) en de Nederlandse Organisatie voor Wetenschappelijk Onderzoek (NWO).

The research described in this thesis has been carried out as part of the scientific programme of the Foundation for Fundamental Research on Matter (FOM) and the Netherlands Organisation for Scientific Research (NWO).

---

Cover: a random configuration of dislocations on a 2D triangular lattice.

# Contents

<b>1</b>	<b>Introduction</b>	<b>1</b>
1.1	Order vs. disorder . . . . .	1
1.2	Correlated electrons and high- $T_c$ superconductivity . . . . .	3
1.3	Motivation and the main results . . . . .	7
1.4	Definitions and conventions . . . . .	9
<b>2</b>	<b>A tutorial: Abelian-Higgs duality</b>	<b>13</b>
2.1	Vortex duality . . . . .	15
2.2	The disorder field . . . . .	20
2.3	Green's functions, the Zaanen-Mukhin relation and the 'dual censorship' . . . . .	26
2.4	Dual view on the critical regime . . . . .	35
2.5	Abelian-Higgs duality in higher dimensions . . . . .	42
<b>3</b>	<b>Elasticity and its topological defects</b>	<b>47</b>
3.1	The potential energy of an elastic medium . . . . .	49
3.2	Path integral formulation . . . . .	54
3.3	Topological defects in solids . . . . .	59
3.4	Topological kinematic constraints: dislocations and the glide principle . . . . .	66
<b>4</b>	<b>Dual elastic theory – nematic phases</b>	<b>77</b>
4.1	Dual elasticity . . . . .	81
4.2	Defect fields and their dynamics . . . . .	86
4.3	Ideal crystal as the dual Coulomb phase . . . . .	96
4.4	The ordered nematic phase of a solid . . . . .	103
4.5	The topological nematic phase . . . . .	122
4.6	Burgers Higgs fields and the isotropic nematic phase . . . . .	131
<b>5</b>	<b>Superconductivity in nematic phases</b>	<b>145</b>
5.1	A tutorial: electrodynamics of elastic media and physical observables . . . . .	148
5.2	Dual electromagnetism . . . . .	156
5.3	Charged isotropic nematic phase . . . . .	161
5.4	Charged ordered nematic . . . . .	177

<b>6 Conclusion</b>	<b>185</b>
<b>A Mapping of a nonlocal interaction to <math>\Psi^4</math> term</b>	<b>189</b>
<b>B Defect current conservation laws</b>	<b>195</b>
<b>C Irreducible tensors of the symmetry group</b>	<b>197</b>
Samenvatting	213
Curriculum Vitæ	217
Publications	219
Acknowledgments	221

# Chapter 1

## Introduction

### 1.1 Order vs. disorder

The ability of physicists to completely enumerate the properties of physical systems is strongly dependent on the strength of interaction among its basic constituents. For example, the non-interacting gas is perfectly described by the ideal gas equation of state which follows entirely from the kinematical considerations of single molecules. In real classical gases, the weak interaction between particles implies that the proper equation of state is not the ideal gas equation of state, but rather the ‘van der Waals’ equation

$$\left(p - \frac{an^2}{V^2}\right)(V - bn) = nRT. \quad (1.1)$$

Due to the limited influence of the interparticle interaction, van der Waals could draw the conclusion that the additional terms, with respect to the ideal gas equation of state, correspond to the interaction among the particles, the ‘long-tail’ attractive forces and the ‘excluded volume’ hard-core repulsion. The exact origin of the interaction (dipolar forces) was later explained by Debye. When the constituents of the same gas condense into the liquid state, e.g. steam condenses into liquid water, the proximity of molecules results in much stronger interactions between them. It is much harder to understand the physics of the liquid state, based only on the premise of interacting particles, and the theoretical understanding is limited to phenomenological theories, where a direct link between the microscopic physics associated with individual particles and the macroscopic behaviour of the liquid is intentionally avoided. Ultimately, the solid state of matter is completely governed by the interaction between the molecules, while their kinetic properties appear only as corrections to the ideal crystal state. The solid loses the knowledge about the internal constituents to such a degree that even if a portion of molecules is removed from a crystal in the form of vacancies, the crystal will still be in the same state. This property of solids, that the global degrees of freedom are effectively independent from these of the individual particles, acts as the major obstacle in the understanding of solids in terms of loose particles.

Nevertheless, our understanding of solids is very strong because it is based not on the single particle approach, but rather on the approach in terms of collective fields. In a classical solid there is a “classical wave function”  $\Psi_{cl.}^0$  corresponding to the ground state and the excitations are parametrized in terms of the phonon excitations. None of these carries any information about the individual molecules. Surely, the phonons, as well as pressure or temperature which are defined throughout all the phases, are emergent concepts. If we would consider two-, three- or ten isolated molecules, no one could say whether the condensation to the solid occurred or what the temperature is. The difference is that the pressure and temperature in the gas have emerged from the collective kinetic properties, whereas in the solid they originate in the interactions. The emergence of phonons in solids is the more interesting feature. An observer embedded in a solid could only measure the properties of its vacuum implied by the classical state  $\Psi_{cl.}^0$ , i.e. the vacuum excitations dispersing linearly as phonons and he or she could hardly anticipate that there might exist different vacua or that his/her ‘theory of everything’ inside the crystal is just an effective theory emerging from another, more complicated, universe. This idea of emergence is directly related to the concept of duality which will be one of the key ingredients of this thesis. Namely, the universe of our ‘crystal embedded’ experimentalist is a very simple one, with linear dispersing phonons acting as the unique force carrying particles, while the crystalline defects act as massive particles, being the sources for the phonons. This physicist does not need to have any knowledge of individual molecules, nor of strong interactions which would make his life as a physicist tough. So, when it comes to understanding a state of matter which is not a solid, but close to a solid with respect to the relevance of the interparticle interaction, the ‘solid experimentalist’ will have serious advantages over his/her colleague who uses ‘single-particle’ type of theories. At the same time, the theory of solid is still a robust construct able to cope even with some flaw in the crystalline order, like the mentioned vacancy disorder.

The scale based on the strength of the interactions extends between two extremes. One extreme is the ‘gas limit’, already mentioned, which serves as a starting point for the theories in the weak coupling regime. The other one has just been discussed: the ‘solid limit’ offers an easy description of strong coupled systems in terms of the collective fields. Each of the limiting theories sees the vacuum and the excitations of the other theory as a complicated mixture of its own excitations. This underlies the basic idea of the duality: the state which is complex due to the dominant interactions compared to the kinetic energy can alternatively be seen as the order state in terms of the collective emergent fields, which significantly simplifies the description. There may still be a range where interactions compete with the kinetic energy and perturbative methods starting from either of the two limiting theories require more attention to obtain good physical predictions.

## 1.2 Correlated electrons and high- $T_c$ superconductivity

The same hierarchy of interactions and phases as in the classical physical systems occurs in the quantum realms, where the phases of matter are determined by the level of quantum fluctuations, rather than by thermal disorder [1]. In the absence of any interactions, quantum matter can exist in only two ‘gaseous’ states, pending the irreducible representation of the permutation group they belong to. For bosonic systems, the symmetric representation results in the Bose-Einstein gas which may eventually condense into the BEC condensate, the feature originally predicted by Bose and Einstein [2, 3] and only recently experimentally demonstrated [4, 5, 6, 7]. When the interactions among the constituents are much stronger, such as in Helium-4, the Bose-Einstein gas picture requires significant modifications, as first pointed out by Landau [8], in order to describe the phase that can be called the Bose-Einstein liquid, rather than the Bose-Einstein gas. A prominent feature of superfluid helium is the roton minimum in the excitation spectrum which is yet another signature of the competition between the interacting and non-interacting states of matter. At large scales, helium shows the collective superfluid behaviour which does not reveal any information regarding individual constituents. However, at short scales the behaviour of its particle degrees of freedom resurfaces. The unique way to ‘patch’ the spectra of these two worlds is through the roton minimum.

Helium-4 represents a bosonic system without Umklapp. In the bosonic systems where Umklapp processes become relevant, the ordered- and disordered phases of matter are given by the superfluid and the bosonic Mott-insulator. In recent years, the physics of bosonic matter in optical lattices has flourished. A commonly studied bosonic model with relevant Umklapp processes is the Bose-Hubbard model which will be addressed in this thesis for the demonstrational purposes.

Fermions are particles corresponding to the antisymmetric representation of the permutation group. The most obvious example of the fermionic gas is the state of electrons in metals. Other interesting quantum fermionic states of matter are found in Helium-3, but here we are more interested in the electronic systems which are at the focus of our attention. In a metal, the perfect Fermi gas is never literally realized. The interactions can be usually treated perturbatively, leading to the theory of Fermi liquid, a state whose innate excitations (quasiparticles) are electrons ‘dressed’ with interactions.

The Umklapp processes are important for the fate of the strongly interacting state of fermionic matter too. When the Umklapp is absent and there are no other relevant fields, there are basically two states of matter: the Fermi liquid realized at high electron densities and the Wigner crystal [9] which is realized in the low density limit, when electrons form a triangular lattice. The entire scale of the electron density/interaction on the phase diagram should be covered by either one or the other phase with a first order transition between the two. In a recent work, Jamei *et al.* [10] demonstrated that this direct transition may be obstructed if the Coulomb force is weaker than some critical value when ‘microemulsion’ phases of matter set in between the Wigner crystal and Fermi liquid phase. These

intermediate phases consist of bubbles or stripes of Fermi liquid inside a Wigner crystal or vice versa, of Wigner crystal inside a Fermi liquid.

When the weak coupling of electrons to the lattice phonons is considered, another limit arises, namely the BCS superconductor state. The experimental discovery of the superconductivity was made by Kamerling-Onnes in Leiden almost one hundred years ago [11]. In the next forty years the understanding of the superconductivity slowly progressed driven by experimental discoveries, such as the Meissner effect [12] and more or less successful theories of which the London [13] and Ginzburg-Landau phenomenological theory [14] are worth noticing. In the 1950-s, the dependence of the superconducting transition temperature on the isotopic mass of the constituents [15, 16] pointed at the relevance of electron-phonon interactions which soon led to the BCS theory [17] which can be considered as the first complete microscopic description of the conventional superconductivity. This turned out to be another fundament for the development of more complete theories of interacting fermions on which theories, such as the Eliashberg [18, 19] theory of superconductivity.

When the magnetic fields are high, the electronic matter without Umklapp processes realizes itself in the form of the incompressible quantum Hall state of matter. The time scale for the development of the fundamental understanding of the quantum Hall effect was shorter than the corresponding time for the BCS superconductivity. The theory by Laughlin [20, 21] appeared shortly after the experiments by Von Klitzing [22] and by Tsui and Störmer [23]. There were even some approximate calculations, that preceded the experiments, suggesting the quantization of Hall resistance [24]. From this emergent concept, many new ideas in physics flourished, let us just mention the smectic and nematic quantum Hall stripe phases [25, 26], the ingenious concept of composite fermions [27, 28] and generalizations thereof like the C<sup>2</sup>F theories [29].

The presence of the Umklapp in electron systems implies, as by rule, a nontrivial physics even in the limit of high electron densities. Examples include Mot insulators, spin liquids, high- $T_c$  superconductors, stripes, quantum liquid crystals, non-Fermi liquids, etc. We are particularly interested in the high-temperature superconductors. Their discovery by Bednorz and Müller [30] sparked a giant quest in physics which is still going on with considerable intensity. The high- $T_c$  superconductors are just a subclass of a broader family of strongly correlated electron systems. In the BCS superconductors a simple canonical transformation connects Cooper pairs and the original electrons as shown by Bogolyubov [31]. In contrast, the adiabatic continuation between the constituting electrons and the genuine excitations of the high-temperature superconductors appeared as a hard nut to crack.

For almost twenty years, both theoretical and experimental physicists strove to understand better the strongly correlated electron systems and particularly the unconventional superconductivity found in these systems. An early idea which was widely accepted among physicists refers to the application of the two-dimensional Hubbard model. The physical arguments are reasonable: the parent compounds consist of alternating layers of rare earths and perovskite planes. In the perovskite planes one finds a density of one missing electron per CuO<sub>2</sub> unit cell and in the absence of interactions this should be a metal. Experi-

ments, however, show that these are antiferromagnetic insulators. This is well understood in terms of the language of the Hubbard model: these are so-called Mott-insulators, which are insulating because of the strong local Coulomb repulsions. The role of the “charge reservoir” layers is to dope these Mott-insulators with free charge carriers in a way which is quite similar to what is happening in simple semiconductors. While armies of men and women produced countless publications on every possible variation of the Hubbard model, the answer to the ultimate question of why  $T_c$  is high or even regarding the basic physics of these electron systems is still in the air.

There were, however, many useful and fundamental results among which the presence of stripes plays an important role in the motivation for the ideas in this thesis. Stripe order can be imagined as follows: the magnetic coupling between the electrons in the perovskite planes is antiferromagnetic which results in the Néel ground state for the undoped compound. This state is a Mott-insulator, which cannot conduct charge due to the strong local Coulomb potential, when the charge density is commensurate with the lattice potential. The doping removes some electrons out of the perovskite planes, i.e. it introduces holes, which leads to the destruction of the Néel state already at doping levels of  $x \approx 0.02$ . At the doping levels slightly higher than the 0.02, the introduced holes would like to delocalize in order to reduce their kinetic energy. However, due to the antiferromagnetic interaction, the delocalization costs energy instead of gaining it. The tendency toward the stripe formation just means that the holes arrange into lines of missing charges/spins to minimize the energy. In this respect, the stripe phase can be seen as a discommensuration of lattice associated with the commensurate Mott-state. The first theoretical predictions of stripes came soon after the discovery of the high- $T_c$  superconductivity [32], with few others that followed [33, 34]. The experimental confirmation of stripes however had to wait until 1995 when the incommensurate charge and spin peaks were found in the neutron experiments on the underdoped cuprates and nickelates [35, 36].

The presence of static stripes in the underdoped regime of high- $T_c$  cuprates and some early experiments suggesting the presence of dynamical stripes in the optimally doped regime, led Kivelson, Fradkin and Emery [37] to suggest that the phase diagram of the superconductivity may be understood as associated with zero temperature quantum electronic liquid crystal phases. In contrast with the classical liquid crystals where the disorder is of thermal origin, in the quantum version it is driven by quantum fluctuations induced by doping. The Néel state, underdoped-, optimally- and overdoped regimes correspond to the crystal, smectic, nematic and isotropic state of a liquid crystal as seen in Fig. 1.1. The presence of static stripes [32, 34, 33] observed in the cuprates [35, 36, 38], and their disordering and fractionalization [39, 40] finds a natural place in this picture.

It was demonstrated by various experiments that the previous claims are not just a theoretical speculation, but have a real support in strongly correlated electron systems. For example, the incommensurate spin fluctuations associated with the stripes were found in various neutron scattering experiments on optimally doped YBCO [41], but the signal was present only above a certain energy gap. This means that although the static stripes cannot exist in the superconducting phase, some notion of spatial order is still present in the superconducting phase. The order is however transient and can persist only for

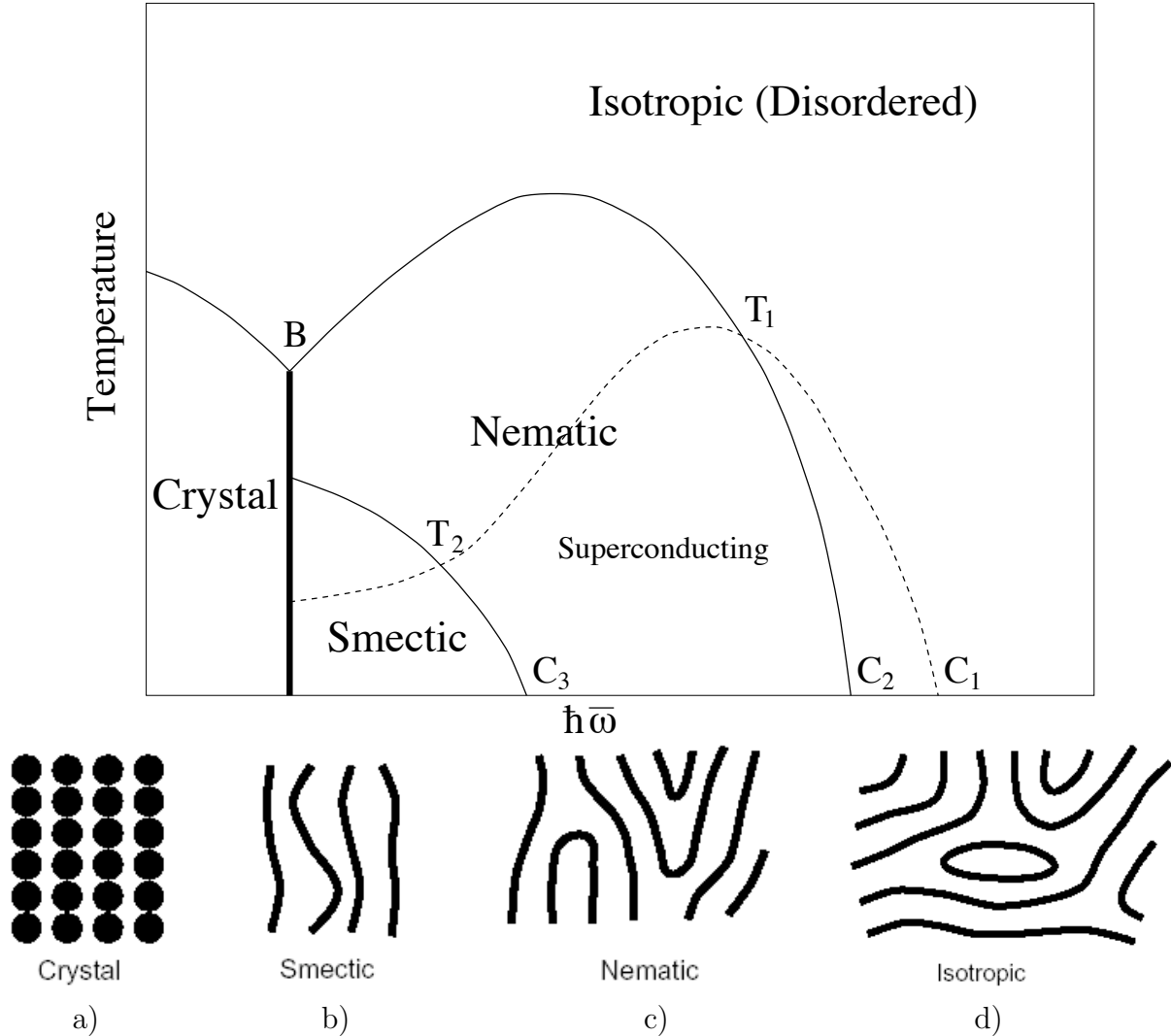


Figure 1.1: The phase diagram of electronic liquid crystals (taken from Ref. [37]): The temperature is on the vertical and doping on the horizontal axis. The Mott-insulator corresponds with a) commensurate crystal; the regions with the static stripe order corresponds to b) a smectic phase of the liquid crystal; the ‘superconducting dome’ on the phase diagram corresponds with c) a nematic phase and the overdoped region on the phase diagram is related to d) the isotropic phase.

relatively short times and lengths. Another relevant experiment is the scanning tunneling spectroscopy of magnetic vortex cores in BiSCO2212 by Davis *et al.* [42] where the presence of a spatially ordered electron state (mutually perpendicular layers of stripes or checkerboard) in the vortex core is observed. An interpretation could be that the ‘transient’ fluctuations become static when the superconductivity is suppressed by the external magnetic field. Finally, recent experiment employing the neutron scattering on optimally

doped ‘untwinned’ YBCO123 crystals [43] shows an anisotropy in the superconducting gap which appears to be much higher than one would expect it from the anisotropy implied by the CuO chains located between the perovskite planes.

## 1.3 Motivation and the main results

These ideas about liquid crystalline electronic order and the experimental signs of fluctuating order in the superconducting state form the main motivation for the scope of this thesis. The mainstream in the theory of high- $T_c$  superconductivity is preoccupied with a microscopic description of electrons in the cuprate planes. This approach has had only a limited success, especially considering the amount of energy invested in it. Even the plausible theories are fairly complicated, which is not surprising when one realizes how distinct bare electrons and, for example,  $d$ -way Cooper pairs are, which these theories wish to adiabatically connect. Bearing these fact in mind, the approach employed in this thesis starts from the opposite, collective limit. We expect that in this way the handicap of the approach by means of the individual degrees of freedom can be avoided, in analogy with the classical solids where the interaction is dominant.

The pioneering work in this direction was presented by Zaanen, Mukhin and Nussinov [44], where the quantum melting of a crystal is considered in terms of the dual gauge field theories. In this thesis we take up the considerable challenge posed by this research program. We identify several shortcomings in the original approach. By curing these, we manage to generalize these ideas further with, as the main result, that we arrive at a variety of predictions which can be tested experimentally, at least in principle, but it seems also experimentally.

In this approach, the notion of liquid crystals appears in the context of the famous Nelson, Halperin and Young [45, 46, 47] theory of classical melting (NHY). The aim is to keep some residual order in the melted phase, because some residual order was measured in the electronic liquid of cuprates. This is possible to achieve if the melting is driven exclusively by dislocation topological defects. In that respect the melted phases can be regarded as the quantum generalization of the NHY melting. In analogy with the liquid crystal nematic and smectic phases, which are on a halfway between the solid and the liquid, the ‘hexatic’ phase of NHY or the quantum melted crystalline phases, presented in Ref. [44] and here, represent the nematic phases of a matter.

One of the important conclusions in Ref. [44] was that the charged crystal that undergoes quantum melting transition driven by dislocation defects, develops a (unconventional) Meissner term, i.e. it becomes impenetrable for the electromagnetic fields, which is the exclusive trademark of superconductors. Thus, next to the experiments supporting the claims of Kivelson *et al.* [37], the theory of a melted quantum solid seems as a perfect candidate for the liquid crystalline theory that may deliver an unconventional superconducting state. We know that the cuprates exhibit many properties not innate to the conventional BCS superconductors.

The results presented in this thesis treat the problem of the quantum nematic state of

matter in a detailed manner including the physically relevant electromagnetic observables that can be measured in experiments in order to put the theory under the test. In the course of developing the theory, as a sideline two novel results were found. One pertains to the duality and the possibility to measure the correlation of the disorder operators by means of the order operators. We call the screening of the disorder correlation the ‘dual censorship’ and show that it is not absolute, i.e. that some of the disorder operators may show up in the order-fields correlation functions due to the dual representation of the degrees of freedom. By investigating the critical regime, a connection between the modes of ordered and disordered phase is established. The other result deals with the kinematical constraint on the topological crystalline defects which is known as the glide constraint. Given the fact that the work in this thesis rests on the dual field theory of elasticity, the constraint had to be implemented in a strict mathematical way. The proof is presented first in its original form, but the later additions to the proof including the higher order corrections and the conservation laws for the topological defect currents in solids are also given.

The key results found in this thesis may be split in two conceptual parts. The first group of results is relevant for the electrically neutral quantum solids and their melting. The dislocation dynamics which was absent in Ref. [44] is considered and new modes in the elastic response function (phonon propagators) are found. The phase diagram of the quantum solid is presented and a novel phase is predicted. From the other two phases predicted in Ref. [44], one is recalculated with the dynamical dislocation gas, resulting in some quite unconventional and counterintuitive properties. For the other, the claim is made that it requires ‘beyond Gaussian’ treatment in order to encapsulate all the effects of the dynamical condensate. The other group of results pertains to the charged media and in that respect it is crucial since it represents a candidate theory for the electronic liquid in cuprates. The results obtained are astonishing, unconventional and very counterintuitive. The theory predicts magnetic and electric screening with unconventional overscreening as one of the features and the effect that the propagation of electromagnetic photon (light) becomes diffusive. Finally, due to the dynamical dislocation condensate in the superconducting phase, we predict the presence of additional poles in the response functions. Some unconventional experiments are suggested that could prove or disprove the relevance of these findings for strongly correlated electron systems.

This thesis is organized in the following way: The main part of the thesis is composed of six chapters. Beside this introductory- and concluding chapter, two of the four remaining chapters have more of an introductory/tutorial character, while the two other chapters consist of mostly new results. The next chapter is aimed to accustom the reader to the ideas associated with the duality. For that purpose, the Abelian-Higgs duality in 2+1-dimensions is considered, both for its educative value, for explaining duality, and its actual implementation in the remainder of the thesis. This chapter contains original results on the ‘dual censorship’ and it closes with an overview of higher dimensional generalization of the Abelian-Higgs duality. The third chapter introduces the other basic ingredient of the theory, the theory of elasticity. After the basics of the theory are reviewed and the phonon propagators are introduced as the physically relevant quantities, we proceed with

the introduction of the description of crystalline topological defects. The final section introduces a novel result: the formulation of the glide constraint in terms of the dynamical defect currents.

The fourth chapter starts with the construction of the dual elasticity theory, inspired by the work of Kleinert [48], representing the unification of the key concepts introduced in the two previous chapters. After constructing the Ginzburg-Landau-Wilson theory for dynamical dislocation condensate, the phase diagram of the quantum solid is discussed with one section devoted to each specific phase. Because of some controversy regarding some of the presented results, the last section shows that some of the ‘self-inconsistent’ results actually have a different physical interpretation and belong to a different phase than originally anticipated, based on the input to the theory. This novel phase is characterized by isotropy and the rotational symmetry breaking at the same time, which may seem contradicting at first, having however some interesting physical consequences. Chapter five applies the previously developed dual elasticity theory to a charged medium. This involves a generalization of the dualization of elasticity, now including the EM fields. After this has been done, the two next sections present the physically relevant EM response functions, discussing possible experiments which require some unconventional techniques in order to detect the weak fingerprints of the liquid crystalline order in the charged liquids.

In addition, there are three appendices to the thesis. The first presents the mapping of the loop gas onto the GLW action, as originally developed by Kiometzis *et al.* [49] with one novel addition: the arbitrary non-local inter-particle potential. The second appendix has detailed proofs for the dynamical defect current conservation laws which were originally published as a part of the paper on the glide constraint [50]. The final appendix discusses the role of the symmetry in the problem. Using the irreducible representations of the group of point symmetries of the action, degrees of freedom are separated according to their transformation properties under the symmetry group action.

## 1.4 Definitions and conventions

This final part of this introductory chapter is dedicated mostly to introducing a few technical details in order to remove these from the main part of the text where they could distract the attention of the reader. We also add a few general remarks about the imaginary time path-integral formalism.

Let us first note that we employ by rule the imaginary time formalism with the Euclidian positive signature. There are a few reasons for this. First, we are interested in the quantum theory and in order to get the statistics of the fields in the problem right, it is necessary, as standard text books demonstrate [51, 52], to consider a path integral over the configuration space where the temporal direction is either compactified with radius  $\hbar/(k_B T)$  at finite temperatures or not compactified at zero temperature. In this way, the braiding of the particle world-lines brings in nontrivial imaginary contributions to the action (Berry phases), that yield the statistics of the underlying particles. Then, there is the issue of the equivalent treatment of the temporal- and spatial coordinates and positive

Euclidian signature, which will prove useful at some stages of the work. Nevertheless, in most of the text we will insist on the ‘space-time puritanism’, treating temporal and spatial fields on different grounds. This is often necessary, as we argue in the next chapter in detail, because both us and our experiments are fixed in a certain reference frame which promotes the temporal direction to a special one. Finally, when the work is finished, one would like to have a theory which gives prediction in real time and that is possible using an inverse Wick rotation  $\tau \rightarrow it$  on any desired quantity.

Most of our work will be done in the Fourier-Matsubara transformed fields. It is useful to introduce a three-momentum  $p_\mu$  (we are considering only 2+1D theory) having a temporal component equal to the Matsubara frequency  $p_\tau = \omega_n$  and other two components proportional to the momentum  $q$ . However, there is an issue that we use different units for the momenta and frequencies and in order to have them expressed in the same units, we convert the momenta by  $q \rightarrow cq$ . In a standard theory, the velocity  $c$  should be the velocity of light as pointed out by Einstein. We have a different view on this problem. As it turns out, in our work the ‘space-time isotropy’ is achieved with use of some other velocities, like the spin-wave and the phonon velocity. Therefore, we decided not to implement the relativistic velocity of light as the conversion velocity and instead we will note it by  $c_l$  when it becomes relevant in chapter 5. Another standard convention which is implemented regards the Planck constant:  $\hbar = 1$ .

Let us now turn to the bases defined by these momenta that, when used, greatly simplify our work, e.g. the propagators have a (block)diagonal form. Due to the inequivalent treatment of space and time in some segments of our problem, there are two types of momentum basis. One is used in situations when time is separated from space components and it is known under the name of ‘zweibeinen’ (with a third temporal direction added to complete the space-time):

$$\tilde{\mathbf{e}}_L = \hat{q} = \frac{\mathbf{q}}{q} = (\cos \phi, \sin \phi, 0), \quad (1.2)$$

$$\tilde{\mathbf{e}}_T = \times \hat{q} = \frac{\times \mathbf{q}}{q} = (-\sin \phi, \cos \phi, 0), \quad (1.3)$$

$$\mathbf{e}_\tau = (0, 0, 1). \quad (1.4)$$

Clearly, the first vector is parallel to the spatial momentum  $\mathbf{q}$  and the next one is its orthocomplement. Crossproduct  $\times$  acts as the antisymmetric tensor rank-2 in two dimensions: acting on a pair of vectors it produces a scalar (one could think of a vector oriented in the temporal or ‘ $z$ ’ direction); acting on a single vector it produces a vector.

When both time and space are treated equally, one uses set of three vectors – ‘dreibeinen’. This basis is not independent of the choice for the velocity  $c$  used to convert time and space to the same units. The relativistic three-momentum momentum defines the linear polarized version of ‘dreibeinen’:

$$\mathbf{e}_0 = \hat{p} = \frac{\mathbf{P}}{p} = (\sin \theta \cos \phi, \sin \theta \sin \phi, \cos \theta), \quad (1.5)$$

$$\mathbf{e}_{+1} = (-\cos \theta \cos \phi, -\cos \theta \sin \phi, \sin \theta), \quad (1.6)$$

$$\mathbf{e}_{-1} = (\sin \phi, -\cos \phi, 0). \quad (1.7)$$

Angles are defined by momentum to Matsubara frequency ratio  $\text{tg}\theta = \frac{cq}{\omega_n}$ .

This linear choice of polarizations still splits the relevant directions into purely spatial  $\mathbf{e}_{-1}$  and admixed one  $\mathbf{e}_{+1}$ . An alternative is the basis with helical polarizations

$$\mathbf{e}_{\pm} = \frac{1}{\sqrt{2}}(\mathbf{e}_{+1} \pm i\mathbf{e}_{-1}), \quad (1.8)$$

each one being conjugate to another and admixing the spatial and temporal directions equally.

Any tensor can be decomposed into components defined by any of the bases introduced in the above, Eq. (1.3), Eq. (1.6) or Eq. (1.8). However, one has to be careful with the symmetry transformational properties since these basis vectors are well defined only in Fourier space and one should maintain the important relation of the Fourier components

$$A(-p_{\mu}) = A(p_{\mu})^{\dagger}. \quad (1.9)$$

Acting with the inversion operator ( $p_{\mu} \rightarrow -p_{\mu}$ ) on the unit vectors, we find that  $\mathbf{e}_{\tau}$ ,  $\mathbf{e}_{+1}$  and  $\mathbf{e}_{\pm}$  are invariant while all the others change sign. Components associated with the latter basis vectors have to acquire an additional  $i$  prefactor in order to conform with the symmetry transformation property Eq. (1.9). Hence, a single component vector is expanded according to

$$A_{\mu} = e_{\mu}^{\tau}A_{\tau} + i\tilde{e}_{\mu}^E A_E = ie_{\mu}^0 A_0 + e_{\mu}^{+1}A_{+1} + ie_{\mu}^{-1}A_{-1} = e_{\mu}^0 A_0 + e_{\mu}^h A_h. \quad (1.10)$$

For multiple indices, the generalization is straightforward.

Needless to say, summation over repeated indices is always assumed, unless stated otherwise, and while Greek letters represent that the index may take both temporal and spatial values, small Latin indices are reserved for spatial indices exclusively. Sometimes we wish to stress that the indices belong to a certain basis: each basis has its own ‘reserved letters’: We already used  $h$  for helical components and we will continue to do so, both for linear and helical basis. When referring exclusively to spatial components of the ‘zweibeinen’ basis (twiddled basis), letters  $E$ ,  $F$  and  $G$  will be used, and when both spatial and temporal direction have to be included, letters  $M$  and  $N$  are used.

Finally, in many places we will use projector onto spatial part of the momentum and its orthocomplement projector. These projectors are defined as

$$\hat{P}_{ij}^L = |\hat{q}\rangle\langle\hat{q}| \xrightarrow{i,j} \frac{q_i q_j}{q^2}, \quad (1.11)$$

$$\hat{P}_{ij}^T = \hat{\mathbf{1}} - |\hat{q}\rangle\langle\hat{q}| \xrightarrow{i,j} \frac{q^2 \delta_{ij} - q_i q_j}{q^2} \quad (1.12)$$

in operator and matrix form respectively.



# Chapter 2

## A tutorial: Abelian-Higgs duality

The concept of duality [53, 54, 55, 56, 57] has been around for a long time in the high energy and statistical physics communities, but only in relatively recent times has its powers become increasingly appreciated in the condensed matter community. Although there is yet no unifying formalism that could relate all known examples of duality, the general working mechanism of duality follows a certain pattern. Consider a general physical system (model) described in terms of certain observables (variables, operators, fields, either quantum or classical) and suppose that it undergoes a phase transition from an ordered into a disordered phase. The transition is characterized by vanishing expectation values of the initial observables and by rule, these observables become ill-defined or unpractical to work with in the disordered phase. Initially it seems that one can say little or nothing about the system beyond the phase transition. Fortunately, there is a way to circumvent this problem and give a proper description for the system on the disordered side – via disorder operators. These entities, as their name suggests, measure the amount of disorder in the system and their eigenstates are the states whose presence indicates the disordered phase. Accordingly, in the disordered phase, the disorder operators become well-defined and the disordered states have the highest weights. The duality in this context simply means that the disordered phase of the system can be viewed as the phase which experiences order as expressed by the disorder operators. The disordered state can now be analysed using many of the known techniques developed for ordered systems. The duality works the other way around too: the initial operators, the ones that were ordered in the ‘ordered phase’ and became disordered in the ‘disordered’ phase, play the role of disordering agents in the disordered phase: their reappearance implies that the order of the disorder operators is destroyed and that the system is back in the ordered phase. Therefore, the duality makes the meaning of words ‘order’ and ‘disorder’ relative to what one chooses as the appropriate observables.

Let us illustrate this by a very simple (and historically the first) example of the duality, the Kramers-Wannier duality construction for the Ising model. In terms of Ising spins, the theory knows two phases, the ordered phase at low temperatures with all spins pointing in the same direction and the disordered phase, experienced at high temperatures where the average magnetization vanishes. An experimentalist equipped only with a machine capable

of measuring spins would agree with the previous statement and there would be very little to say about the disordered phase except that it appears as an entropy driven state with no correlations whatsoever. Consider now what may happen if the same experimentalist could build a machine that measures magnetization domain walls and their correlations instead of spins. The experimentalist would decide that the high temperature phase appears ordered as the domain walls are present everywhere and their correlations extend over the whole system. The low temperature phase, on the other hand, seems disordered in terms of domain walls. With the duality in charge, the disorder is the order in disguise and it seems that this camouflage act is perfect.

When performing the dualization, perhaps the most difficult task is to identify the disorder operators. In general, the dual order is carried by the topological excitations of the direct order. In continuum field theories these topological excitations are contained in field configurations that are singular (multivalued) and these will translate into topological operators carrying quantized charges. It takes an infinite number of order operators to construct a topological excitation so it seems fundamentally impossible for an ‘order experimentalist’ to observe any kind of correlations in the disorder phase. This statement on ‘dual censorship’ is surely correct for the Ising model in 2D where the domain wall correlations cannot be measured by means of pure spin experiments. However, the statement above is too strong as in certain cases of the duality, the disorder correlations can be probed by means of order variables.

For our needs, we concentrate on a model that is very popular and used often as a toy model for the dualization of a continuum field theory. It is the vortex duality in 2+1-dimensions [58, 59, 60], also known as the Abelian-Higgs duality. In the quantum context this model may be alternatively interpreted as the Bose-Hubbard model in 2+1D at zero chemical potential [61]. The ordered phase represents a neutral superfluid, whereas the quantum disordered phase corresponds to a dual Meissner phase characterized by Bose condensed vortex-particles. This incompressible state corresponds to the Bose Mott-insulator [61].

On the ordered side, the excitation spectrum consists only of XY magnons. When on the ‘dual side’, the excitations of the Mott-insulator are massive degenerate doublets corresponding to particle and hole states (see Fig. 2.1). However, using the dual description of the XY model, one finds one Higgs (amplitude) mode (irrelevant for the case of strong type-II transitions) and two massive photons. As it will turn out, linear combination of these two photons become the massive particle and hole excitations. Furthermore, with the help of a simple expression relating the order and dual propagators (Zaanen-Mukhin relation, Eq. (2.55)), we will demonstrate that the correlations of the dual order can in principle be measured by means of order operators circumventing the principle of the ‘dual censorship’.

This connection between the order and disorder based on the concept of duality seemed to have been overlooked for quite a while and it was presented in a paper (co-authored with Zaanen) [62]. In that paper, whose main ideas are part of this chapter, special attention was given to the critical regime of the Abelian-Higgs model. This is a necessity since the model in 2+1D is below its upper critical dimension and its critical state is strongly

interacting. We present the complete description of this critical state (due to Hove and Sudbø [63]) and derive the Green's functions (superfluid velocity-velocity propagators) in the critical regime relying on the dual critical propagators. Surprisingly, the transversal and longitudinal dual photons appear to be quite different even though they are governed by the same anomalous dimension, again reflecting the rather different status of 'order' (transversal) and 'disorder' (longitudinal) when measured through velocity correlators.

In our work on the disordering of elastic solids, this model plays a central role as the theory of elasticity can also be dualized and the dual model is by construction equivalent to the dual XY model with additional (Burgers) flavors. The nature of topological defects in an elastic medium is far richer than that of a simple dual model and the aforementioned duality works only if the topological defects driving the duality are limited only to dislocations. That state of matter corresponds precisely with the nematic phase of the elastic media as described in the introductory chapter and resting on the fact that 'dual censorship' is violated in the Abelian-Higgs duality, the properties of the 'dislocation disordered' solid, i.e. nematic phases, will be investigated later.

This chapter is organized in the following way: in the first section we review the XY model used as a playground for the Abelian-Higgs duality. Consequently, we perform the dualization where the main step is the introduction of dual gauge fields [60]. The disordering operators, vortices in this case, couple to gauge fields. We will devote the second section to finding an effective theory describing the disorder operator dynamics. The third section analyses Green's functions of the model and calculates them (to Gaussian order) both in the ordered and the disordered phase. The disordered phase Green's functions can be found only after the Zaanen-Mukhin relation is derived from the Legendre transformation in the same section. In this third section we also invoke different gauge fixings which can shed light on the physical interpretations of the gauge field degrees of freedom. The next section presents novel results for the critical regime of the Abelian-Higgs model. The critical response is used to patch the excitation spectrum between the ordered and the disordered side of the model. Finally, the last section speculates on extensions to higher dimensions based on some existing work [64] and suggests where the lessons of the 2+1-dimensional case might be used.

## 2.1 Vortex duality

The system of interest is the well-known Bose-Hubbard model in 2+1D at vanishing chemical potential [61]. Due to many interesting applications there is a vast amount of literature about this model [53, 61, 63, 65, 66, 67, 68]. A short exposition of the dualization procedure can be found in a paper by Zee [59].

The model is defined on a bipartite 2D lattice and in phase representations its Hamiltonian is

$$\hat{H} = \frac{1}{C} \sum_i n_i^2 - J \sum_{\langle ij \rangle} \cos(\phi_i - \phi_j); \quad (2.1)$$

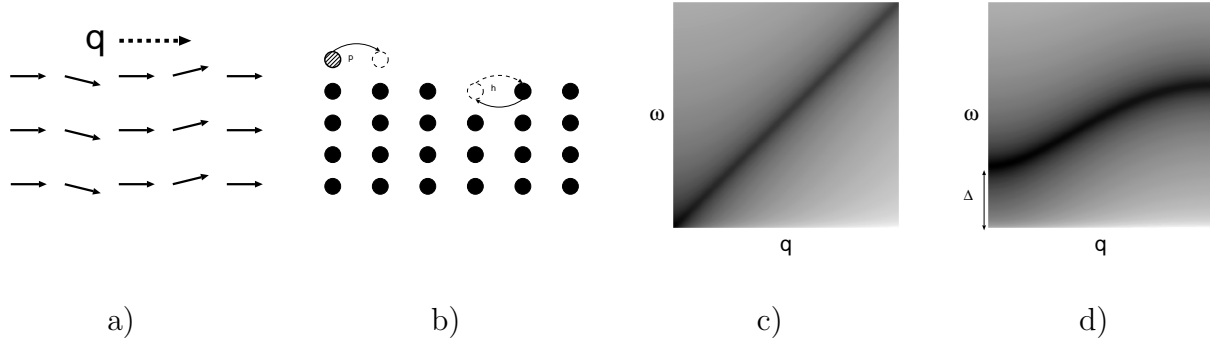


Figure 2.1: The excitations in the weak/strong coupling limits of the Bose-Hubbard model at zero chemical potential: The Goldstone boson (second sound) with linear dispersion (c) is associated with the superfluid (phase ordered) state (a) at weak coupling. In the strong coupling limit (b) a doublet of massive ‘excitons’ are found with gap  $\Delta$  (d) corresponding to propagating unoccupied and doubly occupied sites, which can be alternatively understood at  $q \rightarrow 0$  as the  $\pm 1$  angular momentum eigenstates of an  $O(2)$  quantum rotor.

$n_i$  and  $\phi_i$  are the number and phase operators on site  $i$ , satisfying the commutation relation  $[n_i, \phi_j] = i\delta_{ij}$ . The first and second terms in Eq. (2.1) represent the charging and Josephson energy respectively. When the coupling constant  $\tilde{g} = 2/(JC)$  is small, the Josephson energy will dominate and the phase is ordered at zero temperature, while the excitation spectrum consists of a single Goldstone mode (phase mode or second sound) shown in Fig. 2.1a, c. On the other hand, when  $\tilde{g}$  is large the phase is quantum disordered while the number operator condenses such that  $n_i = 0$  modulo local fluctuations, signaling the Mott-insulator. It is worth noticing that there are no finite temperature phase transitions as the partition function is a smooth function of the temperature [69]. Of central interest is the excitation spectrum of the Mott-insulator. In the rotor language [1], the ground state of the Mott-insulator is the angular momentum singlet while the lowest lying excitations consist of a doublet of propagating  $M = \pm 1$  modes characterized by a zero-momentum mass gap (Fig. 2.1d). In the Bose-Hubbard interpretation these have a simple interpretation in the strong coupling limit ( $\tilde{g} \rightarrow \infty$ ) as bosons added ( $M = +1$ ) or removed ( $M = -1$ ) from the charge-commensurate state (Fig. 2.1b), while their delocalization in the lattice produces a twofold degenerate dispersion due to the charge conjugation symmetry of the model Eq. (2.1).

We leave the propagator related questions aside for now as we first wish to establish a connection between the original Bose-Hubbard model written in the Lagrangian formalism and its dual counterpart that will turn out to be the Maxwell EM theory in 2+1D. To do so, we expand the cosines and take the continuum limit, and obtain the effective long-distance action density (Lagrangian)

$$\mathcal{L}_{XY} = \frac{1}{2g} \left[ \frac{1}{c_{ph}^2} (\partial_\tau \phi)^2 + (\nabla \phi)^2 \right] = \frac{1}{2g} (\partial_\mu \phi)^2. \quad (2.2)$$

The coupling constant  $g$  is proportional to the original coupling constant  $\tilde{g}$ . The spin-wave velocity is given by the ratio of the stiffness and compression moduli  $c_{ph}^2 = \rho_s/\kappa_s$  and set to 1 in the last step to express time in units of length  $\tau' \rightarrow c_{ph}\tau$ . This velocity is supposed to have the status of the ‘velocity of light’ in the theory. It is left implicit that the phase field is compact,  $\phi = \phi + 2\pi$ . The phase variable  $\phi$  is our order operator and it is well defined as long as  $g \ll 1$  since its fluctuations are strongly suppressed. The resulting state of matter is a superfluid. On the other hand, in the limit  $g \gg 1$  the phase can freely fluctuate so it averages to zero. In the disordered phase, the phase  $\phi$  is not a well-defined object (multivaluedness) and it is better if we can substitute it with a (universal) field that has well-defined values in both phases. The Hamiltonian strong-coupling regime of Eq. (2.1) suggests that the number operator  $n_i$  becomes well-defined in the Mott-insulating phase. This is correct, but the number operator is not defined in the ordered phase, thus it is not a universal field either. Besides, the ‘dual’ action has to be expressed in terms of topological operators of the original model and these will originate in the phase degree of freedom.

When one deals with a compact  $U(1)$  field, the standard trick is to split the phase field  $\phi$  into a smooth and a multivalued part [70]

$$\phi = \phi_{sm} + \phi_{MV}. \quad (2.3)$$

$\phi_{sm}$  is a non-compact (unbounded) field describing the smooth (non-topological) fluctuations of the phase variable.  $\phi_{MV}$  enumerates the topological defects corresponding, in this  $U(1)$  case, with vortices only. The vorticity is characterized through the non-trivial quantized circulation acquired by the multivalued field

$$\oint d\phi_{MV} = 2\pi N. \quad (2.4)$$

$N$  is the (integer) winding number of the encircled area, being invariant under the group of all smooth transformations of the phase.

Villain obtained quite accurate predictions for the disordered phase by taking the path integral over the vortex charges  $N_i$  and treating the smooth part as a non-compact field [71]. As we mentioned before, the aim of the duality is to remove the ill-defined phase field  $\phi$  and instead use the omnipotent dual operators. There are a number of different methods to construct the dual theory having, naturally, the same outcomes. We use the one that utilizes the Legendre transformation of the action (based on Ref. [60]). An alternative approach is to employ Hubbard-Stratanovich fields taking the role of dual variables (see Ref. [44]).

Let us begin by writing the partition function corresponding to the action density Eq. (2.2):

$$Z = \int \mathcal{D}\phi e^{-\int d^{d+1}x_\mu \mathcal{L}_{XY}[\phi, \partial\phi]}. \quad (2.5)$$

The action density is a functional of the phase field  $\phi$  and its derivatives  $\partial_\mu\phi$ , and at first we wish to get rid of these derivatives. Conjugate fields are introduced, playing the role of

momenta

$$\xi_\mu = -i \frac{\partial \mathcal{L}_{XY}}{\partial(\partial_\mu \phi)} = -\frac{i}{g} \partial_\mu \phi. \quad (2.6)$$

In a neutral superfluid, the fields  $\xi_\mu$  have the physical interpretation of supercurrents. The temporal component  $\xi_\tau$  is conjugate to the time derivative of the phase and, henceforth, corresponds to the number density. Notice that we work in the Euclidian space-time with a conventional prefactor  $-i$  in the definition Eq. (2.6) [60]. In the real-time duality formalism this factor is usually omitted. Inverting Eq. (2.6), phase field derivatives are expressed in terms of the momenta (and eventually phase  $\phi$ ). Using these, we construct the Hamiltonian density

$$\mathcal{H}_{XY}[\phi, \xi_\mu] = -i \xi_\mu \partial_\mu \phi(\phi, \xi_\mu) + \mathcal{L}_{XY}[\phi, \partial_\mu \phi(\phi, \xi_\mu)] = \frac{g}{2} \xi_\mu \xi_\mu. \quad (2.7)$$

which is by construction a functional of the phase field  $\phi$  and its conjugate momenta  $\xi_\mu$ . Our intention is to recover relevant physical quantities from the partition function which is now defined as the integral over all the paths in phase space  $(\phi, \xi_\mu)$ . However, the weighting in a partition function is never given by the Hamiltonian, but rather by the dual action

$$Z = \int \mathcal{D}\phi \mathcal{D}\xi_\mu e^{-\int d^{d+1}x_\nu \mathcal{L}_{dual}}. \quad (2.8)$$

To obtain the dual action (density) we have to ‘undo’ the Legendre transformation in Eq. (2.7)

$$\mathcal{L}_{XY,dual} = \mathcal{H}_{XY} + i \xi_\mu \partial_\mu \phi. \quad (2.9)$$

The last term is treated differently in this step as we do not wish to return to an action which is a function of the phase field  $\phi$ . Therefore, the derivatives  $\partial_\mu \phi$  are not reexpressed in terms of momenta  $\xi_\mu$ , but instead split into the smooth and the multivalued part as in Eq. (2.3). The smooth part can be first integrated by parts  $i \xi_\mu \partial_\mu \phi \rightarrow -i \phi \partial_\mu \xi_\mu$  and then integrated out producing the momentum conservation law (continuity equation of the superflow)

$$\partial_\mu \xi_\mu = 0. \quad (2.10)$$

The momentum conservation law is a direct consequence of the translational symmetry of the action. The Euler-Lagrange varying principle gives

$$\partial_\mu \xi_\mu = \partial_\mu \frac{\partial \mathcal{L}}{\partial(\partial_\mu \phi)} = \frac{\partial \mathcal{L}}{\partial \phi} = 0. \quad (2.11)$$

The speciality of the 2+1-dimensional model is that a divergenceless vector field obeying conservation law Eq. (2.10) can be written as the curl of another vector field

$$\xi_\mu = \epsilon_{\mu\nu\lambda} \partial_\nu A_\lambda. \quad (2.12)$$

This vector field  $A_\mu$  has the property of an  $U(1)$  gauge field. The physical variable momentum  $\xi_\mu$  as well as any other physically relevant quantity stays unchanged if we perform a gauge (also referred to as gradient) transformation

$$A_\mu \rightarrow A_\mu + \partial_\mu \alpha(x^\nu), \quad (2.13)$$

where  $\alpha(x^\nu)$  is an arbitrary *smooth* scalar function. The vector field  $A_\mu$  is called the dual gauge field and after the construction is complete, it will play the role of gauge potentials in the dual Maxwell theory.

That the dual theory has to do with the Maxwell theory becomes clear directly after the definition Eq. (2.12) is inserted back into the dual action Eq. (2.9). The term with the singular part of the phase field is partially integrated with respect to the gauge field

$$i\xi_\mu \partial_\mu \phi_{MV} = i\epsilon_{\mu\nu\lambda} \partial_\nu A_\lambda \partial_\mu \phi_{MV} \rightarrow iA_\lambda \epsilon_{\lambda\nu\mu} \partial_\nu \partial_\mu \phi_{MV} = iA_\lambda J_\lambda. \quad (2.14)$$

The minimally coupled topological current is

$$J_\lambda = \epsilon_{\lambda\nu\mu} \partial_\nu \partial_\mu \phi_{MV} = \epsilon_{\lambda\nu\mu} \partial_\nu \partial_\mu \phi. \quad (2.15)$$

This is the vorticity current enumerating the density of singularities, as well as their kinematic currents. Indeed, the temporal current component (charge density) integrated over some area gives the vorticity (number of vortices  $N$ ) of that area

$$\int dx dy J_\tau = \int dx dy \epsilon_{\tau ab} \partial_a \partial_b \phi = \oint dx^a \partial_a \phi = \oint d\phi = 2\pi N. \quad (2.16)$$

The spatial components  $J_i$  represent kinematical vortex currents. These can be thought of as the product of topological charge and the velocity of the defect. The vortex current is conserved

$$\partial_\mu J_\mu = \epsilon_{\mu\nu\lambda} \partial_\mu \partial_\nu \partial_\lambda \phi \equiv 0. \quad (2.17)$$

If we introduce the field strengths in the usual way  $F_{\mu\nu} = \partial_\mu A_\nu - \partial_\nu A_\mu$ , the Hamiltonian part Eq. (2.7) will play the role of Maxwell dynamical term and we arrive at the total dualized action Eq. (2.9))

$$\mathcal{L}_{XY,dual} \rightarrow \mathcal{L}_{EM} = \frac{g}{4} F_{\mu\nu} F_{\mu\nu} + iJ_\mu A_\mu. \quad (2.18)$$

This construction shows that vortex particles described by the current density  $J_\mu$  act as sources for the gauge field  $A_\mu$  and the latter plays the role of electromagnetic gauge potential carrying force between the ‘charged’ vortices. Conversely, one can view the Maxwell theory of electromagnetism (at least in 2+1D) as a description of the ordered phase of an XY model in disguise.

## 2.2 The disorder field

For any small but finite coupling constant  $g$ , closed loops of vortex-antivortex pairs will appear in the system. By increasing the charging energy in the starting model Eq. (2.1), i.e. by increasing the coupling constant  $g$ , the characteristic size of the loops increases. At the critical value of coupling  $g_c$  the size diverges and the system turns into a dense system of strongly interacting vortex lines. According to Eq. (2.18) these lines behave precisely like the world-lines of electrically charged particles. The unbinding transition and formation of a dense tangle of world-lines is something we are familiar with: the system becomes an Anderson-Higgs superconductor in terms of vortex charges [72, 73].

The Anderson-Higgs superconductor follows from the effective Ginzburg-Landau-Wilson action [60] describing the tangle of electrically charged particles. This is the last piece in the complete dual description of the model Eq. (2.1), the dynamics of the dual gauge fields is already recovered in Eq. (2.18) and we repeat here the famous proof from statistical physics [60, 74, 75] that a gas of bosonic particles in  $d$  dimensions (or equivalently gas of loops in  $d+1$  dimensions with the extra dimension interpreted as time) can be mapped onto the GLW action.

We now give one version of the proof for the ‘free bosons – GLW action’ mapping based on Ref. [44]. Let us start with a single vortex. It behaves as a random walker in the system with action proportional to the length of its world-line. The loop has to be closed because the vorticity is conserved or in other words, a vortex in a superfluid cannot be created out of nothing. A *relativistic* treatment means that the time direction is made equivalent to the spatial directions. There is precisely one velocity  $c_V$  that yields an isotropic space-time configuration space by  $\tau' \rightarrow c_V \tau$ . The space-time is ‘isotropic’ when a contribution of a world-line segment of length  $\Delta x$  is equal to that of a line segment that extends for  $\Delta \tau = \Delta x / c_V$  in a temporal direction. If  $\epsilon$  is the ‘action cost’ per loop length, then the total action of a single loop is given by the *relativistic* expression

$$\mathcal{L}_V = \epsilon \oint ds \sqrt{\dot{x}_\mu \dot{x}_\mu} = \epsilon \oint ds \sqrt{c_V^2 \dot{\tau}(s) \dot{\tau}(s) + \dot{\mathbf{x}}(s) \cdot \dot{\mathbf{x}}(s)}. \quad (2.19)$$

One could ask why we do not employ the ‘non-relativistic’ action for a boson particle (standard kinetic energy term  $\mathcal{L} \sim \frac{m}{2} (\partial_\tau \mathbf{x})^2$ )? The reason is that the initial action Eq. (2.2) is *relativistic*, i.e. invariant under ‘Lorentz boosts’ where the phase velocity  $c_{ph}$  plays the role of light velocity. If vortices inherit their dynamical properties exclusively from the Lagrangian Eq. (2.2) and if the temperature is precisely zero (this ensures that the configuration space is truly *relativistic*), the resulting effective theory of defects must also be invariant under the relativistic boosts. It is well known from special relativity that the length of a particle world-line as given in Eq. (2.19) is invariant under boost transformations (with the velocity  $c_V$  used as the light velocity in the boosts) and that it defines the ‘Lorentz-invariant’ action [76]. Thus, for a zero temperature *relativistic* XY model, the vortex velocity  $c_V$  is identical to the phase velocity  $c_{ph}$  and as we will argue later this degeneracy in velocities is necessary in order to connect the spectrum of the dual Maxwell theory to that of the Bose-Hubbard Mott-insulator as we did [62].

Even if there were another mechanism responsible for the dynamics of the vortices, or if the temperature were finite (implying the compactified time axis), the underlying theory ultimately has to reflect the dynamics of the vortices by having some other, vortex propagation, velocity  $c_V$  in place of the phase velocity as the only difference. In the case of the BCS superconductor [17] the velocity associated with the condensate is proportional to Fermi velocity  $v_F$  [77, 78]. As a consequence, the electric and magnetic screening in a superconductor, although originating in the same superconducting gap  $\Delta$ , have highly discrepant characteristic lengths. The magnetic sector (the transversal photon) is governed by the light velocity  $c$  and the London penetration length is  $\lambda_L = c/\Delta$ . This length is many orders of magnitude larger than the electric screening length  $\lambda_e \sim v_F/\Delta$ .

The velocity  $c_V$  is alternatively implied by the (relativistic) Klein-Gordon equation for the bosonic vortex field. A bosonic field has to obey equation of motion [79].

$$0 = (\partial_\mu^2 + m^2)\Psi = \left( \frac{1}{c_V^2} \partial_\tau^2 + \partial_i^2 + m^2 \right) \Psi. \quad (2.20)$$

The collective field  $\Psi$  is the wave function of a single or multiple bosons and it relates to (bosonic) matter currents via

$$J_\mu = \frac{i}{2} [(\partial_\mu \bar{\Psi})\Psi - \bar{\Psi}\partial_\mu \Psi]. \quad (2.21)$$

These currents must obey the current conservation law

$$0 = \partial_\mu J_\mu = \frac{i}{2} [(\partial_\mu^2 \bar{\Psi})\Psi - \bar{\Psi}(\partial_\mu^2 \Psi)] \quad (2.22)$$

and this will be the case if we use the velocity  $c_V$  to convert time to length in the definition (2.21) for the static charge

$$J_\tau = \frac{i}{2} \frac{1}{c_V^2} [(\partial_\tau \bar{\Psi})\Psi - \bar{\Psi}\partial_\tau \Psi]. \quad (2.23)$$

After this interlude on the velocities, let us now return to a partition function corresponding to one loop/random walker. For convenience, consider the problem on a (hyper-)cubic lattice with spacing  $a$  (which acts as a necessary cut-off). Note that the discretisation in the temporal direction is implied as  $\Delta\tau = a/c_V$ . A single loop of length  $aN$  is a random walker which returns to its initial position (loop has to be closed). Knowing that the action is proportional to the world-line length, we can write the partition function of a single defect loop as

$$Z_1 = \sum_{x_\mu, N} \frac{C_N(x_\mu, x_\mu)}{N} e^{-\epsilon a N}. \quad (2.24)$$

The length  $N$  of the loop can run from zero to infinity, but longer loops will be exponentially suppressed. The denominator factor  $N$  ensures that each loop is counted only once and  $C_N(x_\mu, y_\mu)$  is the number of loops of length  $N$  running from  $x_\mu$  to  $y_\mu$ . The problem of

finding  $C_N$  is equivalent to the diffusion problem in a  $d + 1 = D$ -dimensional embedding space. The number of possible loops is determined from the recursion relation

$$C_N(0, x_\mu) = \sum_{a_\mu} C_{N-1}(0, x_\mu - a_\mu). \quad (2.25)$$

The vector  $a_\mu$  points toward nearest neighbours where the particle was present in the previous step (time  $(N - 1)\Delta\tau$ ). The ‘diffusion’ equation Eq. (2.25) is easier to solve in Fourier-transformed form

$$C_N(p_\mu) = \int dx_\nu C_N(x_\mu) e^{-ip_\mu x_\mu} = C_{N-1}(p_\mu) \sum_{a_\mu} e^{-ip_\mu a_\mu}. \quad (2.26)$$

The boundary condition  $C_0(0, x_\mu) = \delta(x_\mu)$  together with Eq. (2.26) implies a solution

$$C_N(p_\mu) = [P(p_\mu)]^N \quad (2.27)$$

where we introduced the ‘sum of cosines’  $P(p_\mu)$ , often seen in problems on cubic lattices. At large distances (small wavelengths) it can be expanded up to quadratic order

$$P(p_\mu) = \sum_{a_\mu} e^{-ip_\mu a_\mu} = 2D - a^2 p_\mu p_\mu + O(p^4). \quad (2.28)$$

In the partition function Eq. (2.24), the solution Eq. (2.27) together with expansion identity  $\sum_{N=1}^{\infty} \frac{x^N}{N} = -\ln(1 - x)$  yields the partition function

$$Z_1 = - \sum_{p_\mu} \ln [1 - P(p_\mu) e^{-\epsilon a}]. \quad (2.29)$$

The grand canonical partition function of a gas of non-interacting loops is obtained by exponentiation of the single loop partition function

$$\Xi = e^{Z_1} = \prod_{p_\mu} \frac{1}{1 - P(p_\mu) e^{-\epsilon a}} \equiv \prod_{p_\mu} [G_0(p_\mu)]^{-1}. \quad (2.30)$$

The same product of the propagators is, on the other hand, reproduced if we perform a Gaussian integration over the complex fields  $\Psi$

$$\Xi = \int \mathcal{D}\bar{\Psi} \mathcal{D}\Psi e^{-\frac{1}{2} \int dx_\nu \bar{\Psi}(x_\mu) G_0(x_\mu) \Psi(x_\mu)}. \quad (2.31)$$

The inverse propagator in the coordinate space with the continuum limit becomes the bosonic (Klein-Gordon) propagator

$$G_0(x_\mu)^{-1} = (a^2 e^{-\epsilon a}) [-\partial_\mu \partial_\mu + m^2], \quad (2.32)$$

with the ‘mass’ defined by

$$m^2 = \frac{e^{\epsilon a} - 2D}{a^2}. \quad (2.33)$$

The stability of the ground state with no vortices present (vacuum) depends on the sign of the mass Eq. (2.33). When the energy/action costs of vortices are high, they can be present only as bound pairs in the system. This is reflected in positive mass term Eq. (2.33). On the other hand, if energy cost  $\epsilon$  is small, the meandering entropy of vortex world-lines can overcome it and the defects proliferate. This is seen through the mass term Eq. (2.33) that becomes negative. The transition between the two phases occurs when at critical value of coupling constant

$$\epsilon_c = \frac{1}{a} \ln [2D + a^2 m^2]. \quad (2.34)$$

When the vortices condense one has to regulate the density of the vortex tangle (average number of vortices per volume). This is solved by a short-ranged repulsion term  $\omega|\Psi|^4$  which represents a ‘steric’ repulsion between the world-lines. In the appendix A we treat a problem of non-relativistic diffusion based on results by Kiometzis *et al.* [75], generalizing their findings to a system of random walkers with an arbitrary repulsion potential between them. As it turns out, the two-body repulsion can always be mapped to a  $\Psi^4$  term.

The Gaussian part of the random walker action Eq. (2.32) and the ‘steric’ repulsion together yield the action describing systems such as the vortices in the Abelian-Higgs duality. This action is precisely the Ginzburg-Landau-Wilson  $\Psi^4$  action

$$\mathcal{L}_{GLW} = \frac{1}{2}|\partial_\mu \Psi|^2 + \frac{1}{2}m^2|\Psi|^2 + \omega|\Psi|^4, \quad (2.35)$$

so we have a proof that vortices can be mapped onto a GLW action.

The ordered and disordered phases of the XY model Eq. (2.2) have other names, based on the vortex duality and their interpretation in terms of the standard Maxwell theory. The ordered (superfluid) phase of the XY model is called Coulomb (vortex vacuum) and it is characterized by massless gauge fields  $A_\mu$ . On the other hand, the disordered (Mott-insulating) phase is interpreted as a superconductor in the dual theory and it is also called the dual Higgs phase. The Higgs phase is a fully gapped (incompressible) superconductor unless there are additional constraints on gauge fields or currents that can interfere with the Higgs mechanism.

The vacuum state of the Higgs (vortex-condensed) phase is determined by the minimum of the static potential between vortices (last two terms in Eq. (2.35)). The absolute value of the GLW order parameter field is

$$\Psi_0 = \sqrt{\frac{-m^2}{4\omega}}, \quad (2.36)$$

and it represents the vortex tangle density at which the energy gains through further proliferation of vortices are exactly compensated by their repulsion. Fluctuations in the

Higgs field amplitude can be ignored (strong type-II superconductor limit). The phase of the complex field, on the other hand, appears as the physical degree of freedom and if the bosons (vortices) were not interacting with the gauge fields, this degree of freedom would correspond to the Goldstone mode of the broken global  $U(1)$  symmetry [80].

The above picture is, however, not complete as we still need to find the role of coupling between the vortices and the gauge fields in the GLW action Eq. (2.35). To do so, we again analyse a single vortex excitation. At this point we have to go back to 2+1D duality for the reasons that originate in geometrical structure of defects. Namely, the vortex defects are point particles (tracing world-lines in the imaginary direction) only in the 2+1D Abelian-Higgs model. In any higher dimension of the embedding space, the vortices become lines, branes, etc. and action Eq. (2.35) is not applicable anymore. Later, in section 2.5 we will analyse higher-dimensional Abelian-Higgs duality and review problems associated with the dimensionality of vortex excitations in higher dimensions.

Let us parametrize the vortex world-line as  $\bar{x}_\mu(s')$  where the parameter  $s'$  runs from 0 to  $s$  and the boundary condition  $\bar{x}_\mu(s) = \bar{x}_\mu(0)$  is imposed in order to have a closed defect loop. This vortex excitation carries vortex current, expressed in terms of path  $\bar{x}_\mu(s')$  as

$$J_\mu(x_\nu) = 2\pi N \delta_\mu(x_\nu). \quad (2.37)$$

The winding number of the vortex is  $N$ . The line-delta function is defined as the tangent of the world-line path, i.e.

$$\delta_\mu(x_\nu) = \oint_0^s ds' \partial_{s'} \bar{x}_\mu(s') \prod_\nu \delta[x_\nu - \bar{x}_\nu(s')]. \quad (2.38)$$

The current conservation law Eq. (2.17) can be easily demonstrated using total derivative identities

$$\begin{aligned} \partial_\mu J_\mu &= 2\pi N \partial_\mu \oint_0^s ds' \partial_{s'} \bar{x}_\mu(s') \prod_\nu \delta[x_\nu - \bar{x}_\nu(s')] \\ &= 2\pi N \oint_0^s ds' \partial_{s'} \bar{x}_\mu(s') \delta' [x_\mu - \bar{x}_\mu(s')] \prod_{\nu \neq \mu} \delta[x_\nu - \bar{x}_\nu(s')] \\ &= 2\pi N \oint_0^s d\delta [x_\mu - \bar{x}_\mu(s')] \prod_{\nu \neq \mu} \delta[x_\nu - \bar{x}_\nu(s')] \equiv 0. \end{aligned} \quad (2.39)$$

The definition of the vortex current Eq. (2.37) can be substituted in the minimal coupling term of the action to obtain the coupling of a single vortex line to gauge degrees of freedom

$$\begin{aligned} S_{AJ} &= i \int dx_\nu A_\mu(x_\nu) J_\mu(x_\nu) = i \int dx A_\mu(x_\nu) \oint_0^s ds' \partial_{s'} \bar{x}_\mu(s') \delta[x_\nu - \bar{x}_\nu(s')] \\ &= i \oint_0^s ds' \partial_{s'} \bar{x}_\mu(s') A_\mu(\bar{x}_\nu(s')) = i \oint d\bar{x}_\mu A_\mu(\bar{x}_\nu). \end{aligned} \quad (2.40)$$

This tells us that a vortex behaves as a free particle moving in the gauge field potential  $A_\mu$ . The canonical momentum immediately follows as

$$P_\mu = p_\mu + A_\mu = i\partial_\mu + A_\mu, \quad (2.41)$$

which in turn implies that instead of the regular derivatives in the Ginzburg-Landau-Wilson action Eq. (2.35), one should use the covariant derivatives  $\partial_\mu - iA_\mu$ . The total action, including both the dynamic Maxwell term and the Ginzburg-Landau-Wilson action of the vortex condensate is

$$\mathcal{L}_{EM,full} = \frac{g}{4}F_{\mu\nu}F_{\mu\nu} + \frac{1}{2}|(\partial_\mu - iA_\mu)\Psi|^2 + \frac{1}{2}m^2|\Psi|^2 + \omega|\Psi|^4 \quad (2.42)$$

corresponding to the partition function

$$Z = \int \mathcal{D}A_\mu \mathcal{D}\bar{\Psi} \mathcal{D}\Psi \mathcal{F}(A_\mu, \bar{\Psi}, \Psi) e^{-\int dx_\mu \mathcal{L}_{EM,full}}. \quad (2.43)$$

An alternative way to deduce the minimal coupling Eq. (2.41) in the GLW action Eq. (2.42) is related to the fact that vortices behave as charged particles in an electromagnetic field governed by the potentials  $A_\mu$ . It is well-known that, in order to preserve gauge invariance of the action, the hopping in the EM field must change the phase of the wave function by  $iA_\mu dx_\mu$  (i.e. the Wilson loop [55]). This adds to the standard phase change which equals  $ip_\mu dx_\mu$ , so the standard derivative has to be replaced by the covariant derivative Eq. (2.41).

The Maxwell part of the action Eq. (2.42) is invariant under the gradient transformation Eq. (2.13). The same holds for the second, GLW part of the action provided that the transformation of the gauge fields is accompanied by the change in the phase of the collective bosonic field  $\Psi(x_\nu) \rightarrow \Psi(x_\nu)e^{i\alpha(x_\nu)}$ . In order to keep the integration only over physically distinct configurations, i.e. to avoid redundant configurations implied by the arbitrariness of the gradient function, we restrict the path integral only to one particular choice of the gradient function, that is to one particular gauge fix. The gauge fix is implied by a constraint  $\mathcal{F}$  that acts both on the gauge fields and the phase of the bosonic field. In the next section, some particular choices will be made for the gauge fix, pending the content of the problem. The gauge fix is usually chosen in such way to either simplify the work or to give valid interpretations to physical results of the theory. However, regardless of the choice of the gauge fix, the physical results must always be the same.

The most important consequence of the coupling between the disorder field and the gauge field is that the global phase symmetry of the disorder field  $\Psi$  has changed into a local (gauge) symmetry. The complex phase mode in the disordered phase is therefore not a Goldstone mode. Instead, it plays the role of the vortex condensate sound as will become clear in the next section. In the Higgs/Meissner phase, the complex phase degree of freedom will be represented by a gapped EM photon and eventually the spectrum of the incompressible Mott-insulator will be recovered. It should be noted that, in contrast to a popular belief, a gauge symmetry cannot be broken [81] and the order carried by this phase is in fact the topological order [82, 83]. Accordingly, we never call the phase with massive gauge fields the phase with the broken gauge symmetry. Instead, it is referred to as the Higgs phase of the gauge theory.

## 2.3 Green's functions, the Zaanen-Mukhin relation and the 'dual censorship'

Our toy model, the XY spin model given by Eq. (2.2), is formulated in terms of spins and one would like to think of the excitations in the model as magnons (at least in the ordered phase). On the other hand, in the previous section we hopefully managed to convince the reader that the model can alternatively be viewed as a Maxwell theory with photons as the primary degrees of freedom. The duality presented in the previous section can be utilized only when we are able to express the propagators of the original XY model in terms of photon propagators. It seems that until recently a direct relation between the order propagators and the dual propagators was not established. In Ref. [44] such a relation (Zaanen-Mukhin) was derived for the case of elastic propagators and their dual counterparts (and we will use it in later chapters). In a follow up paper [62] (together with Zaanen), the Zaanen-Mukhin relation was used to address the Green's functions of the XY model, showing that the dual censorship between the order and disorder phase is not absolute as in the case of Kramers-Wannier duality. In other words, even when the system is in the disordered XY phase, it is possible to observe correlations of the topological disorder operators by means of order operators. In this section these matters are reviewed, the Zaanen-Mukhin relation is derived, the spectrum of the model is found in both ordered and disordered phase and a link with the strong coupling expansion of the model is established. The dual gauge fields are given the status of physical degrees of freedom by imposing appropriate gauge fixes for each separate phase.

Let us begin our exploitation of the XY model by asking the most natural physical question: what are the Green's functions, i.e. XY phase propagators of the model? The time has a specific role in these matters. For example, despite the 'relativistic' form of the XY action Eq. (2.2), in the 'Josephson junctions' action Eq. (2.1) time had a specific role, different from the spatial components. This is true for most other physical applications of the XY model, as well as for other physical theories like the elasticity theory introduced later. Any finite temperature, although not at the focus of our attention, isolates the time direction from the spatial counterparts by its compactification. One should not forget how much relativistic our experiments are. Namely, all our laboratories and machines are static only in a specific reference frame and their 'world-lines' define a preferred direction in space-time which is observed (by a machine or a person sitting next to it) as the time direction in that frame of reference. Therefore, measurable quantities involving spatial components of fields usually have different status from their 'temporal' counterparts. In this section the superfluid velocity is put forward as the experimentally relevant observable of the model and we calculate its correlation functions. The superfluid velocity is related to gradients of the phase field from the model Eq. (2.2). Based on the arguments presented here, we are interested only in the spatial superfluid velocities ( $\partial_i\phi$ ) whereas the temporal component ( $\partial_t\phi$ ) is left out.

The claims in the previous paragraph are true for most of the physically relevant questions, like the outcomes of the human-devised experiments. Nevertheless, there are still

### 2.3 Green's functions, the Zaanen-Mukhin relation and the 'dual censorship' 27

some situations left where the 'relativistic' nature of the action should be appreciated and where time and space have to be treated on equivalent footing. This will certainly be the case when the elastic theory is utilized to recover the emerging theory of gravity [84, 85], but also in cases of loop gas formulation (appendix A), introduction of true topological defects and many other technical details that are resolved straightforwardly in the 'relativistic' interpretation. Signifying the importance of both cases, both relativistic and non-relativistic versions of the physical variables will be defined. However, due to the special direction of time in the rest frame of experiments, the non-relativistic versions will receive the full treatment and they will be in charge when it comes to interpretation of experimental observables. The difference in status of order and disorder correlations probed by means of order operators has much to do with the special role of the time direction.

The first natural order observable to consider should be the XY phase  $\phi$ , but since it becomes ill-defined in the disordered phase, we take the superfluid three-velocity

$$v_\mu(\mathbf{x}) = \partial_\mu \phi(\mathbf{x}) \quad (2.44)$$

as the natural, 'primitive' observable of the orderly side. In the ordered phase, the momentum space velocity-velocity propagator is proportional to the phase-phase propagator,  $\langle\langle v_\mu | v_\nu \rangle\rangle_{q,\omega} = q_\mu q_\nu \langle\langle \phi | \phi \rangle\rangle_{q,\omega}$  and the latter suffices to calculate the order parameter propagator  $\langle\langle e^{i\phi} | e^{i\phi} \rangle\rangle$  (e.g., Ref. [61]). In the disordered phase,  $\phi$  itself becomes multi-valued and meaningless, but  $v_\mu$  continues to be single-valued and meaningful.

In the phase-ordered state the theory Eq. (2.2) is Gaussian and the velocity propagator is easily computed by adding the external source term to the Lagrangian,

$$\mathcal{L}[\mathcal{J}_\mu] = \mathcal{L}_{XY} + \mathcal{J}_\mu \partial_\mu \phi, \quad (2.45)$$

followed by taking the functional derivative of the generating functional

$$\langle\langle v_\mu | v_\nu \rangle\rangle = \frac{1}{Z} \left. \frac{\partial^2 Z[\mathcal{J}_\mu]}{\partial \mathcal{J}_\mu \partial \mathcal{J}_\nu} \right|_{\mathcal{J}_\mu=0}. \quad (2.46)$$

The non-relativistic propagator measured in condensed matter experiments represents only the subset of components of the relativistic propagator Eq. (2.46) with spatial indices:  $\langle\langle v_i | v_j \rangle\rangle$ . In the phase ordered state of the XY model one can integrate the Gaussian Goldstone fields in Eq. (2.45) with the result,

$$Z[\mathcal{J}_\mu] = \prod_{p_\mu} \sqrt{\frac{2\pi g}{p^2}} e^{\frac{g}{2} \mathcal{J}_\mu \frac{p_\mu p_\nu}{p^2} \mathcal{J}_\nu}. \quad (2.47)$$

and the propagators follow immediately from the identity Eq. (2.45). The relativistic and non-relativistic versions are respectively,

$$\langle\langle v_\mu | v_\nu \rangle\rangle = g \frac{p_\mu p_\nu}{p^2}, \quad (2.48)$$

$$\langle\langle v_i | v_j \rangle\rangle = g \frac{c_{ph}^2 q^2}{\omega_n^2 + c^2 q^2} P_{ij}^L, \quad (2.49)$$

denoting the three-momentum by  $p_\mu = (\omega_n, c_{ph}\mathbf{q})$  and the spatial part of the momentum by  $\mathbf{q}$ . The longitudinal projection operator Eq. (1.11) is defined in the introductory chapter. There is just one propagating degree of freedom in the system and it can be thought of as a XY magnon which is the Goldstone mode of the broken global  $U(1)$  symmetry.

Of course, the above procedure no longer works in the absence of the phase condensate. At any finite disorder there are configurations present containing topological defects (vortices), which are ignored in the path integral Eq. (2.47) but these are easily handled in the language of the dual disorder field theory. There is, however, one important step to be made that we already announced: the dual theory is expressed in terms of dual (gauge) fields and we need to make a connection between the dual and the original Green's functions. Although one might be tempted to think that, due to the linear relation Eq. (2.6), the propagators differ only by a prefactor, the nature of the Legendre (or alternatively the Hubbard-Stratanovich) transformation yields a different identity. Begin with the action Eq. (2.45) and repeat the dualization as given in section 2.1. Interestingly, the conjugate momenta acquire an additional term from the external source current term Eq. (2.45)

$$\xi_\mu = -\frac{i}{g}\partial_\mu\phi - i\mathcal{J}_\mu. \quad (2.50)$$

When this identity is used in place of Eq. (2.6) to substitute derivatives  $\partial_\mu\phi$ , the Hamiltonian density Eq. (2.7) acquires additional terms

$$\mathcal{H}_{XY} = \frac{g}{2}\xi_\mu\xi_\mu - \frac{g}{2}\mathcal{J}_\mu\mathcal{J}_\mu + ig\mathcal{J}_\mu\xi_\mu. \quad (2.51)$$

The double derivative of the partition function yields

$$\left. \frac{\partial^2 Z[\mathcal{J}_\mu]}{\partial \mathcal{J}_\mu \partial \mathcal{J}_\nu} \right|_{\mathcal{J}_\mu=0} = \int \mathcal{D}\xi_\mu \mathcal{D}\phi \left. \frac{\partial^2}{\partial \mathcal{J}_\mu \partial \mathcal{J}_\nu} e^{\int dx_\nu \left( \frac{g}{2}\mathcal{J}_\mu\mathcal{J}_\mu - ig\mathcal{J}_\mu\xi_\mu - \frac{g}{2}\xi_\mu\xi_\mu - i\xi_\mu\partial_\mu\phi \right)} \right|_{\mathcal{J}_\mu=0} \quad (2.52)$$

$$= \int \mathcal{D}\xi_\mu \mathcal{D}\phi (g\delta_{\mu\nu} - g^2\xi_\mu\xi_\mu) e^{\int dx_\nu \left( -\frac{g}{2}\xi_\mu\xi_\mu - i\xi_\mu\partial_\mu\phi \right)} \quad (2.53)$$

$$= Z (g\delta_{\mu\nu} - g^2\langle\langle\xi_\mu|\xi_\nu\rangle\rangle), \quad (2.54)$$

which implies the following exact relationship between the velocity and the supercurrent propagators

$$\langle\langle v_\mu | \partial_\nu \phi \rangle\rangle = g\delta_{\mu\nu} - g^2\langle\langle\xi_\mu|\xi_\nu\rangle\rangle. \quad (2.55)$$

Because  $\xi_\mu = \epsilon_{\mu\nu\lambda}\partial_\nu A_\lambda$  this implies that in fact the phase velocity/spin wave propagator is proportional to a linear combination of the physical photon propagators of the dual gauge disorder-field theory. This implies that the poles of the magnon and photon propagator have to coincide and this has to be because both describe the same physics. However, the pole strengths might be quite different reflecting the ‘dual relativity principle’: pending the use of either order or disorder ‘tools’ one might get a very different view of the same underlying reality. The result Eq. (2.55), first derived in Ref. [44], shows that at least in the

### 2.3 Green's functions, the Zaanen-Mukhin relation and the 'dual censorship' 29

Abelian-Higgs case, the two observers should actually agree more on what they see than one could have expected a-priori. The key is that although the vortex condensate falls prey to dual censorship, the observer equipped with the 'orderly measuring machines' can still learn much about the dual world because he/she can probe the dual photons according to Eq. (2.55).

Let us exercise these notions in the simple case of the phase ordered state. We know the answer (the Goldstone mode, Eq. (2.48), we know the dual side (Maxwell theory,  $F_{\mu\nu}F^{\mu\nu}$ ), and we know how these relate (the 'Zaanen-Mukhin' relation, Eq. (2.55)). It is indeed a straightforward exercise.

Although the dynamics is fully relativistic, the questions of relevance to condensed matter experimentalists are not relativistic: only the spatial components of the propagator are measurable (Eq. (2.49)). This makes it convenient to use the Coulomb gauge fix. The Maxwell action in momentum-Matsubara frequency space becomes, including the external sources  $J_\mu^{ext.}$ ,

$$\mathcal{L}_{EM} = \frac{g}{2} (A_\tau^\dagger, \mathbf{A}^\dagger) \begin{pmatrix} q^2 & -i\omega_n \langle \mathbf{q} | \\ i\omega_n | \mathbf{q} \rangle & \omega_n^2 \hat{\mathbf{1}} + c_{ph}^2 q^2 \hat{P}^T \end{pmatrix} \begin{pmatrix} A_\tau \\ \mathbf{A} \end{pmatrix} + iJ_\tau^{ext.} A_\tau + i\mathbf{J}^{ext.} \cdot \mathbf{A} \quad (2.56)$$

where we have explicitly indicated the time ( $X_\tau$ ) and space ( $\mathbf{X}$ ) components of the gauge fields and currents. The bra and ket in the gauge field propagator represent rows and columns  $q_i$ , respectively.

Provided that we choose a gauge fix  $\mathcal{F}$  that does not act on the temporal component  $A_\tau$ , the temporal component can be integrated out. This yields the usual Lagrangian with Coulomb interactions between static sources,

$$\begin{aligned} \mathcal{L}_{EM} = & \frac{1}{2g} \frac{J_\tau^\dagger J_\tau}{q^2} + \frac{g}{2} (\omega_n^2 + c_{ph}^2 q^2) \mathbf{A}^\dagger \hat{P}^T \mathbf{A} + \\ & + i(J_L - \frac{i\omega_n}{q} J_\tau) A_L^\dagger + i\mathbf{J} \hat{P}^T \mathbf{A}^\dagger. \end{aligned} \quad (2.57)$$

The longitudinal component  $A_L$  is unphysical (its source is  $i\omega_n J_\tau - qJ_L \rightarrow \partial_\tau J_\tau + \partial_i J_i = 0$ ) and it should be removed by the Coulomb gauge

$$0 = \partial_i A_i = -qA_L. \quad (2.58)$$

We end up with two propagators for the gauge fields, as it should in 2+1D. We find one dynamical photon,

$$\langle \langle A_i^\dagger | A_j \rangle \rangle = \frac{P_{ij}^T}{g(\omega_n^2 + c_{ph}^2 q^2)}. \quad (2.59)$$

and a propagator taking care of the Coulomb interactions between the static sources,

$$\langle \langle A_\tau^\dagger | A_\tau \rangle \rangle = \frac{1}{gq^2} \quad (2.60)$$

This is of course textbook electromagnetism, but be aware of the twist in the interpretation. The outcome is: the theory is carrying a 'Goldstone photon' ( $A_T$ , Eq. (2.59)) and it can mediate as well interactions between static vortices ( $A_\tau$ , Eq. (2.60)).

Although a relativity textbook issue, let us make an observation on the seemingly paradoxical nature of the Coulomb gauge fix. At this point one might object that the Coulomb law given by the first term of the action Eq. (2.57) violates the causality of the standard Maxwell electrodynamics. First of all, in imaginary time formalism there is no causality issue as the disorder is just represented via path integral over all possible configurations, including the ones that would correspond to motions with velocities greater than that of light when imaginary time is rotated to real time. However, disregarding the contribution to the action from the thermal disorder, one finds, after rotation to the real time, term  $\frac{e^2}{q^2}$ . Interpreting this naively, an appearance of a charge at a certain point in the system would be immediately detectable in the whole system, rendering the causality principle invalid. However, the appearance of the charge (spontaneous or not) is strictly forbidden due to the current conservation law Eq. (2.17). The direct violation by inserting extra charges is therefore not possible. Nevertheless, one might consider a rearrangement of charges that would be detected instantaneously, due to a change in dipole, quadrupole, octupole, etc. potentials. Such a process is in fact used for radio transmission. All antennae play the role of oscillating dipoles. Due to the oscillating charge, a current occurs coupling to the transversal electromagnetic field. It is these photons, travelling at the velocity of light, that transport information from site to site. The dipole and higher order potentials on the other hand cannot be detected instantaneously due to the advanced potentials in the actions that cancel their strength.

We are now in the position to evaluate the 'Zaanen-Mukhin' relation Eq. (2.55). For this purpose, we are only interested in the spatial components of the supercurrents  $\xi_\mu$ . The supercurrent propagator is easily found by using the definition Eq. (2.12), and the results for the gauge field propagators Eqs. (2.59, 2.60). We find for its spatial components,

$$\langle\langle \xi_i^\dagger | \xi_j \rangle\rangle = \frac{1}{g} \left[ \frac{\omega_n^2}{\omega_n^2 + c_{ph}^2 q^2} P_{ij}^L + P_{ij}^T \right]. \quad (2.61)$$

Using now the Zaanen-Mukhin relation Eq. (2.55),

$$\begin{aligned} \langle\langle v_i | v_j \rangle\rangle &= g\delta_{ij} - g^2 \langle\langle \xi_i | \xi_j \rangle\rangle = g[P_{ij}^L + P_{ij}^T] - g \left[ \frac{\omega_n^2}{\omega_n^2 + c_{ph}^2 q^2} P_{ij}^L + P_{ij}^T \right] \\ &= g \frac{c_{ph}^2 q^2}{\omega_n^2 + c^2 q^2} P_{ij}^L. \end{aligned} \quad (2.62)$$

After this long detour, we indeed have managed to recover the spin wave propagator Eq. (2.49)!

The lesson following from this simple exercise is that the dual photon language is in a way more complete than the description in terms of phase fields, in the sense that the gauge fields keep track in an explicit way of both the capacity of the medium to propagate

### 2.3 Green's functions, the Zaanen-Mukhin relation and the 'dual censorship' 31

Goldstone bosons and the fact that it mediates interactions between its topological excitations. The Zaanen-Mukhin relation filters out the Goldstone sector from the 'omnipotent' dual gauge sector, keeping its topological side (the Coulomb propagator, requiring vortex sources) completely hidden from the eye of the 'orderly' observer.

Surely, this dual route is a rather inefficient way to derive the propagator of a Goldstone mode. This changes drastically in the phase disordered state. Resting on the fact that the dual gauge theory is now governed by order, precise information on the second sound propagator can be extracted with barely any extra investments. The only other option is the strong coupling expansion in the Hamiltonian language and this becomes very tedious at intermediate couplings.

The phase disordered state corresponds to the Higgs phase of the gauge theory Eq. (2.42), corresponding to the state where vortex loops have blown up and the vortices have Bose-condensed. As a consequence, the bosonic disorder field  $\Psi = |\Psi_0|e^{i\phi_V}$  acquires a finite expectation value. This theory is fully relativistic, as we explained, and this vortex condensate is literally like the  $U(1)$  Higgs phase of high energy physics [86]. It will turn out to be quite convenient for the interpretation of the results to consider a non-relativistic extension of the theory characterized by a condensate velocity  $c_V$ , which is different from the spin-wave velocity  $c_{ph}$ , entering the time components of the covariant derivatives  $\sim \frac{1}{c_V}(\partial_\tau - iA_\tau)$ .

Let us employ the usual unitary gauge, corresponding to fixing the condensate phase  $\phi_V = 0$ . The finite expectation value of the disorder field results in the familiar Higgs term in the action

$$\mathcal{L}_{Higgs} = \frac{1}{2}|\Psi_0|^2 \left[ \frac{1}{c_V^2} A_\tau A_\tau + A_i A_i \right]. \quad (2.63)$$

The only specialty is the velocity  $c_V$ . In high energy physics this is the light velocity while in the non-relativistic condensates of condensed matter physics  $c_V$  is the sound velocity (in BCS theory  $\sim v_F$  [72, 73, 77, 78]), which is vanishingly small compared to the light velocity with the consequence that one can get away with a time independent Ginzburg-Landau theory.

We now follow the same route as in the case of the ordered phase. Adding the Higgs term the Lagrangian becomes,

$$\mathcal{L}_{full} = \frac{g}{2} \begin{pmatrix} A_\tau \\ \mathbf{A} \end{pmatrix}^\dagger \begin{pmatrix} q^2 + \frac{\Omega^2}{c_V^2} & -\omega_n \langle \mathbf{q} | \\ -\omega_n \langle \mathbf{q} | & (\omega_n^2 + \Omega^2) \hat{\mathbf{1}} + c_{ph}^2 q^2 \hat{P}^T \end{pmatrix} \begin{pmatrix} A_\tau \\ \mathbf{A} \end{pmatrix} + iJ_\tau A_\tau^\dagger + i\mathbf{J} \cdot (\mathbf{A}^\dagger \hat{P}^T) \quad (\mathbf{A}^\dagger \hat{P}^T) \quad (2.64)$$

We introduced a convenient notation for the Higgs gap  $\Omega$ , defined by

$$\Omega^2 = \frac{|\Psi_0|^2}{g}. \quad (2.65)$$

Since the gauge has already been fixed, the temporal components  $A_\tau$  can be safely

integrated out,

$$\begin{aligned} \mathcal{L}_{full} = & \frac{g}{2} \mathbf{A}^\dagger \left[ \frac{\Omega^2(\omega^2 + c_V^2 q^2 + \Omega^2)}{c_V^2 q^2 + \Omega^2} \hat{P}^L + (\omega_n^2 + c_{ph}^2 q^2 + \Omega^2) \hat{P}^T \right] \mathbf{A} + \\ & i \mathbf{J}^{ext.} \left[ \hat{\mathbf{1}} - \frac{c_V^2 q^2}{c_V^2 q^2 + \Omega^2} \hat{P}^L \right] \mathbf{A}^\dagger + \frac{1}{2g} \frac{J_\tau^{ext. \dagger} J_\tau^{ext.}}{q^2 + \frac{\Omega^2}{c_V^2}}. \end{aligned} \quad (2.66)$$

The external currents  $J_\mu^{ext.}$  are separated from the internal ones (disorder currents) as they do not have their own dynamics and are rather controlled from the outside (by experimentalists). From the way these currents couple to the gauge fields we can interpret the external source fields physically as infinitesimal test charges or currents associated with the experiment. The last term corresponds to the interactions between the static vortices which are now short-ranged. The interest is in the dynamics of the gauge fields itself. As before, we find a transversal photon  $A_T$  characterized by a spin-wave (second sound) propagator which has acquired a Higgs mass. In addition, we find an extra longitudinal photon (the first term) which is now physical. This is also characterized by the same Higgs mass but it is propagating at the condensate velocity, showing that it represents the phase rigidity of the dual superconducting matter sector.

The propagators for the gauge fields are easily determined from the inverse of the full action Eq. (2.64). The superfluid current propagator is decomposed into longitudinal and transversal parts  $\xi^{L,T}$  (parallel and perpendicular to the momentum  $\mathbf{q}$  respectively) and the propagators are found to be

$$\langle\langle \xi_L | \xi_L \rangle\rangle = \frac{1}{g} \frac{\omega_n^2}{\omega_n^2 + c_{ph}^2 q^2 + \Omega^2}, \quad (2.67)$$

$$\langle\langle \xi_T | \xi_T \rangle\rangle = \frac{1}{g} \frac{\omega_n^2 + c_V^2 q^2}{\omega_n^2 + c_V^2 q^2 + \Omega^2}. \quad (2.68)$$

Using now the Zaanen-Mukhin relation 2.55 and the momentum propagators Eq. (2.67 - 2.68), we obtain the result for the non-relativistic propagator for the superfluid velocity in the disordered phase,

$$\langle\langle v_i | v_j \rangle\rangle = g \left[ \frac{c_{ph}^2 q^2 + \Omega^2}{\omega_n^2 + c_{ph}^2 q^2 + \Omega^2} P_{ij}^L + \frac{\Omega^2}{\omega_n^2 + c_V^2 q^2 + \Omega^2} P_{ij}^T \right]. \quad (2.69)$$

The spectral response from this propagator is plotted on Fig. 2.2b.

The longitudinal (first) term represents, as before (Eq. (2.62)), the correlations associated with the smooth part of the phase field : this is literally second sound (or the XY spin-wave) acquiring a mass associated with the disappearance of the superfluid rigidity at large lengths and times. We notice that in the static limit ( $\omega_n \rightarrow 0$ ) the longitudinal part becomes a constant, signaling that even at the shortest distances superfluid correlations have disappeared. This makes sense: when vortices populate the whole system, then any long-living correlation is destroyed even between two neighboring sites when one waits long enough.

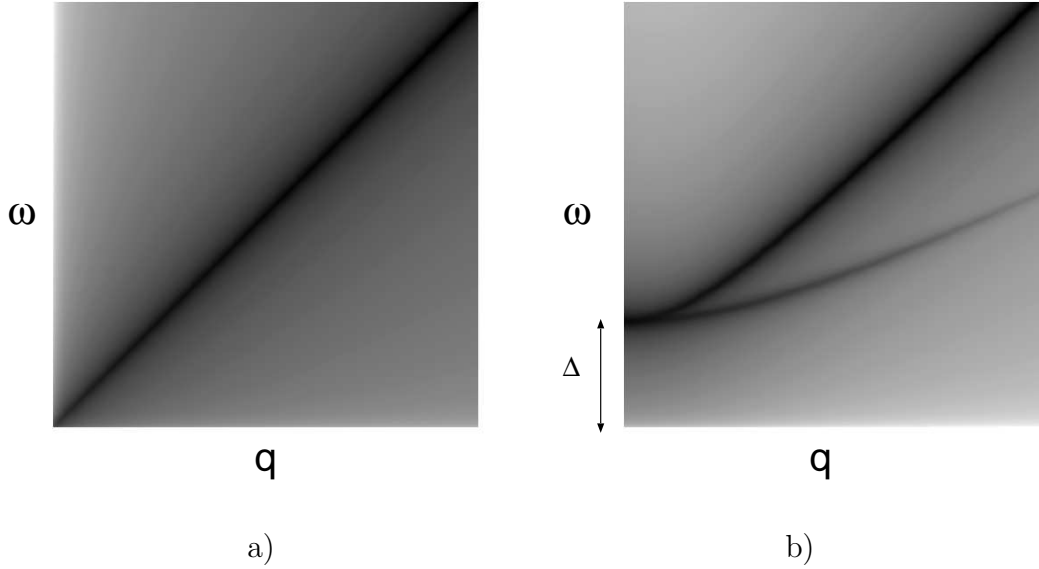


Figure 2.2: Spectral functions associated with the superfluid velocity-propagator, computed on the Gaussian level using the dual theory . These results should be accurate deep inside the ordered and disordered phase. (a) The ordered (superfluid) phase: the second sound pole of Fig. 2.1c is recovered as it should. (b) The disordered (Mott insulating) phase: we used here a condensate velocity ( $c_V$ ) which is half the phase velocity  $c_{ph}$  for the mere purpose to make visible the different behaviors of the strength of the second sound (higher branch) and dual (vortex) condensate (lower branch) poles. In reality these velocities are the same and the modes are degenerate. For  $q \rightarrow 0$  the pole strengths of the two modes are the same, while they are governed by the same Higgs mass, and they can be combined in the  $\pm 1$  helicity modes as expected from the strong coupling expansion in the Hamiltonian formalism (Fig. 2.1d). However, for increasing momentum the condensate pole gradually loses strength while the second sound pole becomes more and more like the 'orderly' result of (a), reflecting that at distances short compared to the dual London penetration depth the medium 'rediscovers' the order.

The second, transversal term is the interesting one: we indeed find a second mode and although it has the same mass as the gapped second sound it propagates with the condensate velocity. It is of course the longitudinal photon reflecting the dynamics of the dual superconducting vortex matter. In order for the superfluid velocity correlator to acquire a non-zero transversal component it is actually a requirement that the phase field becomes non-integrable. This becomes clear by inspecting the transversal part of the supercurrent Eq. (2.68),

$$\begin{aligned}
 \xi_T &= -ie_i^T \xi^i = -e_i^T \frac{\partial_i(\phi_{sm} + \phi_{MV})}{g} \\
 &= -\frac{1}{g} e_i^T (iqe_i^L \phi_{sm} + \partial_i \phi_{MV}) = -\frac{1}{g} e_i^T \partial_i \phi_{MV},
 \end{aligned} \tag{2.70}$$

where the smooth part has disappeared since it makes no sense to have derivatives in the

transversal direction for the case of smooth fields.

Let us analyse the result Eq. (2.69) in more detail. The velocity  $c_V$  has done its job in establishing that the transversal poles of Eq. (2.69) are indeed due to the superconducting vortex matter. Now we can analyse the special case of the *relativistic* zero-temperature XY model where the vortex condensate velocity is the same as the spin-wave velocity  $c_V = c_{ph} \equiv c$ . In this setup, the longitudinal and transversal modes become degenerate as they should because of the degeneracy associated with the  $n = \pm 1$  excitons, trivially seen in the Hamiltonian formalism. A different issue is the pole strength of the second sound ( $I_L$ ) and condensate poles ( $I_T$ ) as measured by the velocity-velocity correlator, characterized by the ratio,

$$\frac{I_L}{I_T} = 1 + \frac{c^2 q^2}{\Omega^2} \quad (2.71)$$

Giving this a minute of thought this makes a perfect sense. First, at  $q = 0$  both modes at real frequency  $\omega = \Omega$  have the same weight. It follows from the Hamiltonian formalism that at wavelengths large compared to the London length the excitons correspond with the helicity  $\pm 1$  eigenstates of the angular momentum of the  $O(2)$  quantum rotors. The supercurrents have the status of canonical momenta and should therefore be combined in currents with definite helicity  $\xi_{\pm 1} \sim \xi_L \pm i\xi_T$ . The implication is obvious: at  $q \rightarrow 0$  the longitudinal and transversal poles of the velocity propagator should have the same strength because all what exists in this limit is the helicity eigenstates.

What is changing at smaller distances? The characteristic momentum scale is of course the inverse dual London penetration depth  $q_L \simeq 1/\lambda_L = \Omega/c$  and from Eq. (2.71) it follows that at larger momenta the strength of the dual condensate pole decreases quadratically in momentum relative to that of the second sound pole. Within the confines of this Gaussian treatment this makes again sense. At these short times and distances one enters a regime where one is probing mainly the phase ordered matter forming the background in which the vortices move. This matter is the same stuff as the fully phase ordered matter and accordingly it should carry the same Goldstone excitation. Eq. (2.69) tells how to interpolate between the disorder physics at  $q \rightarrow 0$  with its number eigenstates and the phase ordered regime at large momenta: the dual condensate pole loses its weight gradually, in fact in the same way as the Higgs mass loses its influence on the dispersion.

How to interpret the results Eq. (2.67 - 2.68) in terms of the dual EM fields? From the definition of the conjugate momenta in terms of the dual gauge fields Eq. (2.12) it follows that these momenta represent strengths of 2+1D EM fields: the spatial indices correspond to electric field components ( $E_i = \epsilon_{\tau ij} \xi_j$ ) and the temporal component is simply a (scalar) magnetic field ( $B = \xi_\tau$ ). Therefore, the propagators may also be interpreted as field permeabilities of the medium. The presence of gaps means that both electric and magnetic fields are screened and that the medium is in the Meissner phase. The implications of the vortex dynamics (ballistic objects with characteristic propagation velocity  $c_V$ ) also has an EM corresponding phenomenon: a discrepancy in the London and the electric screening lengths. This result was first obtained by Anderson through a RPA diagrammatic expansion [87] added on a top of the classical, non-relativistic ( $c_V \rightarrow \infty$ ) BCS condensate

[17]. Without the RPA corrections taken into account, the (classical) condensate could not screen the electric field, apart from the inherited Fermi liquid screening [72, 73, 88]. With the proper velocity taken in the Higgs term, the RPA diagrammatic contributions are in Gaussian order, reproduced and the appropriate screening length related to the superconducting gap is recovered.

Another physical quantity measurable by means of dual operators, is the longitudinal conductivity that can be extracted from the Kubo formula [51]. The Higgs phase of the dual XY model Eq. (2.42) has a conductivity equal to

$$\sigma_L = \omega_n \frac{\omega_n^2 + c_V^2 q^2 + \Omega^2}{\omega_n^2 + c_V^2 q^2}. \quad (2.72)$$

In the case of the ordered phase ( $\Omega \rightarrow 0$ ), the conductivity is the one associated with the vacuum of the Maxwell electromagnetism:  $\sigma_L = \omega_n \rightarrow i\omega$ . The disordered phase is, on the other hand, an ideal conductor as the conductivity Eq. (2.72) diverges in the appropriate limit ( $q \rightarrow 0$ , then  $\omega_n \rightarrow 0$ ) [51].

Let us finally consider what would happen if one decides to use some other gauge fix, different from the unitary one. The complex field phase  $\phi_V$  is now a real degree of freedom, and in order to get the gauge field propagator that has to be used in the Zaanen-Mukhin relation Eq. (2.55), we have to remove that degree of freedom by Gaussian integration. What is recovered is a superior version of the unitary Higgs term Eq. (2.63) which is valid with any arbitrary gauge fix choice. The two versions differ by the gauge variant part

$$\mathcal{L}_{Higgs,gauge.inv.} = \mathcal{L}_{Higgs} - \frac{1}{2} |\Psi_0|^2 \frac{\left| \frac{1}{c_V^2} \partial_\tau A_\tau + \partial_i A_i \right|^2}{\omega_n^2 + c_V^2 q^2} = \frac{1}{2} |\Psi_0|^2 A_\mu \left[ \delta_{\mu\nu} - \frac{p_\mu p_\nu}{p^2} \right] A_\nu. \quad (2.73)$$

The velocity used in the last version of Higgs term is the vortex velocity  $c_V$  (also note  $p^2 = \omega_n^2 + c_V^2 q^2$ ). This form of the Higgs term is sometimes found in textbooks under the name of the “gauge invariant Higgs term”. Inspection of the numerator of the gauge variant part shows that the Higgs term Eq. (2.63) is valid not only under the unitary gauge fix, but also if the Lorentz gauge fix with the vortex velocity  $c_V$  is chosen

$$0 = \frac{1}{c_V^2} \partial_\tau A_\tau + \partial_i A_i. \quad (2.74)$$

Later, when working with the Higgs phase of the dual elastic theory, we’ll utilize a gauge fix of that kind; the calculation is simplified and the physical outcomes may be traced back to interpretations obtained in this simple Maxwell theory.

## 2.4 Dual view on the critical regime

We are not done yet. We have implicitly assumed up to this point that the fields are non-interacting. Modulo perturbative corrections this would have been fine in dimensions above the upper critical dimension but the Abelian-Higgs model in 2+1D is below its upper

critical dimension  $d_{uc} = 3 + 1D$ . One has now to be cautious with considerations like the one in the previous section. Upon exceeding the scale  $\Omega$  one does not re-enter the ordered phase but instead one enters the quantum critical regime which has no longer to do with order or disorder but has acquired an identity of its own due to the strongly interacting nature of the critical point. Away from the critical coupling, the order (second sound) and dual order (longitudinal and transversal photons) excitations discussed so far still make sense because they will appear as bound states pulled out from the low energy side of the continuum of critical modes, with a pole-strength and binding energy diminishing upon approaching the critical coupling. The missing link at this point is the appearance of the continua of critical modes as picked up by the velocity propagator. After some preliminaries we will derive their form resting on the large body of knowledge on the 3D XY critical state. These critical continua turn out to behave in a quite surprising way, with the second sound and condensate contributions showing a completely different behavior away from  $q = 0$  (see Fig. 2.3a,b). We will subsequently focus in on the detailed way the quasiparticle poles (second sound, the excitons) develop as function of the distance from the critical point, making the case that the critical continua have to be as they appear in order to be consistent with the quasiparticle poles.

In order to describe the system close to and right at criticality, we introduce renormalized parameters and critical exponents. The role of reduced temperature is taken by the quantity  $\epsilon = \frac{g-g_c}{g_c}$ , which is the reduced coupling constant. If  $\epsilon < 0$  or  $\epsilon > 0$ , we approach the quantum critical point at  $g_c$  from the ordered and disordered side, respectively. Depending on whether we approach the critical point from the order or disorder side, the system will scale either to the stable fixed points associated with phase order and non-interacting second sound ( $g = 0$ ) or with non-interacting rotors ( $g = \infty$ ). The reduced coupling constant  $\epsilon$  is therefore a relevant operator with scaling dimension  $y_\epsilon > 0$ . Another relevant field, which plays the role of the magnetic field in the standard scaling analysis, is the external source field  $\mathcal{J}_\mu$ . Since it is relevant at the transition, its scaling dimension is also positive  $y_{\mathcal{J}} > 0$ .

The model we consider is relativistic, with dynamical critical exponent  $z = 1$ , and its critical behaviour will coincide with that of the 3D XY-model. We use the state of the art for the exponents, based on analytic methods (high-temperature expansion [89], vortex-loop scaling [90], one-loop renormalization group [91]) as well as numerical results from Monte Carlo simulations [63, 92, 93]. The critical exponent  $\eta$  for the order parameter propagator  $\langle e^{i\phi_j} e^{-i\phi_i} \rangle$  has been studied in great detail [61, 94, 95, 63, 68, 96]. However, our interest is in the velocity correlation function Eq. (2.49) which is not straightforwardly related to the vertex correlator. Instead, we will use the knowledge of the scaling dimensions of the dual field  $\eta_A$  to derive the form of the velocity propagator in the critical regime.

Let us first analyse the model and its propagators right at the critical point  $g = g_c$ . The exponent  $\eta_A$  is usually defined as the critical exponent of the gauge fields correlation function right at the critical point  $g = g_c$ , i.e.  $\langle\langle AA \rangle\rangle \propto 1/p^{2-\eta_A}$ . To be consistent with the literature [63, 91], we have to change the gauge fix from ‘our’ Coulomb/unitary gauge fix to the Lorentz gauge fix ( $\partial_\mu A_\mu = 0$ , i.e. the vector potential is purely transversal). In this gauge fix, the gauge field can be projected onto a 3D linearly polarized basis (defined

as  $\mathbf{e}_0 = \frac{\mathbf{p}}{p}$ ,  $\mathbf{e}_{-1} = -\mathbf{e}_T$  and  $\mathbf{e}_{+1} = \mathbf{e}_{-1} \times \mathbf{e}_0$ . The component  $A_0$  is set to zero by the gauge fix, with only the space-time transversal components of the fields being physical. The spatially transversal photon (second sound) degree of freedom  $A_T$  is now represented by  $A_{-1}$ . The remaining component  $A_{+1}$  that admixes the Coulomb and the longitudinal photons plays the role of the vortex phase degree of freedom in this particular gauge fix. On the Gaussian level of the previous sections, the propagators for the gauge fields within the Lorentz gauge fix become degenerate and are given by

$$\langle\langle A_h^\dagger | A_{h'} \rangle\rangle = \rho_s \frac{\delta_{h,h'}}{\omega_n^2 + c^2 q^2 + \Omega^2}. \quad (2.75)$$

In the Coulomb phase one finds the same propagator with a vanishing gap,  $\Omega = 0$ . The indices take ‘transversal’ values  $h, h' = \pm 1$ . The coupling constant in the prefactor is expressed in terms of the superfluid stiffness  $\rho_s = 1/g$  which is a quantity which does renormalize. It follows that the residues of the quasi-particle poles (order/disorder excitations) are also renormalized which would not be the case if the prefactor would correspond to the bare coupling  $g$ . The overall prefactor in the expression for the velocity propagators corresponds to  $g_b^2 \rho_s$  in this scheme. The  $g_b^2$  is the bare critical coupling since the relation between the dual and original propagators Eq. (2.55) is an exact relation from the Legendre transformation, which is also valid in the critical regime. Accordingly, both the second sound of the ordered side and the excitons of the disordered side lose their pole strength approaching the critical point and this is governed by the renormalization of the superfluid density  $\rho_s$  which we will deduce starting from the known critical behaviour of the dual gauge field propagators.

Herbut and Tešanović [91] analysed the charged XY model which is equivalent to the dual action Eq. (2.42). From their expression for the  $\beta$ -function governing the renormalization of the electrical charge, it follows that at the fixed point

$$0 = \hat{e}_0^2 (D - 4 + \eta_A). \quad (2.76)$$

Assuming that the charge scales to a finite value  $\hat{e}_0$ , it follows that  $\eta_A = 4 - D \equiv 1$ . The same result was obtained by Hove and Sudbø [63], using Monte-Carlo to determine the exponent  $\eta_A$  from the vortex correlations at the critical point. They introduced a relation between the correlation function of the vortex tangle  $G(p)$  and the dual gauge field propagator,

$$\langle \mathbf{A}^\dagger \mathbf{A} \rangle = \frac{2\beta}{p^2} \left( 1 - \frac{2\beta\pi^2 G(p)}{p^2} \right) \quad (2.77)$$

valid for the case of the uncharged original/charged dual action. Notice that in Ref. [63]  $\mathbf{h}$  is used for the dual gauge fields and  $\mathbf{A}$  for the original gauge fields. At the critical point the vortex correlator is given by  $\lim_{p \rightarrow 0} 2\beta\pi^2 G(p) = p^2 - C_3(g)p^{2+\eta_A} + \dots$  and using Eq. (2.77) it follows that

$$p^2 \langle \mathbf{A}^\dagger \mathbf{A} \rangle = C_3(g)p^{\eta_A} + \dots \quad (2.78)$$

According to their numerical simulation, Eq. (2.78) shows a linear behaviour and Hove and Sudbø[63] conclude that  $\eta_A = 1$ .

The critical propagator of the dual gauge fields, Eq. (2.78), can be used to establish the form of the velocity propagator Eq. (2.49) in the critical regime. Comparing Eq. (2.78) with our form of the gauge field propagator Eq. (2.75), and bearing in mind the degeneracy, we conclude that each field component propagator corresponds to one half of the propagator Eq. (2.78),

$$\langle\langle A_h^\dagger A_{h'} \rangle\rangle = \frac{C_3}{2} p^{\eta_A - 2} \delta_{h,h'} + \dots \quad (2.79)$$

We can now use again the universal Zaanen-Mukhin relation Eq. (2.55) to obtain the velocity propagator

$$\langle\langle v_i | v_j \rangle\rangle \sim P_{ij}^L \left[ \frac{-\omega_n^2}{p^{2-\eta_A}} + \dots \right] + P_{ij}^T [p^{\eta_A} + \dots] \quad (2.80)$$

right at  $g = g_c$ . This is the first main result of this section. The dots represent constant terms with no imaginary parts as well as short distance corrections. At least deep in the critical regime the Wick rotation to real time is simple [1] because scale invariance implies that Euclidean propagators are power laws, turning into branch cuts in real frequency. With  $\eta_A = 1$ , right at the criticality, the spectral function has two quite different branch cuts in the longitudinal and the transversal channels

$$\text{Im}\langle\langle v_i | v_j \rangle\rangle_L \sim \theta(\omega^2 - c^2 q^2) \frac{\omega^2}{\sqrt{\omega^2 - c^2 q^2}}, \quad (2.81)$$

$$\text{Im}\langle\langle v_i | v_j \rangle\rangle_T \sim \theta(\omega^2 - c^2 q^2) \sqrt{\omega^2 - c_{ph}^2 q^2}, \quad (2.82)$$

and we sketch both pieces of the velocity correlator in Fig. 2.3a.  $\theta(x)$  is the Heaviside unit step function.

This is quite an unexpected result. At  $q = 0$  we find both spectral functions to be simply proportional to frequency, a simple behavior which of course originates in  $\eta_A = 1$ . Upon increasing momentum, the ‘sound’ and ‘condensate’ spectral functions start to behave very differently near the threshold  $\omega = cq$  although at large  $\omega$  they merge together again. The sound part shows the usual [1] divergence  $\omega^2/(\omega - cq)^{2-\eta_A} \sim \omega^2/(\omega - cq)$  while the condensate piece behaves like  $(\omega^2 - c^2 q^2)^{\eta_A/2} = \sqrt{\omega^2 - c^2 q^2}$ . The degeneracy of the two contributions at  $q = 0$  rings a bell: at infinite wavelength it should be that the critical fluctuations are eigenstates of rotor angular momentum, ‘equalizing’ the condensate and sound contributions as we found for the propagating excitations. To better understand why these contributions should become different at finite momenta, we should first analyze in more detail what happens with the quasiparticle poles close to the critical point.

To analyse the behavior of the quasiparticle poles in the ordered- and disordered phase close to the critical coupling, we need hyperscaling. Although one has to be careful [97, 98], recent numerical simulations [93] show that there is none or a very small violation of

hyperscaling for 3D XY. Let us first repeat the standard hyperscaling arguments applied to the velocity-velocity propagators. We denote the propagators of the gauge field in real space as  $G_A(x, \epsilon)$ . They are generated by the term  $\mathcal{J}_h A_h$  in the action and this external source term of the gauge fields  $\mathcal{J}_h$  plays a role similar to a magnetic field. It is a relevant field with scaling dimension  $y_{\mathcal{J}}$ . Hyperscaling requires that such fields act on a block of  $b^{d+1}$  points in space-time, treated as a single variable. After a scale transformation, the new propagator is related to the original one by

$$G_A\left(\frac{r}{b}, \mathcal{J}'\right) = \frac{\partial^2}{(\partial \mathcal{J}')^2} \ln Z[\mathcal{J}] \sim \frac{b^{2(d+1)}}{\lambda_{\mathcal{J}}^2} G(r, \mathcal{J}) \quad (2.83)$$

where  $\lambda_{\mathcal{J}} = e^{y_{\mathcal{J}}}$  is the scaling factor of the external source field for the gauge fields.

Repeating the scale transformation  $n$  times in the vicinity of the critical point, we obtain

$$G_A(r, \epsilon) = \frac{\lambda_{\mathcal{J}}^{2n}}{b^{2n(d+1)}} G(r/b^n, \lambda_{\epsilon}^n \epsilon), \quad (2.84)$$

with the scaling factor  $\lambda_{\epsilon} = e^{y_{\epsilon}}$  associated with the reduced coupling constant. Choosing  $n$  such that  $(\lambda_{\epsilon})^n b = \text{const}$ , it follows from Eq. (2.84) that the propagator behaves universally on both sides of the critical point as

$$G_A(r, \epsilon) \propto |\epsilon|^{\frac{2}{y_{\epsilon}}(d+1-y_{\mathcal{J}})} \Phi_{\pm}(r/|\epsilon|^{-\frac{1}{y_{\epsilon}}}). \quad (2.85)$$

The functions  $\Phi_{\pm}$  are universal functions associated with the ordered and disordered sides of the critical regime, and given in terms of  $G(r, \text{const})$ . The denominator in its argument is the correlation length that diverges at the critical point with exponent  $\nu$ , implying the familiar relation  $\nu = 1/y_{\epsilon}$ . The relation of the ‘magnetic field’ exponent  $y_{\mathcal{J}}$  to the scaling exponent  $\eta_A$  follows when we set  $\epsilon = 0$  in Eq. (2.84),

$$y_{\mathcal{J}} = \frac{d+3-\eta_A}{2} \rightarrow 2 \quad (2.86)$$

using the known value  $\eta_A = 1$ . Together with the relation for  $\nu$ , Eq. (2.85) can be written as

$$G_A(r, \epsilon) \propto |\epsilon|^{\nu(d-1+\eta_A)} \Phi_{\pm}(r/|\epsilon|^{-\nu}) \quad (2.87)$$

$$\rightarrow |\epsilon|^{2\nu} \Phi_{\pm}(r/|\epsilon|^{-\nu}). \quad (2.88)$$

This is just the familiar result that the behaviour of the correlation function close to the critical point is governed by the exponents  $\nu$  and  $\eta$  (with  $\eta = 1$  in the present case), and the crossover functions  $\Phi_{\pm}$ .

Let us first approach the critical point from the disordered side, i.e.  $\epsilon \rightarrow 0^+$ . This phase is characterized by the gap Eq. (2.65), which we can call (compare Ref. [1])  $\Delta_+ = \Omega$ . This gap is proportional to the inverse correlation length of the vortex tangle  $\xi = c/\Omega$ . Upon approaching the critical point, both the correlation length vanishes and the gap diverges

with characteristic exponent  $\nu$  as  $\xi \propto \epsilon^{-\nu}$  and  $\Delta_+ \propto \epsilon^{z\nu}$ , where  $z$  is the dynamical exponent which equals one in this specific (relativistic) case. The 3D XY correlation length exponent  $\nu = 0.66 - 0.67 \approx \frac{2}{3}$  according to a large body of work [89, 90, 92, 93]. Given that there are two dynamical fields in the problem ( $A_T$  and the vortex phase field phase  $\phi_V$ ) one could be tempted to think that there are two correlation lengths in the problem, but this is not the case. The problem is effectively Lorentz invariant, consistent with numerical work [63, 67, 68, 95] and an argument [94] linking it to the anomalous dimension of the gauge field  $\eta_A$  [63, 91].

The scaling dimension of the superfluid density can be deduced from Eq. (2.75). After Fourier transformation to space-time, the Gaussian propagator Eq. (2.75) behaves like

$$\langle\langle A_{h'}^\dagger | A_{h'} \rangle\rangle = \rho_s \frac{1}{x^{d-1}} \Psi_+\left(\frac{x}{\xi}\right) \quad (2.89)$$

$$= \rho_s \xi^{-(d-1)} \Phi_+\left(\frac{x}{\xi}\right) \quad (2.90)$$

$$= \rho_s \epsilon^{\nu(d-1)} \Phi_+\left(\frac{x}{\xi}\right). \quad (2.91)$$

Comparing it with the hyperscaling form for the gauge field propagator Eq. (2.85) we conclude that the superfluid density scales as

$$\rho_s \propto |\epsilon|^{\nu(2-\eta_A)} \rightarrow |\epsilon|^\nu \quad (2.92)$$

at the disordered side of the critical point.

We have now arrived at a point where we can determine the behaviour of the two quasi-particle poles upon approaching the critical point from the disordered side. Using Eq. (2.80), the fact that  $g \rightarrow g_b^2 \rho_s$  and the scaling of both  $\rho_s$  and  $\Omega$ , we conclude that the vortex-condensate pole  $\sim P^T$  has a strength proportional to  $\rho_s \Omega^2 \propto \epsilon^{2z\nu + \nu(2-\eta_A)} \rightarrow \epsilon^{3\nu}$ , vanishing upon approaching the critical point with an exponent  $3\nu \approx 2$  while its strength disappears in the critical continuum as indicated in Fig. 2.3b. Turning now to the second sound pole  $\sim P^L$ , we observe that at long wavelength ( $q \rightarrow 0$ ) its strength behaves exactly like the condensate pole. This has to be because eventually, at large enough distances, one should recover the fact that these excitons correspond to the exact rotor angular momentum eigenstates. However, for increasing momenta the term in the numerator  $\sim c^2 q^2$  takes over, and the strength of the large momentum second sound pole is scaling more slowly to zero upon approaching the critical point, governed now by the superfluid density exponent  $\nu(2 - \eta_A) \cong \frac{2}{3}$ . This is of course not different from what we found on the Gaussian level, with the second sound pole overtaking the condensate pole when the vortex condensate is ‘losing its grip’, governed by the Higgs mass  $\Omega$ .

To complete the picture, let us finally consider what happens with the second sound pole approaching the critical point from the ordered side. This is straightforward: as before, we should substitute  $g \rightarrow g_b^2 \rho_s$  in the Gaussian result Eq. (2.49) and  $\rho_s \sim |\epsilon|^\nu$  because  $\rho_s$  renormalizes in the same way on both sides of the transition [99]. In other words, the strength of the second sound pole on the ordered side coincides with its behavior at large momenta on the disordered side.

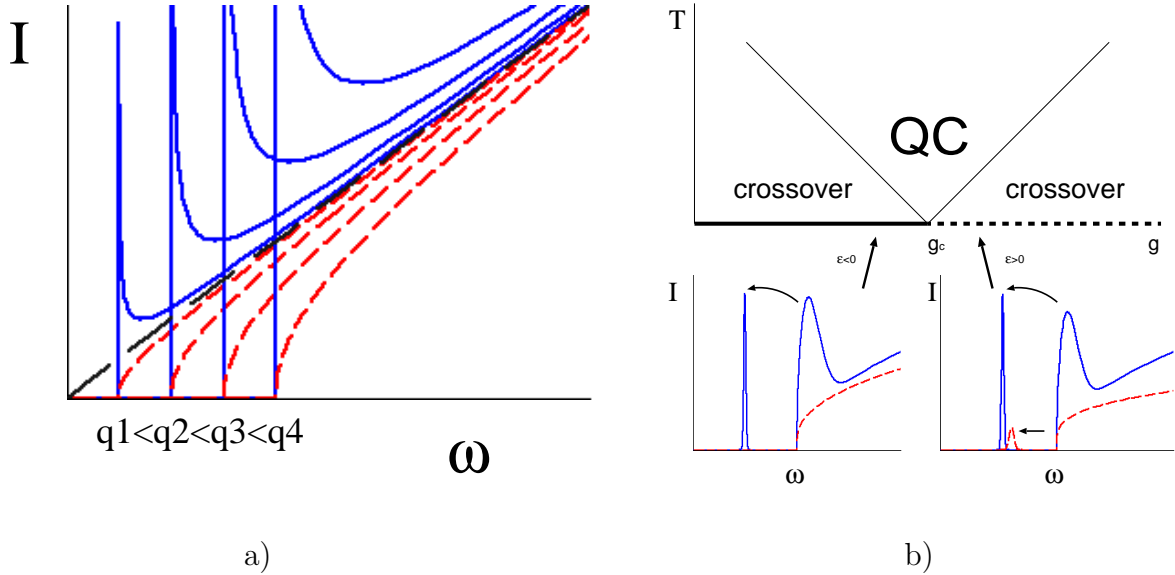


Figure 2.3: The spectral functions at and near the critical point: a) The spectral functions associated with the second sound (solid lines) and condensate (dashed lines) pieces of the velocity propagator in the critical regime for various momenta (Eq. (2.82)). At  $q = 0$  both critical continua become degenerate and linear in  $\omega$  reflecting the simple correlation function exponent  $\eta_A = 1$  associated with the dual gauge fields. However, at finite momenta it is seen that the second sound continuum diverges at threshold while the condensate piece is actually suppressed, although both continue to be governed by the same scaling dimension. At finite momenta this different behavior of the critical continua has to be present in order for them to be consistent with the momentum dependence of the pole strengths of the propagating disorder excitations appearing at the moment one moves from the critical coupling. b) Cartoon of the appearance of the second sound (solid lines) and dual condensate (dashed lines) contributions to the velocity spectral functions at finite momentum in the close vicinity of the quantum critical point, both on the ordered (left) and disordered (right) side. Although the critical continua are expected to have a very similar appearance, on the ordered side only a second sound pole is found. However, on the disordered side the system scales to dual superconducting order with the effect that one finds both a propagating second sound and condensate excitations with strengths governed by the XY correlation length exponent. However, the way their pole strengths develop as a function of momentum tracks the Gaussian result shown in Fig. 2b and it turns out that the momentum dependence of the critical continua is just of the right kind to be consistent with the behavior of the disorder poles.

Not surprisingly, we have found that the ‘order poles’ behave quite like the results we found on the Gaussian level in the previous sections except that renormalized mass scales and quasiparticle residues have to be used, all governed by the same correlation exponent  $\nu$  because  $\eta_A$  ‘magically’ drops out. We can now use this knowledge to comprehend why the critical continua of Fig. 2.3a behave the way they do. We already argued that at energies

far away from the threshold  $\omega = cq$  the second sound and vortex condensate pieces picked up by the velocity correlator merge in the same linear  $I \sim \omega$  behavior. At finite  $q$  the differences between the two are large near the threshold. With the knowledge regarding the behavior of the quasiparticle poles at hand, this now makes sense.  $\rho_s$  being a relevant operator, its influence at high energies is small while growing when times get longer. A bit away from the critical point, it takes over at a length  $\sim \xi$  where the system gets under control of the stable fixed points at zero or infinite coupling, which are also in charge of protecting the quasiparticle poles. Surely, the quasiparticles close the critical point can be viewed as bound states pulled out of the critical continuum due to the effect of the relevant operators (Fig. 2.3b). However, because of the way the latter scale, the quasiparticles are formed from the *low energy end* of the critical continuum. What does this mean for our velocity propagator, ‘watching’ the true critical excitations through the ‘duality filter’? We derived some clear rules for how the weights should be distributed over the quasiparticles: the condensate and sound poles of the disordered state should have equal weight at  $q = 0$ , but the former should lose its weight rapidly for increasing momentum. Inspecting now the low energy end of the critical continua for various momenta we see this rule also at work (Fig. 2.3a)! We notice that this ‘weight-matching’ of the critical continua and the quasiparticle poles is to an extent even quantitative. For this purpose we inspect the pole strength ratio Eq. (2.71) close to the critical point. For fixed  $q$ , due to the gap in the denominator, we learned already that the ratio diverges like  $\sim q^2/\epsilon^{2\nu}$ . However, the prefactor of the second sound pole strength is proportional to  $q^2$ . Comparing it with the ratio of the spectral responses right at the critical point and near threshold ( $\omega \approx cq$ )

$$\left(\frac{I_L}{I_T}\right)_{g_c} = \frac{\omega^2}{\omega^2 - c^2q^2} \xrightarrow{\omega \approx cq} q^2 \times \text{“divergent part”}. \quad (2.93)$$

We find a perfect match – the strengths of the spin-wave and the condensate excitations are proportional to the strengths of their respective critical continua where they have their ‘origin’.

Surely, this does not explain everything, and to a degree Eq. (2.82) is a result which stands on its own. However, given the simple integer  $\eta_A$  exponent, it appears to us to be a unique analytical form which obeys the general requirements of scale invariance and Wick rotation, having at the same time the right form to be consistent with the evolution of the spectral weights in the quasiparticle poles.

## 2.5 Abelian-Higgs duality in higher dimensions

It appears that the content of this chapter up to this point has answered all relevant questions concerning the Abelian-Higgs duality in 2+1D. If we were only after the theory of high  $T_c$  superconductivity as realized in quasi-2D cuprate planes, the previously given formalism would suffice. There are, however, many other applications that require a different spatial dimension. Let us just name few: our embedding space is three-dimensional and one would like to know the theory dual to XY model in three or more dimensions. A direct

consequence would be a generalization of the quantum dislocation melting, as presented in this thesis, to 3+1-dimensional elastic media. Finally, one would like to address how the complete elastic theory in higher dimensions could relate to the models of emergent gravity.

Unfortunately, until the present day, only some futile attempts to construct the Abelian-Higgs duality in 3+1D or more dimensions have been undertaken. The shortcoming of the Abelian-Higgs duality as presented before, is that it works as a completely closed formalism only in 2+1D (or classical 3D). At first, the geometrical properties of the theory and constraints do not allow mapping to the standard Maxwell theory. Although this problem seems not to be of great importance, the main obstacle comes from the geometrical structure of the defects and our subsequent inability to construct the second-quantized action equivalent to the GLW action Eq. (2.35). This section will therefore only present the current state of matter hoping that in the near future a breakthrough can be achieved.

The vortices of the XY model Eq. (2.2) are point-like defects only in two spatial dimensions. As the dimensionality increases, the dimensionality of the vortex manifold increases accordingly. In three spatial dimension vortices become lines, in four they are sheets and in general, in  $d$ -dimensional medium, vortex excitations, i.e. set of singular points of the phase  $\phi$  correspond to  $d - 2$ -branes. This result is implied by the beautiful theorem due to Hopf stating that all but one homotopy groups of  $U(1)$  are trivial [100]

$$\pi_m [U(1)] = \begin{cases} \mathbb{Z}, & m = 1 \\ \mathbf{1}, & m \neq 1 \end{cases} . \quad (2.94)$$

Each homotopy group has a physical interpretation:  $\pi_0$  counts how many disconnected subspaces exist in the configuration space and for the  $U(1)$  group the trivial homotopy group means that all the configurations for the phase are smoothly connected. Nontrivial  $\pi_0$  would mean that different regions of the system could end in different disconnected vacua with domain walls (of dimensionality  $d - 1$ ) between them acting as the topological operators.

For us, the homotopy group  $\pi_1$  is of importance as the only nontrivial homotopy group of  $U(1)$ . What Eq. (2.94) means is that one can make loops inside the XY parameter space by winding the phase by an arbitrary integer number. That is, if one puts a phase field on a closed loop (i.e.  $\bar{x}_\mu(s)$  with  $\bar{x}_\mu(0) = \bar{x}_\mu(L)$ ), after one circulation around the loop, a multiple of  $2\pi$  is collected by the phase (i.e.  $\phi(\bar{x}_\mu(L)) = \phi(\bar{x}_\mu(0)) + 2\pi m$  although we describe the same point in space). Given that any value of the phase from 0 to  $2\pi$  can be taken as a vacuum of the XY model, it follows that a path can exist in a system around which a nontrivial circulation of the phase is recorded. Such paths cannot be smoothly removed from the system because they encircle a singularity in the phase field. We already know that the singularity of the XY model is represented by a vortex, but from Eq. (2.94) it follows that a vortex is a manifold of dimension  $d - 2$ , just as mentioned before.

Higher homotopy groups  $\pi_{m \geq 2}$  work in the same way except that a nontrivial configuration on a closed  $m$ -sphere is considered. If any other homotopy group  $\pi_m$  had been nontrivial, it would imply the existence of topological defects (sets of singular points) that are  $d - m - 1$ -dimensional manifolds.

Forgetting the geometrical structure of the vortices for a moment, let us try to generalize the Abelian-Higgs dualization to a 3+1D XY model first. The part which precedes introduction of the dual gauge fields Eq. (2.12) is identical to the 2+1D duality: conjugate momenta are given by  $\xi_\mu \sim \partial_\mu \phi/g$  and the original and ordered propagators are connected by the Zaanen-Mukhin relation Eq. (2.55). The difference arises when the supercurrent conservation law Eq. (2.10) is invoked in order to define dual gauge fields. The four-dimensional curl can be constructed by means of an antisymmetric tensor contracted with an antisymmetric rank-2 dual gauge field

$$\xi_\mu = \epsilon_{\mu\nu\rho\lambda} \partial_\nu A_{\rho\lambda}. \quad (2.95)$$

The gauge transformations leaving the physical fields unchanged are defined by a four-component gradient function  $g_\mu$ :

$$A_{\mu\nu} \rightarrow A'_{\mu\nu} = A_{\mu\nu} + \partial_\mu g_\nu - \partial_\nu g_\mu. \quad (2.96)$$

One should notice that there is a redundancy in the space of gradient functions. Two transformations  $g_\mu$  and  $g'_\mu$  differing only by a smooth function gradient  $g'_\mu = g_\mu + \partial_\mu \Lambda$  produce the same gauge transformation Eq. (2.96).

In the current duality mapping, we can go one step further and consider coupling of the conjugated momenta to singular configurations of the phase. In analogy with Eq. (2.14), we find a minimal coupling of antisymmetric gauge fields Eq. (2.95) to defect currents:

$$i\xi_\mu \partial_\mu \phi_{MV} \rightarrow iA_{\mu\nu} \epsilon_{\mu\nu\rho\lambda} \partial_\rho \partial_\lambda \phi_{MV} = iA_{\mu\nu} J_{\mu\nu}. \quad (2.97)$$

The two antisymmetric indices in the current  $J_{\mu\nu}$  reflect that that the defect world-sheet has two tangent directions. If one of the indices is temporal (say the first one), then the component  $J_{\tau i}$  corresponds to static density of vortex lines extending in the  $i$  direction. When both indices are spatial, the component  $J_{ij}$  is simply the current (charge times the velocity) in the  $i$  direction of the vortex lines stretching in the  $j$  direction minus the current in the  $j$  direction of the  $i$ -direction stretching vortex lines (due to antisymmetry in indices). Current components with both indices identical do not exist since sliding of a vortex along its line has no physical consequences and cannot be observed.

For a single (closed) vortex world-sheet defined by  $\bar{x}_\lambda(s, t)$ , the currents are defined in the same manner as for point-like vortices Eq. (2.37). This time, the antisymmetric sheet-delta function is introduced

$$\delta_{\mu\nu}(x_\lambda) = \oint ds dt (\partial_s \bar{x}_\mu \partial_t \bar{x}_\nu - \partial_s \bar{x}_\nu \partial_t \bar{x}_\mu) \delta[x_\lambda - \bar{x}_\lambda(s, t)] \quad (2.98)$$

leading to the definition of the current

$$J_{\mu\nu}(x_\lambda) = 2\pi N \delta_{\mu\nu}(x_\lambda), \quad (2.99)$$

where  $N$  is the winding number of the vortex line.

Vortex currents are conserved in the following sense

$$0 = \partial_\mu J_{\mu\nu} \quad (2.100)$$

which trivially follows from the identity on the sheet delta function

$$0 = \partial_\mu \delta_{\mu\nu}(x_\lambda). \quad (2.101)$$

This one is checked in analogy with Eq. (2.39) using the properties of total derivative (the vortex world-sheet has no edges!).

The minimal coupling of a single vortex world-sheet to the gauge fields is accordingly

$$S_{AJ} = \oint A_{\mu\nu}(\bar{x}_\lambda) d\bar{x}_\mu d\bar{x}_\nu. \quad (2.102)$$

At this point we are stuck. In contrast with the minimal coupling of point-particles Eq. (2.40), the minimal coupling Eq. (2.102) has no corresponding GLW-like action, translating into a covariant derivative of an order parameter field. Such an effective action does not exist yet for strings and although some works on phase transitions of strings (crumpling) have been presented in the past, these relate to a structural transition of strings rather than to the transition between a vacuum with no strings at all and a dense packed tangle of strings.

One of the problems associated with the formulation of the second-quantized string action (analogous to GLW) is related to the ‘natural’ (Lorentz-invariant) way of defining the action in terms of the surface of a world-sheet (a moving string draws a sheet behind). This is precisely the Nambu-Goto action for strings but when one wants to average over the all possible disorder configurations, singularities that cannot be removed are brought in the action. Namely, while ‘spiky’ trajectories of particles were possible but exponentially suppressed by the loop-length action Eq. (2.19), there are many ‘spiky’ surfaces extending to infinity with finite surface measure. A trivial example is a funnel (generalized Gabriel’s horn) defined by

$$z^\alpha = x^2 + y^2 \quad (2.103)$$

where  $-2 < \alpha < 0$ .

Since we cannot give a valid description of the 3+1D ‘Higgs’ phase of the XY model Eq. (2.1), let us at least tackle the problem from the ordered side. In analogy with the Coulomb gauge fix employed for the ordered phase of 2+1D XY model, we separate the temporal component from the other gauge field components. The components to be integrated out are  $A_{\tau\pm}$ , while the longitudinal static current  $A_{\tau L}$  has no propagator and it falls prey to one of the gauge fixing conditions. The resulting ‘Coulomb’ action is

$$\mathcal{L}_{EM} = \frac{1}{g} \frac{J_{\tau+}^\dagger J_{\tau+} + J_{\tau-}^\dagger J_{\tau-}}{q^2} + g(\omega_n^2 + c_{ph}^2 q^2) A_{+-}^\dagger A_{+-} + i2J_{+-} A_{+-}^\dagger. \quad (2.104)$$

All of the longitudinal components  $A_{L\mu}$  have been fixed by a generalized Coulomb gauge fix

$$0 = \partial_i A_{i\mu} = -q A_{L\mu}. \quad (2.105)$$

The static interaction between segments of vortex loops is governed by the Coulomb law (the first term of Eq. (2.104)). One should note, however, that charges can exist only as strings, not as point particles, and also that the sign of the ‘Coulomb’ force depends on the relative orientation of the strings. The force law in the three-dimensional case is reminiscent of the Ampere law for closed current loops. The remaining gauge field component  $A_{+-}$  works as the ‘transversal photon’ and carries the physical Goldstone mode – XY magnon which is the unique excitation of the XY model.

The generalizations of the Abelian-Higgs duality can be continued in this manner to an arbitrary dimensional XY model. The difference is that both the gauge fields and defect densities acquire an extra index per increased dimension. Defects, being  $d-2$ -branes, have their densities given in terms of antisymmetric brane (manifold) delta function

$$\delta_{\mu_1 \dots \mu_{d-1}}(x_\nu, \Sigma) = \oint_{\Sigma} ds_1 \dots ds_{d-1} \epsilon_{i_1 \dots i_{d-2}} \partial_{s_{i_1}} \bar{x}_{\mu_1} \dots \partial_{s_{i_{d-2}}} \bar{x}_{\mu_{d-2}} \delta[x_\nu - \bar{x}_\nu(\{s\})]. \quad (2.106)$$

In the XY ordered (Coulomb) phase, the Coulomb gauge fix yields the physical correspondence of gauge degrees of freedom and physical observables. All fields components with a temporal index will be non-dynamical and result in the Coulomb force law between defect branes. There is always precisely one dynamical degree of freedom, namely the gauge field component with all the transversal indices. It is massless, propagates with velocity  $c_{ph}$  and obviously represents the XY magnon in this, dual formulation of the model.

# Chapter 3

## Elasticity and its topological defects

The basics of the theory of elasticity are easy to understand thanks to our everyday encounter with solids. The roots go back to Hook, who was the first to realize a simple mathematical law relating a force acting on a spring and its deformation. With later additions, the whole field developed into what seems to be the first emergent physics theory – the theory describing elastic properties of a solid is universal and independent of microscopic details. The only allowed microscopic detail that may enter the elasticity theory is the point group of the lattice symmetries. Its effects are represented by an elastic response which is dependent on the relative orientation between crystal facets and the applied force or stress. Even this detail is vanishing in a solid like a piece of steel where the “self-averaging” yields a perfectly isotropic elastic energy.

When the forces exerted on a solid become sufficiently large, the crystalline constituents may stray away from their equilibrium positions and the resulting deformations are said to be plastic. When this happens, the simple ‘Hooke’ laws become invalid. The plastic deformations of solids are closely related to the elastic topological defects, but this was not realized until the 1930s. At that time, the existing models of plastic deformation in solids (based on “sliding planes”) predicted stress values needed for plastic deformation that were some four orders of magnitude higher than the experimentally observed ones [48]. Roughly simultaneously, Orowan [101, 102], Polanyi [103] and Taylor [104] realized that plastic deformations occur due to development of dislocation defects, analysed at the beginning of the century by Volterra. A complete new field in material science developed, largely driven by importance of the defects in metallurgy. For instance, cold working as known for millennia is the process where dislocation defects are ‘inserted’ in the solid in order to improve its stiffness, but the theory behind it is relatively new.

From the theoretical point of view, it has long been recognized that the energy-entropy balance of the topological defects was responsible (via deconfinement) for the melting processes [70, 105, 106, 107, 108, 109, 110, 111, 112, 113]. Topological defects often display sharp dynamical imprints and when present in low concentrations as in standard solids, they play an important factor in determining the plastic properties of the medium. In glasses, an extensive configurational entropy of these defects [114] (from which ensuing restrictive slow dynamics might follow [115, 116, 117, 118]) may be sparked. In recent

years, attempts were made to lift defect dynamics from the classical realms to the quantum theory [44] aiming at a description of quantum (electronic) liquid crystals [37] and other phases [37, 44]. The electronic constituents favor, in a certain parameter regime, the formation of a crystal-like stripe pattern which may then be perturbed, through a cascade of transitions, to produce a rich variety of phases. Such stripe patterns are observed in the high-temperature superconductors and other oxides [35, 36] and in quantum Hall systems [119]. Defects naturally alter the local electronic density of states allowing for spatial (and temporal) inhomogeneities of electronic properties [120, 121, 122]. Following the general notion that melting occurs by the condensation of topological defects (e.g. [70]), we may naturally anticipate that the study of topological defects is pertinent to the understanding of quantum phase transitions between various zero-temperature states.

There is yet another, ‘modern’, view of the elastic theory, which reformulates the theory in terms of differential geometry [123, 124, 125]. This conception will become convenient in this section for certain proofs, but its true power lies in the connection of the elasticity theory to gravity (at least in 2+1D), as has been shown in some recent works [84, 85]. It has only recently been recognized that the presence of defects in a crystal and the subsequent quantum ‘melting’ can lead to an unconventional superconductor state that will be presented in chapter 5 as one of the central results of this thesis [44].

We shall interpret the theory of elasticity as a literal quantum theory formulated in a Euclidian path integral formalism. The first section of this chapter deals with the elastic potential, shared by both classical and the more interesting quantum crystals. Our primary interest lies in elasticity in two spatial dimensions. However, to get a more general view, we present the basic linear and second order gradient elasticity in a form applicable to an arbitrary  $d$ -dimensional elastic medium. In the second section the complete theory of elasticity is given via its path integral formulation. Green’s functions (phonon propagators) are introduced and we evaluate them in the ‘smooth-only field’ approximation and leave the dual description for later chapters. In the next section we are interested in elastic defects, where we will pay special attention to dislocation and disclination defects. The Weingarten theorem that leads to definitions of the defect densities and the conservation laws for these densities, is shown in its dimension independent form (the original proof was devised only for the 3D elastic medium). In the final section we take care of an important dynamical constraint on the dislocation dynamics, the “glide constraint”. This constraint was known for some time in metallurgy, but only recently new results were presented (coauthored with Nussinov and Zaanen) where the constraint was formulated in a form applicable to field theories of elasticity [50]. This constraint can be proven in many ways and we give two natural paths for its formulation, but in the end it is naturally rooted in the conservation of the crystalline bulk material and has a special importance for the compressional properties of the solid. We give the basic, linearized version and later discuss the more general expression that may improve the field theory by allowing the inclusion of interstitial excitations.

### 3.1 The potential energy of an elastic medium

The elastic theory of solids is built on the premise that every constituent (atom, molecule, vortex, etc.) of a solid has its own equilibrium position [126]. The equilibrium configuration is determined by the global minimum in the interaction energy between the particles. This principle is violated for example when entropy of disordered configurations starts to compete with the energy of the solid (the melting process) or if the system relaxes and locks itself in a local minimum of its potential energy (like in glasses). If a relatively small force is applied to a solid, all of the constituents displace, but still do not move far away from their equilibrium positions and the mutual spatial arrangement is unaffected. This condition is necessary in order to have purely elastic forces in the system.

When a defect is subjected to a deformation, the relative positions between the constituents change, resulting in a slightly higher interaction energy. This change in energy is responsible for the elastic response of solids. Assuming that the potential is a smooth function of inter-particle distance, the effective elastic energy emerges from the microscopic theory losing all knowledge regarding the detailed nature of the constituents.

Suppose that a constituent with the equilibrium position  $\mathbf{R}_0$  finds itself in a new position  $\mathbf{R} = \mathbf{R}_0 + \mathbf{u}$  after an elastic deformation. The vector  $\mathbf{u}$  defines the (crystalline) displacement. In practice, each particle has its own displacement. However, when we work with systems where the lattice constant (or more generally the average interparticle distance) is sufficiently small, we are allowed to coarse-grain the displacements and define the displacement field on a (continuum) real space. In order to have a well-defined continuum field theory, the displacements have to be finite, so it is a necessary condition that the crystalline displacements are large as compared to the lattice constant ( $u \gg a$ ).

The total potential energy  $\mathcal{V}$  can be expanded in small displacements. Since it is a function of multiple arguments (relative positions)

$$\Delta \mathbf{R}_{ij} = \mathbf{R}_i - \mathbf{R}_j = (\mathbf{R}_i^0 + \mathbf{u}_i) - (\mathbf{R}_j^0 + \mathbf{u}_j) \equiv \mathbf{R}_{ij}^{(0)} + \mathbf{u}_{ij}, \quad (3.1)$$

the expansion will depend only on relative displacements  $\mathbf{u}_{ij} \equiv \mathbf{u}_i - \mathbf{u}_j$  and not on the displacements alone. The zeroth-order term in the expansion is just the equilibrium energy of the solid and it plays no role in the elastic theory. Terms linear in the relative displacements are strictly forbidden as their presence would imply uncompensated forces acting on the constituents and the equilibrium position would not be a minimum of the potential energy as assumed. We are interested in the second order terms, written as

$$\mathcal{V}^{(2)} = \frac{1}{2} \frac{\partial^2 \mathcal{V}}{\partial R_{ij}^a \partial R_{kl}^b} u_{ij}^a u_{kl}^b. \quad (3.2)$$

These terms will contain all the relevant contributions to the potential energy. The third and higher order terms in the expansion contain the interaction physics which becomes relevant beyond the Gaussian order, i.e. for processes such as scattering of the crystalline excitations (phonons). These processes cause the dressing of the phonon propagators leading to their finite lifetime and eventually may render the ground state of the solid unstable.

Such effects are not of interest to us since a) the stability of solids is well established and is robust up to a certain level of disorder or external stress, and b) the quantitative predictions rest on free parameters such as compression and shear rigidities, but in experiments concerning phonons we measure only their ‘dressed’ values.

Let us analyse what kind of elastic energy terms arise from the Gaussian part, Eq. (3.2). The relative displacements have to be expanded in a series

$$u_{ij}^a = u_i^a - u_j^a = R_{ij}^{(0)m} \partial_m u^a + \frac{R_{ij}^{(0)m} R_{ij}^{(0)n}}{2} \partial_m \partial_n u^a + \dots \quad (3.3)$$

As it will be explicitly demonstrated at the end of this section, the higher derivatives become relevant only when elasticity is considered at small distances, while these terms become irrelevant in the long wavelength limit. Therefore, we keep only the first-derivative term in Eq. (3.3) to recover the familiar linearized elastic energy.

Using the expansion Eq. (3.3) and the Gaussian potential energy Eq. (3.2), the following potential energy functional is obtained

$$e(\mathbf{x}) = \frac{1}{2} \frac{\partial^2 \mathcal{V}}{\partial R_{ij}^a \partial R_{kl}^b} R_{ij}^{(0)m} R_{kl}^{(0)n} \partial_m u^a \partial_n u^b \equiv \frac{1}{2} \partial_m u^a C_{mnab} \partial_n u^b. \quad (3.4)$$

Partial derivatives of the displacement field ( $\partial_n u^a$ ) are called strains. The second derivatives of the microscopic potential  $\mathcal{V}$  are collected in the tensor  $C_{mnab}$ , which is known as the elastic tensor of the solid. Therefore, regardless of the microscopic details reflected in the potential  $\mathcal{V}$ , the effective theory of elasticity has a rather universal status which qualifies it as a theory dealing with faithful emergence.

The elastic tensor  $C_{mnab}$  has in total  $d^4$  elements in a  $d$ -dimensional solid. However, due to symmetries of space-time as well as due to the symmetries implied by the lattice (point symmetry group), only a few will be independent. The universal property of the elastic energy is that (at least in the linear order) it cannot depend on a local rotation since a pure rotation does not change the relative spacings between the crystalline constituents. This property is deeply wired into the invariance of the model under global rotations and will be elegantly formulated in terms of the Ehrenfest constraint [126] when the dual stress representation of the model is obtained. Due to this requirement, the potential energy Eq. (3.4) has to be independent on the local rotation operators, expressed as antisymmetrized strain components

$$\omega_{a,b} = \frac{1}{2} (\partial_a u^b - \partial_b u^a). \quad (3.5)$$

Hence, the potential energy only depends on the symmetrized strains, which are sometimes simply called ‘strains’ in the literature

$$w_{a,b} = \frac{1}{2} (\partial_a u^b + \partial_b u^a). \quad (3.6)$$

This leads to an alternative way of writing the potential elastic energy as

$$e(\mathbf{x}) = \frac{1}{2} w_{i,j} c_{ij,kl} w_{k,l}. \quad (3.7)$$

The constants  $c_{ij,kl}$  are naturally related to the elements of the elasticity tensor  $C_{m nab}$  and the number of independent elements must be equal. To count them let us consider a  $d$  dimensional solid: there are  $M = d(d + 1)/2$  symmetrized strains; this number implies  $M(M + 1)/2 = [d(d + 1)(d^2 + d + 2)]/8$  independent coupling constants. For a two-dimensional solid there may be up to 6 independent elements, in three and four dimensions 21 and 55 independent elements are possible, respectively.

These numbers reduce further when point group symmetries of the crystals are taken into account. As a first example, let us consider a three-dimensional solid and collect all the symmetrized strains in one column  $u_a = (w_{1,1}, w_{2,2}, w_{3,3}, 2w_{1,2}, 2w_{1,3}, 2w_{2,3})$ . The elastic energy is expressed via yet another version of the elastic tensor, which is the conventional one from material science

$$e(\mathbf{x}) = \frac{1}{2} u_a c_{ab} u_b. \quad (3.8)$$

The triclinic three-dimensional lattice, being the one with the lowest possible symmetry, has all 21 tensor elements independent representing the most general elasticity tensor

$$c_{ab} = \left( \begin{array}{ccc|ccc} c_{11} & c_{12} & c_{13} & c_{14} & c_{15} & c_{16} \\ & c_{22} & c_{23} & c_{24} & c_{25} & c_{26} \\ & & c_{33} & c_{34} & c_{35} & c_{36} \\ \hline & & & c_{44} & c_{45} & c_{46} \\ & & & & c_{55} & c_{56} \\ & & & & & c_{66} \end{array} \right). \quad (3.9)$$

The monoclinic type of lattice has only one symmetry plane (crystallographic point group  $C_2$ ), but that already reduces the number of independent constant to 13. The 32 crystallographic point groups divide into 9 classes for the elastic tensor  $c_{ab}$ . The general rule is that the more symmetries the crystal lattice possesses, the fewer independent elastic constants there are. Groups innate to the cubic type of lattice ( $T$ ,  $T_h$ ,  $T_d$ ,  $O$  and  $O_h$ ) have the highest symmetry and accordingly only three independent elastic constants within the elasticity tensor

$$c_{ab} = \left( \begin{array}{ccc|ccc} c_{11} & c_{12} & c_{12} & & & \\ & c_{11} & c_{12} & & 0 & \\ & & c_{11} & & & \\ \hline & & & c_{44} & 0 & 0 \\ & 0 & & & c_{44} & 0 \\ & & & & & c_{44} \end{array} \right) \quad (3.10)$$

The constants appearing in Eq. (3.10) are familiar constants of the elasticity theory,  $c_{44} = \mu$  is the *shear modulus* and  $c_{12} = \lambda$  is the *Lamé constant*. The remaining constant can be related to the anisotropy of the material

$$\xi = \frac{c_{11} - c_{12}}{2c_{44}}. \quad (3.11)$$

If the anisotropy  $\xi$  is close to or exactly equal to 1, the material has no preferred direction with respect to its elastic properties. These kinds of elastic media will be in the center of our attention because their simple properties are representative for the essence of the quantum phase transition we consider in later chapters.

In the case of a two-dimensional solid there are at most 6 independent coefficients, which is realized for the oblique type of lattice (parallelogram unit cell). The square lattice, on the other hand, contains only three independent elastic constants and the elastic energy has the form

$$e(\mathbf{x}) = \frac{1}{2}c_{11}(w_{1,1}^2 + w_{2,2}^2) + c_{12}w_{1,1}w_{2,2} + 2c_{44}w_{1,2}^2. \quad (3.12)$$

This class of elastic tensors with only 3 independent parameters Eq. (3.10) or Eq. (3.12), is common to any  $d$ -dimensional hypercubic lattice, where the energy has a simple form

$$e(\mathbf{x}) = \frac{1}{2}c_{11} \sum_{i=1}^d w_{i,i}^2 + \frac{1}{2}c_{12} \sum_{\substack{i,j=1 \\ i \neq j}}^d w_{i,i}w_{j,j} + c_{44} \sum_{\substack{i,j=1 \\ i \neq j}}^d w_{i,j}^2. \quad (3.13)$$

The solids with the simplest elastic tensors are the isotropic ones. Generally speaking, a single crystal cannot have isotropic elastic properties with the 2D triangular lattice as the only exception which is accidental. There, the gradient expansion yields isotropic elastic energy. We met another possibility already with the anisotropy given by Eq. (3.11) set to 1, but given the fact that  $c_{11}$  and  $c_{12}$  are derived from a microscopic theory, the probability that all the microscopic couplings conspire to produce two identical elastic constants is very unlikely. Alternatively, real materials like pieces of steel are not made of a single crystal and because they are amorphous on large scales they appear as isotropic elastic entities. Since the symmetry of such a coarse-grained state is the highest and the details of the lattice point group are entirely lost, the elastic properties are defined in terms of only two constants: the compression and shear moduli. The compression modulus  $\kappa$  represents a response of a body to change of volume. It is not exclusively associated with solids since liquids and gases also respond to volume changes. The shear modulus  $\mu$  (introduced in Eq. (3.10)) is associated with the response of a solid when deformed without any change in the volume. Obviously, such stiffness is exclusive to solids and can even be used to make a sharp distinction between a solid and a liquid state of matter. Resting on rotational symmetry principles (for more details see Appendix C), the two rigidities can be associated with two irreducible representations of the rotation symmetry group. The change in the volume is an operator invariant under rotations, and so compression corresponds to the singlet (spin-0) part of the elasticity tensor. Shear, on the other hand, transforms under the spin-2 representation and the corresponding part in the elasticity tensor has spin 2. The two channels are separated by the introduction of  $d$ -dimensional projection operators onto spin-0 (rotation singlet) and spin-2 states (rotation multiplet, e.g. in  $d = 2$  the state is a doublet)

$$P_{ijab}^{(0)} = \frac{1}{d}\delta_{ia}\delta_{jb}, \quad P_{ijab}^{(2)} = \frac{1}{2}(\delta_{ij}\delta_{ab} + \delta_{ib}\delta_{ja}) - \frac{1}{d}\delta_{ia}\delta_{ab}. \quad (3.14)$$

These operators are orthonormal and span the space of all symmetric matrices. They allow us to define the elastic tensor (written in the convenient form of Eq. (3.4)) of an isotropic  $d$ -dimensional solid as

$$C_{ijab} = d\kappa P_{ijab}^{(0)} + 2\mu P_{ijab}^{(2)} \quad (3.15)$$

with the compression and shear moduli  $\kappa$  and  $\mu$  respectively.

There are alternative constants used in the theory of linear elasticity to express elastic properties of a solid [48]. When we introduced the compressibility, the Lamé constant became redundant, because the two are related by

$$\kappa = \lambda + \frac{2\mu}{d}. \quad (3.16)$$

Other constants include the Poisson ratio  $\nu$  and Young modulus  $E$ , with the former used often in combination with the shear modulus  $\mu$  to express the compression modulus

$$\kappa = \mu \frac{2}{d} \frac{1 + \nu}{1 - (d-1)\nu}. \quad (3.17)$$

We shall use a combination of these two parameters most of the time except when we wish to stress that some effect is due to compression, where we will use the compression modulus  $\kappa$  instead.

The Young modulus is defined as the inverse ratio of the relative elongation and the force required to cause this deformation

$$E = 2\mu(1 + \nu). \quad (3.18)$$

In a liquid there are no shear forces and elongation of a liquid is a process which does not cost energy and the Young modulus becomes zero.

It was already mentioned that a local rotation of a solid body or a rotation of a body as a whole does not contribute to its elastic energy. Solids, however, respond to torque deformations: if two adjacent regions are mutually rotated, there are seemingly no deformations inside any of these regions. However, on a larger scale, the distance between two constituents located in two different regions is changed and such a deformation costs a finite energy. The elastic energy associated with these kinds of deformation is clearly related to the derivatives of the local rotation operator Eq. (3.5) and we know where these terms came from: the second derivative term in the relative displacement expansion Eq. (3.3) takes care of this, as well as of other terms of the same order in the number of derivatives. When linearized elasticity is supplemented with these terms, one obtains the so called second-order gradient elasticity which describes the torque effects as well as other elastic effects related to gradients of the linear elastic deformations (strains). In an isotropic medium, only two terms are allowed by symmetry and each of these has a length associated with it. The additional terms are (the local rotation  $\omega_{a,b}$  is defined in Eq. (3.5))

$$e_2(\mathbf{x}) = \frac{1}{2} 2\mu \left[ \frac{1-(d-2)\nu}{1-(d-1)\nu} \ell'^2 \partial_i \partial_j u^j \partial_i \partial_k u^k + \ell^2 \partial_i \omega_{a,b} \partial_i \omega_{a,b} \right], \quad (3.19)$$

with a length  $\ell'$  describing the stiffness of the solid under compression gradient and a length  $\ell$  describing ‘rotational stiffness’ (the response under a gradient of local rotations = torque). The choice of prefactors will become clear when we analyse the excitation spectrum. However, already at this level it is clear that at distances larger than  $\ell'$  and  $\ell$  the contribution from Eq. (3.19) gets overwhelmed by the linear elasticity term Eq. (3.4).

Finally, we must set another condition on the elastic constants of a solid. Namely, the stability of a lattice can be compromised if any of the elastic deformations results in a negative energy. To prevent this from happening, any sub-determinant of elastic tensor Eq. (3.9) must be strictly positive. In terms of (hyper-)cubic elastic constants, this means that

$$c_{11} > 0, \quad c_{44} > 0, \quad c_{11} > c_{12}, \quad c_{11} + 2c_{12} > 0. \quad (3.20)$$

In order for the isotropic elastic medium to be stable, the shear and the compression moduli must be positive. The same is true for the Young modulus while the Lamé coefficient must obey the inequality

$$\lambda > -\frac{2}{d}\mu. \quad (3.21)$$

The Poisson ratio is dimensionless, with allowed values in the range  $-1 \leq \nu \leq \frac{1}{d-1}$ . In most solids its value is positive, as a negative value would imply an elastic medium that reduces its cross section upon pressure, going against our daily intuition. The known exceptions are the Abrikosov lattice in type-II superconductors ( $d = 2$ ) [127] and  $\alpha$ -quartz ( $d = 3$ ) [128]. Recently, phases of biopolymers that experience a negative Poisson ratio have been proposed [129].

## 3.2 Path integral formulation

The elastic theory can be easily constructed as a literal quantum field theory and this section will be devoted to this construction. The continuum field of displacements is interpreted as the order parameter field, the corresponding partition function is defined and the relevant questions such as the Green’s functions of the model are analysed. Although our ultimate aim is to implement the duality in order to deal with defects of a solid within the ‘elastic field theory’, in this section only smooth displacement fields are considered. The results obtained in this way are reminiscent of the results in Eq. (2.49) obtained for the XY model where only the Goldstone mode (magnon) is visible in the spectrum. In the same way, smooth displacements can carry only phonon excitations which are massless Goldstone modes.

Viewing elasticity as a field theory of the displacement field, the corresponding partition function is

$$Z_{el.} = \int \mathcal{D}u^a e^{-\int \mathcal{L}_{el.} dx}. \quad (3.22)$$

The Lagrangian  $\mathcal{L}_{el.}$  is that of the elastic solid and in general, it is a function of displacements as well as their first and higher derivatives (depending on the number of derivative terms considered in Eq. (3.3)). In the case of an electrically neutral solid, next to the elastic energy part Eq. (3.4), the action contains only the kinetic energy part. In a classical crystal, the kinetic energy is given simply as

$$t(\mathbf{x}) = \frac{1}{2}\rho (\partial_t \mathbf{u})^2, \quad (3.23)$$

where  $\rho$  is the mass density of the solid. The kinetic term of a quantum crystal is a more subtle issue, as it must, among other things, encapsulate the statistics of the crystalline constituents. In a crystal with constituents other than bosons, a winding of particle world-lines (extending in the imaginary time direction) may give rise to nontrivial statistics by means of imaginary contributions to the action. Suppose, for example a fermionic crystal, and consider a configuration which contains a pair of fermions exchanging their position over an imaginary time  $\tau = \hbar/k_B T$ . The action of such a configuration has, next to its real part, acquired a contribution of  $i\pi$  that will change the sign of its weight in the partition function Eq. (3.22). The simple statistical methods applicable to bosons are at this point no longer valid and we are confronted with the fermion sign problem which has bothered physicists for quite a long time without any final solution. One could go a step further and imagine the effects on the action of considering configurations of some of the many possible particles with ‘exotic statistics’, which might exist as the effective constituents of strongly correlated condensed matter systems.

In this respect we are safe with the quantum elasticity theory as long as we deal with bosons as the basic quantum solid constituents. Although one might object that in the classical theories the phonons (basically the same as the displacements) are bosons regardless of the statistical nature of the constituents, this is a consequence of the finite temperature compactification where ‘winding configurations’ such as the one mentioned above are highly unlikely (radius of the imaginary time direction  $\hbar/k_B T$  is relatively small compared to other lengths in the problem). If one deals with the quantum crystal at zero temperature, the temporal direction extends to infinity and both space and time become entangled in such way that the statistics of the solid constituents becomes crucial.

The above statement is a bit strong and in fact, even at zero temperature crystalline phonons are bosonic excitations even for fermionic solids (e.g. Wigner crystal). This is true only because expansion around the crystalline ground state involves configurations in which none of the particles is allowed to dwell far away from its equilibrium position. Even when the displacements become larger than the lattice constant, the considered motions are always collective as the phonons are represented only by *smooth* fields. When the singular displacement field configurations are taken into account, as it will be the case in the dual theory of the elasticity, the problem of imaginary action is on the table again and this will be the reason to limit ourselves to the development of a theory applicable only to bosonic crystals in spite of the rich variety of particles seen in nature.

With a bosonic crystal, one can always rely on the classical kinetic term Eq. (3.23) continued to imaginary time by the Wick rotation  $t \rightarrow -i\tau$ . The kinetic term Eq. (3.23)

and the potential energy term Eq. (3.4) can be written in a compact form

$$\mathcal{L}_0(\mathbf{x}) = \frac{1}{2}\rho\partial_\tau\mathbf{u}\partial_\tau\mathbf{u} + \frac{1}{2}\partial_i u^a C_{ijab}\partial_j u^b \equiv \frac{1}{2}\partial_\mu u^a C_{\mu\nu ab}\partial_\nu u^b. \quad (3.24)$$

The extended elastic tensor

$$C_{\mu\nu ab} = \begin{cases} C_{ijab}, & \mu = i, \nu = j \\ \rho\delta_{ab}, & \mu = \nu = \tau \\ 0, & \text{otherwise} \end{cases} \quad (3.25)$$

now includes both elastic constants and the mass density and gives the action more of a *relativistic* appearance, similar to the action Eq. (2.2). The action Eq. (3.24) is unfortunately not Lorentz-invariant, as the gradient expansion leading to the elastic energy Eq. (3.4) assumes that equilibrium positions of the constituents are static in a certain (our) reference frame. The elasticity theory emerges on a *non-relativistic* concept of the equilibrium positions and therefore it must abandon the Lorentz-invariance innate to the fundamental microscopic theory.

We discussed how time has a special role in the physical theories due to our experiments performed in a specific reference frame and this is valid even with models that are originally relativistic, like the XY action Eq. (2.2). In the elastic theory, the special status of time is only amplified on the level of the emergent theory. In addition, the field variables, the displacement, exist only in the spatial direction. The constraint  $u^\tau = 0$  would have to be imposed, had we started with a Lorentz-invariant formulation of the theory equivalent to the one with elastic action Eq. (3.24). These ‘‘upper labels’’ of the displacements, as well as the upper labels that occur in the dual description will be called ‘flavours’.

We have now to ask physical questions such as what are the Green’s functions of the model in terms of the displacement fields? Associated with a displacement  $u^a$ , an external source term is added to the action

$$\mathcal{L}_{\mathcal{J}} = \mathcal{J}^a u^a \quad (3.26)$$

so that the imaginary time propagator is found as the derivative of the generating functional

$$\langle\langle u^a | u^b \rangle\rangle = \frac{1}{Z} \left. \frac{\partial^2 Z[\mathcal{J}]}{\partial \mathcal{J}^a \partial \mathcal{J}^b} \right|_{\mathcal{J}=0}. \quad (3.27)$$

The real time propagator is then obtained by the analytic continuation of the propagator Eq. (3.27) back to real time by  $\tau \rightarrow it - \delta$  (or  $\omega_n \rightarrow -i\omega - \delta$  for the propagator of the Fourier components).

When only smooth displacement configurations are assumed in the path integral Eq. (3.22), one can transform the fields to the momentum-Matsubara frequency space. It is convenient to rotate the displacement flavours to the momentum ( $L, T$ , i.e. ‘zweibeinen’ Eq. (1.3)) basis, but for the moment we keep the Cartesian indices and separate the longitudinal and the transversal displacements by the projection operators Eq. (1.11, 1.12). When the linear isotropic elasticity is considered, the elastic action including the external source terms

turns into

$$\begin{aligned}\mathcal{L} &= \frac{1}{2}u^a \left[ (\rho\omega_n^2 + \mu q^2)\delta_{ab} + \mu \frac{1-(d-3)\nu}{1-(d-1)\nu} q_a q_b \right] u^b + \mathcal{J}^a u^a \\ &= \frac{1}{2}\rho u^a \left[ (\omega_n^2 + c_L^2 q^2) P_{ab}^L + (\omega_n^2 + c_T^2 q^2) P_{ab}^T \right] u^b + \mathcal{J}^a u^a,\end{aligned}\quad (3.28)$$

introducing two velocities

$$c_L^2 = \frac{2\mu}{\rho} \frac{1 - (d-2)\nu}{1 - (d-1)\nu} = \frac{\kappa + 2\mu \frac{d-1}{d}}{\rho}, \quad c_T^2 = \frac{\mu}{\rho}\quad (3.29)$$

which correspond to the longitudinal and transversal phonon velocities of the isotropic  $d$ -dimensional solid.

The Gaussian integration of the (exclusively smooth!) displacements yields the partition function of the solid, including the external source terms,

$$\begin{aligned}Z[\mathcal{J}^a] &= \prod_{\mathbf{q}, \omega_n} \sqrt{\frac{2\pi}{\rho(\omega_n^2 + c_L^2 q^2)}} \sqrt{\frac{2\pi}{\rho(\omega_n^2 + c_T^2 q^2)}} e^{\frac{1}{2}\mathcal{J}^a \left[ \frac{P_{ab}^L}{\rho(\omega_n^2 + c_L^2 q^2)} + \frac{P_{ab}^T}{\rho(\omega_n^2 + c_T^2 q^2)} \right] \mathcal{J}^b} \\ &= Z e^{\frac{1}{2}\mathcal{J}^a \left[ \frac{P_{ab}^L}{\rho(\omega_n^2 + c_L^2 q^2)} + \frac{P_{ab}^T}{\rho(\omega_n^2 + c_T^2 q^2)} \right] \mathcal{J}^b}.\end{aligned}\quad (3.30)$$

The imaginary-time displacement propagator for the elastic ideal solid is found to be

$$\langle\langle u^a | u^b \rangle\rangle = \frac{1}{\rho} \left( \frac{P_{ab}^L}{\omega_n^2 + c_L^2 q^2} + \frac{P_{ab}^T}{\omega_n^2 + c_T^2 q^2} \right).\quad (3.31)$$

The excitation spectrum of an ideal crystal has a massless linear pole associated with the longitudinal displacements, and  $d - 1$  degenerate massless linear poles associated with the transversal displacements. These are of course well-known, and go under the name of the longitudinal and transversal crystal phonons respectively. Liquids differ from solids for having no reactive shear rigidity which implies the absence of massless propagating poles in the transversal response (compare  $\mu = 0$  in Eq. (3.29)). Instead, a liquid responds to shear either by a dissipative response (as in a classical liquid) or it does not respond at all as in superfluid  $^4\text{He}$ . There, a response to shear is not present at all, all the way down to length scales of a few lattice constants, where the shear response is recovered, signaled by the roton minimum in its excitation spectrum.

The displacement propagator for a solid as described by the second order gradient elasticity is straightforwardly found in the same manner as the propagator Eq. (3.31). Two additional terms in the elastic energy density Eq. (3.19) are added to the inverse propagator, resulting in

$$\langle\langle u^a | u^b \rangle\rangle = \frac{1}{\rho} \left[ \frac{P_{ab}^L}{\omega_n^2 + c_L^2 q^2 (1 + \ell'^2 q^2)} + \frac{P_{ab}^T}{\omega_n^2 + c_T^2 q^2 (1 + \ell^2 q^2)} \right].\quad (3.32)$$

The choice of the factors (lengths)  $\ell'$  and  $\ell$  in the second order gradient energy density Eq. (3.19) is now clear: second-order gradient elasticity effects become visible in the phonon

spectra only at lengths smaller than  $\ell'$  in the longitudinal and  $\ell$  in the transversal sector. Although the two lengths are in first instance irrelevant for the long-wavelength behaviour, the length  $\ell$  does regulate the ratio of dislocation and disclination rest mass and it will be necessary to implicitly include it in the formalism in order to achieve the phase transition to the nematic crystal [48, 44].

The existence of separate, decoupled, excitations in the ideal crystal displacement propagators (Eqs. (3.31, 3.32)) allows us to split the propagator into longitudinal and transversal parts. The longitudinal component of the displacement field is proportional to the compressional strain  $\partial_a u^a \rightarrow -qu^L$ . Therefore, the longitudinal propagator is defined as the correlation function of the compression strain

$$G_L = \langle\langle \partial_a u^a | \partial_b u^b \rangle\rangle. \quad (3.33)$$

The transversal part of the displacement is proportional to the local rotation operator Eq. (3.5) and the residual part of the displacement propagator is then the trace of the local rotation correlator

$$G_T = 2\langle\langle \omega_{a,b} | \omega_{a,b} \rangle\rangle. \quad (3.34)$$

The antisymmetric local rotation can in general be represented as a contraction of the Levi-Civita symbol and an axial-tensor of rank  $d-2$ . Thus, in two dimensions there is only one component of the local rotation (axial-scalar)  $\omega^\tau = \frac{1}{2}\epsilon_{ab}\partial_a u^b$ , while in three dimensions the local rotation is represented by an axial-vector  $\omega^a = \frac{1}{2}\epsilon_{abc}\partial_b u^c$ . The transversal propagator Eq. (3.34) is the propagator of the local rotation excitation(s) and it is interesting to see how the antisymmetric strain component, which does not even have an elastic stiffness in the linear elasticity, acquires a nontrivial Green's function.

Use of the strain propagators Eq. (3.33) and Eq. (3.34) ensures that these propagators stay well-defined even in the phase where the displacements are disordered. This choice of Green's functions does, in analogy with the superfluid velocity-velocity correlators Eq. (2.49), break the 'dual censorship' barrier and allows us to measure disorder/topological field correlation in the disordered phase by means of (order) phonon propagators.

Hypothetically, one could construct a correlation function between compression strain and local rotation

$$G_{chiral} = \langle\langle \partial_a u^a | \omega_{b,c} \rangle\rangle. \quad (3.35)$$

Compression is always a true scalar, i.e. a rotation singlet invariant under spatial reflections. The local rotation transforms under a representation that depends on the dimensionality, but it is always an 'axial' object. This means that it changes sign under spatial reflections. Accordingly, the propagator Eq. (3.35) has to be an axial object as well, and it will change its sign under spatial reflection. The only way for this propagator to acquire a non-zero value is that the ground state be chiral, i.e. it breaks the spatial reflection symmetry so that it is not equivalent to its mirror image. In the ideal crystal, the two sectors are decoupled and, as expected, the propagator Eq. (3.35) vanishes as there is no chirality

breaking. Later, in the ordered nematic state, the Fourier transformed chiral propagator will acquire a nonzero value for certain values of angle between Burgers- and wave-vector. This is however not a sign of broken reflection symmetry since one needs to perform the inverse Fourier transformation after which the correlator (in real space) may vanish. When we come to the exact expression of the chiral propagator in the ordered nematic phase, we will use that opportunity to demonstrate conditions on the Fourier transformed correlators implied by (un)broken reflection symmetry.

### 3.3 Topological defects in solids

The theory of the ideal crystal presented in the previous section is heavily used for common solids encountered on a daily basis like metal rods or springs. One might wonder why the gradient expansion works so well for the long-wavelength description of solids experiencing low stress? What causes the simple elasticity picture to fail? The assumption that all the crystalline constituents remain, for infinitely long times, close to their equilibrium positions may be jeopardized by many factors. First of all, no crystal growth process is perfect and occasionally there will be a missing atom (vacancy) or an excess atom (interstitial) in the crystal. Vacancies and interstitial pairs may be introduced by high energy processes such as an irradiation of the crystal where an atom is ‘pushed’ out of its equilibrium position into a new position, far enough away such that the recombination of the interstitial-vacancy pair is not likely to occur. A vacancy or an interstitial can occur due to fluctuations in the system whether they are of classical (thermal) or quantum (zero-point) origin [48]. In real crystals, the formation energy for a vacancy is of order of 0.5eV, resulting in roughly one percent vacant sites for a piece of steel at 1000K, while the vacancy concentration is  $\sim 10^{-7}$  at room temperature. The formation energy of interstitials is even higher, usually like 3-6eV, rendering only few of them at 1000K, while they are virtually non-existent at room temperature. A small concentration of vacancies is not in contradiction with long-range crystalline order: the vacancies by themselves ‘dilute’ the crystal by reducing the crystalline order. In the quantum crystal matters are a bit different, as interstitial-vacancy pairs are bound in virtual pairs at small coupling constant while they might Bose-condense when the coupling constant increases, forming a supersolid (coexisting phase of crystalline order and the vacancy Bose condensate). A further increase in the coupling constant leads to a transition into the superfluid phase where the crystalline order parameter is completely diminished. This scenario becomes relevant when Umklapp scattering dominates, as in popular toy models of the Bose-Hubbard variety [1] studied earlier.

The potential energy per vacancy/interstitial event in a solid is quite high and whenever a multitude of these point defects is present, they will, instead of leading a solitary life, get rather close in order to minimize their potential energy. What usually happens is that interstitials group into line defects, effectively removing a large number of frustrated bonds. In a two-dimensional crystal this is the way in which dislocation and disclination defects are formed. The crystal deforms around the line to repair (remove) high strains caused by interstitial defects which decreases the energy of the defect further, and the only place where

this repair is impossible is close to the line-end where the defect core is formed and where most of the defect energy is stored. In three dimensions, things are less obvious. Namely, following the manner of two-dimensional defects, rows of interstitials in three-dimensions can stack onto each other, with further reduction in the potential energy. In this way sheets of interstitials are created, the crystalline repair may again take place at the surface of the sheet only to fail at the edges which then form a line-like core of dislocation/disclination defects in the three-dimensional solid. However, the three-dimensional interstitials are still point particles and they can significantly reduce the total energy by a delocalization. In this manner, the supersolid ground state can compete with the state dominated by the topological defects even when there are no strong Umklapp processes present. In higher dimensions the topological defects are created by further stacking of interstitials so that in  $d$  dimensions dislocations and disclinations are geometrical  $p$ -branes with  $p = d - 2$ . The increased dimensionality, however, favours even more strongly the realization of the supersolid phase. Notice that the geometrical structure of dislocation/disclination defects in an arbitrary-dimensional medium corresponds to that of vortex excitation in XY model (chapter 2) which will later be crucial in development of the elastic duality.

The coexistence of the solid and interstitial BEC parameter in a supersolid is in a way possible due to the non-topological status of interstitial defects: presence of one of them in the lattice influences only other constituents in the vicinity of the defect. By contrast, the dislocation and disclination defects are topological excitations: whenever a circulation is made around one such defect, the displacement field  $\mathbf{u}$  becomes ill-defined by acquiring a singular part. This multi-valuedness of the displacement field characterizes the defect and, in analogy with the XY singular configurations, yields a precise description of the topological defect as a part of the field theory. The same as with the vortices, the topological defects of the elasticity theory can be ‘measured’ by an encircling contour which counts the discontinuities in the displacement and local rotation field, the former giving the dislocation and the latter giving the disclination charge of the defect [130, 131]. The requirement that symmetrized strains have to be smooth is analogous to the requirement that the superfluid velocity of the XY model is a smooth function.

The discontinuity in the fields can alternatively be expressed as a jump of the corresponding fields across a surface (in 3D) which has the defect line as its only boundary. If a defect is unbound the surface will extend to infinity. If a defect forms a loop, the surface is usually taken to be finite. The choice for this surface, which is known as the Volterra cut, is physically irrelevant. If we imagine that a defect is made ‘by hand’, by cutting the solid and inserting extra material at that plane (as Volterra imagined), the crystal will relax to ‘repair’ along this line (symmetrized strains match precisely) and the only physically observable quantity is the singularity along the defect line which could have been achieved by any other arbitrary Volterra cut, having the defect line at its edge as the only requirement.

A dislocation charge, the Burgers vector, is defined by the displacement discontinuity, regardless of the number of embedding dimensions. A disclination charge is, on the other hand, a dimension-sensitive quantity. This comes from the definition of local rotations as an antisymmetric tensor of rank-2, Eq. (3.5). Alternatively, this tensor (the local rotation field) can be expressed as a contraction of the Levi-Civita tensor and an antisymmetric

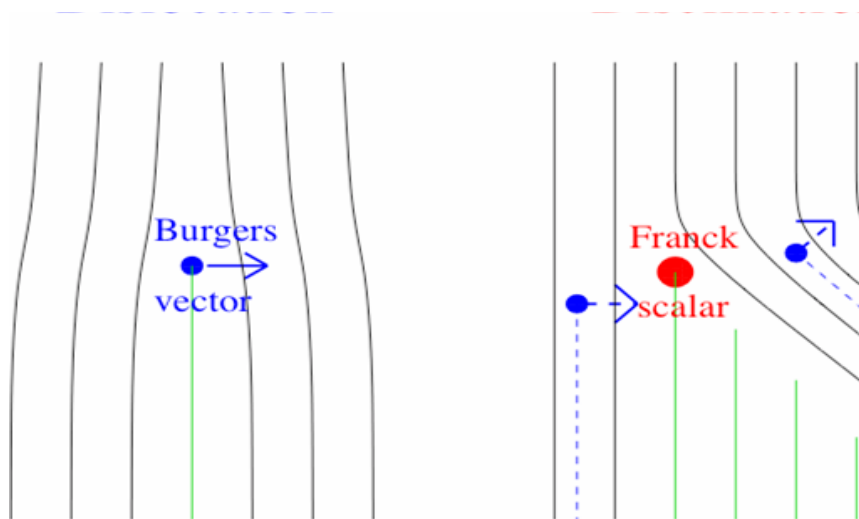


Figure 3.1: Topological defects in 2D: a) dislocation can be regarded as a line of interstitials coming to an end in the bulk of a solid; b) stacking these lines of interstitials yields a wedge of interstitials which is a disclination.

axial-tensor of rank  $d - 2$  which is known as the Frank charge of the disclination. Accordingly, a disclination of a two-dimensional medium has axial-scalar charge (Frank scalar) and one in a three-dimensional medium has axial-vector charge (Frank vector).

In Fig. 3.1 we can see how defects look in a two-dimensional solid. The dislocation can be thought of as a line of atoms coming to an end in a middle of the crystal [132, 133, 134]. It is associated with the restoration of the broken translational symmetry in the crystal and causes discontinuities in the displacement field only. A disclination, on the other hand, looks like a wedge of atoms inserted into the crystal. It is associated with the restoration of the rotational symmetries in the crystal and it causes discontinuities both in the displacement and the local rotation field. Dislocation and disclination defects are not independent: a disclination can be viewed as a stack of dislocations extending to infinity and a dislocation can conversely be seen as a bound pair of an anti-disclination and a disclination. Pursuing the analogy, a whole hierarchy of excitations in solids may be made: interstitials are made of bound dislocation-antidislocation pairs and phonons are just bound interstitial-vacancy pairs (vacancy at the original constituent position  $\mathbf{R}^0$ , interstitial at its true position  $\mathbf{R}^0 + \mathbf{u}$ ).

The geometrical properties of the topological defects, their topological charges and their mutual ‘alignment’ define different types of dislocations and disclinations. In two dimensions defects are point charges and there is no need for a classification although sometimes they are regarded as if they were in slices of a three-dimensional medium (so that they are referred to as ‘edge’ and ‘wedge’ respectively). Three-dimensional defects are lines and topological charges are vectors so the classification is based on their alignment. A dislocation can be edge dislocation, with the Burgers charge perpendicular to the defect line, and

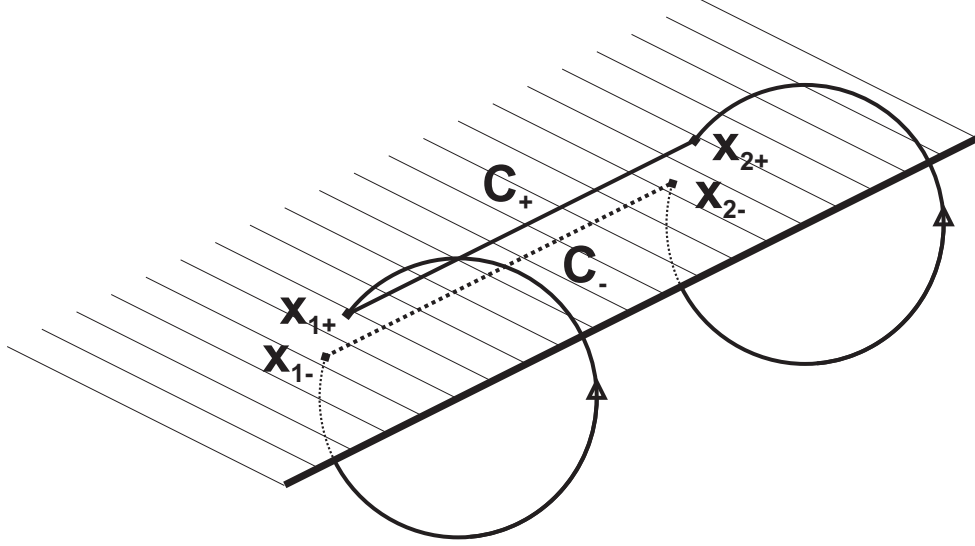


Figure 3.2: Weingarten theorem: a difference in the displacement circulation between contours 1 and 2 is given by Eq. (3.43). The discontinuity occurs at the Volterra cut (rastered plane).

screw dislocation, with the two being parallel; a disclination can be wedge disclination, with the Frank vector and the defect line parallel, splay disclination, with the two being perpendicular, or twist disclination, similar to the splay except with the two lines bypassing each other. Both dislocations and disclinations can also be a mixture of different classes when the angle between the defect line and the topological charge has some intermediate value.

There is a theorem by Weingarten which insures that only these two types of topological defects can exist [135]. While the original work pertained to three-dimensional solids, we present a slight modification that is valid in an arbitrary dimensional medium [50].

Suppose that we have a defect line in a solid and wish to relate the discontinuity in the displacement field at two points 1 and 2 located at the cut (see Fig. 3.2). The discontinuity is recorded by encircling the defect, so we have

$$\begin{aligned}
 \Delta u^a(2) - \Delta u^a(1) &= (u^a(2^+) - u^a(2^-)) - (u^a(1^+) - u^a(1^-)) \\
 &= \int_{1^+(C^+)}^{2^+} dx_i \partial_i u^a - \int_{1^-(C^-)}^{2^+} dx_i \partial_i u^a \\
 &= \int_{1^+(C^+)}^{2^+} dx_i (w_{i,a} + \omega_{i,a}) - \int_{1^-(C^-)}^{2^+} dx_i (w_{i,a} + \omega_{i,a}).
 \end{aligned} \tag{3.36}$$

Contours  $C^+$  and  $C^-$  connect the respective points 1 and 2 and run each on one side of the Volterra cut. The term with the local rotation can be partially integrated

$$\int_{1^\pm(C^\pm)}^{2^\pm} dx_i \omega_{i,a} = [x_i - x_i(1^\pm)] \omega_{i,a} \Big|_{1^\pm}^{2^\pm} - \int_{1^\pm(C^\pm)}^{2^\pm} dx_j [x_i - x_i(1^\pm)] \partial_j \omega_{j,a} \tag{3.37}$$

and since

$$x_i(1^+) = x_i(1^-), \quad x_i(2^+) = x_i(2^-), \quad (3.38)$$

we arrive at

$$\begin{aligned} \Delta u^a(2) - \Delta u^a(1) &= (x_i(2) - x_i(1))(\omega_{i,a}(2^+) - \omega_{i,a}(2^-)) + \\ &\int_{C^+} dx_j [w_{j,a} + (x_i - x_i(1))\partial_j \omega_{i,a}] - \\ &\int_{C^-} dx_j [w_{j,a} + (x_i - x_i(1))\partial_j \omega_{i,a}]. \end{aligned} \quad (3.39)$$

The integrals are calculated over two different sides of the Volterra cut and they can be merged into one integration over a contour  $C$  of the discontinuities

$$\int_{C^+} - \int_{C^-} \rightarrow \int_C dx_j [\Delta w_{j,a} + (x_i - x_i(1))\Delta \partial_j \omega_{i,a}]. \quad (3.40)$$

The discontinuity of the local rotation derivative can be reorganized into

$$\begin{aligned} \Delta(\partial_j \omega_{i,a}) &= \frac{1}{2} \partial_j (\partial_i u^a(\mathbf{x}^+) - \partial_a u^i(\mathbf{x}^+)) - [\mathbf{x}^+ \rightarrow \mathbf{x}^-] \\ &= \partial_i w_{j,a}(\mathbf{x}^+) - \partial_a w_{j,i}(\mathbf{x}^+) + \frac{1}{2} (\partial_j \partial_i - \partial_i \partial_j) u^a(\mathbf{x}^+) - \\ &\quad \frac{1}{2} (\partial_j \partial_a - \partial_a \partial_j) u^i(\mathbf{x}^+) + \frac{1}{2} (\partial_a \partial_i - \partial_i \partial_a) u^j(\mathbf{x}^+) - [\mathbf{x}^+ \rightarrow \mathbf{x}^-]. \end{aligned} \quad (3.41)$$

Since the displacement field is smooth on both sides of the Volterra cut, all terms with two derivatives vanish and the integral Eq. (3.40) turns into

$$\int_C dx_j [\Delta w_{j,a} + (x_i - x_i(1))\Delta(\partial_j w_{j,a} - \partial_a w_{j,i})]. \quad (3.42)$$

It was earlier assumed that both strains and their derivatives are smooth on the Volterra cut. Accordingly, the integral Eq. (3.42) is identically zero. The discontinuity in the local rotation field defines an antisymmetric tensor  $\mathcal{A}_{ij} = \Delta \omega_{i,j}$ , and we obtain the exact formulation of the Weingarten theorem

$$\Delta u^a(2) = \Delta u^a(1) + \mathcal{A}_{ab} [x^b(2) - x^b(1)], \quad (3.43)$$

which states that a discontinuity over a Volterra cut can only be a constant vector plus the action of an antisymmetric tensor. Another way to formulate it is by saying that a discontinuity in the displacement around a defect line is independent of the path and always given in the form

$$\oint_C (d\mathbf{l} \cdot \nabla) \mathbf{u} = \mathbf{u}(\mathbf{x}_+) - \mathbf{u}(\mathbf{x}_-) = \mathbf{b}_0 + \hat{\mathcal{A}}(\mathbf{x} - \mathbf{x}_0). \quad (3.44)$$

We express the antisymmetric tensor  $\mathcal{A}$  as

$$\Omega_{a_1 a_2 \dots a_{d-2}} = \frac{1}{(d-2)!} \epsilon_{a_1 a_2 \dots a_{d-2} ij} \mathcal{A}_{ij}, \quad (3.45)$$

and vice versa:  $\mathcal{A} = \epsilon\Omega$  (in symbolic form) and we recognize the second term of the Weingarten theorem Eq. (3.43) as a  $d$ -dimensional rotation. For a two- or three-dimensional defect line, the Frank scalar and vector respectively coincide with  $\Omega$  and  $\Omega_a$ . Defects with  $\Omega$  equal to zero are pure dislocations with the Burgers vector  $\mathbf{b} = \Delta\mathbf{u}$ . The Burgers vector of a disclination is on the other hand sensitive to the choice of the reference point 1 in the Weingarten theorem Eq. (3.43). The most important consequence of the theorem is, however, that dislocations and disclinations are sufficient to cover any possible discontinuity and therefore there is no other kind of defect permitted.

An elastic topological defect is characterized by discontinuity at the defect manifold (point, line, brane, etc.). In analogy with the vortices of the Abelian-Higgs model, we introduce the density of defects, dislocations and disclinations respectively, as

$$\alpha_{i_1 i_2 \dots i_{d-2}}^a = \epsilon_{i_1 i_2 \dots i_{d-2} j k} \partial_j \partial_k u^a, \quad (3.46)$$

$$\Theta_{i_1 i_2 \dots i_{d-2}}^{a_1 a_2 \dots a_{d-2}} = \epsilon_{i_1 i_2 \dots i_{d-2} j k} \epsilon_{a_1 a_2 \dots a_{d-2} b c} \frac{1}{2} \partial_j \partial_k \partial_b u^c. \quad (3.47)$$

$d-2$  lower indices represent the fact that the defect is an oriented manifold (a  $d-2$ -brane). The upper indices correspond to the Burgers charge (vector regardless of the number of embedding dimension) and Frank charge (tensor of rank  $d-2$ ). By our earlier convention, we will refer to the upper index of the dislocation density as a ‘flavor’ index.

Let us suppose that a general topological defect is defined by singularities on a manifold  $\Sigma$ . The defect densities can be expressed in terms of manifold delta function, Eq. (2.106), used in section 2.5

$$\alpha_{i_1 i_2 \dots i_{d-2}}^a = \delta_{i_1 i_2 \dots i_{d-2}}(\Sigma) (b^a - \mathcal{A}_{ab} x_b), \quad (3.48)$$

$$\Theta_{i_1 i_2 \dots i_{d-2}}^{a_1 a_2 \dots a_{d-2}} = \delta_{i_1 i_2 \dots i_{d-2}}(\Sigma) \Omega^{a_1 a_2 \dots a_{d-2}}. \quad (3.49)$$

Since the topological defects cannot have any edges, the derivative identity Eq. (2.101) is valid for the manifold  $\Sigma$ . Accordingly, the conservation law for disclinations and a similar law for dislocations follow when we differentiate defect densities Eqs. (3.48 - 3.49)

$$\partial_j \Theta_{j i_1 i_2 \dots i_{d-3}}^{a_1 a_2 \dots a_{d-2}} = 0, \quad (3.50)$$

$$\partial_j \alpha_{j i_1 i_2 \dots i_{d-3}}^a = \mathcal{A}_{aj} \delta_{\dots}(\Sigma) = \epsilon_{a j b_1 b_2 \dots b_{d-2}} \Theta_{j i_1 i_2 \dots i_{d-3}}^{b_1 b_2 \dots b_{d-2}}. \quad (3.51)$$

The latter identity can be interpreted as the conservation law for dislocation densities valid only in the absence of disclinations. In the presence of disclinations, it illustrates the interdependence of dislocations and disclinations: ‘peeling’ of dislocations from the infinite stack that builds a disclination is allowed at no cost on the disclination Frank charge. This implies that, in order to create a dislocation, all we have to do is make a disclination move. This law works the other way around also: a moving disclination leaves a trail of free dislocation defects behind it. If these proofs seem superficial, a more precise proof, based on the analogies with differential geometry [48]. and gravity [123, 124, 125], will be presented in appendix B.

Until now we were concerned only with defects of a classical elastic medium. Given that a quantum elastic medium has an additional coordinate, i.e. imaginary time, we

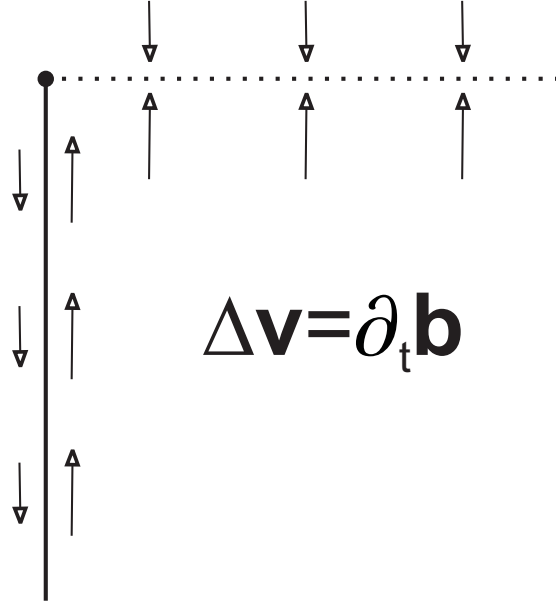


Figure 3.3: Discontinuity in the velocity field or the ‘velocity dislocation’: such a discontinuity, though physically possible, violates the assumptions of the Weingarten theorem Eq. (3.44). Depending on the orientation of the Volterra cut with respect to the ‘velocity Burgers vector’ it represents slip of surfaces (parallel, full line) or adding/removing material (perpendicular, dashed line). For simplicity, we use the word ‘slip’ for both motions.

should repeat the whole procedure, now having the topological densities only as the static (temporal) components of the more general defect currents and generalizing the definitions Eq. (3.46 - 3.47) to accommodate the dynamical currents. The imaginary time direction should have a special role in this generalization. However, it turns out that the generalization to the dynamical currents of a quantum solid is straightforward if we assume a medium with one more dimension which is assigned to the imaginary time and use the definitions, remarks, conservation laws, etc., from the previous paragraphs in this section. There is, however, a subtle change due to the special status of time in the elastic theory – crystalline displacements in the temporal direction ( $u^\tau = 0$ ) are forbidden and this is reflected in the geometrical structure of the defect topological charges. First, we note that the Burgers vector registers the displacement discontinuity which is only possible in the spatial directions. Therefore, the dislocation currents with temporal flavor are not permitted and the definition of dynamical dislocation currents becomes

$$J_{\mu_1 \mu_2 \dots \mu_{d-1}}^a = \epsilon_{\mu_1 \mu_2 \dots \mu_{d-1} \nu \lambda} \partial_\nu \partial_\lambda u^a. \quad (3.52)$$

The Greek indices are now used to signify summing over both spatial and temporal indices while the Burgers flavor is exclusively spatial.

The generalization of the disclination current Eq. (3.47) has to be performed with greater care. Let us naively substitute all the indices in Eq. (3.47) by their Greek counter-

parts (space-time indices) to obtain the definition of the dynamical disclination current

$$T_{\mu_1\mu_2\dots\mu_{d-1}}^{\alpha_1\alpha_2\dots\alpha_{d-1}} = \frac{1}{2}\epsilon_{\{\mu\}\nu\lambda}\epsilon_{\{\alpha\}\beta\gamma}\partial_\nu\partial_\lambda\partial_\beta u^\gamma. \quad (3.53)$$

Braces represent a string of indices (say  $\{\alpha\} = \alpha_1\alpha_2\dots$ ). Since the index  $\gamma$  cannot take the temporal value  $\tau$  in the summation of Eq. (3.53), one of the remaining indices, either any of the  $\alpha_i$  or  $\beta$ , has to be the temporal one. If one of  $\alpha$ 's has taken the value  $\tau$ , the remaining indices are all spatial, including  $\beta$ , and the topological charge operator Eq. (3.53) gives the discontinuity in a local rotation. If, however, one takes the disclination current component with all of the  $\alpha$  indices spatial,  $\beta$  is forced to take the temporal value and the topological charge Eq. (3.53) is not measuring a discontinuity in a local rotation, but rather in the velocity field  $\partial_\beta u^\gamma \rightarrow \partial_\tau u^c \equiv v_c$ . Thus, this kind of generalized disclination current can alternatively be thought of as a disclination in the velocity field. In principle, such events are possible in real solids, but what do they mean physically? In Fig. 3.3, we give an illustration of the effect of a velocity discontinuity. Pending the orientation of the Volterra cut (which is physical now since the velocity field does not repair itself) with respect to the velocity discontinuity, a nonzero value of the current  $T_{\{\mu\}}^{\{a\}}$  means that two crystalline surfaces slip over each other or that some additional material is added or removed from the defect. These effects are in clear violation of the Weingarten theorem as it states that all the symmetrized strains (and the velocity field can be regarded as such) have to be smooth. The conditions violating the Weingarten theorem imply further that the conservation laws Eq. (3.50 - 3.51) are no longer valid. The velocity slips act as defect factories, adding new material from the outside and changing the total amount of crystalline material. As we wish to describe defects which are innate to the solids and conserved (equivalent to the condition that no new matter is introduced into the system), the disclination currents with  $d - 1$  spatial Frank indices are prohibited in the remainder of this work. Therefore, the current Eq. (3.53) is redefined for a non-relativistic solid as

$$T_{\mu_1\mu_2\dots\mu_{d-1}}^{a_1\dots a_{d-2}} = \frac{1}{2}\epsilon_{\{\mu\}\nu\lambda}\epsilon_{\{a\}bc}\partial_\nu\partial_\lambda\partial_b u^c, \quad (3.54)$$

so that only the Frank charge is represented in the upper label(s). It turns out that the dual elastic theory, which is supposed to treat all possible defects, decouples the prohibited velocity slips from the physical dual degrees of freedom at the end of the day.

### 3.4 Topological kinematic constraints: dislocations and the glide principle

Defects such as interstitials/vacancies, dislocations or disclinations perturb the ideal perfectly periodic crystal. Since they play a crucial role in the melting transition by their deconfinement, it is natural to expect that their kinematical and dynamical properties become essential when these transitions are analysed. An important example is the dislocation glide constraint. This constraint is very well known in the materials science community, but the understanding of this constraint was always based on either heuristic

or numerical arguments. Recent work on the melting of quantum crystals [44] signified the importance of the glide constraint for the properties of the new melted phases and it offered a formulation of glide in terms of the novel dynamical dislocation currents Eq. (3.52).

In this section we treat these matters carefully and show that the glide constraint, which is a topological constraint, may be derived from a simple consideration that the matter is conserved inside the solid. To highlight the history of the subject and the beauty of the proof, we first derive the linear glide constraint for a charged solid, and later repeat the procedure for an uncharged solid with the same result. The proof we give is independent of the number of embedding dimensions and it always constrains one of the dynamical currents Eq. (3.52). To give a better feeling for the glide constraint in higher dimensions, the constraint is interpreted in two, three and four dimensions, and we point out how the geometrical structure of the defect can allow local ‘leaks’. Because the constraint, as initially derived by us, represents only the linear approximation to the exact expression, we revisit the proof without the linear approximation, rederive the exact expression and argue that these corrections can accommodate the physics beyond the linear theory, involving interstitial events and finite lattice constant effects. There is another aspect of the glide constraint: its transformation properties under the spatial symmetries of the system. As we show toward the end of this section, the glide constraint prohibits the only singlet current in the system, relieving the compression degree of freedom from the burden of the disorder degrees of freedom. In the dual theory of the elasticity, this condition is sufficient to keep the compression rigidity present at all length scales.

In many standard texts, e.g. [132, 133, 134], the explanation of the glide constraint is not profound. A dislocation corresponds to a row of particles (atoms) ‘coming to an end’ in the middle of a solid. One way to move this entity is to cut the neighboring row at the ‘altitude’ of the dislocation and consequently move over one tail to cure the cut (Fig. 3.4a). The net effect is that the dislocation is displaced. This easy mode of motion is termed ‘glide’. Moving in the orthogonal direction is not as easy. Let us try to move the dislocation ‘upward’. This requires loose particles to lengthen or shorten the row of particles (‘interstitials’ or ‘vacancies’) and since loose particles are energetically very costly and they move very slowly (by diffusion) this ‘climb’ motion is strongly hindered. Estimates on ‘climb’ diffusion rates are provided in e.g. Ref. [136]. Climb is hindered to such an extent in real life situations (e.g. pieces of steel at room temperature) that it may be ignored altogether. The lower dimensional glide motion of dislocations is reminiscent of dynamics in the heavily studied sliding phases [57, 137, 138, 139, 140, 141, 142, 143] in which an effective reduction of dimensionality occurs.

Earlier discussions on the glide constraint present it in a fairly quantitative way by demanding that the dislocation motion obeys conservation of crystalline material. Suppose we have a dislocation line specified by  $\mathbf{x}(s)$  having a Burgers charge  $\mathbf{b}$ . The three-dimensional glide constraint is then expressed as

$$\int_L ds \partial_s \mathbf{x} \cdot (\mathbf{b} \times \dot{\mathbf{x}}) = 0. \quad (3.55)$$

It is given in integral form in order to leave room for the diffusion of the material over

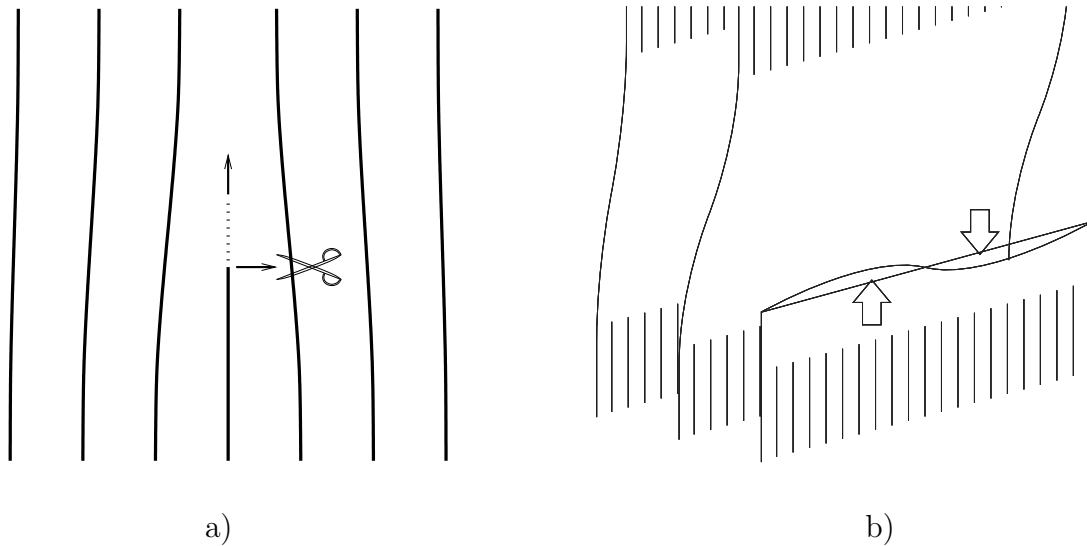


Figure 3.4: Possible motions of dislocation defects in a) two and b) three dimensions a) allowed (matter conserving) cutting and reconnecting of ‘atomic columns’ gives rise to the glide motion of the dislocation line (at the center of figure) in the horizontal direction. By contrast, an emission or absorption of vacancies and interstitials is required for a climb motion (vertical motion of the dislocation in this figure). Thus, an absence of additional material (mass conservation) strictly prohibits the climb within, continuum limit, linear elasticity. b) in three dimensions, the same principle is still valid for a motion of the defect as a whole line parallel or perpendicular to its Burgers vector. However, due to the geometrical structure of the defect, small exchange of material is allowed across the defect line. That way, a segment of the defect line may locally climb at expense of its neighbours’ height.

the line. In spite of the fact that this diffusion process is not intensive, it is usually still much stronger than the diffusion of the external interstitials. This motion, where a segment of the three-dimensional dislocation can move perpendicular to its Burgers vector at the expense of its neighbouring segment is known as restricted climb (see Fig. 3.4b).

The glide formulation Eq. (3.55) may suffice for the needs of metallurgy. However, if we want to write a consistent dual theory of quantum elasticity, the glide constraint should be given in an exact mathematical form, involving the currents Eq. (3.52). This formulation of the constraint is the aim of this section.

Let us begin with the analysis of an electrically charged solid. Such a medium (“bosonic Wigner crystal”) is interesting in itself [9, 144], and will be the central object of our study in the chapter on our novel type of superconductivity (chapter 5). Here, it is merely utilized as a convenient tool for implementing the material conservation law via gauge invariance, to subsequently derive the glide principle. Later on, we will independently derive the glide constraint by direct *mass conservation* without resorting to local gauge invariance to implement it. As mass conservation pertains to a scalar quantity, such a conservation law translates into a condition on a linear combination of the topological defect currents

which is necessarily invariant under spatial rotations. Conservation laws (equivalent to gauge invariance) may greatly restrict the dynamics of the system, leading to an effective reduction in the dimensionality. We will now illustrate how this indeed transpires in solids: in linear elasticity, mass (‘charge’) conservation allows only glide motion of a dislocation.

From chapter 5, we borrow the (linear) EM coupling term Eq. (5.3) of a charged solid and add it to the total action density

$$\mathcal{L}_{EM} = (n_e e^*) [A_\tau \partial_a u^a - A_a \partial_\tau u^a]. \quad (3.56)$$

For the exact derivation of this result we refer the reader to chapter 5. The charge and its density are given by  $e^*$  and  $n_e$ ; the first term in Eq. (3.56) is the Coulomb repulsion energy gained by compression of the solid, while the second term represents the Lorentz potential of a moving charged particle. Charge conservation is closely related to gauge invariance – the gauge invariant action is equivalent to the statement that the charge is conserved. Therefore, we demand that the action Eq. (3.56) is invariant under the  $U(1)$  gauge transformation of the electromagnetic potentials  $A_\mu$  given by

$$A_\mu \rightarrow A_\mu + \partial_\mu \alpha, \quad (3.57)$$

with  $\alpha$  an arbitrarily *smooth* scalar field. Inserting the gauge transformed fields, Eq. (3.57), into Eq. (3.56), and performing an integration by parts, the gauge-variant part is found to be

$$\mathcal{L}_{EM} \rightarrow \mathcal{L}_{EM} + (n_e e) \alpha [\partial_a \partial_\tau u^a - \partial_\tau \partial_a u^a]. \quad (3.58)$$

Since the gradient function  $\alpha$  is arbitrary, the term in the brackets must be identically zero in order to preserve the electric charge, and thus

$$\partial_a \partial_\tau u^a - \partial_\tau \partial_a u^a = 0. \quad (3.59)$$

This will be the glide constraint in terms of strain. Contracting the dynamical current definition Eq. (3.52) with the Levi-Civita tensor and employing the identity

$$\epsilon_{\tau a \mu_1 \dots \mu_{D-1}} \epsilon_{\mu_1 \dots \mu_{D-1} \nu \lambda} = (D-1)! \begin{vmatrix} \delta_{\tau\nu} & \delta_{\tau\lambda} \\ \delta_{a\nu} & \delta_{a\lambda} \end{vmatrix}, \quad (3.60)$$

the glide constraint Eq. (3.59) can be rewritten so that it acts on the dislocation currents in any arbitrary dimension:

$$\epsilon_{\tau a \mu_1 \dots \mu_{D-1}} J_{\mu_1 \dots \mu_{D-1}}^a = 0. \quad (3.61)$$

This is none other than the glide constraint acting on the dislocation current in arbitrary dimensions! This result places on rigid mathematical footing the conventional glide “principle”. As we will illustrate later on, this result, now derived in full generality within the linear regime, is violated by non-linear contributions. Towards the end of this section,

we will derive a complete non-linear glide constraint which will enable us to predict and estimate corrections to the linear order glide constraint in general elastic solids

At first sight this might appear as magic, but it is easy to see what is behind this derivation. In order to derive Eq. (3.56) one has to assume that the gradient expansion is well behaved, i.e. the displacements should be finite. This is not the case when interstitials are present, because an interstitial is by definition an object which can dwell away an infinite distance from its lattice position. Hence, in the starting point, Eq. (3.56), it is implicitly assumed that the interstitial density is identically zero. The gauge argument then shows that gauge invariance exclusively communicates with the *non-integrability* of the displacement fields, Eq. (3.59). These non-integrabilities are of course nothing else than the topological currents – the glide constraint is a constraint on the dislocation current. If the glide constraint were not satisfied, electrical conservation would be violated locally, i.e. electrical charges would (dis)appear spontaneously, as if the dislocation were able to create or destroy crystalline matter. In the absence of interstitials this is not possible and, therefore, dislocations can only glide. The key is, of course, that by default, dislocation currents are decoupled from compressional stress in the linear non-relativistic theory.

We may indeed equivalently derive Eq. (3.61) without explicitly invoking EM gauge invariance to arrive at Eq. (3.59). Instead, we may directly rely from the very start on *mass conservation* – the continuity equation of the mass currents (which, as alluded to above, is equivalent to local gauge invariance),

$$\partial_\tau \rho + \nabla \cdot \mathbf{j} = 0. \quad (3.62)$$

To see how this is done directly, we compute the various mass current components  $j_\mu$ . By simple geometrical considerations, within the linear elastic regime, the mass density is

$$\rho = \rho_0 [1 - \partial_i u^i], \quad (3.63)$$

with  $\rho_0$  the uniform background value: the divergence of  $\mathbf{u}$  (signaling the local volume increase) yields the negative net mass (‘charge’) density variation at any point. Similarly, the spatial current density

$$\mathbf{j} = \rho_0 \partial_\tau \mathbf{u}. \quad (3.64)$$

Compounding the mass continuity equation of Eq. (3.62) with the physical identification of the current (Eqs. (3.63, 3.64)), we obtain Eq. (3.59) from which Eq. (3.61) follows. Later, we will return to such a physical interpretation of the glide constraint from this perspective in order to determine corrections to the glide principle which follow from anharmonic terms. We emphasize that the mass conservation law leading to Eq. (3.59) trivially holds in any medium regardless of the underlying statistics [145] of potential quantum systems or their dimension. Furthermore, within the linear elastic regime, such a discussion highlights the validity of Eq. (3.59) and the ensuing glide equation of Eq. (3.61) (when interpreted as density matrix averages) in crystals at any temperature in which strict linear order mass conservation condition is imposed on all configurations. Needless to say, as temperature

is elevated, a departure occurs from such an imposed linear order condition through the enhanced appearance and diffusion of interstitials and vacancies leading to climb motions. The restriction on the dynamics in this regime is captured by a higher order variant of Eq. (3.61) (Eq. (3.76)) which will be derived later on.

Let us now pause to consider what Eq. (3.61) means physically. In two spatial dimensions, Eq. (3.61) implies that the dislocation currents have to be symmetric [44]:  $\epsilon_{ab}J_a^b = J_x^y - J_y^x = 0$ . Now, consider Fig. 3.4a. Here, the Burgers vector is pointing in the horizontal x-direction implying that  $J_\mu^y = 0$ , while the glide constraint reduces to  $J_y^x = 0$ . This current ( $J_y^x$ ) is, by its very definition, the climb current perpendicular to the Burgers vector.

In three and higher spatial dimensions, the story is less easy, the reason being that the constraint on the motion is less absolute. This is of course known in the classic theory [48, 133], but the reader might convince him/herself that making use of Eq. (3.61) the analysis is much helped as compared to the rather pain-staking effort based on the ‘intuitive’ arguments. In 3+1D, the constraint of Eq. (3.61) becomes

$$\epsilon_{\tau abc}J_{bc}^a = 0. \quad (3.65)$$

Let us first consider a screw dislocation. These correspond to dislocation currents of the form  $J_{a\mu}^a$  (i.e. the static  $\mu = \tau$  component corresponds to the orientation of the dislocation loop being parallel to the Burgers vector). It follows immediately that the constraint Eq. (3.65) is not acting on screw dislocations and, henceforth, screw dislocations can move freely in all directions. Edge dislocations are the other extreme, corresponding to dynamical currents of the form  $J_{b\mu}^a$  where  $a$  and  $b$  are orthogonal. The condition  $\mu = a$  corresponds to glide: an edge dislocation with its loop oriented in a direction ( $b$ ) perpendicular to the Burgers vector ( $a$ ) can still move freely in the direction of the Burgers vector ( $a$ ). The displacement of a dislocation along the line is not a topological object and the current with two identical lower indices ( $\mu = b$ ) vanishes. The glide constraint only strikes when all three labels are different. Let us consider a dislocation line extending in  $z$  direction with Burgers vector in the  $x$  direction (see Fig. 3.4b). The only nonzero components of the current are  $J_{z\mu}^x$  and the glide constraint becomes  $J_{zy}^x = 0$ . This automatically forbids any motion in the  $y$  direction, that is perpendicular both to the dislocation line and its Burgers vector. The constraint is ‘leaky’ due to the extended nature of the defect. The material needed for the climb of one segment of the dislocation can be supplied by an adjacent segment. The glide constraint has therefore only a real meaning through its integral form,

$$0 = \int dV \epsilon_{\tau abc}J_{ab}^c. \quad (3.66)$$

As illustrated in Fig. 3.4b, only the dislocation’s ‘center of mass’ is prohibited to move in the climb direction. Local segments of the line may still move at expense of their neighbors, effectively transporting matter along the defect line. The ‘leaky’, locally defined, constraint of Eq. (3.66) corresponds with the intuitive idea of ‘restricted climb’ found in the elasticity literature.

Having a mathematical definition of the glide constraint at our fingertips enables us to address its incarnations in even higher dimensional systems where direct visualization is of little use. Notwithstanding that such crystals are, of course, not to be found in standard condensed matter, higher dimensional glide constraints might have implications for ‘emergence theories’ of fundamental phenomena resting on elasticity theory [146, 85]. Let us for example look how the constraint Eq. (3.61) acts in a 4+1D crystal. A dislocation is now a 2-brane, say, a plane extending in  $y$  and  $z$  directions. When its Burgers vector lies in this plane, this brane is analogous to a screw dislocation in the sense that its motions are not affected by the glide constraint. The other extreme is the ‘edge dislocation brane’ with a Burgers vector perpendicular to the brane, say in the  $x$  direction. In this case the nontrivial currents correspond to  $J_{yz\mu}^x$ . As noted earlier for three-dimensional defects, topological currents do not record any motion taking place within the defect-brane but only in directions perpendicular to it. The bottom line is that besides the static current (density)  $J_{yz\tau}^x$ , the topological dynamical currents are  $J_{yzx}^x$  and  $J_{yzw}^x$ , representing dislocation glide and climb respectively. The glide constraint Eq. (3.61) forbids the latter ‘in integral form’, allowing climb of a certain brane element only at the expense of the brane volume taken by a neighboring element.

Contrary to our rigorous (‘glide only’) result concerning the linear regime of continuum elasticity, in real crystals dislocations do climb (albeit at small rates). When dislocations collide, interstitial matter will be exchanged and this process releases climb motions [44]. In what follows, we will rederive the glide constraint, yet now do so within a fully general framework which will enable us to address the implications of both (higher order) *non-linear elasticity* and the presence of a lattice cut-off. Higher order corrections to linear elasticity modify the original glide constraints of Eq. (3.61) giving rise to dislocation climb.

To achieve this aim, we could invoke a more precise version of electromagnetic coupling term Eq. (3.56), robust against particles that dwell away from their equilibrium positions (interstitials) and exact up to higher orders is given by

$$\mathcal{L}_{EM} = (n_e e^*) \left[ \frac{A_\tau(\mathbf{R}_0 + \mathbf{u})}{\det(\delta_{ij} + \partial_i u^j)} - A_i(\mathbf{R}_0 + \mathbf{u}) \partial_i u^a \right]. \quad (3.67)$$

The denominator in the first term is the exact volume change due to the compression. The main difference between the approximate coupling Eq. (3.56) and the exact coupling Eq. (3.67) is that now, particles ‘feel’ the EM potential  $A_\mu$  not at their original crystalline positions  $\mathbf{R}_0$  but rather at their true positions, i.e.  $\mathbf{R}_0 + \mathbf{u}$ . Demanding the gauge-invariance of coupling Eq. (3.67) under performed gauge transformation Eq. (3.57) yields the exact glide constraint. However, when we are in search for the exact glide constraint, the uncharged ‘mass conservation’ argument gives a far simpler derivation.

We return to the mass continuity equation invoked earlier (in unison with Eqs. (3.63, 3.64)) yet now, by examining contributions of higher order derivatives of the displacement field, we exercise far greater care in examining its ramifications. The continuity equation of Eq. (3.62) implicitly assumes that the density and current fields are functionals of local Eulerian (distorted lattice) coordinates. On the other hand, the displacement, stress, and other elastic fields are functionals of substantial coordinates (i.e. the coordinates defined

relative to the undistorted lattice coordinates) – the Lagrangian coordinate frame. As was briefly done earlier (Eqs. (3.63, 3.64)), we express the local density and currents of Eq. (3.62) in terms of volume and velocities as  $\rho = \frac{\rho_0}{V}$  and  $\mathbf{j} = \frac{\rho_0 \mathbf{v}}{V}$ , with  $\rho_0$  the mass of the ideal uniform medium in a unit volume in the undistorted original medium (i.e. the ideal background mass density). Following a distortion, a unit volume element of the original medium now occupies a region of volume  $V$ . With these relations in tow, Eq. (3.62) reads

$$\partial_\tau V + (\mathbf{v} \cdot \nabla)V \equiv D_\tau V = V(\nabla \cdot \mathbf{v}). \quad (3.68)$$

This equation can be interpreted as a law governing the change of volume of the elastic medium: the change in volume (the derivative on the left hand side) is exclusively dictated by the motion of the boundaries – the gradient on the right hand side corresponds to a surface integral of the velocity field. This is just a reformulation of the same basic constraint: the conservation of mass (or electrical charge). Throughout this section, mass conservation was the primary ingredient leading to the glide constraint. To invoke the mass continuity equation in the form of Eq. (3.68), let us express the actual atomic coordinates  $R^j$  in terms of the Eulerian coordinates (henceforth denoted by  $r^i$ )

$$\mathbf{r}[\mathbf{R}, \tau] = \mathbf{R} + \mathbf{u}[\mathbf{R}, \tau], \quad \mathbf{R}(\mathbf{r}, \tau) = \mathbf{r} - \mathbf{u}(\mathbf{r}, \tau), \quad (3.69)$$

which gives the identity (valid for finite lattice constant  $a$ ),

$$\left(\frac{\partial R^j}{\partial r^i}\right)_\tau = \left(\delta_{ij} + \sum_{m=1}^{\infty} \frac{a^{m-1}}{m!} \partial_j^m u^i\right)^{-1}. \quad (3.70)$$

Simplifying, we find that Eq. (3.68) may be recast as

$$\partial_\tau V = V \left(\frac{\partial R^j}{\partial r^i}\right)_\tau \partial_i \partial_\tau u^j. \quad (3.71)$$

This is an exact expression (entailing corrections to all order in gradients of  $\mathbf{u}$ ) detailing the glide constraint. Retaining the leading order contributions and employing  $V = 1 + \partial_i u^i$ , we recover the ‘familiar’ linearized glide constraint of Eq. (3.59).

What can we learn from this exact form of the glide constraint? Let us specialize to the simple 2+1D medium. Assuming a vanishing lattice constant  $a$ , the volume of an elementary cell is simply given as  $V = \det(\delta_{ij} + \partial_i u^j)$ . Inserting this in the exact glide expression Eq. (3.71) we find that it simplifies,

$$0 = \epsilon_{ab} J_i^b (\delta_{ia} + \partial_i u^a) = J_x^x \partial_x u^y + J_y^x (1 + \partial_y u^y). \quad (3.72)$$

The displacement derivative  $\partial_i u^a$  includes both regular and singular components. When  $\partial_i u^a$  is small compared to unity, the linearized glide constraint of Eq. (3.61) is recovered. In the second step we chose a specific Burgers vector orientation  $\mathbf{b} = b\mathbf{e}^x$  so that all current components  $J_\mu^y$  have to vanish.

The ‘climb’ current  $J_y^x$  is non-zero in two cases. The dislocation may already glide ( $J_x^x \neq 0$ ) and by following the smoothly displaced crystalline lines, a small climb motion is present in rate of

$$J_y^x \approx -J_x^x \partial_x u^y. \quad (3.73)$$

This is however no true climb as the dislocation is still stuck to one crystalline line and the ‘climb’ we find is just a result of motion of the dislocation conforming to the deformation of the lattice (drag by the underlying lattice). This is by no means a topological climb current! By contrast, when  $\partial_y u^y = -1$  which represents the stacking of material in  $y$  direction, i.e. presence of the interstitial matter, the current  $J_y^x$  may take arbitrary value which means that the dislocation can freely climb.

At this point it seems that the field theory defined in Ref. [48] is not able to capture relevant interstitial physics without inclusion of the anharmonic effects. In the next chapter we’ll however discuss the interstitial dynamical currents (strictly speaking they are not topological) and show their relation to the dislocation current. Given that climbing dislocations represent sources and sinks for the interstitials, we’ll point out how to implement the glide constraint in its local form to explicitly include the previous relation between the interstitials and dislocations.

We reach the conclusion that higher orders in the displacements (non-linearities, anharmonicities) have the effect of restoring the physics of interstitials. Another natural question to ask regarding the continuum limit is whether there may be a hidden dependence on the lattice cut-off  $a$ . To investigate this issue, let us see what happens to Eq. (3.71) when we only keep terms which are harmonic in the displacements, while imposing no conditions on the number of derivatives. These have to do with the volume of the unit cell. Let us specialize to a simple hypercubic lattice with sides defined by the vectors ( $i = 1, \dots, D$ ),

$$u^j(R_i + a_i) - u^j(R_i) = \delta_{ij} + \sum_{m=1}^{\infty} \frac{a^{m-1}}{m!} \partial_i^m u^j. \quad (3.74)$$

The corresponding volume is a determinant of the matrix Eq. (3.74) and in the harmonic approximation only the diagonal elements remain,

$$V = 1 + \sum_{i,j=1}^D \sum_{m=1}^{\infty} \frac{a^{m-1}}{m!} \partial_i^m u^j. \quad (3.75)$$

Using this expression for the volume, the exact equation of constraint (Eq. (3.71)) reads

$$\epsilon_{\tau a i_1 \dots i_{D-1}} J_{i_1 \dots i_{D-1}}^a = -(D-1)! \sum_{i=1}^D \partial_{\tau} \frac{e^{a \partial_i} - a \partial_i - 1}{a \partial_i} \partial_i u^i. \quad (3.76)$$

The remarkable fact is that it is possible to collect all higher order derivatives in a simple exponent. Eq. (3.76) affords us with the general non-linear corrections to the glide constraint of Eq. (3.61). Given any elastic media in which the magnitude of the gradient terms

are known, we may estimate the size of the non-linear corrections to the linear order glide constraint.

Let us finally analyse the symmetry properties of the glide constraint. The static dislocations and disclinations of higher dimensional media are geometrically complex entities such as lines, sheets or  $p$ -branes with Burgers vectors and Frank tensors attached. When in motion, these branes sweep the additional time dimension. For instance, defects in two space dimensions are point-like particles turning into world-lines in space-time, in three space dimensions they form loops spreading out in strings etc. Nevertheless, regardless of the embedding dimensionality, all of these ‘branes’ share a universal property: there is a unique direction perpendicular to the brane. This direction can be related to the dynamical defect currents by contracting it with the  $D - 1$  dimensional antisymmetric tensor having one index set equal to time,

$$\frac{1}{(D-1)!} \epsilon_{\tau i b_1 b_2 \dots b_{D-1}} J_{b_1 b_2 \dots b_{D-1}}^a = \partial_i \partial_\tau u^a - \partial_\tau \partial_i u^a = U_i^a, \quad (3.77)$$

isolating the perpendicular direction  $i$ . Instead of the dislocation current  $J$ , we could have used here also the disclination current  $T$ , but our interest in this subsection will be in the former. The comparison of the tensor Eq. (3.77) with the glide constraint Eq. (3.59) illustrates that the glide condition turns into a constraint on the trace  $U_i^i = 0$ . For rank-2 tensors, the trace is the only invariant tensorial component of the  $D$ -dimensional orthogonal group ( $O(D)$ ), corresponding to all rotations and the inversion in the  $D$ -dimensional medium. It follows that the constrained current is the only ‘singlet’ (scalar) under the point group symmetries of the crystal (point group symmetries constitute a subgroup of  $O(D)$ ). The conjugate degree of freedom must have the same symmetry and this can only be compression, the only physical entity being a singlet under  $O(D)$ . We have identified the fundamental reason that glide implies the decoupling of dislocations and compressional stress [44].

Apart from rotations, the glide constraint is also invariant under Galilean space-time translations. Needless to say, the constraint does not obey Euclidean Lorentz (space-time) invariance as the time direction has a special status both in Eq. (3.59) and Eq. (3.61). The origin of this lies, of course, in the definition of the crystalline displacement  $\mathbf{u}$  and its role in the minimal coupling Eq. (3.56). The displacements are defined under the assumption that every crystalline site has an equilibrium position which implicitly wires in that their world lines extend exclusively in the temporal direction.

We conclude with a speculation. As emphasized throughout, the basic physical ingredient leading to the derived constrained glide dynamics in solids was mass conservation. In a formal setting, similar albeit more restrictive volume conserving diffeomorphisms (parameterized by time) may be directly examined via the  $w_\infty$  algebra in two spatial dimensions and its extensions, e.g. [147, 148, 149]. We suspect that there might be a more fundamental way of casting our relations by relying on the intricacies of such symmetries of space and time.



# Chapter 4

## Dual elastic theory – nematic phases

The previous two chapters were of an introductory nature as we reviewed most of the known results relevant for the Abelian-Higgs duality (chapter 2) and the elastic theory (chapter 3), adding a few novel results to each chapter. Now, having made the reader accustomed to the basic ideas of duality and elasticity, we will proceed in this chapter to unify the two ideas in the dual theory of elasticity. This concept is fairly new in physics: it was introduced by Kleinert [48] and it seems that the scientific community has only recently started to appreciate its full power. This unfortunate fact may be attributed to the ‘sociological distance’ between the fields that dual elasticity binds together: on one end of the spectrum, we have duality, often perceived as a mathematical trick of hard core field theorists, and on the other end of the spectrum, elasticity and its topological defects considered as a closed chapter in theoretical physics and left to material science. Hopefully, the pursuit represented by this thesis will close this gap and demonstrate that abandoned theories can give fundamentally new results when dressed up in a field theoretical setting.

As we learned in chapter 2, ordered and disordered phases are relative concepts, relying directly on the kind of machines our experiments are equipped with. Nevertheless, being in the disordered state does not *a priori* ban us from seeing the correlations of the disorder objects by experiments devised in terms of order observables [62]. Elasticity is superficially similar to the XY model as seen by the comparison between their actions, Eq. (2.2) and Eq. (3.4) respectively. The displacement fields  $\mathbf{u}$  take the role of the phase field  $\phi$  and the difference comes from the ‘flavours’, showing that the dualization has to be performed with respect to  $d$  spatial field components. The tensorial nature of the coupling constant Eq. (3.25) and its symmetry properties, as well as the constraints on the topological defects, enrich the dual theory, leading to many counterintuitive results and interpretations which will be found throughout the present chapter. One of the basic ideas we wish to highlight in this chapter is that the phonon propagators can measure correlations between the topological defects, in a manner analogous to the capacity of the superfluid velocity correlators Eq. (2.49) to penetrate the dual barrier.

The scope of this thesis, and especially this chapter, is largely based on the pioneering work on quantum elasticity by Zaanen *et al.* [44]. Prior to that work there were no other treatises on dual elasticity known to us that had addressed disorder in a way similar to the

Abelian-Higgs duality. Although many older works focused on defect proliferation as the mechanism behind melting transitions [70, 105, 106, 107, 108, 109, 110, 111, 112, 113], it was not before this treatise that the gas of defects had been represented by a GLW action in the context of the dual stress gauge formalism. In the same manner that EM photons acquire mass in a superconductor (chapter 2), the dual stress photons, parameterizing the crystalline degrees of freedom, acquire mass in the melted phase.

The special aspect of the dual elasticity melting presented here is that the GLW action can be invoked only for dislocation defects. In that respect, the phases found initially by Zaanen *et al.* (called nematic phases, which we explain in a moment) are similar to the hexatic phase associated with the triangular lattice solid predicted long ago by Nelson, Halperin and Young [45, 46, 47], where the melting is caused exclusively by dislocation defects. There are, however, a number of differences. The NHY melting was a classical treatise disregarding the statistics of the crystalline constituents and based principally on the Kosterlitz-Thouless [110, 111] destruction of algebraic long-range order in the XY system. Further, the hexatic phase and the entire formalism developed in Refs. [45, 46, 47] is innate to the triangular or hexagonal lattice (lattice point group of  $C_{6h}$  type); on the other hand, the quantum nematic is constructed from the dual action and such a construction is possible regardless the lattice point group. The unique advantage of the NHY construction is that, treating the defects on a classical level, it can handle both dislocation and disclination defects. If a quantum crystal is considered, the geometrical phases associated with the winding of the disclination world lines and the ensuing statistics invalidate the GLW description.

Since the original work Ref. [44] contained a subtle flaw regarding the dynamics of the defect fields – a problem tackled in chapter 2 and a preprint of ours [62], the results presented here are derived with the dislocation condensate treated as a fully ‘relativistic’ entity. The conceptual ideas of Ref. [44] are, however, all retained in this thesis and as a consequence, a new phases of matter and novel mechanism for the superconductivity, based on these new phases, are found. With respect to these result, this and the next chapter represent the core of this thesis. The treatise on neutral solids in this chapter forms a basis for the following chapter where electrically charged solids are considered.

Let us review here the basic ingredients needed for construction of the dual elasticity theory and the GLW disorder action that describes the nematic phases. The construction of the dual theory alone is fairly unrestricted, as was the case with the XY model. The role of the conjugate momenta is taken by stress fields. In more than two spatial dimensions it is still possible to define the dual stress gauge fields, but the dual theory shares a difficulty with the Abelian-Higgs duality: the gauge fields become  $d - 1$  antisymmetric forms as do the defect currents. When we introduce the dual elastic theory, we will proceed as far as possible with a dimension independent formulation of the formalism. Unfortunately, when the disorder fields are introduced in the theory, we will have to restrict ourselves to 2+1D quantum solids, just as was the case with the Abelian-Higgs duality. There is one lucky circumstance for the application of this dual elasticity. It is generally believed that the physics behind high- $T_c$  superconductivity in cuprates is restricted to two-dimensional copper-oxide planes. In this regard, our handicap seems not so important because the most

promising application of our theory is to high  $T_c$  superconductivity. One should however be careful when electromagnetism is incorporated in the theory. The EM fields are in principle 3+1-dimensional and one should pay care to match the dimensions properly; in the next chapter more attention will be paid to this issue.

In the previous chapter we argued that a nontrivial statistics of the solid constituents may give rise to nontrivial (imaginary) contributions to the quantum action. In order to protect the dual disorder theory from these ‘signs’, we consider a solid made exclusively from bosonic (spin-0) particles. This condition implies that, when we wish to apply the model to a certain physical system, there exists a temperature/energy scale where effective bosonic excitations emerge.

Another important condition is that we consider only the so-called extreme type-II kind of melting process where interstitials are prohibited in the formalism. The non-topological status of interstitial events makes it less obvious how to incorporate these in the theory. Although we present some speculations in the conclusion on how to include interstitials defects into the field-theoretical description, the full formalism is still not fully developed and so we leave it as an issue for further investigation. The finite Higgs mass for the stress fields at the same time means that there is a (shear) penetration depth  $\lambda_S$  associated with the dual stress gauge fields. This length has to be large compared to the microscopic scales associated with the constituents (Cooper pairs). This condition also implies that the disordered phase is a quantum liquid crystal of the nematic kind. The quantum phase transition from the crystal to the isotropic superconductor is necessarily of the first order [150] and a continuous transition is required for a large  $\lambda_S$ . In the dual language, the nematic order implies the topological status of the phase in a sense that disclination defects are massive. The only permitted defects are dislocations, which are at the same time “carriers of the disorder”.

In the previous chapter we learned that dislocations have a vectorial Burgers charge. Based on this charge, we introduce a Burgers director – a liquid-crystal like order parameter whose value splits the nematic phase into two subphases: ordered and topological (disordered/isotropic) nematic. In the construction of the disorder field, the Burgers charge acquires the status of a coupling constant with respect to the flavour label of the dual stress gauge fields. The order in the Burgers sector means that only one flavour of the dual gauge fields, the one parallel to the Burgers vector, is minimally coupled to the disorder field and only this flavour will be subjected to the Higgs mechanism. The derivation of results for this phase is straightforward, although it becomes technically tedious here and there. On the other hand, the problem of the disordered Burgers charge in the topological nematic phase has triggered some controversy. When a ‘naive’ (mean-field) average of the Burgers director is used, the ramifications of the dual disorder theory seem in contradiction with the initial assumptions. Nevertheless, these results, still not published, are presented for a few reasons. First, if there is indeed a technical error in the results (inadequate averaging, gauge artifacts, etc.), a reader skillful in these matters might be able to find the correction and this might help us to eliminate the flaw. However, at the end of the section on the topological nematic, a claim will be presented that the three demands imposed on this phase in Ref. [44] (‘isotropy’ in the Burgers sector, GLW action implying a Burgersless

dislocation superfluid and Gaussian treatment) cannot be all simultaneously satisfied, at least in the case when the dislocation condensate is treated dynamically. The last section is devoted to a vindication of the results obtained for the topological nematic by ‘naive’ averaging and in that section it is shown that the controversial results have application to yet another, newly identified phase of the nematic type.

This chapter is organized in the following way. The first section is a straightforward derivation of the dual elastic field theory. It leads to the introduction of dual stress gauge field degrees of freedom and the identification of defect currents from section 3.3 as currents which are minimally coupled to the dual gauge fields. The resulting formalism is a generalization of the work of Kleinert [48], now applicable to an elastic solid of arbitrary dimension. Following the same storyline as in chapter 2, the second section contains the formalism required to treat the disorder field. We are limited to a 2+1D gas of bosonic dislocations and a simple GLW action of type Eq. (2.35) suffices for its description. The problem of order vs. disorder in the Burgers sector is formulated in this section and at this point we rely on the analysis from Ref. [44] where a liquid crystal action is suggested for the Burgers director order parameter. The phase diagram based on these arguments is outlined. In the third section, the dual stress gauge bosons are thoroughly analysed. Initially, the ideal crystal phase is recovered as the Coulomb phase of the dual gauge theory and the dual stress gauge field components are given a physical interpretation within the Coulomb gauge fixing. Subsequently, the Bose-condensation of the dislocations is considered. The Higgs mechanism which is implied in one of the stress gauge field flavours leads to the ordered nematic phase. The symmetry analysis, discussed in detail in appendix C, shows that after all relevant constraints have been implemented, only two ‘shear rigidity’ gauge photons are left to interact with the defects. In the ordered nematic phase the Higgs mechanism acts only on one of the two shear doublet components. In the next section, the ‘naive average’ over the Burgers vector is discussed and the isotropic/topological phase of the solid is obtained. Due to the problems already mentioned, the end of this section analyses consistency of the topological nematic phase. Some physical interpretations of the existing results are offered, based on symmetry arguments. In the last section, an alternative model for the disorder field is considered, which leads to an interpretation of the results of the previous section in a completely different light. The phase to which the controversial results are applicable and which we call the ‘isotropic nematic’, shares some features with the topological nematic: the disclinations are massive and the Burgers director has no vacuum expectation value in either of the two phases. In fact, the last property seems responsible for the misinterpretation of the two phases since the only input in the construction of the disordered nematic phase was precisely that the Burgers director order parameter vanishes ( $\hat{Q}^{ab} = 0$ ). The difference between the phases is in the following: in the isotropic nematic phase there is a multitude of mutually interacting dislocation condensates whose Burgers directors add to zero. At the same time, each condensate has a well-defined conserved Burgers vector. The topological phase, on the other hand, has only one bosonic degree of freedom whose Burgers director is disordered. It will be argued that one must take higher order (interaction) terms into account in order to properly describe the ‘strong interaction’ effects of this phase.

## 4.1 Dual elasticity

The dual elastic theory should in principle be easy to obtain if we stick to the recipe given in chapter 2, applying it directly to the theory defined throughout the action Eq. (3.24). That the procedure is everything but straightforward becomes clear when one is forced to invert the “coupling constant”, the elastic tensor given in Eq. (3.25). Given that the symmetries of space-time require the antisymmetric part of the elastic tensor to be singular, the construction of the dual theory has to be executed with great care. In his book [48], Kleinert considers only the symmetric strains Eq. (3.6) and the dual fields are introduced with respect to these strains. The introduction of conservation laws on conjugate momenta Eq. (2.10) in this approach lacks the symmetry in indices which motivated an alternative procedure in the construction of the dual elasticity presented here for the first time. The procedure is based on the same ideas that inspired Kleinert for his dual elastic theory and in fact it amounts to nothing more than reshuffling of indices. However, due to its apparent symmetry, this construction is tailored in such a way that it is easy to generalize all important steps to a medium of arbitrary dimensions.

After the single curl dual stress gauge fields (in analogy with Eq. (2.12)) have been introduced and the ‘single curl’ dual field theory is found, the remainder of this section is used to show that this dual formulation cannot cope with the presence of disclination defects. It should be improved by the introduction of ‘double curl’ gauge fields. Interdependence of dislocation and disclination currents is cured when the ‘true’ topological current is introduced. This topological current operator collects only the defect degrees of freedom (from both dislocation and disclination currents) that are not redundant in the linear elasticity. Although in the remainder of the thesis the ‘true’ topological currents and the ‘double curl’ dual theory are not of direct relevance, they are presented as part of the elastic duality which cannot be ignored in a general review of the subject. We must also notice that the introduction of the ‘true’ topological currents and their conjugate degrees of freedom, double curl stress gauge fields, differs in this text from all the current literature known to us [48]. When Kleinert introduces the ‘double curl’ stress gauge fields, this is done for a classical crystal and all the indices have spatial values. Hopefully, we have convinced the reader that the generalization to dynamical defect currents is a tricky business due to the lack of temporal displacements ( $u^\tau \equiv 0$ ). We can take two definitions for the disclination currents as an example, Eq. (3.53) that does not respect the temporal displacement constraint and the corrected version Eq. (3.54). In this respect, the ‘double curl’ fields we introduce must take care of the inability of matter to displace in the temporal direction, such that only the physical topological defect currents are tracked.

Let us now return to the initial action of an (electrically neutral) solid as given in Eq. (3.24). The generalized momenta are defined according to

$$\sigma_\mu^a = -i \frac{\partial \mathcal{L}_0}{\partial (\partial_\mu u^a)} = -i C_{\mu\nu ab} \partial_\nu u^b, \quad (4.1)$$

and they have a physical meaning: components  $\sigma_i^a$  represent stress exerted on a portion of the solid and the components  $\sigma_\tau^a$  are kinematical momentum densities. One is supposed

to express all strains  $\partial_\mu u^a$  in terms of the stress fields  $\sigma_\mu^a$ . Unfortunately, Eq. (4.1) cannot be directly inverted due to the singularity associated with the antisymmetric stresses. At this point an elegant way to avoid this singularity is introduced in this thesis. Next to the spin-0 and spin-2 projectors, Eq. (3.14), which span the space of symmetric tensors  $C_{ijab}$ , we introduce the antisymmetric spin-1 projector

$$P_{ij,ab}^{(1)} = \frac{1}{2}(\delta_{ij}\delta_{ab} - \delta_{ib}\delta_{ja}). \quad (4.2)$$

The space of all rank-2-2 tensors is spanned by these three projectors as seen from the closure relation

$$P_{ijab}^{(0)} + P_{ijab}^{(1)} + P_{ijab}^{(2)} = \delta_{ij}\delta_{ab} \equiv \mathbf{1}_{ijab}. \quad (4.3)$$

Projecting the definition of stress Eq. (4.1) on the three possible spin subspaces, the following relations between the stresses and strains are found

$$P_{ij,ab}^{(0)}\sigma_j^b = -id\kappa P_{ij,ab}^{(0)}\partial_j u^b, \quad (4.4)$$

$$P_{ij,ab}^{(1)}\sigma_j^b = 0, \quad (4.5)$$

$$P_{ij,ab}^{(2)}\sigma_j^b = -i2\mu P_{ij,ab}^{(2)}\partial_j u^b. \quad (4.6)$$

These relations are derived for the isotropic elasticity theory characterized by the elastic tensor Eq. (3.15) and we will use them in present work. In analogy with the decomposition Eqs. (4.4 - 4.6), one can find the appropriate relations for an elasticity tensor of a solid with lower point group symmetries.

The substitution of strains by stress fields in the action Eq. (3.24) and the recovery of the Hamiltonian is trivial if we employ the decomposition Eq. (4.3) and the orthonormality of each projector ( $P^2 = P$ ). Inserting the unity operator between stress and strain fields one obtains

$$\begin{aligned} \mathcal{H} &= -i\sigma_\mu^a\partial_\mu u^a + \mathcal{L}_0 = \frac{1}{2\rho}\sigma_\tau^a\sigma_\tau^a - i\sigma_i^a \left( P_{ij,ab}^{(0)} + P_{ij,ab}^{(1)} + P_{ij,ab}^{(2)} \right) \partial_j u^b + \\ &+ \frac{1}{2}\partial_i u^a \left[ P_{ij,ab}^{(0)}d\kappa P_{jk,bc}^{(0)} + P_{ij,ab}^{(2)}2\mu P_{jk,bc}^{(2)} \right] \partial_k u^c = \frac{1}{2}\sigma_\mu^a C_{\mu\nu ab}^{-1} \sigma_\nu^b. \end{aligned} \quad (4.7)$$

The terms containing temporal components  $\sigma_\tau^a$  factorize immediately and are trivially dualized because there is no singularity in that sector. The inverse elastic tensor  $C_{\mu\nu ab}^{-1}$  should not be taken literally. Instead, this is just the symbolic notation for the tensor coupling the stress fields

$$C_{\mu\nu ab}^{-1} = \frac{1}{\rho}\delta_{\tau\mu}\delta_{\tau\nu}\delta_{ab} + \frac{1}{d\kappa}P_{\mu\nu,ab}^{(0)} + \frac{1}{2\mu}P_{\mu\nu,ab}^{(2)} \quad (4.8)$$

$$= \frac{1}{\rho}\delta_{\tau\mu}\delta_{\tau\nu}\delta_{ab} + \frac{1}{4\mu} \left[ \delta_{\mu\nu}^{(2)}\delta_{ab} + \delta_{\mu b}\delta_{\nu a} - \frac{2\nu}{1+\nu}\delta_{\mu a}\delta_{\nu b} \right]. \quad (4.9)$$

The singular direction of the elasticity tensor does not appear in the ‘inverse’ elasticity tensor Eq. (4.9). Instead, the singularity implies the constraint on stresses (see Eq. (4.5)) which is in fact the famous Ehrenfest constraint [126]

$$\sigma_a^b - \sigma_b^a = 0. \quad (4.10)$$

In the previous chapter we argued that, based on the symmetry properties of expansion Eq. (3.2), and the microscopic crystal potential  $\mathcal{V}$ , the elasticity tensor in Eq. (3.4) cannot have an antisymmetric part. The implications are very fundamental. The Ehrenfest constraint Eq. (4.10) is in fact much a deeper statement since the stress fields are defined in all media, be it solids, liquids or gases. The constraint is directly related to angular momentum conservation: its violation would imply a violation of the angular momentum conservation. As it turns out, the symmetry of the elasticity tensor Eq. (3.25) is a fundamental consequence of space isotropy. In contrast with the derivation presented here, it is a physical consequence, and not the cause of the Ehrenfest constraint defined on stresses Eq. (4.10).

Together with the Ehrenfest constraint, the partition function acquires the form

$$Z = \int \mathcal{D}u^a \mathcal{D}\sigma_\mu^a \prod_{a \neq b} \delta(\sigma_a^b - \sigma_b^a) e^{-\int dx^\nu \mathcal{L}_{dual}}, \quad (4.11)$$

with dual action

$$\mathcal{L}_{dual} = \mathcal{H} + i\sigma_\mu^a \partial_\mu u^a. \quad (4.12)$$

Following the duality procedure, the displacement field is decomposed into smooth and singular parts. Integrating out the smooth part, the stress conservation law is obtained

$$\partial_\mu \sigma_\mu^a = 0. \quad (4.13)$$

This constraint is nothing else than the equation of motion for stresses in an elastic medium [126]. The sum over spatial values of index  $\mu$  is the divergence of the stress tensor. It is equal to the negative force, which is, according to the classical Newton law, precisely the kinematic momentum time derivative  $\partial_\tau \sigma_\tau^a$ .

We are more interested in the use of the equations of motion Eq. (4.13), in a similar manner as the momentum conservation law Eq. (2.10) was used. The ‘no divergence’ condition implies that a gauge fields can be introduced, similar to those in Eq. (2.12), in such a way that the stress is defined via

$$\sigma_\mu^a = \epsilon_{\mu\nu\lambda_1 \dots \lambda_{d-1}} \partial_\nu B_{\lambda_1 \dots \lambda_{d-1}}^a. \quad (4.14)$$

In analogy with the higher dimensional Abelian-Higgs duality, the number of lower indices depends on the dimension as  $d-1$ . Also, only antisymmetric (in lower indices) components of the gauge field have a physical meaning, but not all: some are part of the gauge volume

and some are ‘eaten’ by the Ehrenfest constraint. The main difference between the Abelian-Higgs and elastic stress gauge fields is that the latter carry an upper (Burgers) label.

To treat the singular part of the displacement field, a partial integration of the multivalued strain part of Eq. (4.12) with respect to the stress gauge fields is performed in the usual way. This results in the familiar coupling of the elastic gauge fields to the  $d+1$ -dimensional dislocation currents, as defined earlier in Eq. (3.52)

$$\begin{aligned} i\sigma_\mu^a \partial_\mu u_{MV}^a &= i\epsilon_{\mu\nu\lambda_1\dots\lambda_{d-1}} \partial_\nu B_{\lambda_1\dots\lambda_{d-1}}^a \partial_\mu u_{MV}^a \\ &= iB_{\lambda_1\dots\lambda_{d-1}}^a \epsilon_{\lambda_1\dots\lambda_{d-1}\nu\mu} \partial_\nu \partial_\mu u_{MV}^a = iB_{\lambda_1\dots\lambda_{d-1}}^a J_{\lambda_1\dots\lambda_{d-1}}^a. \end{aligned} \quad (4.15)$$

In a shorthand symbolical form, the total elastic action turns, after dualization, into

$$\mathcal{L}_{dual} = \frac{1}{2}(\epsilon\partial B)C^{-1}(\epsilon\partial B) + iJB, \quad (4.16)$$

with the Ehrenfest constraint explicitly imposed on the gauge fields. The partition function, with all of the constraints included, becomes

$$Z = \int \mathcal{D}B_{\{\lambda\}}^a \mathcal{D}J_{\{\lambda\}}^a \prod_b \mathcal{F}^b(B_{\{\lambda\}}^a) \prod_{a \neq b} \delta(\epsilon_{a\nu\{\lambda\}} \partial_\nu B_{\{\lambda\}}^b) e^{-\int dx_\nu \mathcal{L}_{dual}}. \quad (4.17)$$

This result is astonishing, especially so in two spatial dimensions where, in analogy with vortex duality, we recover a Maxwell type of effective action with phonon degrees of freedom represented by gauge photons and dislocations acting as electric charges. There are, however, a couple of important differences. The most important is that this Maxwell theory is about ‘flavored’ gauge fields and currents, the flavour corresponding to one upper (Burgers) index. The ‘coupling constant’ appears in the form of a tensor Eq. (4.9) which couples degrees of freedom in a quite unexpected way (longitudinal and transversal field components are messed up). The final novelty comes from the Ehrenfest constraint which effectively removes some of the gauge degrees of freedom at the expense of inducing a coupling between the remaining ones.

One may wonder what has happened to the disclination defects: why are they missing from the dual action Eq. (4.16)? There must be a way to introduce these defects in a field theoretical formalism. To address this issue, we first check the validity of the dislocation coupling term in the dual action Eq. (4.16). The gauge transformations in the two- and three-dimensional vortex dualities were already introduced in chapter 2. The transformation is easily generalized to higher dimensions in such way that the transformed fields stay antisymmetric. The gauge invariance of the action Eq. (4.16) is tightly linked to the dislocation current conservation condition

$$\partial_\mu J_{\mu\nu_1\dots\nu_{d-2}}^a = 0. \quad (4.18)$$

In the vortex duality no defects other than vortices exist and the vortex currents are always conserved, validating the introduction of the gauge fields  $A_\mu$  and their minimal coupling to the vortex currents. In dual elasticity this is not always the case due to the Weingarten

theorem [135] which states that the dislocations alone do not exhaust the spectrum of all possible topological defects. Contrasting the dislocation conservation law Eq. (4.18) with the exact relation Eq. (3.51), it becomes clear that the ‘single curl’ dual stress gauge fields are no longer valid objects as soon as a single disclination is present in the system. Therefore, in such a case it is necessary to avoid the substitution Eq. (4.14). A natural question which arises is: what can we do to develop a proper treatment of the disclination current densities within the dual field theory formalism? Comparing the definitions of dislocation and disclination currents, Eqs. (3.52) and (3.54) respectively, we observe that the disclinations carry one more derivative of the displacements fields. By introducing an additional curl in Eq. (4.14), the problem is removed, while now both dislocations and disclinations are coupled to the physical stress degrees of freedom. These new fields are called the ‘double curl’ stress gauge fields [48]. Due to the dimension dependent nature of the Frank charge, the introduction of the double curl gauge fields is sensitive to the number of dimensions of the solid. In two and three spatial dimensions it can easily be tracked down to the following relations,

$$\sigma_\mu^a = \epsilon_{\mu\nu\rho} \partial_\nu \left[ \partial_a \bar{h}_\rho^1 + \epsilon_{\tau ab} \partial_b \bar{h}_\rho^2 \right], \quad (4.19)$$

$$\sigma_\mu^a = \epsilon_{\mu\nu\rho\lambda} \epsilon_{\tau abc} \partial_\nu \partial_b \bar{h}_{\rho,\lambda}^c. \quad (4.20)$$

Again, due the special status of time in the theory, these fields are introduced in a slightly different manner compared to Ref. [48].

By means of partial integration, the double curl gauge fields ( $\bar{h}_\mu^{1,2}$  in two and  $\bar{h}_{\rho\lambda}^c$  in three spatial dimensions) couple minimally to field discontinuities given by

$$\begin{aligned} \bar{\eta}_\mu^1 &= \epsilon_{\mu\nu\lambda} \partial_a \partial_\nu w_{\lambda,a}, \\ \bar{\eta}_\mu^2 &= \epsilon_{\mu\nu\lambda} \epsilon_{ab} \partial_a \partial_\nu w_{\lambda b} \end{aligned} \quad (4.21)$$

in two or

$$\bar{\eta}_{\lambda\rho} = \epsilon_{\lambda\rho\mu\nu} \epsilon_{abc} \partial_b \partial_\mu w_{\mu,c} \quad (4.22)$$

in three dimensions. The defect currents  $\bar{\eta}$  are known as the “true defect currents” or “true topological currents”. They are related to the disclination and dislocation currents via relation which holds in all dimensions, although the contraction of the indices does depend on the number of dimensions, namely

$$\bar{\eta} = T + \epsilon \partial J. \quad (4.23)$$

Therefore, the true topological current groups redundant defect densities into one tensorial defect density operator. It is important to notice that the true topological currents are incomplete if the second-order gradient elasticity terms Eq. (3.19) are added to the elastic action. The rotational stiffness term introduces a new dual degree of freedom that should couple to a discontinuity in a local rotation. The true topological currents are all defined

as discontinuities in the symmetrized strains and therefore cannot code for all relevant defects of the elastic theory.

In relativistic solids (relevant for emergent gravity [84, 85]), temporal displacements are possible and the relativistic definition of the true topological currents in arbitrary number of dimensions is the one given by Kleinert [48]

$$\eta_{\mu_1 \dots \mu_{d-1}}^{\alpha_1 \dots \alpha_{d-1}} = \epsilon_{\{\alpha\}\beta\gamma} \epsilon_{\{\mu\}\nu\lambda} \partial_\beta \partial_\nu w_{\lambda,\gamma}. \quad (4.24)$$

which is a *relativistic* tensor. The relativistic true topological current Eq. (4.24) is symmetric under the simultaneous exchange of all the upper with all the lower indices. The relativistic double curl field is given by (compare with Eqs. (4.19 - 4.20))

$$\sigma_\mu^\alpha = \epsilon_{\mu\nu\{\lambda\}} \epsilon_{\alpha\beta\{\gamma\}} \partial_\gamma \partial_\nu h_{\{\lambda\}}^{\{\gamma\}}, \quad (4.25)$$

and due to the Ehrenfest constraint, the double curl gauge field  $h$  has the same symmetry properties as the relativistic topological current Eq. (4.24). The antisymmetric part of the field  $h_{\{\lambda\}}^{\{\gamma\}}$  is unphysical and accordingly the ‘true’ topological currents couple only physical degrees of freedom with singularities relevant for the linear elasticity. These are expressed in the form of linear combinations of dislocation/disclination currents while the irrelevant/redundant components are left out. The number of the physically relevant current components is, in this way, easy to establish.

In a non-relativistic solid, where the temporal dimension is not connected by Lorentz symmetry to the spatial dimensions, the symmetrized strain Eq. (3.6) becomes corrupted in the spatial direction (i.e. we should define  $w_{\tau,a} = \partial_\tau u^a$  in Eqs. (4.21 and 4.22)). Therefore, the previously introduced currents Eqs. (4.21, 4.22) cannot demonstrate, in an apparent way, the reduction of the number of independent components. Nevertheless, the number of independent current components can be deduced from the smoothness requirement on the symmetrized strain Eq. (3.6). It removes precisely one (2+1D) or three (3+1D) components from the theory, corresponding the number of independent double curl gauge field components  $\bar{h}$  with the number of independent true topological non-relativistic current components  $\bar{\eta}$ . Again, when finer details of elasticity (the second-order gradient elasticity) are included, the true topological currents are rendered an incomplete set for a full description of the physics of the crystalline defects.

## 4.2 Defect fields and their dynamics

After the appropriate Maxwell-like dual theory of elasticity is obtained, one has to develop the theory describing the dual disordering field. Complex geometrical properties of topological defects in elastic media, more precisely the non-Abelian character of disclinations, represents a major obstacle for the construction of the complete quantum melting theory. We are only aware of a few attempts (by means of quantum double symmetry groups) to resolve the problem of a second quantization of the disclinations [151]. If disclination defects are entirely prohibited or appear as bound particle-antiparticle pairs, their role in the

long-wavelength theory can be ignored and the effective theory acquires a much simpler form. This is a consequence of the Abelian character of dislocations. The disclinations are non-Abelian objects due to their relation to the curvature/rotational rigidity and rotational symmetry restoration. The dislocations, on the other hand, are related to shear rigidity, and their presence in the system restores the translational symmetry, broken by the crystalline ground state. Since the group of all translations in  $d$ -dimensions is Abelian, the dislocations do not exhibit a nontrivial statistics regardless of the number of the embedding dimensions. By contrast, the Euclidian group  $E(d)$ , containing both translations and rotations, is not Abelian even in the two-dimensional case, implying that the quantum field theory that comprises all the topological defects has to be nontrivial.

As announced in the introduction of this chapter and in the previous section, our treatise of defects will, for the reasons listed above, deal only with the dislocation defects in 2+1D. The dual theory of the Maxwell kind that was constructed in the previous section, Eq. (4.16), is precisely tailored for our needs – the dislocation defects are the exclusive topological defects treated by the theory and the disclinations are (implicitly) assumed to be absent. The ‘single-curl’ dual theory is based on the path integral formulation of elasticity in Eq. (4.17) which is rooted into the path integral formulation of the strain formalism, Eq. (3.22). The latter partition function assumes contributions originating from all possible configurations in the smooth and singular displacement fields. After the duality, the smooth fields are reparametrized by means of dual stress gauge fields Eq. (4.14), while the singularities are recorded by the dislocation currents. Each singularity configuration has its own ‘statistical weight’ in the path integral Eq. (4.17) given by the defect action. However, since we, at that particular step, still had to derive the specific action, the path integration was symbolically marked by quotation marks. In this section, this problem is addressed in more detail. Based on the derivations of Ref. [44], and in analogy with vortex duality, a proper disorder field theory of GLW type is constructed, at least for the ordered phase of a nematic solid. Given that the Burgers vectors correspond to a liquid crystal order parameter, the transition between the ordered and isotropic/topological nematic is modeled in terms of a liquid crystal action, based on the work by de Gennes [150]. Based on these ingredients, a phase diagram following from the theory is sketched and we thoroughly analyse the order of the transition between the various phases.

The guiding principle throughout this chapter is that the vortex duality can be generalized to the tensorial elastic action Eq. (3.24). The question which arises at this stage is if the disorder field can be constructed in the same manner as it was in chapter 2. Naively looking at the problem, one might fear that dislocations do not have much in common with vortices: the displacements, and accordingly dislocation currents, have, in contrast to vortices, Burgers flavors. The same holds for the structure of the gauge theory developed in the previous section. Due to the  $d = 2$  flavours in the displacement field  $u^a$ , the dual theory is a “ $d$ -fold” vortex dual theory at least with respect to the gauge fields: the physical stress fields as defined in terms of the stress gauge fields (Eq. (4.14)) are invariant under gauge transformations of the  $U(1) \times U(1)$  kind

$$B_\mu^a \rightarrow B_\mu^{a'} = B_\mu^a + \partial_\mu \alpha^a, \quad (4.26)$$

where  $\alpha^a$  is an arbitrary smooth vectorial function. Gauge transformation in the form of Eq. (4.26) is the speciality of the duality in 2+1-dimensions. In higher dimensions one cannot just generalize transformation Eq. (4.26) by assuming a vectorial gauge function  $\alpha^a$ . Instead, as we learned in section 2.5, each of the components of the gauge function  $\alpha^a$  becomes an anti-symmetric  $d - 1$ -form.

At this point one might argue that the gauge transformation Eq. (4.26) implies the existence of two  $U(1)$  disorder (matter) wave-functions, one for each Burgers flavour. A claim similar to this one will be presented in the last section of this chapter where a different kind of disorder field is considered. However, in this section, the disordered field theory is constructed following the ideas of Zaanen *et al.* [44] where the final disorder action is a mere clone of the GLW action Eq. (2.35), containing a single  $U(1)$  disorder field. So how do we get rid of one of the  $U(1)$  gauge sectors and connect a gas of dislocations with a GLW type of action? The answer to this question is based on the disorder treatise in the vortex duality, except that one needs to ‘strip off’ the Burgers vector from the dislocation in order to make them bosonic point particles of the same kind as the vortices. The recipe lies in a simple decomposition of the dislocation current Eq. (3.52), taken from Kleinert’s book [48]. If one considers a single free dislocation, it can be viewed as a bosonic particle given by a world-line (or world-loop)  $\bar{\mathbf{x}}(s)$  with a Burgers vector  $\mathbf{n}$  attached to it. The bosonic world-line of the dislocation defines a bosonic current in accordance with Eq. (2.37), which we denote by  $\mathcal{J}_\mu$ . Using the bosonic current and the Burgers vector as two independent degrees of freedom, dislocation current is decomposed simply into

$$J_\mu^a = n^a \mathcal{J}_\mu. \quad (4.27)$$

For simplicity, the Burgers vector  $n^a$  will from now on be always considered as a unit vector, while the intensity of the bosonic current  $\mathcal{J}_\mu$  will take care of the difference in Burgers vectors.

In the ordered nematic, where all the Burgers vectors are aligned, the dislocation current decomposition Eq. (4.27) splits the original  $U(1) \otimes U(1)$  gauge structure into two sectors, one parallel to the Burgers vector and one perpendicular to it:  $U(1)^{\otimes 2} = U(1)_\parallel \otimes U(1)_\perp$ . The parallel gauge sector has one bosonic collective field of dislocations to which it minimally couples and accordingly it can be in Coulomb and Higgs phases. On the other hand, in the perpendicular sector there is no such field and the gauge fields from this sector can experience only the Coulomb phase. The argument is quantitative when we consider a single dislocation world-line and couple it to the dual stress gauge fields as given in Eq. (4.16). In terms of the dislocation world-line the minimal coupling becomes

$$\begin{aligned} S_{BJ} &= i \int d\mathbf{x} d\tau J_\mu^a B_\mu^a \\ &= i \int d\mathbf{x} d\tau n^a \oint_C ds \partial_s \bar{x}_\mu \delta[\mathbf{x} - \bar{\mathbf{x}}(s)] \delta[\tau - \bar{\tau}(s)] B_\mu^a = i \oint n^a B_\mu^a \Big|_{\bar{\mathbf{x}}, \bar{\tau}} d\bar{x}_\mu. \end{aligned} \quad (4.28)$$

This equation is in every respect equivalent to the vortex duality coupling derived in Eq. (2.40). In the ordered nematic phase all the dislocations’ Burgers vectors point in the

same direction. Accordingly, only one kind of dislocation (bosonic) defects exists in the system and they are coupled minimally to an effective  $U(1)$  gauge field, given by

$$\mathcal{A}_\mu = n^a B_\mu^a \equiv B_\mu^\parallel. \quad (4.29)$$

Therefore, only stress gauge field components with their flavour parallel to the Burgers vector interact with the disorder field and can be considered relevant (or true) gauge fields. Their orthogonal (with respect to flavour) counterparts  $B_\mu^\perp = \epsilon_{ab} n^a B_\mu^b$  do not interact with any disorder field and they represent the ‘perpendicular’ gauge fields without an associated disorder field.

At this point we introduced new basis in the two-dimensional space defined by Burgers vectors

$$\mathbf{e}_\parallel = \frac{\mathbf{n}}{n}, \quad \mathbf{e}_\perp = “\mathbf{e}_z” \times \mathbf{e}_\parallel. \quad (4.30)$$

This basis will be used at a couple of other instances in the remainder of this thesis for illustrational purposes.

On a more superficial level, the dislocation current decomposition Eq. (4.27) can be used in a single line identity

$$S_{BJ} = iB_\mu^a J_\mu^a = iB_\mu^a n^a \mathcal{J}_\mu = i\mathcal{A}_\mu \mathcal{J}_\mu \quad (4.31)$$

to argue that the coupling of the dual stress gauge fields and the disorder degrees of freedom are equivalent to that of the vortex duality Eq. (2.14).

Finally, we will have to determine the action describing the gas (tangle) of dislocations. Having their Burgers vector stripped off, the dislocations become bare bosonic point particles and, based on the ‘random walker’ construction of section 2.2, the disorder action follows

$$\mathcal{L}_{dist.} = \frac{1}{2c_d^2} |D_\tau \Psi|^2 + \frac{1}{2} |D_i \Psi|^2 + \frac{1}{2} m_\Psi^2 |\Psi|^2 + \lambda_\Psi |\Psi|^4. \quad (4.32)$$

The form of this action is identical to the vortex GLW action Eq. (2.35) since the bare dislocations do not differ much in their dynamical nature from standard XY vortices.

One might worry that the action Eq. (4.32) cannot deal with the constrained dislocation dynamics (i.e. the glide constraint). However, such a constraint can be implemented on the level of the partition function Eq. (4.17) instead of directly on the bare dislocations. Let us illustrate this idea by the glide constraint studied in detail in section 3.4. Before you start thinking how to impose the glide constraint on each single dislocation (that would automatically reduce the dimensionality of action Eq. (4.32), a dangerous statement!), recall that the whole business with the exact mathematical formulation of the glide principle was motivated by the intuitive nature of the classical formulation. That a single dislocation cannot climb is an intuitive claim, based on an intuitive picture of a single dislocation where it actually turns out to be true. In a tangle of dislocations, the glide constraint on each single defect is something with no support in any physical law. At this moment the strictly

mathematically formulated glide constraint Eq. (3.61) shows its full power. When a tangle is formed out of defect world-lines, the collisions between dislocations allow tunneling of interstitial matter. The climb up is therefore possible if supported in material by a nearby dislocation that climbs down. The glide constraint was derived only as a constraint on the total, coarse-grained current density, and it should be applied in the same manner as we do in the remainder of the text. As a curiosity, let us just say that when the glide constraint is invoked in this manner in the phase with no order in Burgers sector, it effectively reduces the dislocation sound velocity  $c_d$  (introduced in the next paragraph) by a factor  $\sqrt{2}$ . This was already shown in Ref. [44] (Appendix C) where the glide constraint was applied to a free dislocation gas. Here that proof is fully justified by means of the field theory and the implicit representation of the glide constraint in terms of Lagrange multipliers. The ‘glide dressed’ velocity is denoted by  $c_g = c_d/\sqrt{2}$ .

The velocity  $c_d$  in Eq. (4.32) is the dislocation second sound velocity. This velocity defines the *relativistic* dislocation dynamics and in this regard it is completely analogous to the vortex velocity  $c_V$  in the vortex duality of chapter 2. One would like to avoid an additional free parameter in the theory, so let us try to find out if the dislocation sound velocity  $c_d$  can be expressed in terms of the existing parameters of the theory in the first place in terms of the phonon velocities Eq. (3.29). In vortex duality, the apparent Lorentz invariant formulation of the zero-temperature problem in Eq. (2.2), as well as the connection of the order propagator Eq. (2.69), lead to the conclusion that the vortex velocity has to be the same as the phase velocity  $c_V = c$ . The corresponding elastic action Eq. (3.24) does not exhibit Lorentz-invariance and the previous argument cannot be used. There is, however, an estimate for the total energy of a moving 3D screw dislocation in the book by Friedel [132]. The sound velocity is directly related to the energy and according to Friedel’s results it follows that  $c_d = c_T$ , i.e. the propagation velocity in the dislocation gas is dictated purely by shear rigidity. In 2+1D, the dislocations can only be of the edge type and the above analysis is not directly applicable. Nevertheless, from the fact that dislocations are tightly related to the shear rigidity, we could argue that the dislocation sound velocity has to be of order of the shear velocity if not equal to it. There are two other arguments supporting this claim. One says that at zero temperature the dislocation second sound velocity has to be a function of the remaining parameters of the theory. Based on dimensional analysis, the only two other parameters that could combine into a velocity are two phonon velocities Eq. (3.29). According to the other argument, the sound velocity in a medium plays the role of light velocity in the vacuum and any excitation with energy larger than the sound velocity should have diverging energy (when the imaginary time is rotated to its real counterpart). The dislocation sound velocity is precisely the velocity where the dislocation defect energy is supposed to diverge so it must not be larger than the longitudinal velocity  $c_L$ .

Following the discussion in the previous paragraph, we may assure ourselves that the physical predictions of our theory stay accurate when we set  $c_d = c_T$ . Whenever any quantitative result is presented this will indeed be the case. However, as long as the theory of the nematic solids is developed in a general theoretical framework, the two velocities will be considered independent. The motivation lies in what we learned from vortex duality: the

separate tagging of the order (spin-wave or phonon) and the disorder (vortex or dislocation) velocities can aid in the proper interpretation of the physical outcomes.

At this point the story of the disorder dislocation fields is still not over. After the decomposition Eq. (4.27), our work was focused entirely on the bosonic current  $\mathcal{J}_\mu$  while the Burgers vector was treated as a constant effective charge, having uniform precise value throughout the whole system. This is not true at all since Burgers vectors of dislocations may vary in space (and time) and the associated configurations lose weight which is ‘measured’ by additional terms in the action. The argument for the existence of two separate nematic phases is based on the assumption that the theory might favour one or another ground state (with respect to the Burgers vector).

To construct this action, we first have to redefine the order parameter associated with the Burgers sector. Dislocations have an interesting property: a dislocation with Burgers vector  $\mathbf{n}$  and a dislocation with Burgers vector  $-\mathbf{n}$  mutually annihilate, so they may be considered as a particle and an antiparticle of the same defect class. Therefore, two tangles of dislocation world-lines, one with Burgers vectors all pointing in the  $\mathbf{n}$  direction and another with the Burgers vectors pointing in the  $-\mathbf{n}$  directions represent exactly the same tangle (the wave-function  $\Psi$  is bosonic and does not discriminate between particles and antiparticles). This  $\mathbb{Z}_2$  local symmetry in the disorder sector has to be obeyed by the ‘disorder field’ order parameter. This is naturally not possible to obtain with a simple vector order parameter field; instead, an order parameter invariant under  $\mathbb{Z}_2$  local gauge transformations should be constructed. Such an order parameter has been known for a long time in the liquid crystal theory [130, 150]. Classical liquid crystals are composed of microscopic rod-shaped particles whose two ends are identical. Due to this  $\mathbb{Z}_2$  symmetry, an order parameter that transforms as a vector is not a good candidate as the orientational order parameter of the liquid crystal. What one does instead is to construct a spin-2 (traceless) tensor out of the orientation vectors  $\mathbf{n}$

$$Q^{ab} = n^a n^b - \frac{1}{2} \delta^{ab}. \quad (4.33)$$

This tensor is the standard order parameter for any  $O(d)/\mathbb{Z}_2$  invariant theory as it is invariant under the symmetry transformation  $\mathbf{n} \rightarrow -\mathbf{n}$ . It is called the director order parameter. However since we use it not to describe orientations of rods, but orientation of Burgers vectors, whenever the director order parameter is constructed from Burgers vectors, we will use the name ‘Burgers director’ order parameter.

An alternative argument for the nematic liquid crystalline order parameter, presented in Ref. [44] is based on the fact that macroscopic ‘ferromagnetic polarization’ of the Burgers vectors is forbidden on grounds of the topological status of the nematic phases. A dislocation may be regarded as a pairing of a disclination and an anti-disclination, separated by a distance equivalent to the Burgers vector. Therefore, a presence of a total Burgers vector that is macroscopically observable and comparable to the system size means that loose disclinations are present in the system and this is topologically forbidden. The dislocations with Burgers charge  $\mathbf{n}$  have, in that respect, to be accompanied by the same amount of the dislocations of  $-\mathbf{n}$  charge. The only observable quantity associated with this pair of excitations is the Burgers director Eq. (4.33).

The theory of liquid crystals represents a glorious discipline of physics often associated with de Gennes who had made significant contributions to the field and presented us with a book on the subject [150]. One of the most relevant results of the liquid crystal theory is a mean field action in terms of the director order parameter Eq. (4.33), which is reminiscent of the GLW action. Based only on the symmetries of the model, Zaanen *et al.* [44] deduced that the most general action, allowed by symmetry, is

$$\mathcal{L}_Q = \frac{1}{2c_Q^2} \partial_\tau Q^{ab} \partial_\tau Q^{ba} + \frac{1}{2} \partial_i Q^{ab} \partial_i Q^{ba} + \frac{1}{2} (m_Q^2 - r_Q |\Psi|^4) Q^{ab} Q^{ba} + \lambda_Q Q^{ab} Q^{bc} Q^{cd} Q^{da} \quad (4.34)$$

The velocity  $c_Q$  is the second sound velocity associated with the Burgers vector degrees of freedom. After the paragraph on the dislocation velocity  $c_d$ , the ‘Burgers velocity’ and its origin should be self-explanatory. In Ref. [44] this velocity was also not explicitly included.

Notice that the cubic term is not present in the action Eq. (4.34), in contrast with a general liquid crystal GLW actions where this term is allowed. The standard action for a liquid crystal is given for the  $O(3)/\mathbb{Z}_2$  director order parameter, whereas in the case of the two-dimensional theory, the order parameter is rather a ‘semi-circle’ of directions and the cubic invariant is forbidden.

An additional peculiarity of action Eq. (4.34) comes from the term  $r_Q |\Psi|^4 Q^{ab} Q^{ba}$ . Such a term is usually not found in actions associated with liquid crystals. The origin of this term lies in the sequence of orderings for the disorder fields. When the action Eq. (4.34) was introduced in Ref. [44], it was argued that the Burgers director field Eq. (4.33) has no physical interpretation before the dislocations, described by the action Eq. (4.32), proliferate forming a tangle (condensate). Therefore, it appears as a requirement to prevent ordering of the liquid crystalline order parameter Eq. (4.33) in the absence of the dislocation condensate. This condition implies that the bare director mass  $m_Q^2$  must be strictly positive. So, if we prohibit the ‘Burgers mass’ term  $m_Q^2$  from being negative, how can Burgers vectors ever order? The answer to this question follows from the parentheses in the third term of the action Eq. (4.34). One can see that the order and disorder of the Burgers director are governed not by the bare mass term  $m_Q^2$ , but rather by an effective mass  $m_{Q,eff}^2 = m_Q^2 - r_Q |\Psi|^4$ . Assuming a second order transition into the nematic phase of a solid, the expectation value of the dislocation field grows as  $|\Psi|^2 \propto \left(\frac{g_c - g}{g_c}\right)^{2\beta}$  and the effective mass follows as  $m_{Q,eff}^2 = m_Q^2 - r' \left(\frac{g_c - g}{g_c}\right)^{4\beta}$ . The coupling constant  $g$  is a control parameter used to express the transition from the ideal crystal to the nematic solid phase. The transition occurs at  $g_c$ . If the bare mass  $m_Q^2$  is strictly zero, upon proliferation of dislocations, the effective mass becomes negative and the Burgers director parasitically develops the order. The resulting ground state is that of the ordered nematic with all the Burgers vectors oriented along the same direction. However, if this mass term is non-zero, the dimensionless coupling  $\frac{g - g_c}{g_c}$  has to exceed a certain value  $g'$  in order for the effective director mass to become negative. Hence, a state with disordered Burgers vectors is anticipated in the region  $g_c < g < g'$  of the coupling constant.

After the disorder (dislocation) field has been decomposed into a pure bosonic and Burgers sector, and appropriate fields and actions are assigned to each one of them, the

path integral under quotation marks in Eq. (4.17) can be substituted by the precisely mathematically defined path integral over a bosonic dislocation field and over a Burgers vector field

$$Z = \int \mathcal{D}B_\mu^a \mathcal{D}\Psi \mathcal{D}n^a \prod_b \mathcal{F}^b(B_\mu^a, n^a, \Psi) \prod_{a \neq b} \delta(\epsilon_{a\nu\mu} \partial_\nu B_\mu^b) e^{-\int dx_\nu \mathcal{L}_{dual}}. \quad (4.35)$$

The pair of gauge fixing currents  $\mathcal{F}^b$  acts not only on the dual stress gauge fields, but also on the bosonic field since its transformation is governed by the Burgers vector

$$\Psi \rightarrow \Psi' = \Psi e^{in^a \alpha^a}. \quad (4.36)$$

The full dual action of the nematic phase  $\mathcal{L}_{dual}$  contains the stress ‘Maxwell’ part (Eq. (4.16) without the current coupling), the bosonic GLW action Eq. (4.32), and the Burgers liquid crystalline action Eq. (4.34).

The schematic phase diagram of the melting of an elastic solid is given in Fig. 4.1. On the left side, there is the ideal crystal phase with a perfect order of displacement fields and long-range correlations of phonon propagators. This phase is characterized by a ground state that breaks all translational and rotational symmetries. On the right side, we find a superfluid where, due to the complete quantum disorder, the displacement field is completely disordered and, apart from the superfluid sound, there are no long-ranged correlations. In this phase both translational and rotational symmetries are fully restored by the proliferation of disclination defects. With the condensation of the disclination defects, the dislocations come for free in this phase, as suggested by Eq. (3.51). Resting on symmetry arguments, the transition between these two phases has to be first order.

The type of melting that we are interested in is the one where only dislocation defects proliferate while the disclinations stay massive. There is a precisely defined prerequisite in order to keep disclinations massive and allow free proliferation of dislocations. Recall the second-order gradient energy term Eq. (3.19) and its second term that defines the energy costs of curvature in the system. The disclinations are associated with the curvature so a high value of  $\ell$  means that a disclination requires a large amount of energy in order to be created. The dislocations, on the other hand, have their rest mass barely dependent on the curvature rigidity  $\ell$ . It is therefore possible, for large enough values of the rotational stiffness, to achieve proliferation of dislocations while simultaneously disclinations cannot proliferate as their kinetic energy gain cannot compensate for the high potential energy costs. This part of the phase diagram we call the nematic phase – the translational symmetries are restored in one or all directions, while the rotational symmetry is still broken. Such an intermediate phase in classical solids has already been predicted [45, 46, 47, 48], but its splitting into the ordered and topological phases was only recently realized [44]. Close to the end of this chapter, the diagram will be revised and an additional phase will be added. It will also be argued that an emergent rotational symmetry may take place in the topological nematic in spite of the absence of disclinations.

The position of the transition line between the order and disorder in the Burgers sector is tilted so that the ordered nematic phase is closer to the superfluid phase whereas the

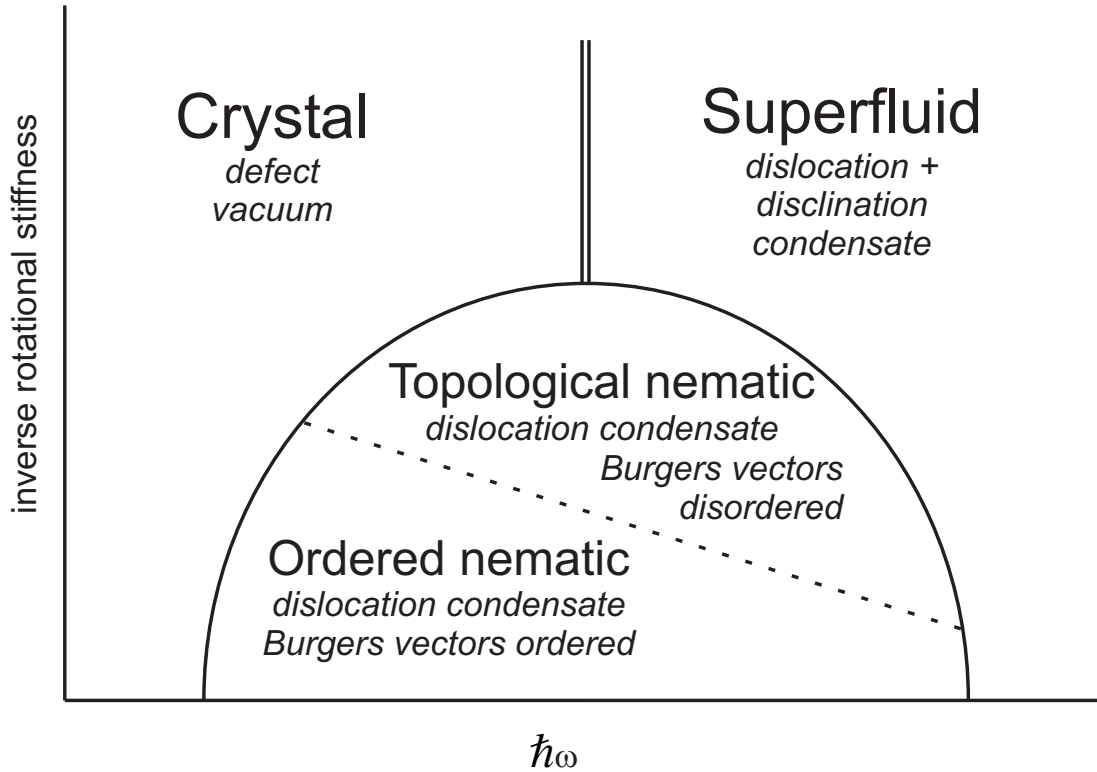


Figure 4.1: Suggested phase diagram of a quantum elastic solid at zero temperature [44]: The disorder is given on the horizontal axis. In the left part of the phase diagram the ideal crystal is realized, representing a defect vacuum in the dual language. On the right, superfluid may be seen as a condensate of both dislocation and disclination defects. On the vertical axis, the inverse rotational stiffness is given. It controls the ratio of dislocation to disclination rest mass, and thus allow the existence of the nematic phases, which are the dual dislocation condensates with disclination defects preserved massive.

ordered nematic phase is closer to the ideal crystal. The location of the transition line between ordered and topological nematic follows from a mere heuristic argument. What is the most important agent that takes care of the disorder of the Burgers directors? As the disorder increases, bound pairs of disclinations and antidisclinations grow in size and right at the transition point to the superfluid phase, their size diverges. It is important to notice that these bound pairs do not have a direct influence on the long-wavelength dynamics in the nematic phase. At short scales, however, a moving dislocation that passes once thorough the loop rotates its Burgers vector precisely by an angle given by its Frank charge [151]. Therefore, in the vicinity of the superfluid phase the ‘angular delocalization’ of the Burgers vector is favoured and one expects a phase where dislocation defects lose any sense of the Burgers vector direction. Unfortunately, currently the ‘topology’ of the phase diagram cannot be determined more precisely, i.e. based on solid arguments we

cannot make any claims regarding the ending points of the topological to ordered nematic transition line.

In Ref. [44] where the topological nematic phase was introduced for the first time, this phase was considered to be a phase of matter where one has to identify dislocations without referral to their Burgers vector. This is an isotropic state of matter which is not the same as an isotropic superfluid because disclination defects are massive. This phase is impossible to envisage starting from the classical picture of a gas of rods. Nevertheless, a topologically ordered state like this was identified before with use of elegant arguments based on gauge invariance. In their papers [152, 153], Lammert, Rokhsar and Toner realized that in a theory based on Eq. (4.34), which is characterized by the Ising ( $\mathbb{Z}_2$ ) gauge symmetry  $\mathbf{n} \rightarrow -\mathbf{n}$ , the only meaningful object is the director Eq. (4.33). They argued that the theory can be generalized by making the gauge symmetry explicit in terms of rotors  $\mathbf{n}$  minimally coupled to Ising gauge fields  $\sigma^z$  living on lattice links (the theory is regularized on a lattice) with Hamiltonian

$$\hat{H} = -J \sum_{\langle i,j \rangle} \mathbf{n}_i \sigma_{ij}^z \mathbf{n}_j - K \sum_{\langle i,j,k,l \rangle} \sigma_{ij}^z \sigma_{jk}^z \sigma_{kl}^z \sigma_{li}^z. \quad (4.37)$$

The first term represents the minimal coupling of the rotors and the gauge field. The second term of the Hamiltonian is the Ising-Wilson action corresponding to a product of Ising variables on a plaquette. This action Eq. (4.37) is gauge invariant under  $\mathbb{Z}_2$  gauge symmetry defined in the following way: each  $\mathbb{Z}_2$  transformation of a rotor at site  $i$  is accompanied by the simultaneous flipping of Ising fields sitting on links that originate from the flipped rotor ( $\sigma_{ij}^z$ ). It is well known that this model has three phases:

1. A Higgs phase, where the rotors are ordered and the gauge fluxes (frustrated plaquettes) are confined;
2. A confining phase, where the rotors are disordered and the gauge fluxes proliferate;
3. A Coulomb phase, with the rotors disordered while gauge fluxes are confined; this state carries topological order.

Identifying the rotor degrees of freedom with Burgers vectors and gauge fluxes with  $\pi$ -disclinations, Zaanen *et al.* concluded that the Higgs phase of the LRT model Eq. (4.37) corresponds to the ordered nematic phase, the confining phase corresponds to isotropic phase, i.e. superfluid (Burgers vectors disordered and disclinations proliferated) and finally, the Coulomb phase should be related to the topological nematic phase (therefore the name, due to the topological order in the Coulomb phase), since the Burgers vectors are disordered and the topological excitations are massive.

The theory of quantum melting presented in this thesis is, however, a much richer theory than the LRT model (Eq. (4.37)). While the LRT theory describes the Burgers sector with great accuracy, the dual elastic theory contains many other degrees of freedom besides the Burgers vector. If the LRT theory offered the entire description of the topological nematic and isotropic phases, there would be no measurable differences between the superfluid and

the topological nematic phase apart from the massiveness of disclinations. We are however equipped with many other correlation functions, primarily phonons expressed by means of displacements. When we try to describe the topological nematic in a later section and arrive at a ‘suspicious’ result, it will seem that the two phases are entirely different, and as if the topological nematic of ours resembles a regular solid at low energies. The first argument for the difference between the topological nematic and the superfluid phase was based on the symmetry restorations in each of the phases. In the absence of disclinations it was expected to have the rotational symmetry still broken. A state with broken global rotational symmetry may develop a Goldstone mode associated with that symmetry breaking [154]. This Goldstone mode is ‘hidden’ behind the translational photon which occurs due to the translational symmetry breaking, but when all the translational symmetries are restored by the ground state, the ‘rotational Goldstone mode’ can show itself in the full light.

However, it turns out after the discussions in the last two sections that the theory developed for the disordered nematic is in fact describing another nematic phase. In place of one Burgers condensate with no well-defined Burgers director, this phase is characterized by many independent condensates that ‘average’ all the directions resulting in the total Burgers director  $\hat{Q} = 0$ . The symmetry argument from the previous paragraph is in fact applicable to this newly found ‘isotropic nematic’ phase. It is left for the discussion in this chapter and later for the conclusion to discuss possible restoration of the rotational symmetry in the phase with *one* dislocation condensate that has no sense of Burgers vectors.

Although counter-intuitive and not easy to accept for many, the concept of an isotropic ground phase with a ground state that breaks the rotational symmetry is repeated in a far more familiar setup: the translational symmetry breaking. There, a solid that is *homogeneous* has a ground state which *breaks the translational symmetry*. Let us just add that the isotropic solid with elasticity tensor Eq. (3.15) is another example of an isotropic system that breaks rotational symmetry.

### 4.3 Ideal crystal as the dual Coulomb phase

That elastic solids can be mapped onto a flavoured Maxwell theory was already demonstrated in section 4.1. At this point in the thesis this fact is used to consider different phases of elasticity theory in terms of the dual theory and their respective phases. In analogy with the Abelian-Higgs duality, here the dual Coulomb phase represents the original ordered phase, which is precisely the ideal crystal phase. This phase, now represented via the dual theory, will be studied in detail in this section. Let us mention the other phases that are considered in later chapters. There are various ways to destroy the crystalline order. The dual theory constructed in the previous two sections cannot deal with the disclination defects and therefore the superfluid phase stays out of our reach. Nevertheless, that phase can be successfully described starting from the opposite limit: the ‘gas’ of free particles. In between, the nematic ‘dome’ represents the phase where the crystal is disordered purely by means of the dislocations. The dual elastic theory seems to be

the right choice for these phases. In the previous section it was demonstrated that out of two ‘flavoured’ dual Maxwell theories, only one, that parallel to the Burgers vector, has a minimally coupled matter field and accordingly only that ‘flavour’ of the Maxwell theory can undergo the transition. In that regard, the ordered nematic phase corresponds to the dual Higgs phase realized in one of the ‘flavours’ and the dual Coulomb phase in the another. Finally, when the dual theories with each of the flavours are treated equally and both undergo the transition to the Higgs phase, the isotropic nematic phase is obtained.

Based on our experience with vortex duality, one might expect that the construction of the dual theory for the ideal crystal is only a slight detour via dual stress gauge fields to trivial results already obtained in section 3.2. Such a fairly simple task could then be joined with some other section and not have a section of its own. However, due to some steps in the dual elasticity which are not trivial even in the Coulomb phase, the treatment of the ideal crystal deserves its own section. As we begin to implement the dual theory and try to obtain the phonon propagators in this section, it will become clear that a direct Zaanen-Mukhin relation, analogous to Eq. (2.55) *cannot* be derived for the dual elastic theory, primarily because of the fact that the elastic tensor is singular. This problem can be circumvented and the phonon propagators can actually be expressed in terms of the gauge field propagators. However, the resulting formalism becomes fairly nontrivial, so only after a quite lengthy detour, we get to the theory resembling the Coulomb phase of the dual vortex model in chapter 2. A few of the tricks that we learn in this section will be quite important in the two following sections and in this respect, this section may be regarded as a tutorial on the proper implementation of constraints and gauge fixing in the dual elastic theory in general. This is another reason for this section to find its place at this stage of the thesis. In spite of the fact that the theory for the dual elastic Coulomb phase, that is the ideal crystal, does not involve any kind of disorder and could have been developed accordingly before the treatment on defects in section 4.2, we thought that it would be better if the three phases are presented together in a sequence of increasing complexity in the underlying physics. In this way, the experience gained in the construction of a theory for each phase is transferred to the next, more complex, section. For example, the ‘modified Zaanen-Mukhin’ relation for the singular elastic tensor is introduced in this section to be further generalized and employed in sections on the ordered and topological nematic. Also, the Higgs mechanism exhibited by the dual stress gauge fields in the ordered nematic is in a way further generalized in the section on the topological nematic.

After the problem with the singular coupling constant related to the Ehrenfest constraint is removed, this section continues with the interpretation of the dual stress gauge fields as photons and dislocation Coulomb forces in analogy with the Coulomb phase of the Maxwell theory.

The easiest way to probe an elastic solid is by means of phonons defined via propagators Eqs. (3.33) and (3.34). When the dual theory is in charge, these propagators have to be expressed in terms of the dual stress field propagators. The naive generalization of the Zaanen-Mukhin relation Eq. (2.55)

$$\langle\langle\partial_\mu u^a|\partial_\nu u^b\rangle\rangle = C_{\mu\nu ab}^{-1} - C_{\mu\kappa ac}^{-1}C_{\nu\lambda bd}^{-1}\langle\langle\sigma_\kappa^c|\sigma_\lambda^b\rangle\rangle \quad (4.38)$$

is not well-defined as the elastic tensor Eq. (3.25) does not have an inverse ( $C^{-1}$ ) and we cannot use it directly. This is at least true for the transversal propagator because it is defined as the propagator between the local rotations for which the singularity is present. Although we cannot use the direct ‘Zaanen-Mukhin’ relation Eq. (4.38), the wisdom that led to the original relation Eq. (2.55) can be used here with a careful eye on the singularity in order to obtain the relation between the dual and phonon propagators. When we are not interested in elastic propagators, as in the following chapter, the dualization as explained in section 4.1, with the singularity implemented in the form of the standard Ehrenfest constraint, is sufficient.

In order to derive the relation between the dual and original propagators, we begin in the style of the ‘Zaanen-Mukhin’ derivation, by adding two external source terms to the action Eq. (3.24),  $\mathcal{K}$  for the longitudinal and  $\mathcal{J}$  for the transversal propagator

$$\mathcal{L}_0[\mathcal{K}, \mathcal{J}] = \mathcal{L}_0 + \mathcal{K}\delta_{ia}\partial_i u^a + \mathcal{J}\epsilon_{\tau ia}\partial_i u^a = \mathcal{L}_0 + \mathcal{K}\delta_{ia}P_{ijab}^{(0)}\partial_j u^b + \mathcal{J}\epsilon_{\tau ia}P_{ijab}^{(1)}\partial_j u^b. \quad (4.39)$$

The closure relation Eq. (4.3) is inserted in the external source terms, leaving only the relevant projections. The action Eq. (4.39) can now be dualized using the recipe described in section 4.1. The difference between this case and the one in the former section, without the external source terms, is that Eqs. (4.4 - 4.6) now change into

$$P_{ij,ab}^{(0)}\sigma_j^b = -id\kappa P_{ij,ab}^{(0)}\partial_j u^b - i\mathcal{K}P_{ij,ab}^{(0)}\delta_{jb}, \quad (4.40)$$

$$P_{ij,ab}^{(1)}\sigma_j^b = -iP_{ij,ab}^{(1)}\epsilon_{\tau j b}\mathcal{J}, \quad (4.41)$$

$$P_{ij,ab}^{(2)}\sigma_j^b = -i2\mu P_{ij,ab}^{(2)}\partial_j u^b. \quad (4.42)$$

Two of the strain projections  $P^{(0)}\partial u$  and  $P^{(2)}\partial u$  can be found from the relations Eq. (4.40) and Eq. (4.42) respectively. The spin-1 relation just imposes the Ehrenfest constraint on the gauge fields, letting the generating functional  $\mathcal{J}$  be the difference of two antisymmetric stresses

$$\epsilon_{\tau ia}\sigma_i^a = -i2\mathcal{J}. \quad (4.43)$$

The Ehrenfest constraint is however not lifted as the external sources are set to zero at the end of calculation.

The remaining strain components  $P^{(1)}\partial u$  cannot be expressed in terms of dual stress fields but this does not pose any problem as it completely drops out of the Hamiltonian

$$\mathcal{H}[\mathcal{K}, \mathcal{J}] = -i\sigma_\mu^a\partial_\mu u^a + \mathcal{L}_0[\mathcal{K}, \mathcal{J}] = \frac{1}{2}\sigma_\mu^a C_{\mu\nu ab}^{-1}\sigma_\nu^b - \frac{1}{2}\frac{\mathcal{K}^2}{\kappa} + \frac{i}{\kappa}\mathcal{K}\sigma_a^a. \quad (4.44)$$

Given that the dual Lagrangian contains the Hamiltonian Eq. (4.44) and given that the dislocation currents do not couple to the external source field  $\mathcal{K}$ , the longitudinal propagator follows directly as

$$G_L = \langle\langle\partial_a u^a|\partial_b u^b\rangle\rangle = \frac{1}{\kappa} - \frac{1}{\kappa^2}\langle\langle\sigma_a^a|\sigma_b^b\rangle\rangle. \quad (4.45)$$

This result is in agreement with the incomplete Mukhin-Zaanen relation Eq. (4.38), as expected. In the longitudinal sector, relation Eq. (4.38) does not involve the singular subspace of the elasticity tensor. In the remainder of the text, there is no need for the external source field  $\mathcal{K}$  since relation Eq. (4.45) is valid in all phases. Therefore, we keep only the transversal phonon external source field  $\mathcal{J}$  explicit in the remainder of the text and use the ‘longitudinal Zaanen-Mukhin’ relation Eq. (4.45) when we need the longitudinal phonon propagator.

With the transversal propagator and its external source field  $\mathcal{J}$  the derivation is more subtle as we observe that it is missing from the Hamiltonian Eq. (4.44). A general formalism is not easy to obtain and we are left to explicitly impose the Ehrenfest constraint with the external source term, Eq. (4.43). After that step, explicit external source terms are found in the dual action and the ‘singular Zaanen-Mukhin’ relation follows directly. Before doing that, let us first write the partition function (generating functional)

$$Z[\mathcal{J}] = \int \mathcal{D}B_\mu^a \mathcal{D}J_\mu^a \mathcal{F}^b(B_\mu^a) \delta(\partial_a B_\tau^a - \partial_\tau B_a^a + i2\mathcal{J}) e^{-S_{dual}[B_\mu^a]}. \quad (4.46)$$

Although we set internal currents strictly to zero in the ideal crystal, the path integral over currents in Eq. (4.46) is kept since this partition function can be used in the next two sections. In this section, we can freely remove that term and allow only external dislocation currents (controlled from the outside) as the only source terms for the dual stress gauge fields.

For simplicity, the fields are Fourier transformed and their components are expressed in the momentum basis (‘zweibeinen’, Eq. (1.3)) rather than in the Cartesian one. The dual action splits into two decoupled parts: longitudinal, governing the physics related to the longitudinal propagator

$$\begin{aligned} \mathcal{L}_L = & \frac{1}{2} \frac{1}{2\mu(1+\nu)} \begin{pmatrix} B_\tau^T \\ B_L^T \\ B_T^L \end{pmatrix}^\dagger \begin{pmatrix} q^2 & -iq\omega & -i\nu q\omega \\ iq\omega & \omega^2 & \nu\omega^2 \\ i\nu q\omega & \nu\omega^2 & \omega^2 + (1-\nu^2)c_L^2 q^2 \end{pmatrix} \begin{pmatrix} B_\tau^T \\ B_L^T \\ B_T^L \end{pmatrix} \\ & + iB_\tau^{T\dagger} J_\tau^T + iB_L^{T\dagger} J_L^T + iB_T^{L\dagger} J_T^L; \end{aligned} \quad (4.47)$$

and transversal

$$\begin{aligned} \mathcal{L}_T = & \frac{1}{2} \frac{1}{4\mu} \begin{pmatrix} B_\tau^L \\ B_L^L \\ B_T^T \end{pmatrix}^\dagger \begin{pmatrix} q^2 & -iq\omega & iq\omega \\ iq\omega & \omega^2 & -\omega^2 \\ -iq\omega & -\omega^2 & \omega^2 + 4c_T^2 q^2 \end{pmatrix} \begin{pmatrix} B_\tau^L \\ B_L^L \\ B_T^T \end{pmatrix} \\ & + iB_\tau^{L\dagger} J_\tau^L + iB_L^{L\dagger} J_L^L + iB_T^{T\dagger} J_T^T. \end{aligned} \quad (4.48)$$

All the dislocation currents are written without the usual *ext.* label, but we implicitly assume that their origin is external – someone has introduced them in the system as part of a (linear response) experiment.

There is some similarity between the dual vortex action Eq. (2.9) and the dual elastic action Eqs. (4.47) and (4.48). In each sector there is a non-dynamical Coulomb force photon  $B_\tau^{L,T}$  and one longitudinal and one transversal photon (with respect to lower indices).

Notice however, that each transversal photon, supposed to carry order excitations, *is not decoupled* from the other two (Coulomb and longitudinal) photons in its sector. Their bare propagation velocities are also not the respective phonon velocities. This should not worry us since the gauge fields are a mathematical construct which, as we learned in chapter 2, acquires true physical meaning only after the gauge fixing condition(s) have been implemented and non-dynamical degrees of freedom have been removed. An additional subtlety lies in the transversal sector, where the Ehrenfest constraint removes one additional degree of freedom. After all such considerations are taken into account, the phonon propagation velocities get dressed to their true values and all degrees of freedom decouple in a natural way.

Let us start with the longitudinal sector. In the ideal crystal there are no other constraints in this sector apart from the gauge fixing which allows us to integrate out the Coulomb photon  $B_\tau^T$  which has no dynamics (propagator is  $q^2$ ). This photon is minimally coupled to dislocation current with transversal label  $J_\tau^T$ , but it also couples to the other two photons. When removed the following longitudinal action is obtained

$$\begin{aligned} \mathcal{L}_L = & \frac{1}{2} \frac{4\kappa\mu}{\kappa + \mu} \frac{J_\tau^{T\dagger} J_\tau^T}{q^2} + \frac{1}{2\rho} B_T^{L\dagger} \left( \frac{\omega_n^2}{c_L^2} + q^2 \right) B_T^L + \\ & iB_L^{T\dagger} \left( J_L^T - \frac{i\omega_n}{q} J_\tau^T \right) + iB_T^{L\dagger} \left( J_T^L - \nu J_L^T \right). \end{aligned} \quad (4.49)$$

The first term represents the static Coulomb interaction between defects of the same, transversal, Burgers flavour. In two cases the interaction energy between the dislocations vanishes, when either the shear or compression modulus is zero. The former corresponds to a liquid where dislocations come for free, while the latter case cannot exist in nature: However it would correspond to a ‘compressionless’ solid where the excess row of atoms (constituting a dislocation) can be stacked on a top of another row at no energy costs. The second term contains the propagator for the longitudinal phonon, represented here by the transversal gauge field photon  $B_T^L$ . The transversal photon carries smooth (phonon) excitations in analogy with the dual vortex theory, except that the dual elastic gauge fields carry flavours. Its propagation velocity is dressed back to the expected longitudinal phonon velocity  $c_L$ . The third term couples the longitudinal photon  $B_L^T$  to a linear combination of currents which vanishes since even the externally added currents must obey the conservation law. The longitudinal component is anyway not physical and is removed in the Coulomb gauge

$$0 = \partial_i B_i^T = -q B_L^T \quad (4.50)$$

The minimal coupling between the photon  $B_T^L$  (corresponding to the longitudinal phonon) and the defect currents is again nontrivial, owing to the tensorial nature and symmetries of the system. Coupling to the dislocation current  $J_L^T$  is acquired from the removed unphysical longitudinal gauge field  $B_L^T$ . Identifying the current components as irreducible representations of the rotation symmetry group (appendix C), the coupled current is expressed as a linear combination of the external glide (compression) and ‘electric’ shear

dislocation currents

$$J_T^L - \nu J_L^T = \frac{1 + \nu}{2}(J_T^L - J_L^T) + \frac{1 - \nu}{2}(J_T^L + J_L^T). \quad (4.51)$$

It readily follows that the longitudinal phonon couples to a mixture of the two defect currents, depending on the Poisson ratio  $\nu$ . In the unphysical limit of the compressionless solid  $\nu = -1$ , only shear rigidity exist and, accordingly, only the shear current couples to the physical degrees of freedom. In the opposite limit,  $\nu = 1$ , the liquid has no shear rigidity and only the glide current couples to the longitudinal phonon. Although one may think that the glide current in Eq. (4.51) should be set to zero as a consequence of the glide constraint, this is not correct. The glide constraint Eq. (3.61) was derived for internal dislocation currents without external influence. Currents in Eq. (4.51) are, on the other hand, external currents and there is no reason that an outside observer/experimentalist cannot violate the glide principle by simple particle injection.

Let us now tackle the transversal sector, Eq. (4.48), where the situation is more subtle due to the indirect action of external source field  $\mathcal{J}$  via the Ehrenfest constraint Eq. (4.43). One of the ways to implement the constraint Eq. (4.43) is via a Lagrange multiplier term that would couple both to the external source field  $\mathcal{J}$  and to the gauge fields. Then, after the gauge fixing has been implemented and the gauge fields have been integrated out, the Lagrange constraint acquires a propagating nature (quadratic term) which allows us to integrate it out by means of a Gaussian integration. This produces an expression which should yield the transversal propagator through the generating functional. Although seemingly quite universal, this implementation of the Ehrenfest constraint involves a gauge fixing procedure which has to be different from phase to phase. We therefore eschew such a procedure and instead invoke the Ehrenfest constraint in the most natural way, by explicit removal of one of gauge field components in favour of other two fields and the generating constraint.

After the Fourier transformation, the Ehrenfest constraint Eq. (4.43) becomes

$$-qB_\tau^L + i\omega_n B_E^E = -2i\mathcal{J}, \quad (4.52)$$

and we eliminate the Coulomb photon  $B_\tau^L$  in favour of the other two. Generally, the physical results are the same if we remove any other component. We wish, however, to make an action in the transversal sector where one can directly interpret gauge photons in terms of physical degrees of freedom. Since we expect the transversal photon  $B_T^T$  to carry smooth (transversal) displacements, it is better to leave it explicit in the action. Whether one choses to remove the Coulomb  $B_\tau^L$  or longitudinal  $B_L^L$  photon, the final action remains the same.

We choose the Coulomb photon since it is usually removed first in any treatment of gauge theories. In the dual elastic gauge theory, the absence of the Coulomb photon in the transversal sector has a precise physical implication: in an elastic solid described by a linear elastic theory, there are no forces between static dislocations with longitudinal Burgers charges. When the second-order gradient terms are in charge, the dual theory admits

additional dual degrees of freedom (fields called  $\tau$  and  $\tau'$ , for details see Kleinert, Ref. [48]) corresponding to second order gradient rigidities. The Ehrenfest constraint appears to be softened as it acts not only on gauge fields, but also on the new dual degree of freedom  $\tau$ . Hence, one can remove the new, curvature degree of freedom and keep the ‘longitudinal’ Coulomb interaction. The interaction is however short-ranged with a characteristic fall off length  $\ell$ . Thus, when interested in physical answers at length scales greater than  $\ell$ , the Coulomb interaction between Burgers longitudinal flavours becomes irrelevant.

Upon elimination of the Coulomb photon, the action including the external currents reads

$$\begin{aligned} \mathcal{L}_T = & \frac{1}{2\rho} B_T^{T\dagger} \left( \frac{\omega_n^2}{c_T^2} + q^2 \right) B_T^T + i B_L^{L\dagger} (J_L^L - \frac{i\omega_n}{q} J_\tau^L) + i B_T^{T\dagger} (J_T^T - J_L^L) \\ & - \frac{1}{2\mu} \mathcal{J}^\dagger \mathcal{J} + \frac{1}{\mu} i \omega_n B_T^{T\dagger} \mathcal{J} - \frac{2}{q} J_\tau^{L\dagger} \mathcal{J}. \end{aligned} \quad (4.53)$$

The first term is the propagator of the transversal photon  $B_T^T$  which has taken the role of the transversal phonon as expected. The propagation velocity is  $c_T$  in contrast with Eq. (4.48). The second term contains the coupling of a non-physical longitudinal photon  $B_L^L$  to the current conservation identity, as usual. The longitudinal photon is removed by the second Coulomb gauge fixing  $B_L^L = 0$ . The third term couples the transversal photon to a specific external dislocation current, namely the magnetic shear current  $J_T^T - J_L^L$  (see Appendix C). This current, together with the electric shear dislocation dynamical current, represents the shear current doublet which transforms under the spin-2 irreducible representation ( $E_{2,-2}$ ). The remaining ‘rotation’ current  $J_T^T + J_L^L$  is decoupled as a consequence of the Ehrenfest constraint, or equivalently the absence of the rotational rigidity in the elastic action Eq. (3.24).

At last, the external source field  $\mathcal{J}$  is present explicitly in the second line of Eq. (4.53). We may neglect the last term since we are not interested in the influence of external dislocation currents on the elastic propagators. In fact, such a term exists even in the longitudinal sector, coupling the external source field  $\mathcal{K}$  with the external dislocation currents, as well as in the dual vortex theory where the external source field  $\mathcal{J}_\mu$ , which was the key ingredient in the derivation of the Zaanen-Mukhin relation, is coupled to the external vortex currents in Eq. (2.55). Just as here, they were left out.

Relying only on the first two terms in the second line of Eq. (4.53), the ‘transversal Zaanen-Mukhin’ relation is found to be

$$G_T = \frac{1}{\mu} - \frac{1}{\mu^2} \omega_n^2 \langle\langle B_T^{T\dagger} | B_T^T \rangle\rangle. \quad (4.54)$$

This relation reproduces the transversal propagator of the ideal crystal, Eqs. (3.31, 3.34). We must notice that Eq. (4.54) is unfortunately not the general relation applicable in all phases. Namely, we circumvented the problem of the singular elasticity tensor by an explicit elimination of one of the gauge fields. In the process we used the gauge field propagator from Eq. (4.48) which are valid only in the Coulomb phase – the ideal crystal.

Whenever the gauge field propagator in the transversal sector acquires additional terms, the ‘second line’ in action Eq. (4.53) has a different form, a major consequence is that a new ‘Zaanen-Mukhin’ relation has to be derived in the transversal sector. This is of great importance to us since additional (Higgs) terms are present in the nematic phases and we will have to recalculate the ‘Zaanen-Mukhin’ relations for both the ordered and the topological nematic.

At this point, the lengthy detour amounting to exercising the duality of the ordered phase of a solid is completed. We have demonstrated that the phonon propagators can be recovered in the dual language. The dual elastic theory is quite similar to the vortex dual theory except that “it repeats itself twice”, once in the longitudinal and once in the transversal sector. In analogy with vortex duality, in the ideal crystal a Coulomb gauge fixing is imposed in each sector so that the gauge fields acquire a specific physical interpretation. The most important part of this section is that we learned how to treat the Ehrenfest constraint in a way such that the appropriate ‘Zaanen-Mukhin’ relations can be derived despite the singular nature of the elasticity tensor Eq. (3.25).

## 4.4 The ordered nematic phase of a solid

In the previous section we have presented the dual treatment of the elastic theory for the simplest case of the ideal crystal. Next to getting some familiarity with dual gauge fields, we learned how to treat the Ehrenfest constraint in a proper way in order to extract the ‘transversal Zaanen-Mukhin’ relation Eq. (4.54) which is otherwise not possible to obtain due to the singularity in the elasticity tensor. In this section, we derive the first truly novel results of this chapter, the theory of the ordered nematic phase of a solid. When the dual elastic theory was derived in section 4.1, the next step was relatively easy to guess from the parallels drawn between vortex and elastic duality. One needs to introduce the disorder in the system via a condensate of defects and the disordered phase is easily accessible by means of dual fields. In vortex duality, the disordered phase corresponds to the incompressible Bose-Mott insulator. In the dual elasticity theory, the richer defect structure makes possible several disordered phases (Fig. 4.1). Each of these states of matter can be regarded as a melted solid given that some kind of crystalline order has been destroyed. Conceptually, condensates of topological defects were recognized a long time ago as the proper way to describe disordered/melted phases of solids [70, 105, 106, 107, 108, 109, 110, 111, 112, 113]. Beginning in this section we employ that wisdom in order to construct new interesting quantum phases of matter.

In this particular section, we focus on the ordered nematic phase. Given that this phase is characterized by a well-defined value for the Burgers director, we leave out its fluctuations as they would be beyond the scope of Gaussian/mean field theory. Therefore, the effective field theory is derived without explicit use of the Burgers field action Eq. (4.34). In the remainder of this section every time we encounter the Burgers vector, it will be assumed that this vector has a predefined value, constant throughout the entire system. Resting on this assumption, we can construct two ‘flavour’ components of the gauge fields, the parallel

and perpendicular ‘flavoured’ gauge fields  $B_\mu^\parallel$  and  $B_\mu^\perp$  respectively. Based on the dislocation action Eq. (4.32) that was constructed in the section on defect dynamics, we conclude that the stress gauge field components with ‘parallel flavour’ exhibit the Higgs mechanism and as a consequence become short ranged when the dislocation defects proliferate. One has to be careful, however, since there are two important constraints lurking in the theory, the Ehrenfest constraint in its ‘external source term’ form Eq. (4.43) and the glide constraint Eq. (3.61). The latter played no role until now, but since we now invoke internal dislocation currents, it has to be strictly imposed. These two constraints influence the stress gauge fields and the Higgs term in a way such that it is still possible to have some degrees of freedom which are massless despite their presence in the bare Higgs term. The degree of freedom associated with compression rigidity is of this kind. Due to the form of the glide principle, the elastic solid never loses its long-range compression rigidity, at least as long as it does not have a reservoir to exchange particles with it.

In the case of vortex duality, we learned that the Coulomb gauge fixing used in the previous section, is not the best choice for the gauge fixing in the Higgs phase. Instead, it is better to use Lorentz gauge fixing with the vortex sound velocity Eq. (2.74). In the case of the elastic Higgs phase, the disorder is caused by the dislocation tangle and hence the best choice for the gauge fix seems to be Lorentz gauge fixing with the dislocation velocity  $c_d$ . Using that gauge fixing, we first find the ‘ideal crystal’ contribution to the gauge field propagator in matrix form and subsequently define the bare Higgs term and implement the constraints in a proper way that takes care that degrees of freedom such as compression are not subject to the Higgs mechanism. The ‘ideal crystal’ and the ‘constrained Higgs’ contributions constitute the total propagator of the gauge fields. In the process, the ‘transversal Zaanen-Mukhin’ relation is obtained for the ordered nematic. One expects intuitively that the ordered nematic phase be highly anisotropic with a liquid-like behaviour along the Burgers vector direction, where the translational symmetry is restored, and a solid-like behaviour in the perpendicular direction, owing to the persisting symmetry breaking. The results we obtain show anisotropy, but the periodicity of screening, as we rotate our ‘experiment’, is not  $\pi$  as expected from the previous argument but  $\pi/2$  instead. Although counterintuitive at first, this result makes perfect sense once we realize where the Higgs gap of the dual stress fields comes from. When the constraints are imposed in the dual theory of the ordered nematic, the only two allowed dislocation currents will be the electric and magnetic shear currents (see Appendix C), and in fact only one of them will be responsible for the Higgs mechanism. Given that these two currents transform as a spin-2 doublet under spatial rotations, the screening periodicity begins to make sense. We do not wish to give away already which shear component is screened in what direction before we obtain the final results towards the end of the section. Let us just suppose that we orient our ‘experiment’ with respect to the Burgers vector in such a way that the magnetic shear is screened whereas the electric shear stays unaffected by the Higgs mechanism. If the experiment is rotated by 90 degrees, the screened shear component transforms into itself modulo a minus sign, which is of no importance since the observables associated with Higgs gap are always about its absolute value. Quite counterintuitively, one should rotate

the screening direction by 45 degrees in order to cause screening in the longitudinal sector (electric shear) and keep the transversal sector unchanged. Hopefully, we managed to convince the reader using only words, that the screening has a spin-2 character, based on symmetry arguments. The argument becomes precise when the Higgs term is determined later in this section.

When the propagation of a phonon makes an intermediate angle value (not 0,  $\pi/2$  or  $\pi/4$ ), the screened shear component is a mixture of both electric and magnetic shear. The Higgs term therefore creates coupling between the longitudinal and the transversal sector of the action. Due to this coupling, computing the phonon propagators in the intermediate propagation directions becomes tedious, involving bi-cubic roots as poles of the propagators. We will find the exact inverse propagators for the dual stress gauge field, but to avoid work that is of little physical significance, the elastic propagators will be fully analysed only in the ‘decoupled’ directions where either electric or magnetic shear is exclusively screened. In all the intermediate directions, only the long wavelength leading expansions of the phonon propagators will be addressed.

The coupling of the longitudinal and transversal sectors of the action has another, potentially dangerous, consequence. Recall the ‘chiral propagator’ Eq. (3.35). In the previous chapter, we argued that this propagator has to be strictly zero or otherwise the parity symmetry of the space is broken by the ground state. The ordered nematic ground state *should not* break the spatial parity symmetry (its order parameter, the Burgers director Eq. (4.33) is  $\mathbb{Z}_2$  invariant) and we expect the chiral propagator Eq. (3.35) to be strictly zero. Nevertheless, the coupling between two sectors may and will produce nonzero values for the  $\langle\langle\partial_a u^a|\epsilon_{ab}\partial_a u^b\rangle\rangle$  propagator which can spark some worries. We should note that we work with Fourier transformed fields and the chiral propagator written in the above is nonzero only when it measures correlation between the Fourier transformed strains. To obtain the chiral propagator in real space one has to perform the inverse Fourier transformation of the propagator Eq. (3.35). As it turns out, the nonzero chiral propagator of the ordered nematic that we find in Fourier representation, averages to zero when the inverse Fourier transformation is performed. In fact, the broken parity has a different consequence in the Fourier space: the chiral propagator has to be an odd function of relative angle between the director and wave-vector. This simple statement is a consequence of the fact that in Fourier space, the only reflection symmetry left is with regard to a line parallel to the wave vector. While the compression strain is invariant under this transformation, the local rotation is not, so any “evenness” in the chiral propagator implies that system prefers one state over its mirror double.

Another ingredient required for the realization of the nematic phase is a high curvature stiffness given by the value of  $\ell$  in the potential energy density Eq. (3.19). Let us here repeat the argument, first given by Kleinert [48], that the disclination rest mass is an increasing function of the stiffness  $\ell$  while the rest mass of dislocations is barely dependent of the curvature stiffness. For a high enough value of the curvature stiffness  $\ell$ , there is a certain range of disorder (see Fig. 4.1), where the “meandering entropy” of defect world-lines overwhelms the dislocation energy cost, while it still falls short for the unbinding of the disclination loops. One may wonder why we have not explicitly included the term

Eq. (3.19) in the starting action Eq. (3.24), given that it is necessary for the nematic phase formation? As mentioned before and demonstrated in the case of the dislocation Coulomb force, the effects of the second order gradient terms are visible only at length scales shorter than the characteristic lengths  $\ell$  and  $\ell'$ . If these lengths are “microscopic” or eventually a few orders of magnitude larger than the lattice constant, but still below the length scales that we can access in our experiments (we are ultimately interested in the longwavelength behaviour), then our experiments cannot resolve the difference between the  $\ell \equiv 0$  and finite  $\ell$  results. In the concluding chapter we will shortly discuss the dual theory of second order gradient elasticity. The results we obtained for this theory are not included in this thesis as the entire formalism would take a whole new chapter to explain all the relevant steps as well as its peculiarities. The concluding chapter contains only some final results that do not differ significantly from the  $\ell = 0$  case, so it readily follows that for any measurement at scales large compared to  $\ell$  is completely blind to its direct effects.

Before we delve into the technicalities of the dual theory of the ordered nematic phase, let us make one more comparison of the ordered nematic with a classical phase that breaks the symmetries in the same manner. We notice that the ordered nematic phase has the symmetry properties of the “smectic-C” phase [130]: the translation symmetry is broken only in one direction and fully restored in the other direction. When the response of the ordered nematic is established towards the end of this section, it will be clear that the elastic properties do not match. When it comes to the smectic phase, it was shown independently by Peierls and Landau [126] in the 1930’s, based on symmetry arguments (even before they knew that smectics existed!), that the elastic energy density of a layered elastic medium can be written as

$$e(\mathbf{x}) = \frac{1}{2} [B(\nabla_{\parallel}u)^2 + K(\nabla_{\perp}^2u)^2]. \quad (4.55)$$

When we compare the elastic response of the ordered nematic phase that we will find later with the one that follows from the elastic energy Eq. (4.55), it becomes immediately clear that the two phases, apart from the symmetry breaking pattern, have not much in common. The main difference comes from the presence of an additional mode in the ordered nematic phase which can be tracked down to the dislocation condensate. Such mode is not present at all in the smectic state of matter since the energy Eq. (4.55) does not deal with a displacement parallel to the planes. Neither of the two remaining poles in the response function of the ordered nematic resembles the excitations of the “smectic-C” phase. We put emphasis that this fundamental difference in the excitation spectrum shows unambiguously that the ordered nematic is *not* a stack of decoupled sliding liquid layers as one might be tempted to think from the intuitive perception of the glide constraint. If that had been the case, the whole work presented here would not make much sense since the Higgs mechanism is based on the long-range order assumption for the Higgs field. Due to Mermin-Wagner-Hohenberg theorem [155, 156], uncoupled layers, which are effectively one-dimensional systems, cannot exhibit long-range order even at zero temperature.

After this lengthy introduction let us begin with the technical part of this section. At the beginning of the section we mentioned that a ‘Lorentz’ gauge fix will be imposed on the

gauge fields. The reason for this is the following: one would like to use ‘interpretational’ gauge fixes, the Coulomb gauge fix for  $B_\mu^\perp$  flavour and the unitary gauge fix for the  $B_\mu^\parallel$  flavour, so that the remaining gauge field components (photons) have an easy physical interpretation. Although perfect for interpreting the final results, this choice of gauge fixes would force us to perform the entire calculation three times: once for the propagation parallel to the Burgers vector, once for the perpendicular propagation, and finally for intermediate values of the angles. This is necessary since the Ehrenfest constraint acts differently depending the ‘orientation’ of the Coulomb photon  $B_\tau^L$  relative to the Burgers director.

An additional difficulty comes from the glide constraint. We learned that the glide constraint acts exclusively on the dislocation currents Eq. (3.61). On the other hand, working in the unitary gauge fix means that the gauge fields take the role of currents. This is best illustrated by the simple case of the vortex duality. Recall the definition of bosonic current Eq. (2.21) and its form in the Higgs phase ( $\Psi_0$  is the expectation value of the bosonic collective field)

$$J_\mu = |\Psi_0|^2(\partial_\mu\varphi - A_\mu). \quad (4.56)$$

With the unitary gauge imposed ( $\varphi \equiv 0$ ), the vortex currents become proportional to the dual gauge fields. This consequence of the unitary gauge fix is rooted in the fact that the complex phase of the bosonic field, which usually determines the currents, transferred its degree of freedom to the longitudinal gauge field  $A_L$ . Surprisingly (or not), with the unitary gauge fix, the constraints that are originally acting on currents, have now to be imposed on the gauge fields.

In the dual elastic theory, at least when applied to the ordered nematic phase, the dislocation currents are given by

$$J_\mu^a = n^a |\Psi_0|^2(\partial_\mu\varphi - n^b B_\mu^b) = n^a |\Psi_0|^2(\partial_\mu\varphi - B_\mu^\parallel). \quad (4.57)$$

With the unitary gauge fix as our preference, the glide constraint implemented on the current Eq. (4.57) reads

$$0 = \epsilon_{ad} J_d^a = -|\Psi_0|^2 \epsilon_{ad} n^a n^b B_d^a = -|\Psi_0|^2 B_\perp^\parallel. \quad (4.58)$$

In analogy with the Ehrenfest constraint, the ‘unitary gauge fix’ glide constraint Eq. (4.58) acts, pending the alignment of the wave-vector and the Burgers vector.

Bearing in mind everything said in the last two paragraphs, we have decided to sacrifice the physical interpretation of the gauge photons in exchange for a more concise derivation of the dual theory in the ordered nematic phase. It will be fairly easy to track down the physical interpretations for these results, based on the experience we have obtained with the vortex duality.

The choice for the gauge fix is therefore not governed by its elegance, but rather by the simplifications it brings to the calculation. Since the unitary gauge fix is ruled out, the

Higgs term must be written in gauge invariant form like in Eq. (2.73). The most desirable gauge fix that we can work in is

$$0 = \frac{1}{c_d^2} \partial_\tau B_\tau^a + \partial_i B_i^a, \quad (4.59)$$

because, as we mentioned in chapter 2, the bare Higgs term (before the constraints are implemented) is simply proportional to  $n^a n^b B_h^{a\dagger} B_h^b$  with  $h = \pm 1$ , where the summation goes over the components in the linear polarized basis (‘dreibeinen’, Eq. (1.6)).

By using the gauge fix Eq. (4.59), the Coulomb and longitudinal photons are merged in one, temporally-spatially admixed transversal component  $A_{+1}$ . For future purposes, we define the dislocation three-momentum as  $p_d^\mu = (\omega_n, c_d q_i)$  and its scalar value by  $p_d = \sqrt{\omega_n^2 + c_d^2 \mathbf{q}^2}$ . The linearly polarized basis (‘dreibeinen’, Eq. (1.6)) that we use, is defined in terms of the three-momentum

$$\mathbf{e}_\mu^{(0)} = \frac{p_d^\mu}{p_d} = \left( \frac{\omega_n}{p_d}, \frac{c_d q_x}{p_d}, \frac{c_d q_y}{p_d} \right)^T = (\cos \theta, \sin \theta \cos \phi, \sin \theta \sin \phi)^T; \quad (4.60)$$

$$\mathbf{e}_\mu^{+1} = \left( \frac{c_d q}{p_d}, \frac{-\omega_n q_x}{p_d q}, \frac{-\omega_n q_y}{p_d q} \right)^T = (\sin \theta, -\cos \theta \cos \phi, -\cos \theta \sin \phi)^T; \quad (4.61)$$

$$\mathbf{e}_\mu^{-1} = \left( 0, \frac{q_y}{q}, \frac{-q_x}{q} \right)^T = (0, \sin \phi, -\cos \phi)^T. \quad (4.62)$$

Any of the gauge fields components with Cartesian indices and flavours has to be expressed in the linear polarized basis Eqs. (4.60 - 4.62). The general identity connecting components of a vector in the two bases is given in the introduction. However, the dual stress gauge fields also carry flavours that can take spatial values and these have to be changed to the momentum basis too (‘zweibeinen’, Eq. (1.3)). The gauge fields with Cartesian indices are therefore expressed in terms of linearly polarized basis via

$$B_\mu^a = i \tilde{e}_a^E [e_\mu^{+1} B_{+1}^E + i e_\mu^{-1} B_{-1}^E]. \quad (4.63)$$

Components  $B_{(0)}^a$  are absent since they are set to zero by gauge fix Eq. (4.59). As usual, the prefactors  $i$  take care that two fields with opposite momenta  $B(p^\mu)$  and  $B(-p_\mu)$  are conjugate to each other.

Let us now rewrite the gauge field propagator originating in the first term of Eq. (4.16). It is common to all phases of a solid and in the previous section where the Coulomb gauge fix was chosen, the longitudinal and transversal sectors of the propagator were found in Eqs. (4.47, 4.53). To find the propagator with the gauge fix Eq. (4.59) imposed, we first have to find the action of the Ehrenfest constrain on the new fields and then use it to remove one gauge photon. When the gauge fields in the Ehrenfest constraint Eq. (4.43) are written according to Eq. (4.63), the Ehrenfest constrain reads

$$B_{+1}^L = -i \frac{\omega_n}{p_d} B_{-1}^T + \frac{2}{p_d} \mathcal{J}. \quad (4.64)$$

Similar to before, the gauge field component  $B_{+1}^L$  is removed in favour of the component  $B_{-1}^T$  which is left (it is proportional to the transversal phonon-photon  $B_T^T$ ). The remainder fields are independent degrees of freedom and we put them in a column/row  $\mathcal{B} = (B_{+1}^T, B_{-1}^L, B_{-1}^T)^T$ . The dual action contribution from the Eq. (4.16) reads

$$\begin{aligned} \mathcal{L}_{ideal} = & \frac{1}{2} \mathcal{B}^\dagger \mathcal{G}_0^{-1} \mathcal{B} - \frac{1}{2} \frac{\mathcal{K}^\dagger \mathcal{K}}{\kappa} - \frac{1}{2} \frac{\mathcal{J}^\dagger \mathcal{J}}{\mu} \\ & + i \mathcal{K}^\dagger \frac{p_d B_{+1}^T + i \omega_n B_{-1}^L}{2\kappa} + i \mathcal{J}^\dagger \frac{\omega_n B_{-1}^T}{\mu}, \end{aligned} \quad (4.65)$$

where we left both external source terms,  $\mathcal{J}$  and  $\mathcal{K}$ , explicit so that the ‘Zaanen-Mukhin’ relation can be recovered for the chiral propagator Eq. (3.35). Notice that external dislocation currents are left out for simplicity.

The inverse gauge field propagator is given as

$$\mathcal{G}_0^{-1} = \frac{1}{\mu} \begin{pmatrix} \frac{p_d^2}{2(1+\nu)} & \frac{i\nu p_d \omega_n}{2(1+\nu)} & 0 \\ \frac{-i\nu p_d \omega_n}{2(1+\nu)} & \frac{\omega_n^2 + (1-\nu^2)c_T^2 q^2}{2(1+\nu)} & 0 \\ 0 & 0 & \omega_n^2 + c_T^2 q^2 \end{pmatrix}. \quad (4.66)$$

The connection between the degrees of freedom in the action Eq. (4.65), and the degrees of freedom in the combined actions Eqs. (4.49) and (4.53) is the following: the transversal sector is trivially identified since we already noticed that the gauge field components  $B_T^T$  and  $B_{-1}^T$  differ only by a minus sign. The absence of a Coulomb force between dislocations with longitudinal Burgers vectors is manifested by the constrained photon  $B_{+1}^L$ . The longitudinal sector is spanned by the remaining two gauge fields  $B_{+1}^T$  and  $B_{-1}^L$ . As in the transversal sector, photon  $B_{-1}^L$  is the  $B_T^L$  photon with opposite sign. The remaining gauge field  $B_{+1}^T$  carries the Coulomb interaction between dislocations with transversal flavour.

The action Eq. (4.65) recovers the ideal crystal phonons as its Green functions. Any other result would mean that something went wrong with the gauge fix Eq. (4.59). We are, however, not interested in yet another derivation of the very well known phonon propagators in the ideal crystal. Since our aim is the ordered nematic phase (and the disordered one in the next section), which is nothing else than the dislocation melted phase, we want to include dislocation defects in the dual theory and to extract consequences coming from their proliferation. The defect action has already been constructed in section 4.2. Due to the striking resemblance between the dislocation GLW action Eq. (4.32) and the vortex GLW action Eq. (2.35), we already anticipate the Higgs term for the dual stress gauge fields when dislocation defects proliferate in the system. Unlike the situation in the vortex duality, the construction of the Higgs term in elastic medium has to take into account two constraints that are central to the dual elastic theory. One is the Ehrenfest constraint Eq. (4.64), which we implement as usual, by removal of the gauge field  $B_{+1}^L$  in favour of the transversal photon  $B_{-1}^T$ . When the constraint is implemented, there is however a generating functional  $\mathcal{J}$  involved. It follows that the Higgs term changes both linear and quadratic terms in the external source field  $\mathcal{J}$ , so that the ‘transversal Zaanen-Mukhin’ relation Eq. (4.54) acquires additional terms.

At an earlier stage, we mentioned that the glide constraint Eq. (3.61) is only a coarse-grained (averaged) constraint and that it should not be imposed on independent dislocations, but instead, it should constrain only the total ‘climb’ of the dislocation world-lines tangle. Such an action of the glide constraint is attainable by means of the Lagrange multiplier term added to the total dual action

$$\mathcal{L}_{glide} = i\lambda\epsilon_{\tau\mu a}J_\mu^a. \quad (4.67)$$

The major consequence of the glide constraint invoked in the form of Eq. (4.67) is that the covariant derivative obtained from Eq. (4.28) acquires an additional term and, in the ordered nematic phase, it reads

$$\partial_\mu\Psi \rightsquigarrow D_\mu\Psi = (\partial_\mu - in^a B_\mu^a - i\lambda\epsilon_{\tau\mu a})\Psi. \quad (4.68)$$

When the Higgs term is constructed, the minimal coupling Eq. (4.68) implies that, in place of the curly gauge fields Eq. (4.29), one has to work with the constrained counterparts

$$\mathcal{A}_\mu^{eff.} = n^a(B_\mu^a + \lambda\epsilon_{\tau\mu a}). \quad (4.69)$$

The effective gauge field yields linear and quadratic terms in the Lagrange multiplier  $\lambda$  so, after it is integrated out, the glide constraint is effectively in charge.

In the ordered nematic, the action of the Burgers sector Eq. (4.34) is not explicitly included. We assume that the effects of this action have been exhausted when all the Burgers vectors are ordered in a particular direction  $\mathbf{n}$ . Thus, instead of performing the path integral over the Burgers vectors, we calculate the total partition function Eq. (4.35) with a contribution from a single Burgers vector orientation. This value corresponds to the mean-field treatment of the Burgers sector. The Burgers director is substituted by the mean-field value  $\hat{Q}$  and its excited states couple only via higher order couplings with the gauge degrees of freedom, so these terms are left out.

The bare Higgs term we want to add to the action is initially written as

$$\begin{aligned} \mathcal{L}_{Higgs} &= \frac{1}{2}\frac{\Omega^2}{\mu}(\hat{Q}^{ab} + \frac{1}{2}\delta^{ab})(B_\mu^a + \lambda\epsilon_{\tau\mu a})\left[\delta_{\mu\nu} - \frac{p_d^\mu p_d^\nu}{p_d^2}\right](B_\nu^b + \lambda\epsilon_{\tau\nu b}) \\ &= \frac{1}{2}\frac{\Omega^2}{\mu}(\hat{Q}^{EF} + \frac{1}{2}\delta^{EF})(B_h^{E\dagger} + \lambda^\dagger\epsilon_{\tau\mu a}e_\mu^h\tilde{e}_a^E)(B_h^F + \lambda\epsilon_{\tau\nu b}e_\nu^h\tilde{e}_b^F). \end{aligned} \quad (4.70)$$

While the first line is universal and written in Cartesian coordinates, in the second one we summed exclusively over helical components  $h, h' = \pm 1$ . The flavours  $E, F$  in the ‘zweibeinen’ basis Eq. (1.3) take values  $L, T$ .

A Higgs gap is introduced in the Eq. (4.70) as  $\Omega = |\Psi_0|/\sqrt{\mu}$ . The expectation value for the dislocation field  $\Psi$  follows from action Eq. (4.32). When the effective dislocation mass  $m_\Psi^2$  has become negative, the average dislocation density is controlled by the short-range repulsion term  $\lambda_\Psi$  so that  $|\Psi_0|^2 = \sqrt{-m_\Psi^2/\lambda_\Psi}$ . When the elastic response of the nematic phase is found, a gapped mode will occur which will always have a gap precisely equal to  $\Omega$ .

The first line of the Higgs term Eq. (4.70) is written as the gauge invariant Higgs term Eq. (2.73). Although it was earlier stated that the ‘Lorentz’ gauge fix Eq. (4.59) does not require this term to be explicitly included, when the Lagrange multiplier term Eq. (4.67) is added to the action, the new effective minimally coupled gauge field Eq. (4.69) does not obey the gauge fix Eq. (4.59) any more. Therefore, we have either to change that gauge fix to include the Lagrange multiplier  $\lambda$  or just work with the gauge invariant Higgs term. We choose the latter. The advantage of the helical basis Eqs. (4.60 - 4.62) is that the bracket term in Eq. (4.70) is realized by summation over  $h = \pm 1$  polarization indices, whereas the  $h = 0$  component is omitted.

The final comment about the action Eq. (4.70) concerns the use of the Burgers director field Eq. (4.33). This Higgs terms was derived under the assumption that the Burgers vector is oriented in a particular direction  $\mathbf{n}$  throughout the entire system. From this Burgers vector, the Burgers director order parameter is constructed, acquiring the value

$$\hat{Q} = \frac{1}{2} [| \parallel \rangle \langle \parallel | - | \perp \rangle \langle \perp |] \quad (4.71)$$

in the ordered nematic phase. Vectors  $| \parallel \rangle$  and  $| \perp \rangle$  are unit vectors parallel and perpendicular to the Burgers vector  $\mathbf{n}$  respectively, Eq. (4.30). In the following section we are concerned with the topological nematic phase, characterized by the disorder in Burgers vector. Quantitatively, this is expressed through the zero expectation value of the Burgers director. In the treatment that will follow, we will ‘naively’ use the bare Higgs action Eq. (4.70) in the topological nematic phase. Since this action is valid, in a strict mathematical sense, only for the values of  $\hat{Q}$  that belong to the ordered nematic phase Eq. (4.71), the generalization to the disordered nematic phase will bring some difficulties, but these are left for the discussion in the next section.

In the remainder of this section, we do not need the bare Higgs term expressed in terms of the Burgers vector, so one may assume that each instance of  $\hat{Q}^{ab} + \frac{1}{2}\delta^{ab}$  in Eq. (4.70) should be simply replaced by  $n^a n^b$ . Given that the entire theory is presented in the Fourier space, the Burgers vector components bear  $L, T$  indices instead of the Cartesian ones ( $x$  and  $y$ ). Since  $\mathbf{n}^2 = 1$ , only one parameter will be used to describe the orientation of the Burgers vector. We define angle  $\eta$  as the angle between the Burgers vector and the wave-vector so that  $\mathbf{n} = (\cos \eta, \sin \eta)^T$ .

Let us now return to the bare Higgs term Eq. (4.70) and treat the glide constraint first. From a direct calculation, it follows that the Lagrange multiplier  $\lambda$  becomes a ‘dynamical field’ with propagator term

$$\frac{1}{2} \frac{\Omega^2}{\mu} \lambda^\dagger \frac{\omega_n^2 + c_d^2 q^2 \cos^2 \eta}{p_d^2} \lambda \equiv \frac{1}{2} \Omega^2 \mu \lambda^\dagger \frac{p_\eta^2}{p_d^2} \lambda. \quad (4.72)$$

introducing a new ‘momentum’  $p_\eta^2 = \omega_n^2 + c_d^2 q^2 \cos^2 \eta$  only for notational purposes.

Besides the quadratic term, the Lagrange multiplier  $\lambda$  couples linearly to the dual stress gauge fields as

$$\lambda^\dagger \left( \frac{i\omega_n}{p_d} \cos \eta \sin \eta B_{+1}^L - \frac{i\omega_n}{p_d} \sin^2 \eta B_{+1}^T - \cos^2 \eta B_{-1}^L + \cos \eta \sin \eta B_{-1}^T \right). \quad (4.73)$$

When it is removed by Gaussian integration, it produces a counter term in the bare Higgs term Eq. (4.70) with the effect that the Higgs term acquires a simpler form

$$\mathcal{L}_{Higgs} = \frac{1}{2} \frac{\Omega^2 |n^E (n^L p_d B_{+1}^E + n^T i \omega_n B_{-1}^E)|^2}{\mu p_\eta^2}. \quad (4.74)$$

We see that despite the presence of all gauge field components in Eq. (4.70), the glide constraint allows that only one gauge field component acquires mass in the Higgs term Eq. (4.74). This degree of freedom can be identified on the basis of symmetry principles. The advantage of the gauge fix Eq. (4.59) is that it allows initially only four gauge degrees of freedom. Out of these four degrees of freedom, one transforms under the  $B_0$  irreducible representations of the group of all rotations  $O(2)$

$$\mathcal{B}_R = |B_0\rangle = B_{+1}^L + i \frac{\omega_n}{p_d} B_{-1}^T. \quad (4.75)$$

Physically, the  $B_0$  irreducible representation is associated with rotation and this field component indeed represents the rotational stress gauge boson. However, we know that the elastic action Eq. (3.24) excludes any rotational rigidities so this stress gauge boson has to disappear, which is precisely the statement of the Ehrenfest constraint (compare Eq. (4.75) with Eq. (4.64)). From the remaining three independent degrees of freedom, one is invariant under all rotations (irreducible representation  $A_0$ ) and this is precisely the compression degree of freedom

$$\mathcal{B}_C = |A_0\rangle = B_{+1}^T + i \frac{\omega_n}{p_d} B_{-1}^L. \quad (4.76)$$

The remainder pair of the dual stress gauge bosons transform as a spin-2 doublet ( $E_{2,-2}$  irreducible representation). They correspond to the shear rigidity, which we split into ‘electric’ (present in the longitudinal sector) and ‘magnetic’ (present in the transversal sector) shear

$$\mathcal{B}_{el.sh.} = |E_{2,-2}^L\rangle = B_{-1}^L + i \frac{\omega_n}{p_d} B_{+1}^T, \quad (4.77)$$

$$\mathcal{B}_{m.sh.} = |E_{2,-2}^T\rangle = B_{-1}^T + i \frac{\omega_n}{p_d} B_{+1}^L. \quad (4.78)$$

The gauge field component that acquires the Higgs mass Eq. (4.74) belongs to the spin-2 subspace spanned by shear bosons Eqs. (4.77 - 4.78) and we conclude immediately that the Higgs mass can be acquired only by shear gauge bosons whereas the compression is protected by the proper implementation of the glide constraint Eq. (3.61).

An alternative way to identify shear as the unique entity subjected to the action of the Higgs mechanism is to represent the specific stress boson from Eq. (4.74) in terms of physical stress fields. Through direct comparison, one finds that the stress gauge field appearing in Eq. (4.74) is precisely given by

$$n^a n^b (\partial_\tau B_a^b - \partial_a B_\tau^b) = \epsilon_{ac} n^a n^b \sigma_c^b. \quad (4.79)$$

This stress component can be seen as one of the shear stresses. It has a zero overlap with the compression stress  $\sigma_i^i$  and pending the orientation of the Burgers vector this is either electric or magnetic stress or their mixture. Let us try to explain this for specific values of angle  $\eta$ . Take first a propagation parallel to the Burgers vector, the shear component Eq. (4.79) becomes  $\sigma_T^L$  which corresponds precisely to the magnetic shear stress. The same is true for  $\eta = \pi/2$  since  $\sigma_L^T = \sigma_T^L$ , except that the massive shear component acquired one minus sign. This is precisely what one expects from spin-2 fields, after rotation by  $\pi/2$  they change sign. According to the spin-2 representation rules, one component of the doublet should transform into its counterpart if rotated by  $\eta = \pi/4$ . We check this case ( $n^L = n^T = 1/\sqrt{2}$ ) and it follows immediately that the massive shear stress Eq. (4.79) turns into the ‘electric’ shear stress  $\sigma_T^T - \sigma_L^L$ . Naturally, for all other, intermediate values, the massive shear admixes two shear components.

Finally, let us add the Ehrenfest constraint to the action. We remove the gauge field component  $B_{+1}^L$  according to the Ehrenfest constraint in form of Eq. (4.64). This results in the final Higgs terms for the ordered nematic phase

$$\mathcal{L}_{Higgs} = \frac{1}{2} \frac{\Omega^2 p_d^2}{\mu p_\eta^2} \left[ \mathcal{B}_H^\dagger \mathcal{B}_H - \frac{4 \cos^4 \eta}{p_d^2} \mathcal{J}^\dagger \mathcal{J} - i \frac{4 \mathcal{J}^\dagger}{p_d} \mathcal{B}_H \right], \quad (4.80)$$

introducing the ‘Higgs shear gauge field’

$$\mathcal{B}_H = -\sin 2\eta \frac{B_{+1}^T - i \frac{\omega_n}{p_d} B_{-1}^L}{2} - i \frac{\omega_n}{p_d} \cos 2\eta B_{-1}^T \quad (4.81)$$

which equals precisely the screened component of shear, Eq. (4.79), with the Ehrenfest constraint explicitly invoked. The external source field  $\mathcal{J}$  is kept here in order for us to recover the transversal propagator. In the next chapter, when we ask questions about the electric properties of the nematic phases and ignore the phonon propagators, terms containing  $\mathcal{J}$  can be removed from the Higgs term Eq. (4.80).

Bearing in mind that the inverse gauge field propagator in the ideal crystal, Eq. (4.66), can be regarded as the ‘unperturbed’ gauge field propagator in matrix form  $\mathcal{G}_0^{-1}$ , the first term of Eq. (4.80) may be written as a self-energy contribution to the action as  $-\frac{1}{2} \mathcal{B}^\dagger \Pi_H \mathcal{B}$ . The self-energy matrix  $\Pi_H$  originating in the Higgs mechanism is given by

$$-\Pi_H = \frac{\Omega^2 \left( \frac{p_d}{2} \sin 2\eta, \frac{-i\omega_n}{2} \sin 2\eta, -i\omega_n \cos 2\eta \right) \otimes \left( \frac{p_d}{2} \sin 2\eta, \frac{i\omega_n}{2} \sin 2\eta, i\omega_n \cos 2\eta \right)}{\mu p_\eta^2}. \quad (4.82)$$

Following this notation, the total inverse propagator for the elastic gauge fields is written as

$$\mathcal{G}^{-1} = (\mathcal{G}_0)^{-1} - \Pi_H \quad (4.83)$$

and this form will be used not only for the recovery of the phonon propagators, but also in the next chapter where we analyse how the self-energy Eq. (4.82) influences the electromagnetic response of a solid.

When the inverse total gauge field propagator matrix Eq. (4.83) of the ordered nematic phase is inverted, the result is the stress gauge field propagator matrix with elements corresponding to propagators of different pairs of dual stress gauge fields. The dual stress gauge bosons always represent physical degrees of freedom, even in gauge fixes that have the effect of encrypting the physics, so they have to be related to phonon propagators. In order to recover the connection, which is nothing else than a generalized ‘Zaanen-Mukhin’ relation Eq. (2.55), we resort to the external source fields  $\mathcal{K}$  and  $\mathcal{J}$  that we kept explicit in the action all along.

Let us begin with the longitudinal propagator. The propagator can be directly extracted from the action Eq. (4.65) since the external source field  $\mathcal{K}$  is not influenced by presence of the Higgs field. Therefore, the relation which is universal to all the phases is recovered

$$G_L = \frac{1}{\kappa} - \frac{p_d^2}{\kappa^2} \langle \langle \mathcal{B}_C^\dagger | \mathcal{B}_C \rangle \rangle. \quad (4.84)$$

This is the same relation as Eq. (4.45) except that we expressed the compressional stress in terms of the compression gauge photon Eq. (4.76). Eventually, this could have been obtained by using directly the relation Eq. (2.55), since the longitudinal sector contains no singularity in the elasticity tensor Eq. (3.25).

The transversal phonon propagator, on the other hand, is a subject of a significant change as compared to its ideal crystal form Eq. (4.54). The Ehrenfest constraint implies a coupling of the external source field  $\mathcal{J}$  to the Higgs field and the presence of the dislocation condensate has consequences as seen from Eq. (4.80). The Zaanen-Mukhin relation for the transversal phonon now becomes

$$G_T = \frac{1}{\mu} \left( 1 + \frac{4\Omega^2 \cos^4 \eta}{p_\eta^2} \right) - \frac{\omega_n^2}{\mu^2} \langle \langle \mathcal{B}_T^\dagger | \mathcal{B}_T \rangle \rangle. \quad (4.85)$$

where we introduce a new linear combination of gauge fields which we call the ‘dressed’ transversal phonon

$$\mathcal{B}_T = \frac{2p_d \Omega^2 \cos^2 \eta}{\omega_n p_\eta^2} \mathcal{B}_H + B_{-1}^T. \quad (4.86)$$

The physical content of Eq. (4.85) can be understood as follows: due to the presence of the dislocation condensate, experiments that are designed to measure the transversal phonon response now couple to new degrees of freedom reflected in the ‘dressed transversal phonon’ Eq. (4.86). A physical interpretation of the photon “dressing” can be found in the earlier claim (section 3.4 on glide) that dislocations live in the solid and therefore have to conform to smooth elastic deformations. In a way defects ‘clutch’ to the medium. When the transversal elastic response is measured, the medium is forced from the outside into a ‘whirling motion’ at the probing points: the transversal phonons are defined as a response of the solid to external local rotation, see Eq. (3.34). It follows that the defect degrees of freedom are excited also when a local deformation is made in order to probe the transversal phonon. The defect excitations then become visible in the phonon propagators,

demonstrating that the ‘dual censorship’ can be broken even in a more direct way than originally thought when the dual ‘Zaanen-Mukhin’ relation was derived. At the end of the section, when we analyse the phonon propagators for specific values of angle  $\eta$ , we will give a pictorial representation of the dressed transversal phonon Eq. (4.86), at least for values  $\eta = 0$  and  $\eta = \pi/2$ .

After the derivation of the longitudinal and transversal propagator, we could employ the external source terms to derive the ‘chiral’ propagator Eq. (3.35). The propagator correlates the compression and the local rotation strains which belong to the longitudinal and transversal sector respectively. This correlator will therefore be nonzero only if the two sectors are coupled and that is indeed the case when angle  $\eta$  takes an intermediate value (not a multiple of  $\pi/4$ ). The chiral propagator is obtained as a second derivative of the partition function  $Z_{el.}[\mathcal{K}, \mathcal{J}]$ , once with respect to  $\mathcal{K}$  and once with respect to  $\mathcal{J}$  and it reads

$$G_{chiral} = G_{LT} = \langle\langle \partial_i u^i | \epsilon_{ab} \partial_a u^b \rangle\rangle = \frac{\Omega^2 p_d^2}{\kappa \mu p_\eta^2} \langle\langle \mathcal{B}_C^\dagger | \mathcal{B}_T \rangle\rangle. \quad (4.87)$$

Its conjugate propagator  $\langle\langle \epsilon_{ab} \partial_a u^b | \partial_i u^i \rangle\rangle$  is a chiral propagator too.

Having introduced all four elastic propagators between spin-0 excitations, the compression  $\partial_a u^a$  and the local rotation Eq. (3.5), we can represent them in a matrix of the form

$$\hat{G} = \begin{pmatrix} G_L & G_{LT} \\ G_{TL} & G_T \end{pmatrix} = \langle\langle (\partial_a u^a, \epsilon_{ab} \partial_a u^b)^{\otimes 2} \rangle\rangle, \quad (4.88)$$

If the phonon propagator of the ideal crystal is denoted by  $\hat{G}_0 = \text{diag}(G_L^0, G_T^0)$ , while the phonon propagator of the ordered nematic phase is  $\hat{G}$ , one can introduce the ‘phonon self-energy matrix’  $\hat{\Pi}$  in a standard way:

$$\hat{G} = \frac{1}{(\hat{G}_0)^{-1} - \hat{\Pi}}. \quad (4.89)$$

All four phonon propagators of the ordered nematic phase can be expressed in a very convenient way if one uses the phonon self-energy Eq. (4.89). Avoiding steps with explicit forms of inverted matrices that are required in order to obtain the phonon propagators, we present only the final step where the ‘phonon self-energy’ becomes a projector to a specific ‘vector’

$$-\hat{\Pi} = \frac{\mu \Omega^2}{c_T^2 q^2} \frac{1}{c_T^2 q^2 (\omega_n^2 + \cos^2 \eta c_d^2 q^2) + \Omega^2 (\omega_n^2 + 4 \cos^2 \eta c_T^2 q^2)} \begin{pmatrix} \cos \eta \sin \eta c_T^2 q^2 \\ \omega_n^2 + 2 \cos^2 \eta c_T^2 q^2 \end{pmatrix}^{\otimes 2}, \quad (4.90)$$

where the ‘tensorial square’ represents the outer product of the column with itself. This self-energy makes the anisotropic character of the screening apparent: tuning the Burgers orientation from  $\eta = 0$  to  $\eta = \pi/2$ , the screening alternates from being purely in the transversal sector to being exclusively in the longitudinal sector and than back. In the

static limit ( $\omega_n \rightarrow 0$ ), the glide constraint has disappeared and the ‘phonon self-energy’ Eq. (4.90) collapses to a far simpler expression

$$-\hat{\Pi}_{\omega_n \rightarrow 0} = \frac{\mu}{4 + \lambda_d^2 q^2} \begin{pmatrix} \sin \eta \\ 2 \cos \eta \end{pmatrix}^{\otimes 2}. \quad (4.91)$$

The dislocation correlation length  $\lambda_d = c_d/\Omega$  is introduced here, and it represents the length above which the dislocation excitations as represented by the complex phase gradient lose their correlation (kinematical range of the dislocation second sound). From Eq. (4.91) one can read the static screening anisotropy which is closer to our intuitive expectations: the screening properties parallel and perpendicular to the (Burgers) director are in complete contrast. The continuous changes of angle  $\eta$  drive the screening between the transversal and the longitudinal correlator, but it takes angle  $\pi$ , not  $\pi/2$  as in the dynamical case, to return to the same static correlator.

Until now, this whole section was dedicated to the derivation of the phonon propagator with all the peculiarities coming from the constraints in the dual elasticity theory, succeeding when the phonon self-energy was finally obtained in Eq. (4.90). This job is not done yet, because we need to analyse the phonon propagator Eq. (4.88) to find out the features of the ordered nematic solid that make it distinct from the ideal crystal or the superfluid phases of matter. In the few remaining paragraphs of this section, the experimentally measurable phonon propagators are therefore carefully studied in relevant limits. Because of the anisotropy of the ordered nematic phase, the phonon propagators are analysed thoroughly only in the cases when the two sectors of the action are decoupled ( $\eta$  is  $\pi/4$  times an integer). The propagators for intermediate  $\eta$  values are analysed only in the long-wavelength limit which is in fact the most relevant one for the comparison with experiments. In this analysis, we will continue to use Matsubara frequency  $\omega_n$  when searching for poles. One should notice however that physical properties as obtained in experiments are trivially recovered by rotation to real time/frequency  $\omega_n \rightarrow -i\omega + \delta$ .

Let us begin with the case of  $\eta = \pi/2$ , i.e. propagation perpendicular to the Burgers vector. The longitudinal propagator is the same as in the ideal crystal, but the transversal propagator becomes

$$G_T = \frac{1}{\mu} \frac{c_T^2 q^2 + \Omega^2}{\omega_n^2 + c_T^2 q^2 + \Omega^2} \quad (4.92)$$

developing a gap  $\Omega$  for its only pole. This result is intuitively comprehensible imagining dislocation currents that can run only in a perpendicular direction and their implied effect on the screening of the magnetic shear. The longitudinal propagator is of course unaffected because the translational symmetry is still broken in the propagation direction.

The propagation along the Burgers direction is the first piece of physics defying our intuition. Setting  $\eta = 0$  in the phonon self-energy Eq. (4.90), we find that the longitudinal propagator is again unchanged, but the transversal propagator turns into

$$G_T = \frac{1}{\mu} \frac{c_T^2 q^2 (\omega_n^2 + c_d^2 q^2) + \Omega^2 (\omega_n^2 + 4c_T^2 q^2)}{(\omega_n^2 + c_T^2 q^2)(\omega_n^2 + c_d^2 q^2) + \Omega^2 \omega_n^2}. \quad (4.93)$$

This propagator experiences one massive pole at  $i\omega_n = \Omega$ , however an additional pole appears with no mass and quadratic dispersion  $i\omega_n = c_d c_T q^2 / \Omega^2$ . Based on the previous arguments on the spin-2 nature of the screening, we should understand why the longitudinal sector is unaffected. An additional argument comes from the geometrical nature of the electric shear: the electric shear requires that the deformation is simultaneously contraction in the longitudinal and expansion in the transversal directions (or the opposite). Therefore, although one may anticipate a liquid-like behaviour along the Burgers vectors, the electric shear seeks “support” in the transversal direction where the system still remembers its solid rigidities.

Now we have to find out where the extra mode in the transversal propagator comes from. Naively looking at the number of independent gauge degrees of freedom, one might be tempted to think that there is no more room for new modes in the transversal sector, but that is a misconception. Namely, by choosing gauge fix Eq. (4.59), we deliberately abandoned the Coulomb/unitary gauge fix where one physical mode corresponds to one gauge field component. In order to retrieve that point of view, we do not have to repeat the entire calculation. In fact, it is sufficient to recall the ‘dual censorship’ violation in the vortex duality. It is all about the phase degree of freedom of the condensate and its emergence in form of the longitudinal photon. In the vortex duality, the condensate propagator became visible in the superfluid velocity correlator Eq. (2.69). Here, the dislocation condensate wave-function  $\Psi$  has a phase degree of freedom translating in this dislocation second sound which is reborn (if the unitary gauge fix is chosen in the  $\parallel$  flavor) in the form of the dual stress gauge photon  $B_L^\parallel$ . When  $\eta = 0$ , the phase becomes  $B_L^L$  which turns from an entity in the gauge volume into a real physical degree of freedom.

The appearance of an additional mode is therefore justified. However, we still have to understand why only one mode in the transversal phonon propagator is gapped, while the other is massless and quadratic. The proper answer to this question can be obtained only after the intermediate  $\eta$  behaviour has to be found and analysed at small  $\eta$  values. Therefore, this discussion is left for the end of this section when the transversal phonon propagator Eq. (4.93) will be revisited.

At this point we may return shortly to the case of the perpendicular Burgers vector ( $\eta = \pi/2$ ) and clarify why there is no third mode in this particular Burgers orientation. Now, we know that the dislocation condensate materializes itself in form of the stress gauge field  $B_L^\parallel \rightarrow B_L^T$ , but, at the same time we know that the glide constraint (in the unitary gauge fix) constrains pair of gauge fields  $B_L^T$  and  $B_T^L$ . Therefore, it follows that the dislocation phase degree of freedom is eaten by the glide constraint before it could appear in a phonon propagator. The mass term was “awarded” to the (transversal phonon) photon  $B_T^T$  (it develops the gap) and to the Coulomb photon  $B_T^T$ : a careful analysis of the external current couplings show that the Coulomb force becomes shortranged with a characteristic length  $\lambda_d$ . The longitudinal photon  $B_L^T$  is forbidden to show up due to the glide constraint.

The remaining value of  $\eta$  where the ramifications of the Higgs mechanism in the ordered nematic phase are expected to be simple is  $\eta = \pi/4$ , with the electric shear as the massive shear component Eq. (4.79). Because the magnetic shear component does not participate

in the Higgs term, one expects consequences exclusively in the longitudinal propagator. This is partially true. The longitudinal propagator is

$$G_L = \frac{1}{\mu} \frac{c_L^2 q^2}{\omega_n^2 + c_L^2 q^2 - \frac{c_T^2 q^2 \Omega^2}{\omega_n^2 + \frac{c_d^2}{2} q^2 + \Omega^2}}, \quad (4.94)$$

which can be seen as a ‘dressing’ of the longitudinal crystal phonon with a self-energy that corresponds to the interaction with a sliding condensate slanted by  $\pi/4$  (thus the half in the velocity in Eq. (4.94)). In the long-wavelength limit, the only rigidity which survives is the compressional rigidity (propagation velocity is  $\sqrt{c_L^2 - c_T^2} \equiv c_K$ ). Only at distances shorter than the ‘shear screening length’  $\lambda_s = c_T/\Omega$ , the medium recovers its shear rigidity and behaves as a solid.

In the previous paragraph, a comment was made on the triviality of the propagators when  $\eta = \pi/4$ . If one considers the gauge field propagators only, there is indeed only one contribution to the action which screens the electric shear in the longitudinal sector. The difficulty begins with the transversal phonon external source field  $\mathcal{J}$  which appears in additional terms in the action only due to the changes in the ‘dressed transversal phonon’ Eq. (4.86). These changes produce nontrivial results not only in the transversal phonon propagator Eq. (3.34), but also in the off-diagonal terms of the phonon propagator Eq. (4.88), i.e. in the chiral propagators. We leave the results associated with this particular case out.

For the intermediate values of angle  $\eta$  there are three physical excitations in the system: two phonons and the condensate (longitudinal) photon, but due to the coupling between the two sectors, each phonon propagator sees all three poles. Given the length of the analytical work needed to analyse the corresponding bi-cubic equations in detail and the physical (in)significance of the obtained results, the results for intermediate  $\eta$  values are treated only in physically interesting limits, far below and well above the gap. As expected, at lengths shorter than the shear screening length  $\lambda_s$  and frequencies smaller than the shear gap ( $c_T q, \omega_n \gg \Omega$ ), the self-energy contribution Eq. (4.90) is negligible compared to the ideal crystal part of the phonon propagator. Hence, the solid-like properties are recovered as all the elastic degrees of freedom are insufficiently screened at these length scales. The opposite (long-wavelength) limit is more interesting as it yields the hydrodynamical properties of the system which can be related to the symmetry content of the model.

The possible gapped modes are found in limit  $q \ll \omega_n, \Omega$ . We retrieve only one gapped mode with an isotropic gap  $\Omega$ . The massless modes are found in the regime  $\Omega \gg \omega_n, q$ , at inverse lengths and energies significantly smaller than the shear gap. Here, the self-energy Eq. (4.90) simplifies into

$$-\hat{\Pi} = \frac{\mu}{c_T^2 q^2} \frac{1}{\omega_n^2 + 4 \cos^2 \eta c_T^2 q^2} \left( \frac{\cos \eta \sin \eta c_T^2 q^2}{\omega_n^2 + 2 \cos^2 \eta c_T^2 q^2} \right)^{\otimes 2}. \quad (4.95)$$

When the eigenvalues of the phonon propagator matrix are found, the velocities associated

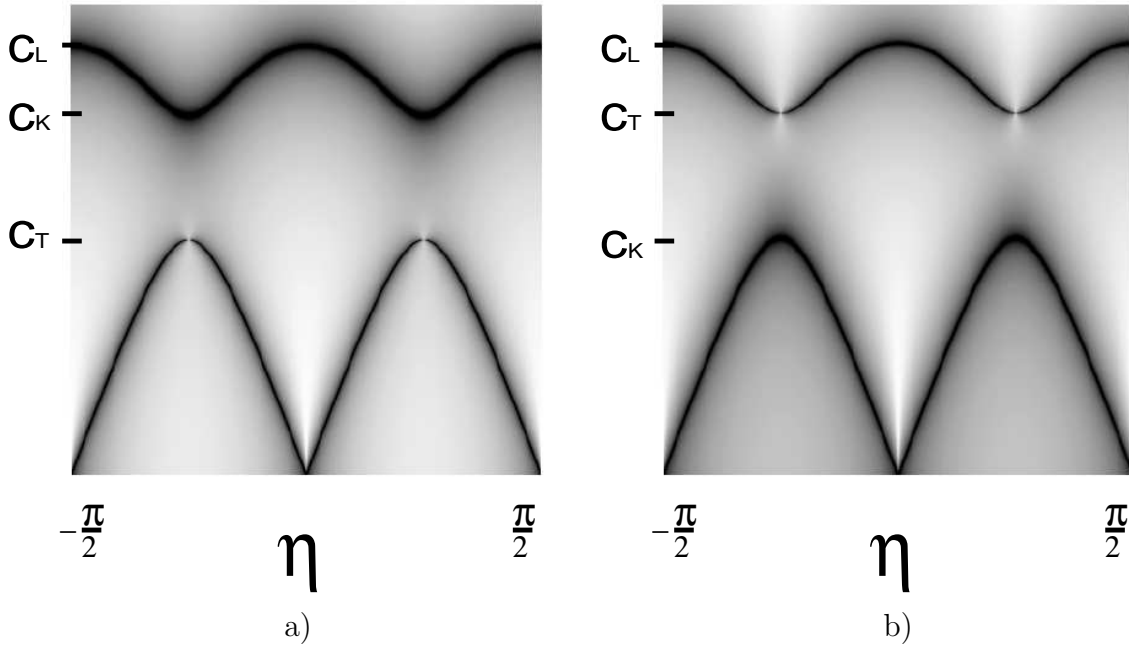


Figure 4.2: The anisotropic velocity softening in the ordered nematic: parallel ( $\eta = 0$ ) and perpendicular ( $\eta = \pm\pi/2$ ) to the Burgers director, the longitudinal velocity is intact, while the transversal phonon, i.e. the ‘magnetic shear’ is completely softened. In contrast, at  $\eta = \pm\pi/4$  the ‘electric shear’ is completely screened leaving the longitudinal phonon with only compressional rigidity, while the transversal phonon is intact. The two figures correspond to a) positive- and b) negative Poisson ratio  $\nu$  when the hierarchy of the compression and shear velocities is interchanged. The thickness of the lines corresponds to the long-wavelength limit pole strength in the longitudinal phonon Eq. (3.33). While for the positive Poisson ratio the transversal phonon has only a weak signal which vanishes at  $\eta = \pm\pi/4$ , when the compressional velocity is lower than the shear velocity, the two poles exhibit the avoided level crossing for the intermediate values of  $\eta$ , so that at  $\eta = \pi/4$  the entire strength of the longitudinal phonon lies in the lower pole.

with the two poles are given as

$$c_{1,2}^2 = \frac{1}{2} \left[ (c_K^2 + c_T^2) \pm \sqrt{(c_K^2 + c_T^2)^2 - 4c_K^2 c_T^2 \sin^2 2\eta} \right]. \quad (4.96)$$

Fig. 4.2 shows the periodic exchange of the shear softening between the longitudinal and transversal sector.

The shear softening in the particular cases of angle  $\eta$  that we analysed earlier are reproduced here (disappearance or quadratic dispersion of a mode are considered to have the vanishing propagation velocity). The general values of the propagation angle  $\eta$  show that propagation velocities have a 4-fold angular periodicity, just as anticipated from the arguments on the spin-2 shear. The 4-fold periodicity is just an artifact due to squaring of spin-2 screening gap (recall relation  $\sin^2 2\eta = \frac{1}{2}(1 - \cos 4\eta)$ ), just like the other physical

spin-2 effects like d-wave superconductivity which shows four nodes).

The angle dependence of the phonon velocities gives a good clue about the quadratic mode in the propagator Eq. (4.93). The magnetic shear, which is the dominant degree of freedom in the transversal sector, becomes entirely gapped both in  $\eta = 0$  and  $\eta = \pi/2$  cases and in the vicinity its velocity vanishes as

$$c_1 \approx \frac{c_K c_T}{c_L} \sin 2\eta = \frac{1+\nu}{2} c_T \sin 2\eta. \quad (4.97)$$

A degree of freedom cannot vanish even when it becomes infinitely soft. It was earlier established that the exception in the  $\eta = \pi/2$  case is due to the glide constraint which ‘eats’ the condensate mode. When  $\eta = 0$ , this is no longer the case. One of the two poles in the transversal propagator become gapped as  $\omega_1^2 = \Omega^2 + (c_d^2 + c_T^2)q^2 + \dots$  and can be thought of as the fully gapped magnetic shear. The other mode lost all of its shear rigidity so one might at first expect that it has no dispersion  $\omega = 0$ . On the other hand, the second mode becomes the dislocation condensate sound at small length scales  $\omega \propto c_d q$ . The only way to ‘patch’ the short-wavelength linear dispersion with the ‘flat’ dispersion in the long-wavelength limit is to make the excitations possible via the second order process. The ‘flat’ mode thus couples to the massive shear with dispersion  $\omega_n = i\omega_1$  so that the first-order perturbation theory gives the dispersion  $\omega_2 = c_d c_T q^2 / \omega_1$  which is exact.

The behaviour of the dislocation condensate second sound is particularly interesting in the physically relevant case of the resonant velocities  $c_d \equiv c_T$ . When the two velocities are different, it is natural to expect that the dislocation sound pole has vanishing strength at short length scales as one wants to recover the ideal crystal response. However, when the two velocities are precisely the same a miracle occurs: two poles of equivalent strengths are present at all wavelengths having dispersions  $\omega \approx c_T q$ . So how does it happen that we never see *two* poles in the transversal phonon propagators but always only one? A closer inspection of the dispersion gives that the two excitations are split by the Higgs gap

$$\omega_{1,2}(\mathbf{q}) = c_T q \pm \frac{\Omega}{2} + \frac{\Omega^2}{8c_T q} + \dots \quad (4.98)$$

Such a spectral response is represented in Fig. 4.3. In order to be able to make the distinction between these poles in an experiment, a resolution higher than the Higgs gap is required. In the ideal crystal this discrepancy between the poles is vanishing and therefore, only one transversal phonon is observed despite the fact that it represents a doublet of two microscopically distinct modes.

The journey through this new quantum phase of matter, the ordered quantum nematic phase is over and let us summarize the most important results. The phase itself is closely related to the famous hexatic phase predicted by Nelson, Halperin and Young [45, 46, 47], apart from being a quantum version including the dynamics. The translational symmetry is restored, but, in contrast to the hexatic phase of NHY where the dislocations proliferate in all three directions permitted by lattice type, here, the lattice artifacts are merged into the effective action Eq. (3.24) and the dislocations are only allowed to have a particular orientation of their Burgers directors. This direction is crucial for the identification of the

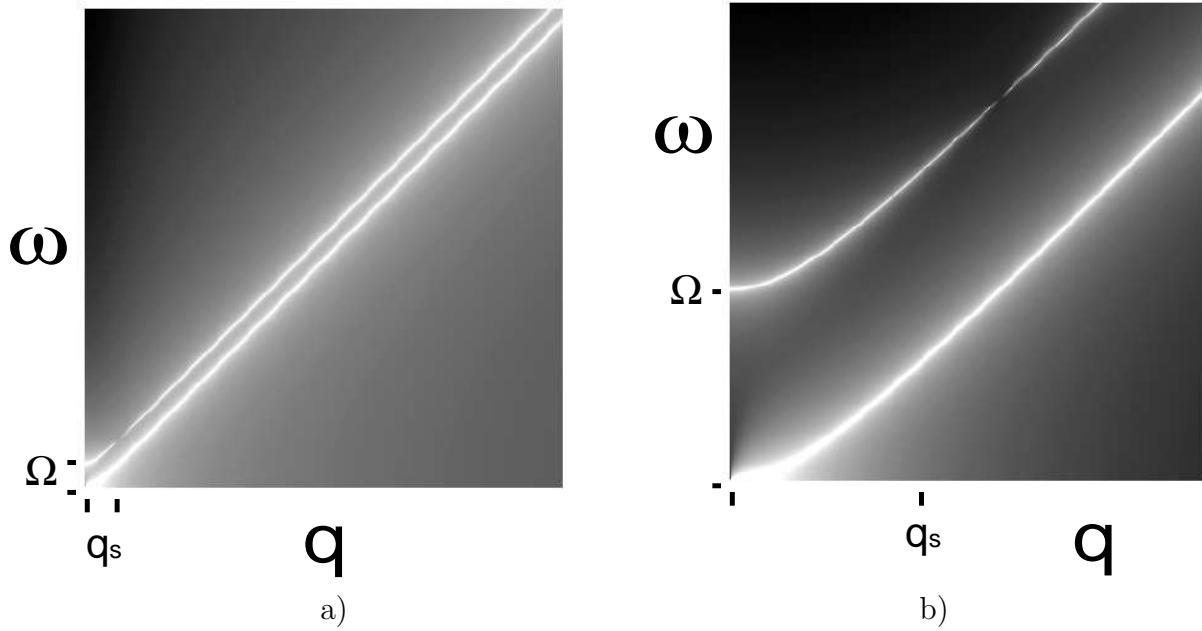


Figure 4.3: The transversal phonon spectral response of the ordered nematic at  $\eta = 0$ : a) in the long-wavelength sector, an additional mode is present originating in the dynamical condensate (longitudinal photon  $B_L^L$ ), one has the shear Higgs gap  $\Omega$ , and another is diffusive; b) at scales smaller than the shear penetration depth, the transversal phonon recovers. However, due to the velocity resonance, it propagates in form of a doublet, split by the minute shear gap  $\Omega$ .

shear component which has to become massive. This degree of freedom materializes itself as the third mode, implying that the shear stress photons and the dislocation degrees of freedom are just two sides of the same coin, and we look at one of them accordingly to the choice of the gauge fix. Since there is always one photon to be gapped, the shear gap is isotropic, but the phonon velocity softening is not, because it is subjected to spin-2 modulations. Clearly, the phase resembles, with regard to the translational symmetry breaking, the smectic phase of liquid crystals, except that the translational symmetry restoration is not implied by geometrical nature of liquid crystalline constituents (rods pointing in one direction), but rather by the dislocations Burgers vectors. In the static limit it even seems as that the strain correlations may match although the smectic phase does not have well-defined in-plane displacements. Nevertheless, once the dynamical features of the theory are considered, the symmetry properties of the shear excitations remove the similarities and the question to ask is if our theory may be dressed, e.g. by interstitial degrees of freedom, to recover the classical smectic phase.

## 4.5 The topological nematic phase

The last phase of matter that we wish to address in terms of Abelian-Higgs dual theory applied to elasticity is the topological nematic phase. This phase is characterized, similarly to the superfluid, by the disorder in the Burgers director degree of freedom, short-ranged shear excitations and isotropy of the phase. This phase is, however, not identical to the superfluid because of the ‘status’ of topological defects therein: in a superfluid disclinations are appearing as free excitations, whereas the nematic phases are by the definition phases where any unbound disclination defects are strictly prohibited. In this respect, this phase represents the topological (or “Coulomb”) phase of the gauge field theory of rotors  $\mathbf{n}$  minimally coupled to Ising gauge fields  $\sigma^z$  as given by Hamiltonian Eq. (4.37). This claim, reviewed in detail in section 4.2 was presented first in Ref. [44], where Zaanen *et al.* realized that the generalization of the famous hexatic phase by Nelson, Halperin and Young [45, 46, 47] to the quantum case offers a richer phase diagram because of the possibility of either (quantum) order or disorder in the Burgers sector. In the previous section we already developed the theory for the case of a nematic characterized by order in its Burgers sector. When the Burgers order parameter Eq. (4.33) becomes disordered a new phase of matter is born and in this section we will try to find an appropriate theory for its physical description.

One can wonder, what is behind the disorder of the Burgers director? Surely, the first term of the action Eq. (4.34) favours ‘angular’ delocalization of Burgers vectors, but one would like to know where it is coming from. From a naive perception of a single dislocation in a solid, but also from the dislocation current conservation law, whose validity is required in phases described by ‘single curl’ stress gauge fields, a Burgers vector appears as a robust topological object that likes to preserve its value over time. This is true as long as there are no disclinations in the vicinity of the dislocations that could interfere with its Burgers vector orientation. Namely, whenever a finite disclination density is present in the system, the dislocation currents are not conserved as seen in Eq. (3.51) and as a consequence the Burgers vector of a dislocation is also not conserved. This can alternatively be seen as a consequence of parallel transport of the Burgers vector in a curved space: in absence of disclinations curvature is absent, resulting in the conservation of the Burgers charge; presence of disclination implies finite curvature and accordingly the Burgers vector is rotated if subjected to the parallel transport in this curvature field. Given that disclination defects are bound in the nematic phases, the dislocation currents and the ‘single curl’ stress gauge field formalism are safe on the global level. Locally however, bound pairs of disclinations and antidisclinations may be present and they will act as the disordering agents in the Burgers sector. This feature is especially prominent in the vicinity of the phase boundary between the ‘nematic’ region and the superfluid phase in Fig. 4.1, where bound pairs of disclinations start to appear in the system with growing characteristic lengths. A large characteristic size of the bound disclination loop greatly enhances the probability for these ‘Burgers scattering’ processes which is the heuristic argument behind the placement of the phase boundary between the ordered and the topological nematic phases in the phase diagram on Fig. 4.1

In order to construct a mathematically consistent theory of the topological nematic in this section, we rely on the ideas and formalisms developed in previous sections of this chapter. The main difference between the ordered and the topological nematic is that the expectation value of the Burgers director order parameter Eq. (4.33) is vanishing which at the same time implies that the Burgers vector  $\mathbf{n}$  is not well defined anymore. A serious problem arises at this point, given that we want to couple ‘Burgersless’ dislocations, dislocations without any notion of the Burgers vector, to the dual stress gauge fields, since it was earlier shown in Eq. (4.29) that this coupling is always determined by the direction of the Burgers vector of the dislocation. One cannot just take the definition of the effective gauge field Eq. (4.29) and make the mean field average with use of  $\langle \mathbf{n} \rangle = 0$  as that would lead to theory without effective Burgers charges (dislocations decouple entirely from the theory). The Burgers director order parameter is, however, the more relevant observable, being well-defined both in the phases with order or disordered in the Burgers sector. In other words, the expectation value

$$\langle n^a n^b \rangle = \langle Q^{ab} \rangle + \frac{1}{2} \delta_{ab} \rightarrow \frac{1}{2} \delta_{ab} \quad (4.99)$$

is finite, in spite of the vanishing expectation value for the Burgers vector alone. Therefore, the mean-field averaging with respect to the Burgers degrees of freedom can be done with meaningful implications on the role of the dislocations in the theory. Using the averaged value Eq. (4.99) for each quadratic appearance of the effective gauge fields Eq. (4.29), one can obtain the Higgs term equivalent to the starting Higgs term Eq. (4.70) with the Burgers director  $Q^{ab}$  set to zero.

At this point we are obliged to provide a scientific disclaimer: the theory which will be developed here is constructed as a pure mathematical treatise of the dual elastic theory as presented in the previous sections of this chapter. All the results are obtained in the Gaussian order and the topological phase is supposed more than anything else to be the representative phase in our theory of the nematic driven quantum melting of solids, if there had not been an inconsistency problem in the formalism that shines some doubts on the final results. Namely, after the ‘naive’ mean-field averaging of the Burgers sector is performed, the number of degrees of freedom in the theory becomes augmented by one. This fact is in contradiction with the property of the Gaussian theories that the number of degrees of freedom should not change, under any circumstances. Nevertheless, the motivation to present the results obtained within this formalism will be explained. If the theory indeed has some kind of glitch (most probably some gauge artifact) due to the ‘naive’ averaging, we hope that an expert in these matters could easily point us the proper way to proceed with the formalism and the new theory should by rule be built on the present state of the formalism. We are however inclined to think that the results we obtain have a physical sense and are relevant to another phase, the one that will be introduced in the next chapter and called the ‘isotropic’ nematic phase. For the moment it will be referred to as the Gaussian topological nematic. The discrepancy in the number of the degrees of freedom is of course related to the ‘naive’ averaging, but we will make the case that the same results are alternatively obtained if one does the exact averaging procedure, based on the path integral, and then keeps only the Gaussian terms in the action. Therefore, one

thing has to be sacrificed. We can keep terms beyond the Gaussian order and obtain the formally correct and exact answers for the topological nematic phase, but the price we pay is the need to calculate higher order corrections to the propagators. If we are determined to keep only the Gaussian order terms in the action, the workings of the Higgs mechanisms are such that the Abelian-Higgs longitudinal photon (which we identified as related to the shear photons) splits its Higgs contribution to both longitudinal and transversal sectors. In fact, our claim is that the only Higgs term permitted by the symmetry requirements, (isotropy in Burgers ‘flavours’) is the one we construct here.

The exact arguments are kept for the end of this section as it will be easier to present them, once we went through the entire formalism. This problem might be viewed as that the Gaussian approximation is in contradiction with itself and that the only way to properly describe the topological nematic is to keep all higher order terms in the action. We do believe that such a treatise would produce the ‘strongly interacting’ topological nematic, the way that Zaanen *et al.* envisaged it, only with a dynamical dislocation condensate. However, having analysed the theory only on the Gaussian level and we want to find out if the Gaussian topological nematic can be ‘repaired’ into a mathematically consistent theory. Based on the arguments in the following section, we believe that the answer is positive, except that the theory of dislocations given in section 4.2 has to be changed. This change implies, as its ultimate consequence, that the phase of matter that we describe in this section, which is at the same time the only isotropic nematic phase on the Gaussian level, is rather a ‘collection’ of dislocation condensates, each with the Burgers director in a particular direction, than a single condensate of ‘Burgersless’ dislocations. Having a myriad of condensates at our disposal, each carrying its own sound degree of freedom, the problem of a missing degree of freedom is trivially patched. Unfortunately, this phase cannot be regarded as topological in a sense of Lammert, Toner and Rokhsar since each of the condensates carries a well defined Burgers vector. The precise details of the construction of the disorder sector are left for the following section.

Let us now, begin with the construction of the action for the topological condensate. In spite of the complicated theory behind the Burgers vector disordering and problems associated with the counting of the degrees of freedom, the technical part of this section is more trivial than its corresponding part in the case of the ordered nematic. This is the consequence of the fact that the coupling terms between the longitudinal and the transversal sector average to zero. Since the two sectors are decoupled, the effective action continues to factorize into longitudinal and transversal ‘sectors’, as was the case in the ideal crystal. In addition, the chiral propagators are strictly equal to zero and the phase is isotropic.

For reasons of compatibility with the previous section, we use the same, ‘Lorentz’ gauge fix Eq. (4.59). This choice for the gauge fix helps us in few aspects. We already found the Ehrenfest constraint in this particular gauge fix in Eq. (4.64). The same is true for the ideal crystal contribution to the propagator, i.e. the first term of Eq. (4.16), which we do not have to recalculate again, but instead we can just reuse the result from the Eq. (4.65). Finally, the Higgs term Eq. (4.70) with the Burgers director order parameter set to  $\langle Q^{ab} \rangle = 0$  is the expression defining the Gaussian topological nematic phase. We, however, decide to

make a detour at this point and instead of Eq. (4.70) we use an alternative route to obtain the Higgs term of the topological nematic phase. The results obtained in this way are naturally the same as if we employed the Higgs term Eq. (4.70). This alternative route to the Higgs term of the topological nematic makes the workings of the disorder currents more apparent by removing the constraint currents and gauge fields from the minimal coupling and leaving only the shear stress fields to be subjected to the Higgs mechanism. The difference with respect to the ordered nematic phase is that there is no notion of preferred direction in the topological nematic phase. Accordingly, the dislocation condensate restores the translational continuous symmetry in all directions which reflects in the fact that both electric and magnetic shear acquire Higgs mass in a democratic fashion.

The separating of the compressional, rotational and shear dual stress photons in the minimal coupling term in Eq. (4.16) is performed by a ‘rotation’ of the original linearly polarized dual stress gauge field components  $B_h^E$ . The minimal coupling is rewritten as

$$\begin{aligned} \mathcal{L}_{BJ} = iB_h^{E\dagger} J_h^E &= \frac{i}{1 + \cos^2 \theta} \left[ (B_{+1}^{L\dagger} - i \cos \theta B_{-1}^{T\dagger})(J_{+1}^L + i \cos \theta J_{-1}^T) + \right. \\ & (B_{-1}^{T\dagger} - i \cos \theta B_{+1}^{L\dagger})(J_{-1}^L + i \cos \theta J_{+1}^T) + (B_{+1}^{T\dagger} - i \cos \theta B_{-1}^{L\dagger})(J_{+1}^T + i \cos \theta J_{-1}^L) + \\ & \left. (B_{-1}^{L\dagger} - i \cos \theta B_{+1}^{T\dagger})(J_{-1}^T + i \cos \theta J_{+1}^L) \right] \equiv i\mathcal{B}_h^{E\dagger} \mathcal{J}_h^E, \end{aligned} \quad (4.100)$$

with the ‘dynamical cosine’ already introduced in the definition of the polarization basis Eq. (4.60 - 4.62) as  $\cos \theta = \omega_n/p_d$ . The unitary transformation behind this rotation is dynamical which is seen from the definitions of the ‘curly’ gauge fields and ‘curly’ dynamical dislocation currents

$$\mathcal{B}_{+1}^L = \frac{1}{\sqrt{1 + \cos^2 \theta}} (B_{+1}^L + i \cos \theta B_{-1}^T), \quad \mathcal{J}_{+1}^L = \frac{1}{\sqrt{1 + \cos^2 \theta}} (J_{+1}^L + i \cos \theta J_{-1}^T) \quad (4.101)$$

$$\mathcal{B}_{+1}^T = \frac{1}{\sqrt{1 + \cos^2 \theta}} (B_{+1}^T + i \cos \theta B_{-1}^L), \quad \mathcal{J}_{+1}^T = \frac{1}{\sqrt{1 + \cos^2 \theta}} (J_{+1}^T + i \cos \theta J_{-1}^L) \quad (4.102)$$

$$\mathcal{B}_{-1}^L = \frac{1}{\sqrt{1 + \cos^2 \theta}} (B_{-1}^L + i \cos \theta B_{+1}^T), \quad \mathcal{J}_{-1}^L = \frac{1}{\sqrt{1 + \cos^2 \theta}} (J_{-1}^L + i \cos \theta J_{+1}^T) \quad (4.103)$$

$$\mathcal{B}_{-1}^T = \frac{1}{\sqrt{1 + \cos^2 \theta}} (B_{-1}^T + i \cos \theta B_{+1}^L), \quad \mathcal{J}_{-1}^T = \frac{1}{\sqrt{1 + \cos^2 \theta}} (J_{-1}^T + i \cos \theta J_{+1}^L) \quad (4.104)$$

The connection to the earlier defined symmetric stress gauge fields,  $\mathcal{B}_C$ ,  $\mathcal{B}_R$ ,  $\mathcal{B}_{el.sh.}$  and  $\mathcal{B}_{m.sh.}$  is obvious, the gauge fields Eq. (4.101 - 4.104) are the normalized versions of the former gauge fields. The labels of the ‘curly’ currents are chosen in such way that each stress gauge field or the dislocation current collapses onto its curly counterpart in the static limit ( $\omega_n \rightarrow 0$ , i.e.  $\cos \theta = 0$ ). Given that the minimal coupling term Eq. (4.100) is split into terms with different symmetry properties, the constraints are fairly trivial to implement at this stage.

Let us first treat the glide constraint. Expressed in terms of the helical components, the constraint Eq. (3.61) transforms into

$$0 = \epsilon_{ab} J_a^b = \epsilon_{ab} e_a^h \tilde{e}_b^E J_h^E = J_{+1}^T + i \cos \theta J_{-1}^L, \quad (4.105)$$

and this is precisely the curly dislocation current  $\mathcal{J}_{+1}^L$ . Since this current cannot contribute to the minimal coupling term, its conjugated stress gauge field is ‘protected’ from the Higgs mechanism. This dual stress gauge field, protected by the glide constraint, is  $\mathcal{B}_{+1}^L$  and this is just the (normalized) compression stress photon  $\mathcal{B}_C$ .

The Ehrenfest constraint is implemented in a similar fashion, except that the corresponding term is not completely removed from the minimal coupling Eq. (4.100). Instead, the Ehrenfest constraint implemented accordingly to Eq. (4.64) requires  $\mathcal{B}_{+1}^L = 2\sqrt{1 + \cos^2 \theta} \mathcal{J}/p_d$ , which introduces the external source field  $\mathcal{J}$  into the Higgs term. The presence of the external source field of the transversal phonon has its influence on the Zaanen-Mukhin relation of the topological phase. When we ask physical questions not directly related to the transversal phonon, this whole term is simply set to zero.

After the constraints have been implemented, the Higgs term of the topological phase in the Gaussian order reads

$$\mathcal{L}_{Higgs} = \frac{1}{2} \frac{\Omega^2}{2\mu} \left[ \mathcal{B}_{+1}^{T\dagger} \mathcal{B}_{+1}^T + \mathcal{B}_{-1}^{T\dagger} \mathcal{B}_{-1}^T - \frac{4(1 + \cos^2 \theta)}{p_d^2} \mathcal{J}^\dagger \mathcal{J} \right]. \quad (4.106)$$

The curly stress gauge fields  $\mathcal{B}_{\pm 1}^T$  correspond to the normalized ‘electric-’ and ‘magnetic’ shear components, and according to the first two terms of Eq. (4.106), both of them acquire a Higgs mass. The presence of the ‘curly’ fields with exclusive transversal flavours in the Higgs term Eq. (4.106) can be interpreted as that the dislocation carry only the transversal Burgers charges. The statement is, however, correct only in the static limit, when the curly stress gauge fields become equivalent to their regular counterparts. At any finite frequency, this is no longer true as can be seen from the unitary transformation Eqs. (4.101 - 4.104) where the dual stress gauge fields with longitudinal and transversal flavours dynamically admix into the shear photons.

The original strains as well as the Zaanen-Mukhin relations are usually given in terms of the linearly polarized dual stress gauge fields  $B_h^E$  so the curly fields in Higgs term Eq. (4.106) have to be ‘rotated’ back, but is also necessary to use the Ehrenfest constraint again as

$$\mathcal{B}_{-1}^T = \sqrt{1 + \cos^2 \theta} B_{-1}^T + \frac{2}{p} \mathcal{J}. \quad (4.107)$$

This leads to the final form of the topological nematic Higgs term

$$\mathcal{L}_{Higgs} = \frac{1}{2} \frac{\Omega^2}{2\mu} \left[ \frac{|B_{+1}^T + i \cos \theta B_{-1}^L|^2}{1 + \cos^2 \theta} + (1 + \cos^2 \theta) |B_{-1}^T|^2 - \frac{4}{p_d^2} \mathcal{J}^\dagger \mathcal{J} + i 2 \cos \theta (B_{-1}^{T\dagger} \mathcal{J} - \mathcal{J}^\dagger B_{-1}^T) \right]. \quad (4.108)$$

Terms not containing the external source term  $\mathcal{J}$  can alternatively be written in terms of the stress gauge fields self-energy matrix as

$$-\square_H = \frac{\Omega^2}{2\mu} \left[ \frac{(p_d, -i\omega_n, 0) \otimes (p_d, i\omega_n, 0)}{2\omega_n^2 + c_d^2 q^2} + \frac{2\omega_n^2 + c_d^2 q^2}{\omega_n^2 + c_d^2 q^2} (0, 0, 1)^{\otimes 2} \right]. \quad (4.109)$$

The tensorial square represents, like in the previous section, the outer product of a vector with itself resulting in a matrix. This self-energy matrix enters the total dual stress gauge fields propagator according to Eq. (4.83).

Now we can ask the ‘measurable’ questions again: what are the phonon propagators of the topological nematic phase described by Higgs term Eq. (4.108)? To answer this question, one needs the Zaanen-Mukhin relations for phonons. The relation for the longitudinal phonon is, as it was the case in the ordered nematic, unchanged in the presence of the condensate, implying that the Eq. (4.45) is still valid. When invoked, this relation yields the longitudinal phonon propagator of the topological nematic phase as

$$G_L = \frac{1}{\mu} \frac{c_T^2 q^2 (\omega_n^2 + c_g^2 q^2 + \Omega^2)}{(\omega_n^2 + c_L^2 q^2)(\omega_n^2 + c_g^2 q^2) + \Omega^2 (\omega_n^2 + c_K^2 q^2)}, \quad (4.110)$$

introducing the ‘glide’ velocity  $c_g = c_d/\sqrt{2}$  in the problem. The effective halving of the dislocation condensate rigidity is not an accident: it is a consequence of the glide constraint applied to the topological nematic [50, 44].

Although we recovered the exact expression for the longitudinal phonon, partially due to the decoupling between the transversal and the longitudinal sector, we may want to analyse Eq. (4.110) in physically relevant cases. However, there is actually no need for that. The topological longitudinal photon Eq. (4.110) is exactly equal to its counterpart in the ordered nematic when the propagation angle is  $\eta = \pi/4$ . In the previous section we analysed this case and found that the longitudinal phonon acquires an additional mode corresponding to the gapped electric shear photon. The original phonon mode stays massless, but at long wavelengths the shear rigidity is gone and the phonon propagates with the compression velocity  $c_K$ . At short wavelengths the shear rigidity is recovered and the original longitudinal phonon velocity is restored.

In the transversal sector, the Zaanen-Mukhin relation is, just as before, sensitive to the presence of the condensate and in order to recover it, a second derivative of the generating functional corresponding with the topological nematic action is found. The resulting relation is

$$G_T = \frac{1}{\mu} \left( 1 + \frac{2\Omega^2}{p_d^2} \right) - \frac{\omega_n^2}{\mu^2} \left( 1 + \frac{\Omega^2}{p_d^2} \right)^2 \langle\langle B_{-1}^{T\dagger} | B_{-1}^T \rangle\rangle. \quad (4.111)$$

When the dual gauge field propagator, extracted from the action with the self-energy Eq. (4.109), is used in the topological nematic Zaanen-Mukhin relation Eq. (4.111), the transversal phonon propagator of the Gaussian topological phase follows as

$$G_T = \frac{1}{\mu} \frac{c_T^2 q^2 (\omega_n^2 + c_d^2 q^2) + \Omega^2 (\omega_n^2 + c_g^2 q^2 + c_T^2 q^2) + \Omega^4}{(\omega_n^2 + c_T^2 q^2)(\omega_n^2 + c_d^2 q^2) + \Omega^2 (\omega_n^2 + c_g^2 q^2)}, \quad (4.112)$$

involving earlier introduced ‘glide’ velocity  $c_g$ .

Before delving deeper into the problems associated with the number of degrees of freedom in Eq. (4.112), let us just quickly review the excitation content and their behaviour

at short- and long-wavelengths. The transversal propagator Eq. (4.112) has two poles. At the length scales smaller than the Higgs gap ( $q, \omega_n \ll \Omega$ ), the ideal crystal transversal photon is recovered. The other mode is the dislocation sound with approximate dispersion  $\omega \sim c_d q$ . In analogy with the ordered nematic phase, the dislocation sound pole strength is vanishing unless the transversal phonon and the dislocation sound velocities are resonant,  $c_T = c_d$ , when the resonant splitting of the transversal phonon by  $\Omega$  is present for any finite dislocation density.

Surprisingly, this phase has a long-wavelength spectrum not much different from that of the ideal crystal. If one considers only the low-energy sector, the massive mode with gap  $\Omega$  is invisible, and the effective propagator

$$G_T(\Omega = \infty) = \frac{1}{\rho \omega_n^2 + c_g^2 q^2} \Omega^2 + O(1), \quad (4.113)$$

has only one massless mode dispersing at the glide velocity. It may seem quite surprising that the glide velocity appears in the transversal sector, given the fact that the glide constraint acts solely in the longitudinal sector. The physical interpretation of this mode, as well as of the other physical features represented by phonon propagators Eqs. (4.110 and 4.112), will be given in the following section in terms of the disorder field that is constructed in an alternative manner. This is necessary since these propagators face a serious problem regarding the number of physical degrees of freedom contained therein.

To explain this, let us count the degrees of freedom in the dual stress gauge field theory as defined by the partition function Eq. (4.35). In the Coulomb phase there were two dynamical degrees of freedom, transversal photons  $B_T^{L,T}$  corresponding to the phonon excitations and one non-dynamical degree of freedom, the Coulomb photon  $B_T^T$ . The other Coulomb photon  $B_T^L$  is removed by the Ehrenfest constraint and the longitudinal photons  $B_L^{L,T}$  are removed by the gauge fix. In the section 4.2, it was demonstrated that only one  $U(1)$  disorder complex field suffices for the description of the ordered nematic phase. When the dislocation condensate is formed, the phase degree of freedom is transferred to the longitudinal photon with the ‘parallel’ flavour, that is to  $B_L^{\parallel} = n^a B_\mu^a$ , which becomes the physical entity. Its counterpart, the ‘perpendicularly’ flavoured longitudinal photon  $B_L^{\perp}$ , remains in the gauge volume, so that it is still an unphysical field. In the case of the ordered nematic, this ‘rule of thumb’ was mathematically consistent and yielded the additional shear/dislocation sound mode.

This is no longer true when one considers the elastic response expressed through the phonon propagators Eqs. (4.110, 4.112). Each of these two propagators carries two poles which adds up to four degrees of freedom in total, which is greater by one than the number of degrees of freedom that the theory started with. Obviously, the treatment of the topological nematic phase presented in this section has introduced an additional mode in the theory. On the other hand, the theory is Gaussian and the Gaussian theories *may not* change the number of degrees of freedom in the theory. So where did we go wrong?

The procedure of ‘naive’ averaging of the Higgs term by invoking the isotropic Burgers director Eq. (4.99) might have already sparked some concern among the connoisseurs

reading this text. Namely, in the phase where the Burgers vector is not well-defined, one cannot decide which flavour is supposed to take the role of the phase degree of freedom and the only isotropic solution is to Higgs both flavours (be it  $x$  and  $y$  or  $L$  and  $T$ ) equally, that is to construct the Higgs term as

$$\mathcal{L}_{Higgs} \sim B_\mu^a B_\mu^a. \quad (4.114)$$

Thus, here lies the answer to the question on the additional degree of freedom. By making the ‘democratic’ Higgs term of kind Eq. (4.114), there is not one, but two longitudinal photons  $B_L^a$  that become physical. At the same time there is only one phase degree of freedom in the disorder field that would like to be represented by the longitudinal photon  $B_L$ , therefore in the Higgs term Eq. (4.114) this degree of freedom got split in two. Since the degrees of freedom are not supposed to split in the treatments of the Gaussian theories, the only logical conclusion is that the Gaussian topological nematic phase is self-inconsistent. This might seem as a big blow to the theory presented in this section, however, the results obtained in this way may be justified, as it will be the case in the next section.

At this point we may try to ‘patch’ the theory in order to obtain the consistent theory of the nematic phase with only one condensate whose Burgers vectors show no preference for any particular direction. The ‘mean-field’ Gaussian treatment with the ‘naive’ implementation of the Higgs term Eq. (4.70) proved to be wrong, so let us step back to the partition function Eq. (4.35) and give the special attention to the path integral over the Burgers vector directions  $\mathcal{D}\mathbf{n}$ . For simplicity, it will be assumed, without a proof, that the path-integrations may exchange their order. The only two terms of the action that depend on the Burgers direction are the Burgers director action Eq. (4.34) and the minimal coupling term which reads

$$\mathcal{L}_{Higgs}[\mathbf{n}] = \frac{1}{2} |\Psi_0|^2 n^a n^b B_h^a B_h^b \quad (4.115)$$

in the Higgs phase. For the sake of simpler notation, the argument is presented with the Higgs term Eq. (4.115) suited for the gauge fix Eq. (4.59). If any other gauge fix was chosen or the gauge invariant Higgs term of kind Eq. (2.73) was used, the arguments would follow the same line.

The Burgers director action Eq. (4.34) is supposed to weight the configurations of the Burgers vector field, i.e. treat it as a dynamical field. If the theory considers excitations of the Burgers field, one of the consequences is the scattering on the Burgers vectors as it would follow from the Higgs term Eq. (4.115). These scattering processes are not Gaussian, and given that we are interested in the Gaussian theory, the Burgers director excitations effectively decouple from the dual stress gauge degrees of freedom. Hence, the Burgers director is treated only as a ‘global’ orientation field, which is the same throughout the entire system. The path integral reduces to a regular integral  $\mathcal{D}\mathbf{n} \rightsquigarrow \mathbf{d}\mathbf{n}$ , and the Burgers director action makes no discrimination between different orientations which results in the following partition function

$$Z = \int \mathcal{D}B_h^E \mathcal{F}_{Ehr.}(B_h^E) e^{-S[B_h^E]} \int \frac{\mathbf{d}\mathbf{n}}{2\pi} e^{-\frac{1}{2} \int d\tau d\mathbf{x} |\Psi_0|^2 n^E n^F B_h^E B_h^F}. \quad (4.116)$$

The action  $S[B_h^E]$  is the total action modulo the Higgs term Eq. (4.115) which is dependent on the Burgers director and therefore separated into the second exponent. The Ehrenfest constraint is imposed by function  $\mathcal{F}_{Ehr}$ .

The integral over the Burgers vector in the partition function Eq. (4.116) can be done analytically and the resulting contribution to the action, which corresponds to the effective Higgs term of the topological nematic, is exactly

$$\mathcal{L}_{top.} = |\Psi_0|^2 \left[ \frac{1}{2} B_h^E (\frac{1}{2} \delta^{EF}) B_h^F + \ln I_0\left(\frac{B_h^L B_h^L}{4}\right) + \ln I_0\left(\frac{B_h^T B_h^T}{4}\right) + 2 \ln I_0\left(\frac{B_h^L B_h^T}{4}\right) \right], \quad (4.117)$$

where  $I_0(x)$  is the modified Bessel function of the first kind.

Let us now expand the Higgs term Eq. (4.117) and keep only terms up to the Gaussian order. Series of the logarithms of the Bessel functions contain only fourth and higher order terms in the dual gauge fields  $B_h^E$ , so the only term that remains in the Gaussian order is the first term. And such a Higgs term is precisely equivalent to the disputed Higgs term Eq. (4.114)! Given the already demonstrated fact that such a Higgs term is inconsistent with the disorder theory constructed from the action Eq. (4.32), it follows that one needs to explicitly treat the non-Gaussian terms caused by the expansion of the exact Higgs term Eq. (4.117), in order to give the valid theory of the topological nematic. Reformulated, this statement reads: without the interaction terms, borne by the series expansion of the exact Higgs term Eq. (4.117), the theory of the topological nematic cannot be consistent.

One should not be surprised that the ‘isotropy’ in the Burgers sector yields the Higgs term of Eq. (4.114) kind. Even before any a priori specific knowledge about the disorder field, there are only two possible bare Higgs terms that are in agreement with the required symmetry. This is the consequence of the fact that there are only two spinless rank-2 tensors in two dimensions. One is the trace and it precisely corresponds to the Higgs term as used in this section or given in Eq. (4.114). While this invariant tensor represented the  $A_0$  irreducible representation tensor, the other spinless tensor belongs to  $B_0$  irreducible representation and it is given by the Levi-Civita symbol

$$\mathcal{L}_{Higgs, B_0} \sim \epsilon_{ab} B_h^a B_h^b. \quad (4.118)$$

Of course, the presence of such a Higgs term would be possible only if the ground state of the disorder field breaks the mirror symmetry of the original action. Even if that was the case, in this particular dual theory, the chiral Higgs term Eq. (4.118) vanishes due to the Abelian character of the dual stress gauge fields. It would be an interesting challenge to construct a non-Abelian dual gauge field theory with a chiral Higgs term like the one in Eq. (4.118).

At the end of the section we give the overview of neither the topological phase nor the interpretation of the results obtained here due to the encountered problems with the self-consistency in the theory. Since it was demonstrated that the topological phase needs non-Gaussian treatment, it will not be in the focus of our attention anymore, apart from some speculations in the concluding sections. Nevertheless, this section has two important ramifications, one of them being the statement on the concurrent consistency of three concepts: a) the ‘isotropy’ in the Burgers sector, b) the disordering dislocation gas described

in terms of a single function GLW action and c) the Gaussian theory. Any two of these three concepts can be featured simultaneously and these cases are represented in Fig. 4.4. A theory which is Gaussian and has its disorder described by a single GLW action is the ordered nematic presented in the previous section. This phase is, however, preferring one ‘flavour’ to the other, based on the orientation of the Burgers director, and therefore it violates the isotropy. The topological nematic, on the other hand, has no preferred ‘flavour’ and it has only one dislocation gas described by the field  $\Psi$ . However, it cannot be formulated in terms of the Gaussian theory as it just has been demonstrated. Finally, what happens when one constructs a Gaussian theory of the nematic state which is isotropic in its ‘flavours’? The answer lies in phonon propagators Eqs. (4.110, 4.112), as well as in the dual gauge field self-energy Eq. (4.109). These results, that represent the second big ramification of this section and of the entire thesis, have been derived from the ‘Burgers isotropic’ Gaussian treatment of the dual stress gauge field theory. However, before we may trust them, find the physical interpretations and employ them in the next chapter where the charged nematic phases are considered, an alternative disorder field theory has to be constructed, yielding the Higgs term Eq. (4.114) in a consistent mathematical manner. Naturally, this disorder theory cannot rely on the GLW action for a single gas.

## 4.6 Burgers Higgs fields and the isotropic nematic phase

Facing the inconsistency problems of the “Gaussian topological nematic” in the previous section, we need to find a different interpretation for its results: the dual stress field self-energy Eq. (4.109) and the phonon propagators Eqs. (4.110 and 4.112). Otherwise, the mere mentioning of these results would not be appropriate for a scientific text such as this thesis. The conclusion in the last section was that, if one wants to have a Gaussian theory with an ‘isotropic’ Higgs term, the only consistent way to do it is to abandon the single GLW approach via the dislocation action Eq. (4.32) and construct a different kind of the disorder theory. Naturally, a modified disorder theory may predict phases which cannot be described in terms of the action Eq. (4.32). In this section, the first task will be to develop that alternative disorder theory, with the Gaussian topological nematic as the primarily objective. However, while the disorder theory is being developed, its ramifications will be much stronger: it will justify use of the bare Higgs term Eq. (4.70) for any possible value of the Burgers director Eq. (4.33). Therefore, the total theory will be able not only to describe the two extreme cases, ordered and isotropic nematic, but in addition, the use of the Higgs term Eq. (4.70) will be justified for all intermediate values of the Burgers director. The phase with such an expectation value for its Burgers director order parameter will be called the “partially ordered nematic phase” and at the very end of the section, the case will be made that all the relevant observables of the partially ordered nematic phase follow if the phase is considered as a mixture of the purely ordered and purely isotropic nematic phases. Before that is done, the physical interpretation of the phonon propagators Eqs. (4.110 and

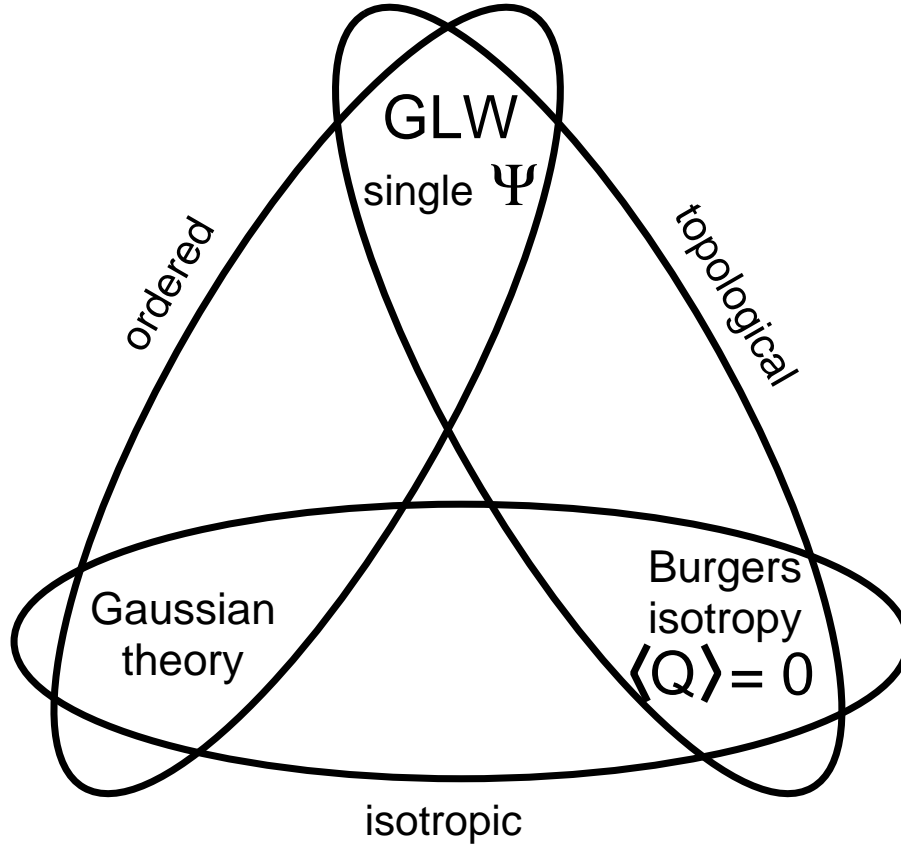


Figure 4.4: “Inconsistency diagram”: a theory that would satisfy all three demands (single wave-function GLW, Gaussian and no order in Burgers sector) is inconsistent. However, by sacrificing one of the demands and keeping the remaining two, a well defined theory can be constructed with different types of the nematic phase as the outcome. These are the ordered, topological and isotropic phase.

4.112) will be presented. That task will not be difficult, once the alternative disorder field theory is understood, because the additional poles and their features will be trivially related to the disorder degrees of freedom.

Let us begin with the considerations for the alternative disorder theory. In the previous section, the discrepancy in the number of degrees of freedom was traced back to the unique form for an ‘isotropic’ Higgs term Eq. (4.114). A single GLW degree of freedom is insufficient to generate the ‘double flavoured’ Higgs term so the first logical solution to the problem would be to introduce an additional bosonic field and use its phase for the physical realization of the second longitudinal dual stress gauge boson. This line of thought seems to be consistent with the structure of the dual gauge theory which is  $U(1) \otimes U(1)$ .

The disorder theory in the section 4.2 singled out one of these two  $U(1)$  gauge theories and associated matter with it. The other stayed decoupled and did not have the ability to undergo the transition into the Higgs phase. Although quite logical and based on the decomposition Eq. (4.27), this kind of action caused quite some trouble when the Burgers vectors became disordered. With two disorder scalar fields the problem with the number of degrees of freedom in the previous section is solved. Let us call the two fields  $\Psi^a$  ( $a = x, y$ ) and minimally couple each of them to the dual stress gauge fields of the same flavour. The two longitudinal photons  $B_L^{x,y}$  can now both become physical, each of them taking the role of the phase of its minimally coupled scalar field.

In spite of the fact that the introduction of an additional scalar disorder field patched the problem associated with the counting of the degrees of freedom, one cannot say much more about the theory unless the scalar fields are given certain physical interpretation and accordingly an action. One might, based on the proposed minimal coupling, assume that the field  $\Psi^x$  corresponds to the gas of dislocations bearing the Burgers director in  $x$  direction and the field  $\Psi^y$  to the dislocation gas with  $y$  flavour. This interpretation might have worked if the theory was considering a square lattice where only these two orientations of the Burgers vector are allowed. However, in the isotropic elastic solid a dislocation may point in any arbitrary direction and at that moment one cannot tell what the overlap between its wave function and either of the fields  $\Psi^{x,y}$  would be. A circumvention of this problem suggested here requires one scalar disorder field for each Burgers direction, which are called ‘‘Burgers Higgs fields’’. There is a grand disorder action associated with these disorder fields. It contains a ‘free’ GLW propagator for each individual Burgers direction and interaction terms between dislocations of different Burgers orientation. The mean-field treatment of this disorder action will produce the long awaited Higgs term for the isotropic nematic phase, but before we get into details, let us first justify the use of a separate disorder field for each particular Burgers orientation.

In order to define the ‘free particle’ action for each of these Burgers orientations, it is necessary that the Burgers vector of a dislocation stays the same along its world-line. This can be checked if the dislocation current conservation is applied to the decomposed current Eq. (4.27) as

$$0 = \partial_\mu J_\mu^a = \partial_\mu (n^a \mathcal{J}_\mu) = (\partial_\mu n^a) \mathcal{J}_\mu + n^a (\partial_\mu \mathcal{J}_\mu) = (\partial_\mu n^a) \mathcal{J}_\mu. \quad (4.119)$$

The second term vanishes since dislocations are conserved objects in the system, i.e. a dislocation cannot be made out of nothing. This conservation law leads to the conclusion that the Burgers vector of a single dislocation does not change along its world-line. In other words, the Burgers vector is a good quantum number, i.e. an integral of motion for a single dislocation.

The argument presented above is true only in the total absence of moving disclinations, because the precise left hand side of the conservation law Eq. (4.119) reads  $-\epsilon_{ab} T_b$ . Of course, any finite density of free disclinations is strictly prohibited in the system, but locally present bound pairs can violate the conservation law Eq. (4.119) and lead to the disorder of the Burgers vectors. However, the disorder of the Burgers vectors means that the

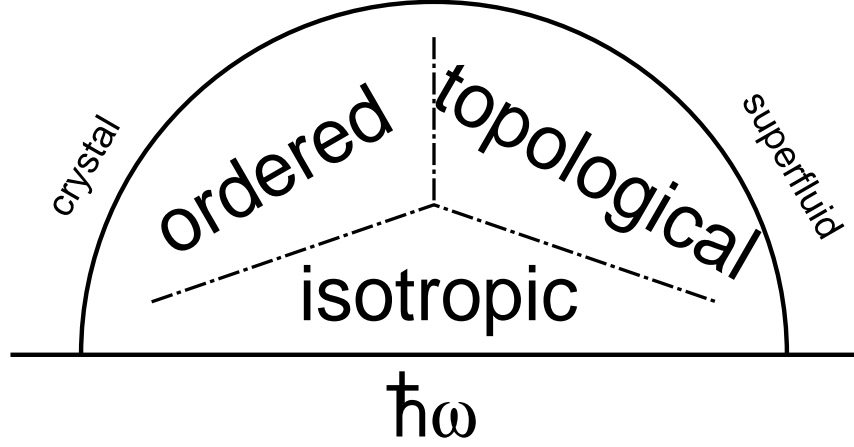


Figure 4.5: Zoom on the ‘nematic dome’ of the newly suggested phase diagram: in addition to the ordered and topological nematic phase, already represented in Fig. 4.1, a new phase is identified which we call the isotropic nematic phase. In order to stabilise each individual dislocation condensate in this phase, the absence of disclinations is required, which is the reason to expect the presence of this phase at very high rotational stiffness parameter  $\ell$ . Compare this phase diagram with Fig. 4.4.

phase is the topological nematic which we wish to avoid due to its notorious non-Gaussian features. Thus, the disorder theory behind the isotropic nematic, which is constructed in this chapter, works only away from the phase transition line to the superfluid phase. Based on these heuristic arguments, an ‘upgraded’ phase diagram for the elastic solid is given in Fig. 4.5.

Let us assign an index  $\mathbf{b}$  to the scalar field corresponding to the gas of dislocation with Burgers vector  $\mathbf{b}$ . Given that the dislocation orientation is a continuous label, all the Burgers fields and associated physical observables will represent the angular density of that field rather than the field itself. In order to obtain the physical fields one has therefore to integrate the Burgers fields over the Burgers angle defined by  $\mathbf{b} = (\cos \eta, \sin \eta)$ . Notice that  $\eta$  measures now the angle between the Burgers vectors and the  $x$ -axis.

With the previously introduced Burgers Higgs fields, the total GLW action can then be written as

$$\mathcal{L}_{dis} = \frac{1}{2} \int \frac{d\eta}{2\pi} \left[ |P_{\mu}^{\mathbf{b}} \psi_{\mathbf{b}}|^2 + m^2 |\psi_{\mathbf{b}}|^2 + \int \frac{d\eta'}{2\pi} |\psi_{\mathbf{b}}|^2 V_{\mathbf{b}, \mathbf{b}'} |\psi_{\mathbf{b}'}|^2 \right], \quad (4.120)$$

where the first two terms represent the ‘free’ particle action and the last term originates in the inter-particle interaction which is proven in the appendix A. The time is converted to the length units with use of the dislocation sound velocity  $c_d$ . The covariant derivative

$$P_{\mu}^{\mathbf{b}} = \partial_{\mu} - ib^a B_{\mu}^a. \quad (4.121)$$

follows from the minimal coupling between a single dislocation with the Burgers vector  $\mathbf{b}$  and the dual stress gauge fields as demonstrated in Eq. (4.28), except that here this scheme is applied to every single direction separately. As usual, the mass term  $m^2$  controls whether bosonic fields are likely to proliferate ( $m^2$  negative) or stay bound ( $m^2$  positive). In an isotropic solid it must be independent on the Burgers vector  $\eta$ . The interaction term, on the other hand, must depend only on the mutual angle between two interacting dislocations ( $\mathbf{b} \cdot \mathbf{b}'$ ). There are further restrictions based on symmetries and they will be discussed in the text that follows.

The minimal coupling Eq. (4.121) also implies the transformational properties of each of the Burgers fields under the gauge transformation Eq. (4.26). In order to keep the disorder action Eq. (4.120), each of the Burgers Higgs fields should transform as

$$\psi_{\mathbf{b}} \rightarrow \psi'_{\mathbf{b}} = \psi_{\mathbf{b}} e^{i\mathbf{b} \cdot \alpha}. \quad (4.122)$$

The Burgers bosonic current is

$$\mathcal{J}_{\mu}^{\mathbf{n}} = \frac{i}{2} [(P_{\mu}^{\mathbf{b}} \bar{\psi}_{\mathbf{b}}) \psi_{\mathbf{b}} - h.c.], \quad (4.123)$$

and together these imply the two-flavoured (physical) dislocation current

$$J_{\mu}^a = \int_0^{2\pi} d\eta b^a \mathcal{J}_{\mu}^{\mathbf{b}}. \quad (4.124)$$

When we have constructed the theory, it will become clear that all but two dislocation current components from Eq. (4.123) decouple from the theory defined in pure strain (phonon) degrees of freedom. Although these currents cannot be measured by means of the phonon propagators, that does not imply that they are unphysical degrees of freedom. The only specialty is that one has to devise an alternative experiment that may capture all the richness of the dislocation dynamical currents with each particular Burgers orientation, Eq. (4.123).

At this point the  $\mathbb{Z}_2$  symmetry in the dislocation field has to be imposed onto the Burgers scalar fields. Recalling the discussion from the section 4.2 about the equivalence between the dislocation with the Burgers vector  $\mathbf{b}$  and the antidislocation with the Burgers vector  $-\mathbf{b}$ , the constraint is imposed by demanding that the Burgers dislocation currents with the opposite Burgers vector are equal modulo the sign change, i.e.

$$\mathcal{J}_{\mu}^{\mathbf{b}} = -\mathcal{J}_{\mu}^{-\mathbf{b}}. \quad (4.125)$$

In terms of the scalar disorder fields, the statement about the  $\mathbb{Z}_2$  symmetry is interpreted as the demand that the Burgers scalar fields with the opposite Burgers vectors are mutually complex conjugate

$$\psi_{\mathbf{b}} = \bar{\psi}_{-\mathbf{b}}. \quad (4.126)$$

To verify the constraint Eq. (4.126), it is substituted in the bosonic current definition Eq. (4.123). What follows is precisely the current constraint Eq. (4.125).

The constraint Eq. (4.126) may be implemented in various manners. One could half the angular domain to the compactified  $[0, \pi)$  and declare the fields in the other half of the Burgers plane dependent. However, this way of imposing the constraint complicates significantly the work later when the angular label  $\eta$  is Fourier transformed. Therefore, the constraint is imposed in a completely different manner: the full domain  $[0, 2\pi)$  is kept in the Burgers label  $\mathbf{b}$ , but only fields  $\psi_{\mathbf{b}}$  are considered independent. The ‘other half’ of the fields, fields  $\bar{\psi}_{\mathbf{b}}$  are constrained fields as implied by Eq. (4.126). As a consequence of this constraint, the absolute values of the Burgers fields in Eq. (4.120) should be replaced by  $|\psi_{\mathbf{b}}|^2 \rightsquigarrow \psi_{-\mathbf{b}}\psi_{\mathbf{b}}$ . One can wonder if there is a problem with the fact that we count the same current twice. This redundancy is merged into definition of the physical currents as seen in Eq. (4.124) where a half should stand in front of the definition. However, this factor is completely irrelevant unless one wishes to perform (an experimentally challenging) direct measurement of the Burgers dislocation currents Eq. (4.123) and relate them to the observables in the phonon realm.

When the dislocation mass  $m^2$  in the action Eq. (4.120) is positive, each of the Burgers scalar fields has no expectation value and the system is in the ideal crystal phase. Let us now assume that  $m^2 < 0$ , so that the Burgers Higgs fields  $\psi_{\mathbf{b}}$  may acquire some nontrivial expectation value  $\psi_{\mathbf{b}}^{(0)}$ . Its precise angular dependence will follow from the repulsive short-ranged potential  $V_{\mathbf{b},\mathbf{b}'}$ , and this will be analysed in some detail in the next paragraph. For now, we can assume that the expectation values are given and proceed with the construction of the Higgs term. It arises from the minimal coupling Eq. (4.121), however, given that the unitary gauge fix cannot be imposed onto all Burgers fields, the Higgs term is written in its gauge invariant form

$$\mathcal{L}_{Higgs} = \frac{1}{2} B_{\mu}^a \left[ \int \frac{d\eta}{2\pi} b^a |\psi_{\mathbf{b}}^{(0)}|^2 b^b \right] \left[ \delta_{\mu\nu} - \frac{p_d^{\mu} p_d^{\nu}}{p_d^2} \right] B_{\nu}^b. \quad (4.127)$$

Comparing this action with the bare Higgs term Eq. (4.70), it readily follows that the disorder theory constructed in this chapter can exactly reproduce that term. In contrast with the derivation from that section, the Burgers director  $\hat{Q}$  does not have to correspond only with the Burgers director of the ordered nematic phase. Its expectation value is actually related to expectation value of Burgers Higgs fields as

$$Q^{ab} = \frac{\int \frac{d\eta}{2\pi} b^a |\psi_{\mathbf{b}}|^2 b^b}{\int \frac{d\eta}{2\pi} |\psi_{\mathbf{b}}|^2} - \frac{1}{2} \delta^{ab} = \frac{1}{\int \frac{d\eta}{2\pi} |\psi_{\mathbf{b}}|^2} \int \frac{d\eta}{2\pi} |\psi_{\eta}|^2 \frac{1}{2} \begin{pmatrix} \cos 2\eta & \sin 2\eta \\ \sin 2\eta & \cos 2\eta \end{pmatrix}. \quad (4.128)$$

The normalization prefactor was chosen in such way to make the ‘modulus’ of the Burgers director Eq. (4.128) equivalent to the one defined by two unit vectors Eq. (4.33), while this prefactor represents the Higgs gap, written in the same notation as

$$|\Psi_0|^2 \equiv \int \frac{d\eta}{2\pi} |\psi_{\mathbf{b}}|^2. \quad (4.129)$$

Notice that the Burgers director defined by Eq. (4.128) transforms as a spin-2 object (sine and cosine of  $2\eta$ ) just as it is expected for a gap related to the shear.

When one realizes that the isotropic expectation value for the Burgers field  $\psi_{\mathbf{b}}^{(0)} = \text{const.}$  yields the Burgers vector of the isotropic nematic phase,  $\hat{Q} = 0$ , then the justification of the use of the ‘naive’ averaging in the Burgers sector is basically done. Before revisiting the results of the previous section, we would like, however, to analyse what sort of potentials favour isotropic or ordered nematic phase.

When looking for the ground state configuration of the Burgers fields, it becomes handy to work with Fourier transformed fields. Due to the  $\mathbb{Z}_2$  constraint on the dislocation currents, the transformation is defined only for

$$\psi_{\mathbf{b}} = \sum_m \psi_m e^{im\eta}, \quad (4.130)$$

while it automatically follows for the constrained conjugate fields. The Fourier coefficients  $\psi_m$  are given by the inverse transformation

$$\psi_m = \int_0^{2\pi} \frac{d\eta}{2\pi} \psi_{\mathbf{b}} e^{-im\eta} \quad (4.131)$$

and each one of them represents spin- $m$  components of the Burgers scalar field. The constraint Eq. (4.126) on the conjugate fields reads

$$\psi_m = \int_0^{2\pi} \frac{d\eta}{2\pi} \psi_{\eta} e^{-im\eta} = \int_0^{2\pi} \frac{d\eta}{2\pi} \bar{\psi}_{\eta+\pi} e^{-im\eta} = e^{im\pi} \bar{\psi}_{-m}. \quad (4.132)$$

The ‘static’ potential energy between dislocations is Fourier transformed

$$\begin{aligned} V[\psi_{\mathbf{b}}] &= \frac{1}{2} \int \frac{d\eta}{2\pi} \left[ m^2 |\psi_{\mathbf{b}}| + \int \frac{d\eta'}{2\pi} |\psi_{\mathbf{b}}| V_{\mathbf{b},\mathbf{b}'} |\psi'_{\mathbf{b}}| \right] \\ &\rightarrow \frac{1}{2} \sum_m (-)^m m^2 \psi_m \psi_{-m} + \frac{1}{2} \sum_{m,n,k} (-)^{m+n} \psi_{-m} \psi_{m+k} V^{(k)} \psi_{-n} \psi_{n-k}, \end{aligned} \quad (4.133)$$

where the amplitude for the spin-exchange  $V^{(k)}$  is given by the standard Fourier transform of the potential

$$V^{(k)} = \int \frac{d\eta}{2\pi} e^{ik\eta} V_{\eta}. \quad (4.134)$$

This amplitude obeys the mirror symmetry which requires that  $V_{\eta} = V_{-\eta}$ . On the level of spin exchange this reads  $V^{(k)} = V^{(-k)}$  making left and right spin exchange equivalent.

When minimizing the static energy Eq. (4.133) we start not from the Higgs fields  $\psi$  but rather from the density operator  $n_{\mathbf{b}} = \bar{\psi}_{\mathbf{b}} \psi_{\mathbf{b}}$  which drives the Higgs term. The Fourier transformed potential is

$$V[n_{\mathbf{b}}] = \frac{1}{2} \int \frac{d\eta}{2\pi} m^2 n_{\mathbf{b}} + \frac{1}{2} \int \frac{d\eta d\eta'}{(2\pi)^2} n_{\mathbf{b}} V_{\mathbf{b},\mathbf{b}'} n_{\mathbf{b}'} \rightarrow \frac{1}{2} m^2 n_0 + \frac{1}{2} \sum_k n_k V^{(k)} n_{-k}. \quad (4.135)$$

Varying the previous expression with respect to the density  $n_k$ , the classical equations are obtained for the density operator that read

$$0 = \frac{1}{2}m^2\delta_{k,0} + V^{(k)}n_k. \quad (4.136)$$

If all the spin-exchange amplitudes Eq. (4.134) are positive, the solution of the Eq. (4.136) is  $n_k = \frac{-m^2}{2V^{(k)}}\delta_{k,0}$ , and that is precisely the state of the isotropic nematic! We conclude that the isotropic nematic ground state is favoured if there is sufficient repulsion between dislocations with closely aligned Burgers vectors.

What happens if one of the spin-exchange amplitudes is zero or negative? If at least one of the amplitudes is negative, say  $V^{(k)} < 0$ , the ‘isotropic’ solution of the Eq. (4.136) represents the state with the maximum energy because populating the  $k$ -th harmonics  $n_{\pm k}$  decreases the total energy. The potential energy Eq. (4.135) does not seem to be bounded from below, as any further increase of the wave-function amplitude  $\psi_{\pm k}$  has the effect of lowering the energy further. However, there is a unilateral constraint on the number operator which has to be positive, following from its definition:  $n_{\mathbf{b}} = |\psi_{\mathbf{b}}|^2 \geq 0$ . Thus, the potential energy Eq. (4.135) has a lower bound due to the restrictions on the number operator of the spin-harmonics  $n_k$ .

This notion may be exercised on a few interesting examples. Let us take a potential  $V_\eta = \omega + U \sin^2 \eta$  with both parameters  $\omega$  and  $U$  positive. It is obvious that this kind of potential favours aligning of the dislocation Burgers vector and minimizes the potential energy when all the Burgers directors are aligned. Therefore it will reproduce the ordered nematic phase. Indeed, by substitution

$$\psi_\eta = \frac{1}{2}\Psi\delta^{(2\pi)}(\eta - \bar{\eta}) + \frac{1}{2}\bar{\Psi}\delta^{(2\pi)}(\eta - \bar{\eta} - \pi), \quad (4.137)$$

with the angular Dirac-delta function defined as

$$\delta^{(2\pi)}(\alpha) = \sum_{k=-\infty}^{\infty} e^{ik\alpha}, \quad (4.138)$$

the dislocation GLW action for the ordered nematic phase Eq. (4.32) is recovered, where the Burgers vector is fixed in the direction  $\mathbf{n} = (\cos \bar{\eta}, \sin \bar{\eta})$ . Hence, the disorder theory presented in this section can describe, among other, the ordered nematic state.

Can this theory also include the quantum version of the NHY ‘hexatic’ with its particularities exactly reproduced, such as the triangular/hexagonal lattice and the dislocation defects with Burgers vectors only in those three directions? It seems that it can. Recall first the comment about the triangular lattice elasticity tensor from the chapter 3. Lattices with this kind of the point group symmetry have their elastic properties indistinguishable from the isotropic elastic solid, at least in the long-wavelength limit. Therefore, the dual theory that has already been constructed in this chapter, is at the same time applicable to the triangular lattice seen in the HNY ‘hexatic’. Now, only the dislocation field has to be adjusted for the triangular lattice, and that is trivially performed by allowing only three

Burgers director orientations

$$\begin{aligned} \psi_\eta = & \psi_1 \delta^{(2\pi)}(\eta - \bar{\eta}) + \psi_2 \delta^{(2\pi)}(\eta - \bar{\eta} - \frac{\pi}{3}) + \psi_3 \delta^{(2\pi)}(\eta - \bar{\eta} - \frac{2\pi}{3}) + \\ & \bar{\psi}_1 \delta^{(2\pi)}(\eta - \bar{\eta} - \pi) + \bar{\psi}_2 \delta^{(2\pi)}(\eta - \bar{\eta} - \frac{4\pi}{3}) + \bar{\psi}_3 \delta^{(2\pi)}(\eta - \bar{\eta} - \frac{5\pi}{3}). \end{aligned} \quad (4.139)$$

In the ‘hexatic’ phase, none of the three lattice vectors is preferred over the other two, which implies that all three Burgers ‘hexatic’ functions  $\psi_{1,2,3}$  have the same expectation value. The use of Eq. (4.128)) gives the isotropic Burgers director  $\hat{Q} = 0$ . Hence, the dynamical ‘hexatic’ phase seems to be no different, at least in the long-wavelength limit, from the isotropic nematic phase.

There is yet another interesting feature of this disorder theory related to the fact that spin-exchange amplitude  $V^{(k)}$  may vanish for a certain  $k$ . In that case, the  $k$ -th spin-harmonic of the number operator  $n_k$  is not defined well by the Eq. (4.136) so it can take any value as long as all  $n_{\mathbf{b}}$  are positive. At this point the ground state is selected by the mechanism of order out of disorder [157, 158] which chooses the ground state with the softest excitations due to the minimized entropy (classical) or zero-point energy (quantum).

Now, we would like to find out which dislocation degrees of freedom admix and get ‘transferred’ to the physical longitudinal dual stress photons in the isotropic Higgs phase. This answer does not have an universal answer because it strongly depends on the Burgers Higgs fields expectation values. As an example, in the ordered nematic phase the longitudinal dual stress photon  $B_L^\parallel$  took the role of the phase degree of freedom of precisely one Burgers field, namely  $\psi_{\mathbf{n}}$ . In the isotropic nematic one expects an answer with a less discrimination between the Burgers angles  $\eta$ . For the purpose of answering this question, the Fourier transformed fields Eq. (4.131) are far more suitable and for this reason the gauge transformation Eq. (4.122) will be revisited.

One of the ways to determine which disorder field degrees of freedom turn into the longitudinal photon(s) is to find the expression for the disorder current without the minimally coupled gauge fields. Observe first that the spin-0 harmonic  $\psi_0$  is real due to the constraint Eq. (4.126). That constraint would have had the same physical meaning if any other complex number had multiplied any of the sides, but it would also have changed the complex phase of  $\psi_0$  to some other fixed value. All the other spin-harmonics have no expectation value in the isotropic nematic phase.

For this occasion, yet another, holomorphic, basis in the flavor space is introduced

$$\mathbf{e}^\pm = \frac{1}{\sqrt{2}} [\mathbf{e}^x \pm i\mathbf{e}^y], \quad (4.140)$$

in which the unit vector making angle  $\eta$  with the  $x$ -axis has coordinates  $e^{\pm i\eta}/\sqrt{2}$ . This simplifies the dislocation current Eq. (4.124) expression to

$$J_\mu^\pm = \int \frac{d\eta}{2\pi} \frac{e^{\pm i\eta}}{\sqrt{2}} \frac{i}{2} [(\partial_\mu \psi_{\eta+\pi})\psi_\eta - h.c.] = \frac{i}{2\sqrt{2}} \sum_k [(\partial_\mu \psi_{-k\mp 1})\psi_k - h.c.], \quad (4.141)$$

which in the isotropic nematic collapses to

$$J_\mu^\pm = \frac{i}{\sqrt{2}} \psi_0 \partial_\mu \psi_{\mp 1}. \quad (4.142)$$

Hence, in the lowest order, the first two spin-harmonics play the role of the ‘complex phases’ of the Higgs field and their signature is seen in the two additional modes in the elastic response of the isotropic nematic solid. Each of these additional modes represents one of the two longitudinal photons  $B_L^\pm$ .

Notice that the spin-1 doublet of wave functions is not compact and has a trivial topology, in contrast with the Abelian-Higgs duality (or the ordered nematic phase), where the complex phase of the disorder wave-function may be wound around magnetic vortices that puncture the dual superconductor. In that respect, one can argue whether the isotropic nematic phase may develop the type-II behaviour. By that, we mean that stress fluxes may appear in the system followed by shear currents with nontrivial circulation that screen these fluxes.

Let us conclude this treatise of the disorder theory with another curiosity. Although not necessary in this thesis, the gauge transformational rules for the spin-harmonics Eq. (4.131) may be required in some future work. When the gauge transformation Eq. (4.122) is utilized in the spin-harmonic definition Eq. (4.131), a rather unusual gauge transformation is obtained

$$\begin{aligned}\psi'_m &= \int \frac{d\eta}{2\pi} \psi'_\eta e^{-im\eta} = \int \frac{d\eta}{2\pi} e^{-im\eta} \psi_\eta e^{i\mathbf{b}\cdot\alpha} \\ &= \int \frac{d\eta}{2\pi} e^{-im\eta} e^{i\mathbf{b}\cdot\alpha} \sum_k \psi_k e^{ik\eta} = \sum_k A_{m,k} \psi_k,\end{aligned}\quad (4.143)$$

introducing the spin-gauge transformation matrix

$$A_{m,k} = \int \frac{d\eta}{2\pi} \psi'_\eta e^{i\eta(k-m)} e^{i(\alpha^+ e^{-i\eta} + \alpha^- e^{i\eta})} = J_{m-k}(f) e^{i(m-k) \arg \alpha^+}.\quad (4.144)$$

The homomorphic gauge components are defined as usual.  $J_{m-k}$  is Bessel function of the first kind.

Having completed the construction of the alternative disorder theory, it is time to return to the results obtained in the previous section and give them the appropriate physical interpretation. We may start with the simpler longitudinal phonon propagator Eq. (4.110). It was mentioned already when this propagator was obtained, that this results is identical to the one found for the longitudinal phonon propagator in the ordered nematic phase for  $\eta = \pi/4$ , Eq. (4.94). In both cases, the electric shear photon is completely screened, while the compression rigidity is ‘saved’ by the glide constraint, so that the longitudinal response resembles that of the liquid at long-wavelengths and recovers its ‘ideal crystal’ form at smaller distances.

The transversal phonon propagator is far harder to understand and its interpretation will introduce a few unconventional concepts. The massive pole of the propagator Eq. (4.112) looks similar to the massive poles in the two cases where the magnetic shear was screened. However, the massless sector is completely different than in any of these cases. This is because in the  $\eta = \pi/2$  case, the photon  $B_T^T$  was screened, but the longitudinal photon in the transversal sector  $B_L^L$  didn’t show up. In this way, the entire magnetic

shear was represented by  $B_T^T$  becoming totally gapped with no other modes appearing. In the other case,  $\eta = 0$ , the longitudinal photon  $B_L^L$  becomes physical, so there are two fields in the transversal sector, but only one, the shear photon  $B_T^T - B_L^L$ , acquires mass, which leaves the photon  $B_T^T + B_L^L$  massless and with quadratic dispersion. In the isotropic nematic, the longitudinal photon becomes physical and both  $B_T^T$  and  $B_L^L$  acquire mass,. However, when the Ehrenfest constraint is imposed, only one of two poles becomes massive, whereas the other acquires the linear dispersion. Similar as to the glide constraint in the longitudinal sector, the Ehrenfest constraint keeps a certain current component conserved in the transversal sector. This is best illustrated recalling the identity between the dual gauge fields and the disorder currents in the unitary gauge fix

$$J_i^a = |\Psi_0|^2 B_i^a, \quad J_\tau^a = |\Psi^0|^2 \frac{1}{c_d^2} B_\tau^a. \quad (4.145)$$

When the Ehrenfest constraint Eq. (4.10) is interpreted in terms of dislocation currents accordingly to the Eq. (4.145), a current constraint follows

$$c_d^2 \partial_a J_\tau^a = \partial_\tau J_a^a, \quad (4.146)$$

which disables the dislocation currents from generating mass for both transversal phonon excitations. Alternatively, when the current definition in terms of the spin-harmonics of the Burgers fields, Eq. (4.142), is substituted in the constraint Eq. (3.52), the identity immediately follows.

Since the massive excitation in the transversal sector is easily traced back to the magnetic shear photon, all what remains is the physical interpretation of the long-wavelength massless excitation. One way to recognize this mode is to directly inspect the long-wavelength propagator Eq. (4.113). In the isotropic nematic phase the displacements are ill-defined, however, the local rotation field is still well-defined due to the absence of disclinations. Given that the transversal photon is actually the local rotation correlator (see Eq. (3.34)), effectively the same dynamical response would have been found if the action was given by

$$\mathcal{L}_\omega = \frac{1}{2} \frac{2\mu}{\Omega^2} (\partial_\tau \omega)^2 + \frac{1}{2} \frac{\mu c_d^2}{\Omega^2} (\nabla \omega)^2. \quad (4.147)$$

The prefactor in front of the angular acceleration  $\partial_\tau \omega$  represents precisely the (density of) moment of inertia of a crystal patch with a size of the shear penetration depth  $\lambda_S = \sqrt{2} c_T / \Omega$ . Hence, the first term in the action Eq. (4.147) is the coarse-grained kinetic energy of a system of rotors. The second term, as usual, couples the rotors locally. We could try to give a physical origin of this term. Since each of the rotors is as big as the shear penetration depth  $\lambda_S$ , it could be considered as an ideal crystal. When two ideal crystals are adjacent to each other, the patching in between requires dislocations and it costs energy which is, in the isotropic nematic phase, given by the correlation length of the dislocation condensate  $\mu c_d^2 / \Omega^2 = c_d^2 / \Omega^2 = \lambda_d^2$ .

Therefore, the isotropic nematic is hydrodynamically equivalent to a liquid, due to the compressional rigidity, carrying a rotor which is in the ordered state. There is, however,

a subtlety related to these rotors. By saying that the rotors are in the ordered state, we assume that the ground state of the isotropic nematic is characterized by disorder of the displacement fields and order of the local rotation  $\omega \equiv 0$ , meaning that the orientation of the crystalline lattice is the same everywhere as it was in the ideal crystal. However, being in the (isotropic) ideal crystal, a special direction implied by the rotor ground state cannot be identified. At the same time, a global rotation to another ground state,  $\omega \neq 0$ , produces the same physical state with no measurable quantity that could distinct between the two of them. Having no preferred direction, the rotor could be thought of as the generalization of the director order parameter. However, while the director had a local  $\mathbb{Z}_2$  symmetry which resulted in the  $O(d)/\mathbb{Z}_2$  order parameter, the local rotation field has a global  $O(2)$  symmetry so it can be regarded as  $O(2)/O(2)$  rotor.

Since the elastic action of the isotropic nematic phase is rotational invariant, while its ground state  $\omega = 0$  is not, it is not surprising that there is a massless linear mode in the rotation correlator – this mode is the Goldstone mode associated with the broken rotation symmetry. According to the folklore, phonons originate in the translational symmetry breaking. When faced with the rotational symmetry breaking which also takes place in the ideal crystal, it is usually assumed that the Goldstone mode of this symmetry is overdamped due to the coupling to the dissipative shear. This is indeed true in the nematic phase of a classical liquid crystal. However, when the theory has no explicit dissipation as it is the case with our theory this argument cannot work. The general truth is that the rotation Goldstone mode is ‘hidden’ behind the Goldstone transversal phonon. In the long-wavelength limit to which the Goldstone theorem applies, the infinitesimal excitations of these two modes are equal [154]. Hence, it takes a theory where the translational symmetries are restored and the rotational left broken, such as the isotropic nematic phase, in order to reveal the rotation Goldstone mode.

To support this claim we may intentionally invalidate the conditions required for the Goldstone theorem, by removing the rotational invariance from the elastic action Eq. (3.24). Consider a solid on some substrate, such that rotations of the solid are energetically costly due to the interaction with the substrate. This is implemented with addition of a local rotation coupling to the elasticity tensor

$$C_{ijab} \rightarrow C_{ijab} + \epsilon \frac{1}{2} (\delta_{ij} \delta_{ab} - \delta_{ib} \delta_{ja}), \quad (4.148)$$

with  $\epsilon$  being the ‘rotational stiffness’. Although it is breaking the Ehrenfest constraint, Eq. (4.10), this assumption is not violating the angular conservation since this solid is not an isolated system and it may exchange the angular momentum with the substrate. In such a setup the Lagrangian has only translational symmetries left over; rotation of a solid as a whole costs a finite amount of energy. When the dualization procedure is repeated, after the lengthy work with details left to an interested reader, the fourth mode is found to acquire a gap equal to  $\Omega_\epsilon^2 = \epsilon |\Psi_0|^2$ . Hence, by violating the global rotational symmetry of the action by addition of term Eq. (4.148) the fourth mode becomes massive.

An alternative way to envisage the transversal excitation of the isotropic nematic is illustrated in Fig. 4.6. In the ideal crystal the response to transversal motion is driven

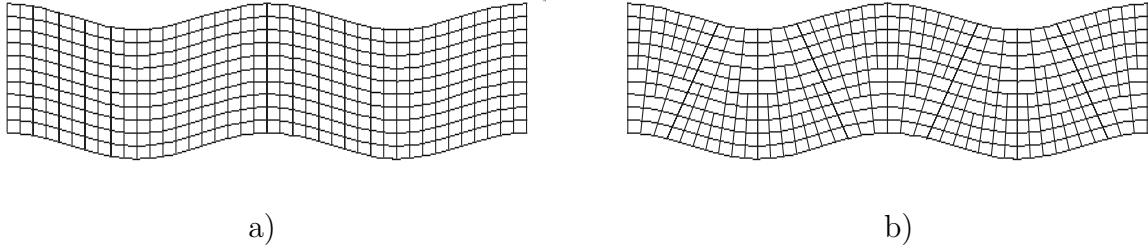


Figure 4.6: An alternative interpretation of the massless excitation in the transversal phonon spectrum: a) in the ideal crystal, the transversal motion induces reactive shear response; b) in the isotropic nematic phase the shear response is massive. However, the transversal motion may cause plastic deformation and the resonance is acquired from the dynamical dislocation condensate.

by the shear rigidity (Fig. 4.6a). In contrast, the isotropic nematic phase has no shear rigidity. Nevertheless, a transversal motion of the system induces a dislocation presence in the system (Fig. 4.6b). The resonance is governed by the velocity at which the dislocations propagate. The factor of  $1/\sqrt{2}$  (the transversal excitation propagates with the glide velocity in the long-wavelength limit) originates in the fact that on average, one half of dislocations have the Burgers vector point along the propagation direction, while the other half is present but do not contribute to the propagation due to their perpendicular Burgers vectors.



# Chapter 5

## Superconductivity in nematic phases

Up to this point, the work presented here was focused exclusively on elastic media which are decoupled from other physical fields. As an outcome, a number of novel phases of solid, like the quantum melted phase, were identified and their physical properties, expressed through the response to external stress, were identified. In the real world, an experimentalist would like to probe the elastic response of a system and make sure if the melting theory developed in chapter 4 is representative for that system. The long wavelength behaviour that was predicted is not sufficient for those purposes. In the ordered nematic phase, the anisotropic phonon velocities may be attributed to anisotropy in the elasticity tensor Eq. (3.7) and the long wavelength response of the topological isotropic nematic predicts a massless mode per each phonon propagator which makes it impossible to see the difference from a standard solid when we are equipped only with *long-wavelength* phonon measurement devices. The only feature of the nematic phases that one would like to measure and be sure that the phase has undergone the transition into the dislocation melted solid, is the shear photon which acquires its own pole in phonon propagators. This pole is however not easy to measure, because it becomes visible only at lengths shorter than the shear penetration depth and at frequencies higher than the shear gap. Recall that the expected values for the shear penetration length have to be larger than the lattice constant (in order for the theory to be applicable), but still in nanometer to micrometer range. When the corresponding shear gap is assessed, it turns out that, in order to test the predictions of the previous sections directly, that is by means of phonon propagators, one needs a machine that could exert stresses at nanometer scales and modulate them with frequencies in giga or terahertz range. While, to the best of our knowledge, the present day AFM tools have cantilevers that may achieve resolution as high as the required nanoscales, the shear gap frequency is many orders of magnitude above the measurable threshold in frequencies.

This unfortunate technological drawback calls for an alternative way to probe an elastic system. In order to do that, the elastic medium must be coupled to another physical field and preferably the experiments related to this additional field should be able to probe terahertz/nanometer regime. The most natural and logical field for this purpose is the electromagnetic field. In fact, dealing with the electron matter (our primary interest), the electrodynamical response is the only way the system can be interrogated. The only

property which counts in the present context is its electrical charge. In this chapter, we develop the extension of the dual theory of nematic solids that will take care of the electromagnetic fields and relate the properties of the nematic phases to measurable EM quantities. The requirement for this theory is, of course, that the crystalline constituents carry electric charge, so this idea will not work for elastic media in general. The charged elastic solids that are described by the theory developed in this chapter can be thought of as Wigner crystals. Traditionally, the name Wigner crystal is reserved for the crystalline state made out of electrons realized in the low density regime. Such a crystal carries fermionic statistic and is thereby beyond the scope of this work. As mentioned before, in order to keep excitations with singular displacements bosonic, we must limit ourselves to a medium made out of electrically charged bosons. To keep matters clear this state of matter will be referred to as the *bosonic* Wigner crystal [144]. What this practically means is that we assume the existence of effective bosonic particles, be it Cooper pairs, holons or whatsoever, below some energy scale.

Although it might appear that we develop the dual theory of a bosonic Wigner crystal for the purpose of detecting nematic phases in standard elastic media, the real motivation is just the opposite. Our primary goal is to construct the dual theory of electronic liquid crystals, and in that respect the previous section may be regarded only as an intermediate step necessary in order to find the action of the dual stress degrees of freedom on the electromagnetic fields. Our motivation in the electronic liquid crystals and, more notably, their quantum version was presented in the introductory chapter, so let us quickly repeat it here. The electron liquid in the high- $T_c$  superconductors is strongly correlated and numerous experiments [35, 36, 41, 42] demonstrate that it is close to the point of crystalizing into the electron (stripe) crystal. The paper by Kivelson, Fradkin and Emery [37] suggests the existence of electronic smectic and nematic phases in the high  $T_c$  superconductors. According to the arguments in the paper, the quantum phase transitions of a high temperature superconductor, with the dopant concentration  $x$  parameterizing the amount of the quantum disorder, can be viewed in terms of an effective liquid crystalline theory for the electrons. The most recent support for the electronic liquid crystal theory comes from the recent experiment employing the neutron scattering on optimally doped ‘untwinned’ YBCO crystals [43] in which an unreasonably high anisotropy in the superconducting gap is found. Could it be that the anisotropy is augmented by an electronic liquid that exhibits spontaneous orientational order?

When we construct the dual theory of the elastic charged media it appears that some of these questions can be answered. The advantage of the duality construction is not only given by the fact that we already developed the formalism that can treat liquid crystal phases, it is also expressed through the idea that the world seen through the duality has a fundamentally different structure, so in a way one could say that the dual view shines a completely different light on the problem. As one of the representative features, let us mention here that in the dual theory every elastic medium has a Meissner term so it qualifies as a bare superconductor. The interaction with the dual stress gauge fields is, however, responsible for dressing of the Meissner term back to its effective value. The short-range propagation of the shear photons in the nematic phases is therefore the key ingredient in

the realization of the superconductivity. The precise statement which will be justified after both topological and nematic phases have been analysed is that the necessary condition for an elastic medium to acquire a finite static Meissner term is that the *magnetic* shear photon is an eigen direction of the shear Higgs term, i.e. there are no long-wavelength, zero frequency parts in its bare propagator.

The presence of the bare Meissner term in the dual language can be understood as follows. The dual theories are naturally tailored to primarily describe the disordered side of the phase diagram. The ultimately disordered state of a zero-temperature quantum elastic medium is the superfluid and there is a theorem due to Wen and Zee [159, 160, 161] which states that a charged superfluid is at the same time a superconductor. This argument works regardless the ‘number of curls’ in the definition of the dual stress gauge fields. Naturally, when there are no defects present, the stress fields are powerful enough to defeat the Meissner term, but as we mentioned, even a partial Higgs mechanism in the stress shear sector is sufficient to liberate the Meissner term which was present all the time in disguise.

This superconductivity mechanism in the nematic phases is not based on the standard BCS paradigm [17] and as it will turn out, the superconductivity is unconventional showing a myriad of electromagnetic features, many of them never predicted before by any existent theoretical model known to us. These effects include an unconventional magnetic and electric static screening, both experiencing overscreening effects, additional poles in the electric response functions and an unconventional propagation of light. From these findings, we will deduce some predictions for novel experiments which up to now have not been carried out, which can serve the purpose to determine whether the theory of dual superconductivity which is constructed here is realized in cuprates. Non-BCS superconductivity models were suggested before, with some of them being closely related to our work. Chronologically the first model was an early attempt to find a theory of conventional superconductivity by Fröhlich [162, 163]. His idea of one-dimensional electrons that couple with phonons and move in a sliding fashion as a whole, resulted in an ideal conductor but also proved vulnerable to infinitesimal pinning. In a similar manner, the ideal Wigner crystal of ours is an ideal conductor since the pinning processes are not incorporated in the theory. Therefore one expects that, in manner of Fröhlich superconductor, this ideal crystal becomes an insulator in the real physical world. Another drawback of the Wigner crystal is that it is not a superconductor, in spite of its vanishing resistivity, since it can admit static magnetic fields. The nematic phases, on the other hand, develop a finite Meissner term, in a mechanism which is similar to the duality between the charge density-wave and superconductor discovered by D.H. Lee [164]. In this phase of matter, ignoring the pinning is justified since its effects are diminished. This is a consequence of the screening of the pinning potential, which is basically transmitted by shear, now screened by the dislocation currents. The remaining phase of matter, the superfluid phase, is not accessible by means of the duality that is presented here, but if one wishes, its properties can be described in the non-interacting gas limit which is the opposite of ours. Some of the answers are already known such as that the phase is superconductor according to the theorem by Wen and Zee [159, 160, 161] we already mentioned. The mechanism of their proof is simple: a compression mode can be dualized into a pair of compression photons that couple to EM

photons. Integrating the former out results in a mass gap for the latter.

This chapter is organized as follows: in the first section we introduce EM (gauge) fields and analyse the way they couple to the displacements of a charged elastic medium. When developing the dual theory of the charged elastic media, our final goal will always be to derive the effective EM gauge field propagators by integrating out all other, in this case dual stress, degrees of freedom. In order to interpret these propagators, we will derive relations connecting the propagators to measurable physical quantities like electric and magnetic susceptibility, conductivity and magnetic and electric screening. As a warm up exercise (but also as a check for the later work), we first analyse the electric properties of the ideal Wigner crystal by means of the strain formalism. In spite of the simplicity of the problem and some intuitive simple expectation for this phase, it will actually show some counterintuitive properties, such as propagation of light by diffusion and a gap in the transversal response. The next section is dedicated to the construction of the dual action for a charged medium. The aforementioned bare Meissner term of the dual theory is found and, after other (stress) degrees of freedom have been integrated out, its fate is determined. In the ideal crystal, the results that were already found in section 5.1 are recovered. Another novel result presented in this section is the ‘dual Kubo’ formula which is engineered to relate the dual stress photon propagators to the conductivity of the medium. The remainder of this chapter will be split in two sections following the discussion of the two (sub)phases with the nematic order. One section deals with the electromagnetic properties of the ordered nematic phase and the other with the properties of the isotropic nematic phase. The order of the phases is permuted with respect to the previous chapter because of the simpler isotropic nature of the topological phase and its representative features. Due to more complicated propagators and the coupling between the longitudinal and the transversal sectors of the ordered nematic phase, only a limited set of its physical quantities is analysed and the discussion is centered on the values of the angle  $\eta$  where the coupling between the elastic sectors is vanishing. We subsequently demonstrate that at all other, intermediate, values of  $\eta$  a coupling is induced between the electric and magnetic properties of the charged medium. Most of the results presented in this chapter are novel and not yet published with the exception of the introductory electrodynamics part and the results on the unconventional static magnetic screening properties which were shortly addressed in the preceding work by Zaanen *et al.* [44].

## 5.1 A tutorial: electrodynamics of elastic media and physical observables

Whenever a new field is introduced into the theory, there are two questions to be addressed: what is the independent dynamics of the field and how does one have to couple the field to the existing theory? These questions are fairly easy to answer when the fields of relevance are the electromagnetic fields, given the status of the Maxwell theory in present day physics as foundational principle. Although the coupling between the elastic media and the EM

fields is discussed in the Landau-Lifschitz books [126], we will rederive these matters in the beginning of this section in order to construct the minimal coupling term that will be easier to treat under the duality. After these terms have been found, together with the (dynamical) Maxwell term for the EM gauge fields, the gauge fix is implemented on the EM gauge fields. For illustrational purposes, the problem of the electric fields coupled to the Wigner crystal is solved and the self-energies for the EM photons are obtained. When the EM observables are related to the self-energies of the EM gauge fields in the remainder of the section, these self-energies will be used to discuss the physics, showing that actually even the bosonic Wigner crystal has untrivial EM properties.

We begin with discussing the minimal coupling between the elastic degrees of freedom and EM fields. Let us start with the contribution to the action associated with a single charged particle that is subjected to an EM field. If the particle's effective electric charge is  $e^*$  and its position at time  $\tau$  is given by  $\mathbf{R}(\tau)$ , then it contributes to the action as [165, 166]

$$\mathcal{L}_{EM,1p.} = ie^* \int d\tau \left[ A_\tau(\mathbf{R}(\tau), \tau) + \dot{\mathbf{R}}(\tau) \cdot \mathbf{A}(\mathbf{R}(\tau), \tau) \right]. \quad (5.1)$$

This action is the origin of the exact EM coupling Eq. (3.67) mentioned in the section 3.4 dealing with the glide principle. The fields that the particle 'feels' at moment  $\tau$  are taken at its precise position  $\mathbf{R}(\tau)$ . The first term corresponds with the energy of the particle in the Coulomb potential field  $A_\tau$ , while the second term represents the generalized potential associated with the action of the Lorentz force on the moving particle. This is the natural interpretation of the EM action in terms of forces in the laboratory reference frame, but the coupling term Eq. (5.1) is Lorentz-invariant. The existence of the minimal coupling Eq. (5.1) in the Lagrangian formalism is a consequence of the fact that the EM forces belong to the class of generalized potential forces [167].

Since the basic action Eq. (3.24) which we use throughout this whole thesis is just an effective action derived in the gradient expansion of true elastic energy Eq. (3.2), there is no need to keep higher order terms in the displacements in the formalism than the ones already present in Eq. (3.24). Therefore, we perform the gradient expansion of the minimal coupling Eq. (5.1), where the particle position is given in terms of its equilibrium position and the displacement  $\mathbf{R}(\tau) = \mathbf{R}^0 + \mathbf{u}(\tau)$ , and keep only terms that are linear in displacement

$$\mathcal{L}_{EM,1p.} = ie^* \int d\tau [(\mathbf{u} \cdot \nabla) A_\tau + \partial_\tau \mathbf{u} \cdot \mathbf{A}] + O(u^2). \quad (5.2)$$

In this step we subtracted the potential coming from the background charge, needed to preserve global electroneutrality. When a large number of these charged particles forms a crystal with density of  $n_e$  particles per unit volume, the coupling term becomes simply

$$\mathcal{L}_{EM} = i(n_e e^*) \int d\mathbf{x} d\tau [-A_\tau \partial_a u^a + A_a \partial_\tau u^a] \equiv i\mathcal{A}_\mu^a \partial_\mu u^a. \quad (5.3)$$

In order to have strains in both terms, a partial integration is performed. The EM potentials turn into effective 'curly' strain potentials

$$\mathcal{A}_\mu^a = (n_e e^*) [\delta_{\mu\tau} A^a - \delta_{\mu a} A_\tau], \quad (5.4)$$

and the EM coupling in this form is naturally married to the stress degrees of freedom when the dual theory is developed in the next section.

Next to the coupling term, the dynamics of EM gauge fields has to be included in the action by means of the Maxwell term

$$\mathcal{L}_{Maxwell} = \frac{1}{4} F_{\mu\nu} F^{\mu\nu} \quad (5.5)$$

with field strengths defined as  $F_{\mu\nu} = \partial_\mu A_\nu - \partial_\nu A_\mu$ . The absence of the prefactor is often encountered in a high-energy physics literature [80] and its advantage is that this form is dimension independent. Given that we restricted ourselves to the 2+1-dimensional universe, it would be wise to keep the number of spatial dimensions that the EM fields are embedded into, which we also take two. Usual prefactors such as  $1/(4\pi c_l)$  in the CGS system of units or  $1/\mu_0 = c_l^2 \epsilon_0$  in the SI system of units have specific values in three dimensions, but in any other number of dimensions they are meaningless. At the end of our exposition it will be shown that this discussion is not crucial at all, because the only physically relevant quantity involving the combination of the effective particle charge  $e^*$ , their density  $n_e$  and the mentioned prefactor, in other words, that is the plasmon energy of the electron system. Notice however, that the specific choice of the prefactor will alter the plasmon gap by a factor of  $4\pi$  relative to commonly used definitions employing the CGS system.

Both the Maxwell part of the action Eq. (5.5) and the minimal coupling to strain fields Eq. (5.3) have to be invariant under gauge transformations of the EM fields  $A_\mu$  which were given earlier by Eq. (2.13). The gauge invariance is, per definition, obeyed by the Maxwell term, while the invariance of the minimal coupling term implies electric current conservation. In the previous chapter, this condition was restated in terms of the glide constraint on the dislocation currents [50]. Due to the gauge redundancy of the EM gauge fields, one has to choose a gauge fix. For the sake of the compatibility with the vast literature (e.g. Ref. [51]), we will employ throughout this chapter the Coulomb gauge fix

$$0 = \partial_i A_i = -q A_L. \quad (5.6)$$

It was already clarified in chapter 2, that this particular gauge fix simplifies matters by decoupling the electric and magnetic effects, while its components can even be directly interpreted as real physical degrees of freedom. One might object at this point that we are after a superconducting phase with massive EM photons, and that the massive gauge fields may be better addressed in terms of the unitary gauge fix. Let us give two arguments in favour of the Coulomb gauge fix Eq. (5.6). In the first place, the final physical outcomes should not be dependent on the gauge fix, so whatever gauge fix we choose the results are the same, and the Coulomb gauge fix will just simplify the computations significantly. There is also a conceptual side: here the unitary gauge fix becomes meaningless since it is proper only when the gauge fields acquire mass due to the Abelian-Higgs mechanism originating in the off-diagonal condensed long-range order in the constituent bosonic fields. Since the superconductivity in our dual theory has a completely different origin while, in

fact, there is even not a bosonic wave-function minimally coupled to the EM gauge fields, the entire gauge redundancy resides in one of the components of the gauge field  $A_\mu$  and the Coulomb gauge fix Eq. (5.6) is just a quite natural choice.

Similarly to the case of the Coulomb phase from section 2.3, the Maxwell term Eq. (5.5) may be expressed in terms of the two remaining photons

$$\mathcal{L}_{Maxwell} = \frac{1}{2}q^2 A_\tau^\dagger A_\tau + \frac{1}{2}(\omega_n^2 + c_l^2 q^2) A_T^\dagger A_T. \quad (5.7)$$

The Coulomb photon  $A_\tau$  is associated with the Coulomb force and the physical longitudinal electric field as  $E_L = iqA_\tau$ , while the transversal photon  $A_T$  represents EM radiation through its physical interpretations in the form of the magnetic field  $B = qA_T$  and the transversal electric field  $E_T = -\omega_n A_T$ .

Let us now switch gear back to the physics of the elastic medium to analyse the electrical properties of the ideal Wigner crystal. For this purpose, the strain formalism with smooth displacement fields  $\mathbf{u}$  is considered. The minimal coupling term Eq. (5.3) is transformed to Fourier-Matsubara frequency space. Only the physical EM gauge fields are left resulting in

$$\mathcal{L}_{EM} = i(n_e e^*) \left[ i\omega_n u^T A_T^\dagger + q u^L A_\tau^\dagger \right]. \quad (5.8)$$

Although one might have noticed it earlier, the exclusive nature of the minimal coupling becomes apparent when given in form of the Eq. (5.8). Here one can convince oneself that the Coulomb photon couples exclusively with the degrees of freedom in the longitudinal elastic sector, while the transversal photon communicates with the transversal elastic sector. In the isotropic phases, this will give rise to the fact that the electric effects are governed by longitudinal elastic properties, whereas the magnetic effects and the light propagation are governed by the transversal elastic properties. The earlier claim of the coupling between the electric and magnetic properties of the charged system is now readily anticipated in the ordered nematic phase.

In order to obtain the effective EM gauge fix propagators, one has to remove the displacement degrees of freedom. In the ideal crystal this invokes a trivial Gaussian integration, using the displacement propagators given in Eq. (3.31). The resulting effective action for the EM gauge fields is

$$\mathcal{L}_{EM,ideal} = \frac{1}{2} A_\tau^\dagger A_\tau q^2 \left[ 1 + \frac{\omega_p^2}{\omega_n^2 + c_L^2 q^2} \right] + \frac{1}{2} A_T^\dagger A_T \left[ \omega_n^2 + c_l^2 q^2 + \omega_p^2 \frac{\omega_n^2}{\omega_n^2 + c_T^2} \right], \quad (5.9)$$

introducing a gap  $\omega_p$  which corresponds to plasmon gap of the charged medium

$$\omega_p^2 = \frac{(n_e e^*)^2}{\rho} = \frac{n_e e^{*2}}{m^*}. \quad (5.10)$$

The effective mass of a constituent is  $m^*$ . This expression differs from the one found in standard literature by factor of  $4\pi$  for reasons we already mentioned (see Eq. (5.5) and the

comment thereafter). An alternative way to represent the propagators in Eq. (5.9) is by means of their self-energies. Defining the vacuum EM gauge field propagators as

$$(\mathcal{G}_\tau^{(0)})^{-1} = q^2, \quad (5.11)$$

$$(\mathcal{G}_T^{(0)})^{-1} = \omega_n^2 + c_l^2 q^2, \quad (5.12)$$

so that the total effective EM action is

$$\mathcal{L} = \frac{1}{2} A_\tau^\dagger (\mathcal{G}_\tau)^{-1} A_\tau + \frac{1}{2} A_T^\dagger (\mathcal{G}_T)^{-1} A_T + i A_\tau^\dagger j_\tau + i A_T^\dagger j_T, \quad (5.13)$$

a self-energy term can be associated with each physical gauge field

$$-\Pi_\tau = \frac{q^2 \omega_p^2}{\omega_n^2 + c_L^2 q^2}, \quad (5.14)$$

$$-\Pi_T = \frac{\omega_n^2 \omega_p^2}{\omega_n^2 + c_T^2 q^2}. \quad (5.15)$$

In the following sections, this will be our standard way to represent the influence of a charged medium on the EM fields.

Let us now turn to the physical interpretation of the propagators Eq. (5.9). Their bare form does not yield much information when we recall the relations between the electric and magnetic fields and the EM gauge fields. At this point it is useful to invoke the substantial Maxwell equations with a spatio-temporal dispersion. The first equation reads

$$\nabla \cdot (\varepsilon \mathbf{E}) = j_\tau^{ext.}, \quad (5.16)$$

but after it has been transformed to the Fourier-Matsubara space and rewritten in terms of the EM gauge fields with the implicit Coulomb gauge fix, it becomes

$$q^2 \varepsilon A_\tau + i j_\tau^{ext.} = 0. \quad (5.17)$$

Comparing this Maxwell equation with the equation of motion that would follow from the action Eq. (5.13), we conclude that

$$\varepsilon = \frac{G_\tau^{-1}}{q^2} = 1 - \frac{\Pi_\tau}{q^2}. \quad (5.18)$$

This dielectric function is commonly known as the longitudinal dielectric function,  $\varepsilon_L$ , because it serves as the propagator of the longitudinal electric field component [168].

Another Maxwell equation with source term is, in two dimensions,

$$c_l^2 \nabla \times \frac{B}{\mu} = \mathbf{j}^{ext.} + \partial_\tau \varepsilon \mathbf{E}, \quad (5.19)$$

introducing the magnetic susceptibility  $\mu$ . It is a habit to set the magnetic susceptibility to unity so that all the magnetic effects are defined in terms of the transversal dielectric function  $\varepsilon_T$  which enters the transversal projection of the Fourier transformed Eq. (5.19)

$$(\varepsilon_T \omega_n^2 + c_l^2 q^2) A_T + i j_T^{ext.} = 0. \quad (5.20)$$

Again, the Maxwell equation Eq. (5.20) is compared with the equation of motion following from the action Eq. (5.13) and the transversal dielectric function is recovered as [51]

$$\varepsilon_T = 1 - \frac{\Pi_T}{\omega_n^2}. \quad (5.21)$$

Of course, the Fourier transformed equation Eq. (5.19) should involve the same dielectric function as the Eq. (5.18) on its right hand side and keep track of the magnetic properties by means of the magnetic permeability  $\mu$ . Thus, the mathematically proper Maxwell equation reads

$$\left( \varepsilon \omega_n^2 + \frac{1}{\mu} c_l^2 q^2 \right) A_T + i j_T^{ext.} = 0 \quad (5.22)$$

so that the magnetic permeability can be given either in terms of the EM photon self-energies or in terms of the already introduced longitudinal and transversal dielectric functions [169]

$$\frac{1}{\mu} = 1 + \frac{\Pi_\tau}{q^2} \frac{\omega_n^2}{c_l^2 q^2} - \frac{\Pi_T}{c_l^2 q^2} = 1 + \frac{\omega_n^2}{c_l^2 q^2} (\varepsilon_T - \varepsilon_L). \quad (5.23)$$

The presence of the light velocity in the denominator in Eq. (5.23) is sometimes used to argue that the effect of a medium on the magnetic fields can be ignored at any finite wavelengths. The smallness of the magnetic permeability Eq. (5.23) is also behind the fact that there are no experiments devised yet that could measure the EM transversal gauge field propagator  $\mathcal{G}_T$  at finite wavelengths. For example, optical conductivity experiments are just one of the many experiments that work effectively at  $q = 0$ . In that respect, experimental physics is still handicapped with regard to probing the nematic phases by means of electromagnetic experiments since only half of the measurable quantities we predict are in principle accessible at this moment, and these are all related to the longitudinal response, i.e. the Coulomb photon and its propagator  $\mathcal{G}_\tau$ . Nevertheless, for completeness and also in the hope that in a near future experiments might be developed that probe the finite-wavelength regime of the transversal EM photon, both results relating to the Coulomb and to the transversal photon propagators will be presented for the various nematic phases.

The electric and magnetic response functions  $\varepsilon_{L,T}$  and  $\mu$  are in last instance associated with experiments and physical effects. Let us start with the static screening effects. The electric static screening is governed by the poles of the inverse dielectric function Eq. (5.18). In the ideal Wigner crystal the dielectric function has the following static limit

$$\varepsilon_{WC} = 1 + \frac{\omega_p^2}{\omega_n^2 + c_L^2 q^2} \xrightarrow{\omega_n \rightarrow 0} 1 + \frac{1}{\lambda_c^2 q^2}, \quad (5.24)$$

introducing the ideal crystal electric screening length  $\lambda_c = c_L/\omega_p$ . The dielectric function Eq. (5.24) has zeros at  $q = \pm i q_c$ , with  $q_c = \lambda_c^{-1}$  the inverse crystalline electric screening length, which implies that instead of the standard Coulomb  $1/r$  electric field fall-off, the

ideal Wigner crystal exhibits electric screening with  $\lambda_c$  as the characteristic length. In a 1D geometry, the profile of the electric field has an exponential fall-off and in a 2D geometry (e.g. electric field flux penetrating the Wigner crystal at a certain point), the inverse Fourier transformation yields a modified Bessel function of the second kind  $\frac{1}{\lambda_L} K_1(\frac{r}{\lambda_L})$  which asymptotically behaves like  $\sqrt{\frac{\pi\lambda_L}{2r}} e^{-\frac{r}{\lambda_L}}$  at large distance.

The magnetic permeability of the ideal Wigner crystal is

$$\frac{1}{\mu_{WC}} = 1 + \frac{c_K^2}{c_l^2} \frac{\omega_p^2 \omega_n^2}{(\omega_n^2 + c_L^2 q^2)(\omega_n^2 + c_T^2 q^2)}, \quad (5.25)$$

which indeed shows minute deviations from unity. In the static limit, the second term vanishes so there are no static magnetic effects.

At the same time, the result in Eq. (5.25) confirms the claim of Bohm and Pines [170] who argued that the discrepancy between the two dielectric functions  $\varepsilon_L$  and  $\varepsilon_T$  is due to the magnetic response of the medium, and corrections have to be of order  $(\frac{v}{c_l})^2$  with  $v$  being the characteristic velocity of the medium material. In the case of the ideal crystal this velocity corresponds to the sound velocity  $c_K$ .

Considering now the dynamical effects, one may want to focus on polaritons, the light excitations dressed by the strong interaction with the medium [171, 172]. Given that the polaritons are, by definition, the same excitations as the transversal EM photons  $A_T$  in the system, their spectra are identical. In general, there is an equation involving both electric and magnetic permeabilities

$$0 = \varepsilon(\omega_n, q) \omega_n^2 + \frac{1}{\mu(\omega_n, q)} c_l^2 q^2. \quad (5.26)$$

which yields the polariton spectrum. In the ideal Wigner crystal these poles are trivial to find and there are two of them. In the long-wavelength limit one of the poles is gapped as  $\omega_1^2 = \omega_p^2 + (c_l^2 + c_T^2)q^2 + O(q^4)$  and this is what one usually finds in a metal – screening of the electric field together with ideal conductivity results in the skin effect and the medium is a mirror, reflecting all incoming EM radiation, provided that the frequency is lower than the plasmon gap. The other mode, however, involves a surprise as it develops a quadratic dispersion  $\omega_2 \approx \frac{c_l}{\omega_p} c_T q$  as a consequence of level repulsion. Can we interpret this mode? A possible answer lies in the fact that the electric field, which is also one of the photon ingredients, is screened in the medium whereas, at the same time the magnetic field is unaffected at large distances. They are both carried by the photon  $A_T$ , i.e. the polariton, which couples with the long ranged transversal mode. In the fight between electric screening and long-ranged shear, the EM photon can still survive but only as a diffusive, not freely propagating, degree of freedom. Alternatively, Eq. (5.26) which is the polariton inverse propagator resembles the inverse propagator of the ordered nematic phase at  $\eta = 0$ , Eq. (4.93). In the same fashion as there, the second pole dispersion can be interpreted as due to the second-order process via the massive first pole  $\omega_2 = c_l c_T q^2 / \omega_1$ , which is the unique way of that mode to ‘catch up’ with the short-wavelength dispersion (decoupled EM photon and the transversal phonon).

Measurements of the dynamical dielectric function are in principle possible, by electron energy loss spectroscopy (EELS) where the amount of energy that an electron leaves behind in the medium is related to the imaginary part of the inverse dielectric function [173]. We however leave the details of this issue for the section on the charged isotropic nematic where an important effect that can be measured by means of an EELS experiment is at the center of the attention. Another experiment which appears to measure the dielectric function is resonant inelastic X-ray scattering [174] although this claim needs further theoretical and experimental scrutiny. The dynamical magnetic permeability is, as we mentioned, at this moment out of reach of the experimentalists.

A medium carrying charge is also characterized by conductivity which is just the ratio between the applied field and the internal currents carried by the constituent (intrinsic) particles. When analysing the conductivity, one can, in the spirit of the Maxwell-Lorentz analysis of Maxwell's substantial equations [166], split the internal currents and charges into the bound and free currents/charges. The bound currents, which have as physical origin constituents that do not move an infinite distance away from their starting points, are supposed to be integrated out to produce corrections to vacuum susceptibilities. On the other hand, the free currents, which represent particles that are not bound to their initial equilibrium position remain in the Maxwell equations. One can eventually invoke the definition of the conductivity and express these free currents in terms of the conductivity tensor as  $\mathbf{j} = \hat{\sigma} \cdot \mathbf{E}$ . The Maxwell equation Eq. (5.19) then becomes

$$c_l^2(\nabla \times B) = \mathbf{j}^{ext.} + \hat{\sigma} \cdot \mathbf{E} + \partial_\tau \mathbf{E}. \quad (5.27)$$

To find the conductivity, one would, however, need to use the full action, together with the elastic part (3.24), Maxwell part Eq. (5.5) and their mutual coupling Eq. (5.3) in order to find equations of motion, which can be compared with Eq. (5.27). Such a procedure seems an unnecessary detour to recover the conductivity, since we already know the electric response functions. As it turns out, the dielectric function and the conductivity are related through a familiar relation

$$\hat{\varepsilon} = \hat{\mathbf{1}} + \frac{i\hat{\sigma}}{\omega}, \quad (5.28)$$

This expression can be interpreted as stating that a conductor with conductivity  $\hat{\sigma}$  can be regarded as a Maxwell dielectric with complex electric susceptibility Eq. (5.28). The components of the dielectric function tensor  $\hat{\varepsilon}$  in the identity Eq. (5.28) are related to the previously defined dielectric functions as  $\varepsilon_{LL} = \varepsilon_L = \varepsilon$  and  $\varepsilon_{TT} = \varepsilon_T$ . The off-diagonal elements  $\varepsilon_{LT}$  and  $\varepsilon_{TL}$  vanish in isotropic media, but in the ordered nematic phase these terms will become nontrivial.

In the ideal Wigner crystal, the conductivity is found using Eq. (5.28),

$$\sigma_{L,T} = \omega_p^2 \frac{\omega_n}{\omega_n^2 + c_{L,T}^2 q^2}. \quad (5.29)$$

The poles of the conductivity are found after the Wick-rotation to real time is carried out. Given that our elastic system is dissipationless, the real part of either of the conductivities

shows only a delta-function pole. This peak is positioned at the phonon frequencies corresponding to the resonant motion in the ideal crystal that would be seen if one applied an oscillating spatially varying electric field. The correspondence between the phonon and the conductivity poles is not an accident. When the ‘dual Kubo’ formula is derived in the next section, it will be clear that the conductivity has to have the same poles as the elastic response of the charged system.

In Eq. (5.29), the longitudinal and transversal pole correspond to field variations parallel or perpendicular to its strength respectively, the difference between the two conductivity components can be attributed to the magnetic response of medium. At  $q = 0$ , the two are equal as we expect (no defined longitudinal and transversal directions). This limit is important since the dc-conductivity of a medium is determined by the ‘ $q \rightarrow 0$  then  $\omega \rightarrow 0$ ’ limiting procedure [51]. For the ideal crystal, we find the perfect conductivity  $\sigma_{dc} = \omega_p^2 \delta(\omega)$  and conclude that our charged ideal crystal would accelerate infinitely in a homogeneous constant electric field revealing that it is a perfect Frölich conductor because pinning is ignored.

## 5.2 Dual electromagnetism

In the above we found that the strain formalism suffices to treat the electrodynamics of the charged ideal crystal, but we already know that the duality has to be employed in order to derive the theory of charged nematic phases described in the previous chapter. In contrast with the dual elasticity theory from the previous chapter, this time the additional terms Eqs (5.3) and 5.5) are present, but the treatment should be straightforward if we apply the same rules as before, paying special attention to the pitfalls caused by the constraints. Although the EM fields lead to new terms in the dual action, slightly complicating the problem, we no longer have to take care of the transversal phonon external source term  $\mathcal{J}$  which had to be handled with great care.

When the duality border is crossed, the physical interpretation of the theory is turned upside-down with respect to that of the ideal crystal: we find that the dual theory provides the system with the EM Meissner term for free, at the same time the couplings between the dual stress degrees of freedom and the EM fields are recovered. These are integrated out removing the dual stress degrees of freedom and we find an effective Meissner term which determines the EM response functions. This expression for the effective Meissner term is the starting point for the two next sections, forming the basis for the response functions in the topological and the ordered nematic. The electric response of the ideal Wigner crystal has already been discussed in terms of the strain formalism and in this section we will confirm these results by means of the dual theory. At the end of this section, a relation between the dual stress gauge fields and the conductivity tensor, which we call the ‘dual Kubo formula’, is derived. The advantage of such relation is that one can calculate the conductivity of a medium, and extract the other electromagnetic response functions therefrom, without invoking directly the EM fields. All that one needs to know is the dual stress gauge field propagator and the plasmon gap corresponding to the charged medium.

To get an overview, let us group together all terms in the action of the charged elastic medium. There are three relevant contributions: the elastic part Eq. (3.24), the Maxwell action responsible for the dynamics of the EM gauge fields Eq. (5.5) and their minimal coupling Eq. (5.3). In combination, they read

$$\mathcal{L} = \frac{1}{2}\partial_\mu u^a C_{\mu\nu ab} \partial_\nu u^b + \frac{1}{4}F_{\mu\nu}F_{\mu\nu} + i\mathcal{A}_\mu^a \partial_\mu u^a. \quad (5.30)$$

The phonon external source terms are intentionally left out as we are no longer directly interested in elastic response. The action Eq. (5.30) is dualized in the standard way. First we define stress fields as conjugate momenta, Eq. (4.1), resulting in an additional term

$$\sigma_\mu^a = -iC_{\mu\nu ab} \partial_\nu u^b + \mathcal{A}_\mu^a. \quad (5.31)$$

The inverse relation  $\partial_\mu u^a = iC_{\mu\nu ab}^{-1}(\sigma_\nu^b - \mathcal{A}_\nu^b)$  is used to obtain the Hamiltonian density

$$\mathcal{H} = \frac{1}{2}\sigma_\mu^a C_{\mu\nu ab}^{-1} \sigma_\nu^b + \frac{1}{2}\mathcal{A}_\mu^a C_{\mu\nu ab}^{-1} \mathcal{A}_\nu^b - \sigma_\mu^a C_{\mu\nu ab}^{-1} \mathcal{A}_\nu^b + \frac{1}{4}F_{\mu\nu}F_{\mu\nu}. \quad (5.32)$$

Given that the field  $\mathcal{A}_\mu^a$  contains no spin-1 parts, the singularity of the elasticity tensor Eq. (3.15) is innocuous and it is safe to use the ‘inverse elasticity tensor’ Eq. (4.9) in the Hamiltonian density. The Ehrenfest constraint, Eq. (4.10) without the external source term, is implicitly imposed.

The treatment of the smooth and the singular displacement fields is identical to that in the previous chapter. First, the smooth displacements are integrated out, producing the stress conservation equation of motion which leads to the introduction of the dual ‘single curl’ stress gauge fields, as in Eq. (4.14). Notice, however, that the stress as introduced in Eq. (5.31), differs from the elastic stress as found in standard textbooks on elasticity [126], because now, a term including the minimal coupling to the EM fields is included. Let us define the ‘standard’ stress as  $\tilde{\sigma} = \sigma - \mathcal{A}$  and rewrite the stress conservation identity Eq. (4.13) as

$$\partial_\mu \tilde{\sigma}_\mu^a = \partial_\mu \mathcal{A}_\mu^a = (n_e e^*)[\partial_\tau A_a - \partial_a A_\tau] = -i(n_e e^*)E_a. \quad (5.33)$$

These are precisely the equations of motion for stress found in the textbooks (factor  $i$  comes from the Euclidian signature). This equation means that the divergence of the stress tensor is equal to the negative force per volume exerted on the elastic medium. The external force originates in the only external, EM field.

The second step in the treatment of the displacements, involving the singular configurations, is identical to the corresponding step in the electrically neutral elastic medium. The result is that the singular configurations in the displacement field (i.e. dislocations) minimally couple to the dual stress gauge field as  $iB_\mu^a J_\mu^a$ . At the same time, this means that the topological defects carry no bare electric charge because they couple exclusively to the dual stress gauge fields. Nevertheless, the dislocations in a charged medium are not completely immune to EM fields, due to the dual stress field which acts as a mediator which couples both to the dislocation and EM fields. The effective interaction is, however,

nonlocal both in time and space, which is easy to understand given the topological nature of the dislocations: a static dislocation present at a certain position will extend its influence on the elastic displacements throughout the whole system, which implies that it will also ‘feel’ the electric field throughout the entire space. Similarly, a dynamical (moving) dislocation couples to the dual stress fields, and these propagate with the phonon velocity to interact with the EM field somewhere else. Therefore, a dislocation’s ‘jitter’ at a certain point in space and time is ‘felt’ by the EM fields at some other point only after the ripples in the fabric of the elastic medium caused by that jitter could have been transmitted there.

Let us now return to the analysis of the dual action, containing the Hamiltonian Eq. (5.32) and the minimal coupling term. A big surprise is associated with the second term in Eq. (5.32). When expressed in terms of EM gauge fields, it yields a bare Meissner term of the dual elastic solid

$$\mathcal{L}_{Meiss.,bare} = \frac{1}{2} \mathcal{A}_\mu^a C_{\mu\nu ab} \mathcal{A}_\nu^b = \frac{1}{2} \omega_p^2 \left[ \frac{1}{C_K^2} A_\tau A_\tau + A_i A_i \right]. \quad (5.34)$$

As it turns out, just by rewriting the model in terms of the dual stress gauge fields, a Meissner term arises even when the charged system is still forming a crystal. In strong contrast with the standard particle language treatment where one has to work hard to derive superconductivity as a ramification of the off-diagonal long range order, the Meissner term comes now for free in this dual language and the difficulty is in fact that one has to get rid of it, knowing that in the ideal crystal it should vanish in static limit (compare with Eq. (5.9)).

The resolution of this problem lies in the third term of Eq. (5.32) corresponding to a linear coupling of the EM gauge fields to the dual stress gauge fields. Could this interaction be sufficient to “dress” the Meissner term back to its expected form Eq. (5.9)? This can be easily checked. Let us first find the explicit form of this coupling. For reasons of convenience and compatibility with the work in the previous chapter, let us choose to impose gauge fix Eq. (4.59) on the dual stress gauge fields. At the same time, we continue to use the Coulomb gauge fix Eq. (5.6) for the EM gauge fields. With these gauge fixes imposed, the coupling term between the EM gauge fields and the dual stress gauge fields becomes

$$\begin{aligned} \mathcal{L}_{EM,coupl.} &= -\sigma_\mu^a C_{\mu\nu ab}^{-1} \mathcal{A}_\nu^b = -\varepsilon_{\mu\lambda\rho} \partial_\lambda B_\rho^a C_{\mu\nu ab}^{-1} \mathcal{A}_\nu^b \\ &= -B_\rho^a \varepsilon_{\rho\lambda\mu} C_{\mu\nu ab}^{-1} \partial_\lambda \mathcal{A}_\nu^b \rightarrow -B_h^{E\dagger} g_{hM}^E A_M. \end{aligned} \quad (5.35)$$

The coupling constants follow, which are all vanishing except for

$$g_{+1,\tau}^T = \frac{(n_e e^*)}{2\kappa} p_d, \quad g_{-1,\tau}^L = -\frac{(n_e e^*)}{2\kappa} i\omega_n, \quad g_{-1,T}^T = \frac{(n_e e^*)}{\rho} q. \quad (5.36)$$

From these coupling constants it becomes apparent which dual elastic degrees of freedom are communicating with which EM sector. The correspondence between the electric and magnetic EM sectors with the longitudinal and transversal elastic sectors, must be preserved since the dualization just offers an alternative way to see the physical phenomena

but should not yield any new ones. In the EM transversal sector the coupling is simpler since there is just one dual stress photon  $B_{-1}^T$  coupled to the EM magnetic field. In the longitudinal sector, there are two nontrivial couplings, but a careful inspection shows that the dual stress field that couples to the Coulomb photon  $A_\tau$  is precisely the compression gauge degree of freedom ( $\mathcal{B}_C$ ). The fact to remember is that the electric shear dual stress gauge field Eq. (4.77) is neutral in the dual theory, and this will turn out to be crucial for the experimental predictions for the nematic phases.

Given that the elastic degrees of freedom are internal degrees of freedom, appearing in the partition function of the problem (e.g. Eq. (4.17), now with the external EM fields added), these have to be removed by Gaussian integration, and we find an effective Meissner term for the EM fields having a general form,

$$\mathcal{L}_{Meissner} = \frac{1}{2}\omega_p^2 \left[ \frac{1}{c_K^2} A_\tau A_\tau + A_i A_i \right] - \frac{1}{2} A_M^\dagger g_{hM}^{E\dagger} \mathcal{G}_{hh'}^{EF} g_{h'N}^F A_N. \quad (5.37)$$

The propagator for the elastic gauge fields  $\mathcal{G}$  should be taken according to the phase whose EM properties we wish to address.

Let us first test the action Eq. (5.37) for the ideal crystal. The bare Meissner term Eq. (5.34) which sparked some worries regarding the dualization is removed when the dual stress gauge field propagator Eq. (4.65) is inserted in Eq. (5.37). Since the elastic degrees of freedom are long-ranged in the ideal crystal, their contribution is sufficient to dress the bare Meissner term to precisely the form we found within the strain formalism: the effective Meissner term of the ideal crystal Eq. (5.9). By doing this we also revealed the weak spot of the superconductivity from the point of view of the dual theory: the normal state of the ideal crystal is a consequence of the long-range propagation of the elastic degrees of freedom which amounts to a cancellation of the bare Meissner term Eq. (5.34). Thus, we can already anticipate that the massiveness of the dual shear degrees of freedom in the nematic phases might lead to superconductivity, because this cancellation can no longer be complete when a gap is present in the dual stress photon spectrum.

Let us conclude this section by deriving a useful relation for the conductivity, which we call the ‘dual Kubo formula’. It allows one to find the electric conductivity of the elastic medium without having to resort directly to the EM fields: all that one needs to know is the dual stress propagator. In a way, all the other EM properties of the medium may be derived via this formula recalling the relation between the conductivity and the dielectric function tensor Eq. (5.28).

In the Coulomb gauge fix Eq. (5.6), the longitudinal electric field component, has a different definition in terms of the EM gauge fields, compared to the transversal field. In order to avoid three different derivations (for the longitudinal, the transversal and the off-diagonal conductivity), we adopt the radiative gauge fix,  $\partial_\tau A_\tau = 0$ , only in this part of the text. This leads to an ‘isotropic’ formulation of the problem where one does not even have to refer directly to the longitudinal and transversal flavours. In this particular gauge fix the electrical field is simply given by  $E_a = i\partial_\tau A_a = -\omega_n A_a$ .

The conductivity tensor is defined usually by

$$J^a = \hat{\sigma}^{ab} E^b = -\hat{\sigma}^{ab} \omega_n A^b, \quad (5.38)$$

where the electric field is expressed in terms of its gauge fields. The electric current carried by the medium is proportional to the charge density and the local velocity field and it can be expressed in terms of dual stress gauge fields as

$$\begin{aligned} J^a &= -i(n_e e^*) \partial_\tau u^a = \frac{n_e e^*}{\rho} \tilde{\sigma}_\tau^a = \frac{n_e e^*}{\rho} [\sigma_\tau^a - (n_e e^*) A^a] \\ &= \frac{n_e e^*}{\rho} \varepsilon_{\tau ij} \partial_i B_j^a - \omega_p^2 A_a = \frac{n_e e^*}{\rho} q B_{-1}^a - \omega_p^2 A_a. \end{aligned} \quad (5.39)$$

If one wishes to work explicitly with the ‘zweibeinen’ directions, Eq. (5.39) has to be contracted with  $-i\tilde{e}_a^E$ , in order to extract the two components  $E = L, T$ . In the remainder of our derivation of the ‘dual Kubo formula’ we do just the opposite: the couplings Eq. (5.36) and the dual gauge field propagators have their ‘flavours’ transformed to Cartesian indices for the purpose of an ‘isotropic’ formulation.

The dual stress gauge field  $B_{-1}^a$  has to be removed from the electric current Eq. (5.39), for which we use the equations of motion obtained by varying the total action with respect to the dual stress gauge field

$$(\mathcal{G}^{-1})_{hh'}^{ab} B_{h'}^b - g_{h,c}^b A_c = 0. \quad (5.40)$$

The coupling constants Eq. (5.36) in the radiative gauge fix have a different form: only two components are nontrivial

$$g_{-1,c}^a = \frac{n_e e^*}{\rho} q \delta_{ac}, \quad (5.41)$$

while all others are identically zero. The dual stress field  $B_{-1}^a$  is found from Eq. (5.40), and together with the coupling Eq. (5.41), the electric current Eq. (5.39) becomes

$$J_a = \omega_p^2 A_a - \left( \frac{n_e e^*}{\rho} \right)^2 q^2 \mathcal{G}_{-1,-1}^{ab} A_b. \quad (5.42)$$

Comparing this with the definition of the conductivity tensor Eq. (5.38), it follows that

$$\hat{\sigma}^{ab} = \frac{\omega_p^2}{\omega_n} \left[ \delta^{ab} - \frac{q^2}{\rho} \mathcal{G}_{-1,-1}^{ab} \right]. \quad (5.43)$$

This is the ‘dual Kubo formula’ expressing the conductivity in terms of the dual stress field propagator  $\mathcal{G}$ . This expression has much in common with the standard Kubo formula. The current Eq. (5.38) is the current measured by experimentalists, which is just the average local velocity of the charged medium. In contrast, the current that minimally couples to the external fields in the Hamiltonian is proportional to the conjugate momentum  $\sigma_\tau^a$ ,

$$j_a = \frac{n_e e^*}{\rho} \sigma_\tau^a = \frac{n_e e^*}{\rho} q B_{-1}^a. \quad (5.44)$$

Thus the two dual stress photons that correspond to the longitudinal and transversal phonon degrees of freedom  $B_{-1}^{L,T}$  are at the same time proportional to the electric currents Eq. (5.44). The dual stress propagator  $\mathcal{G}$  appearing in the dual Kubo formula Eq. (5.43) represents therefore the current-current correlator, modulo a constant, meaning that the dual Kubo formula Eq. (5.43) is equivalent to the standard Kubo formula

$$\hat{\sigma}^{ab} = \frac{\omega_p^2}{\omega_n} \delta^{ab} - \frac{1}{\omega_n} \langle\langle j^a | j^b \rangle\rangle. \quad (5.45)$$

Apart from serving the purpose of the direct derivation of the conductivity, the dual Kubo formula Eq. (5.43) reveals also that direct measurements of the conductivity will reveal poles which are identical to the poles of the dual stress gauge propagator  $\mathcal{G}$ , which again are just the propagators that could be seen in the elastic response.

In the ideal crystal, the dual Kubo formula Eq. (5.43) reproduces known results Eq. (5.29). In the isotropic nematic phase, the conductivity will be a diagonal tensor, due to the decoupling of the longitudinal and transversal sector, but as the ordered nematic phase has these coupled, the off-diagonal terms in the conductivity tensor Eq. (5.43) will be nontrivial. This, does not mean that an effect analogous to the anomalous Hall effect (off-diagonal terms without external magnetic field) appear. Using the wisdom applied to the chiral propagator Eq. (3.35), due to the symmetry properties of the medium, in the real space the off-diagonal terms vanish.

### 5.3 Charged isotropic nematic phase

The hard work has been done. In order to find the EM gauge field propagators, all that one needs to do is to take the effective Meissner term Eq. (5.37) and plug in one of the possible dual stress gauge field propagators derived in chapter 4. This yields self-energies for the EM gauge fields, and one can find the physical observables using the simple relations derived in section 5.1, which are universal. In the previous section, it was already demonstrated that the EM self-energy for the ideal crystal is recovered in this way. In this and the next section, this straightforward exercise is repeated for the cases of the isotropic and ordered nematic phases. We choose to invert the order of these phases for the following reasons: in spite of the nontrivial physical picture behind the isotropic nematic phase, one can convince oneself that this phase shows simple isotropic electromagnetic behaviour, which is not the case with the ordered nematic. At the same time, given the discussion from the previous section, we anticipate that the shear screening in this phase will produce a nontrivial Meissner term. Hence, this phase is a representative example for the dual mechanism of superconductivity, which is the main message we want to get across in this thesis.

Given the fact that the quest for quantum liquid crystals began in the context of the strongly correlated electronic liquid, the results for a charged medium presented here form the highlight of this thesis. This is true not only because a novel fundamental mechanism for superconductivity is proposed, the results from this section correspond to predictions

for physical properties that can, in principle, be measured. The practical problem with these measurements is the following: our ‘ordered’ superconductor is a unconventional type of superconductor, exhibiting a host of properties which are not found in the conventional BCS superconductors, and accordingly, have never been subject of attention for the experimentalists. Some of these require either experimental setups that operate at the edge of the limits of the present day technology or require a substantial modifications of existing techniques. The features we find include unconventional static screening of both electric and magnetic fields, the existence of additional poles in the electric response functions and the presence of a weak massless pole in the optical (transversal) conductivity at finite wavelengths. Experiments capable of detecting any of these features can prove crucial for answering fundamental questions regarding the nature of high- $T_c$  superconductors such as the presence of the fluctuating order in the superconducting phase.

We are unaware of any experimental technique that can measure directly the profile of a static field, be it magnetic or electric, at microscopic lengths. Experiments measuring the London penetration depth exist. However, these assume conventional BCS-type magnetic screening which renders them inapplicable for our purposes. For this reason, we only present possible screening scenarios and speculate about their possible effect on (frustrated) charge separation, as observed in strongly correlated electron systems. For the similar reasons, we also present a prediction for the transversal conductivity to discuss briefly what we expect from an experimentalist will find in an optical conductivity measurement if these could be extended to finite wave-vectors.

Our most promising prediction is to our opinion related to the longitudinal dielectric function Eq. (5.18), where a new pole will appear in the nematic phases, corresponding to the ‘dual shear’/‘dislocation sound’ degree of freedom. In principle, this response can be directly measured in electron energy loss spectroscopy (EELS) experiments [173]. Unfortunately, the ‘shear fingerprint’ pole has a strength which is roughly proportional to the inverse square of the wavelength, which requires a very high resolution ( $\approx 10\text{meV}$ ) measurement of the electron energy loss function at small but finite (“mesoscopic”) wavenumbers. An experimental technique is at present under development using low-energy electrons which is promising in this regard [175]. An alternative experiment having this potential is resonant inelastic X-ray scattering although this technique is still under development [174].

Finally, let us make a remark about the ‘orderly’ status of the nematic superconductor. From the construction of the nematic phases, it follows that the superconducting state that is implied by it has the maximum possible crystalline order. This claim will be further substantiated by the results of this and the next section. In particular, the parameter measuring the remaining order in the nematic phase is the shear penetration depth  $\lambda_S$ , which is inversely proportional to the shear Higgs gap  $\Omega$ . The unconventional properties we identified here will be most prominent when this gap is small such that the system is in close proximity to the solid state. As this gap grows and the shear penetration depth is reduced, the superconducting state becomes more conventional. When the shear penetration depth (and the closely related dislocation correlation length) becomes of order of the microscopic electric screening length  $\lambda_c$ , the crystalline order is completely destroyed and the resulting superconductor cannot be distinguished anymore from the BCS ‘gaseous’ state. Due to the

large difference between the phonon and light velocities, an exception to this rule is offered by the London penetration depth. This length is many orders of magnitude larger than the electric screening length, requiring that the shear penetration depth is at least of that order of magnitude or larger in order to exhibit unconventional screening effects. Although our the initial theory does not prohibit an arbitrary small dual Higgs gap, the necessity of a first order transition between the ideal crystal and an isotropic superconductor may prove an insurmountable obstacle for the realization of the unconventional magnetic screening effects.

After this discussion, we turn to the technical part of the section deriving the EM gauge field propagators first. Using the procedure we explained and invoking the dual stress gauge fields propagator (i.e. self-energy term Eq. (4.109) for the isotropic nematic phase, the inverse EM propagators are found, which we write as

$$(\mathcal{G}_\tau)^{-1} = q^2 \left( 1 + \frac{\omega_p^2(\omega_n^2 + c_g^2 q^2 + \Omega^2)}{(\omega_n^2 + c_L^2 q^2)(\omega_n^2 + c_g^2 q^2) + \Omega^2(\omega_n^2 + c_K^2 q^2)} \right), \quad (5.46)$$

$$(\mathcal{G}_T)^{-1} = \omega_n^2 + c_l^2 q^2 + \omega_p^2 \frac{\omega_n^2(\omega_n^2 + c_d^2 q^2) + \Omega^2(\omega_n^2 + c_g^2 q^2)}{(\omega_n^2 + c_T^2 q^2)(\omega_n^2 + c_d^2 q^2) + \Omega^2(\omega_n^2 + c_g^2 q^2)}. \quad (5.47)$$

These are the key expressions in this section since all the results in the remainder follow. Before proceeding further, one can convince oneself that the propagators Eq. (5.46 - 5.47) do not vanish taking the order of limits  $\omega_n \rightarrow 0$  then  $q \rightarrow 0$ . In short, the physical meaning of this nonvanishing limit is that both electric and magnetic static fields are expelled from the charged nematic phase which qualifies it as a superconducting state. Hence, the bare Meissner term Eq. (5.34) which is tailored by the dual theory for the maximally disordered, superconducting superfluid state, finally becomes ‘liberated’ when the shear stress photons acquire a Higgs mass so that they lose their powers they have in the ideal crystal phase.

Let us start the analysis of Eq. (5.46 - 5.47) with the static magnetic screening of the isotropic nematic phase for the reason that this was the first identified EM property of the dual elasticity theory. Its unconventional properties were already pointed out by Zaanen *et al.* [44], and we repeat their discussion here. For this static property, the problems associated with the dynamical dislocation condensate are irrelevant. Since magnetic fields are carried by the transversal EM photon, its static correlator is proportional to the static limit of Eq. (5.47)

$$G_{mag}^{-1} = \left. \frac{\mathcal{G}_T^{-1}}{c_l^2 q^2} \right|_{\omega_n=0} = 1 + \frac{1}{\lambda_L^2 q^2} \frac{1}{1 + \lambda_s^2 q^2}, \quad (5.48)$$

introducing the bare London length  $\lambda_L = c_l/\omega_p$  and using the already introduced shear penetration depth  $\lambda_s = \sqrt{2}c_T/\Omega$ .

The poles of the  $q$  dependent propagator Eq. (5.48) are given by

$$q_0 = \pm \frac{i}{\sqrt{2}} q_s \left[ 1 \pm \sqrt{1 - \frac{4q_L^2}{q_s^2}} \right]^{1/2}, \quad (5.49)$$

introducing the momenta corresponding to the London ( $q_L = 1/\lambda_L$ ) and shear ( $q_s = 1/\lambda_s$ ) penetration depths. There are two different ways that one can interrogate the poles Eq. (5.49). Either a magnetic charge (monopole, dipole, multipole, vortex, ...) can be inserted from the outside in the system and its influence can be deduced through the pole strengths of the propagator Eq. (5.48), or one can just take the homogenous solutions following from the poles Eq. (5.49) and impose boundary conditions in order to find the magnetic field profile. In the case of the magnetic field we opt for the latter one. Let us, for the sake of simplicity, first analyse what happens in 1D-geometry: in the ‘right’ semiplane  $x > 0$ , the magnetic field obeys the equation  $G_{mag}.B = 0$ , with solutions in this specific type of geometry given as  $e^{iq_0x}$ . Patching these homogenous solutions to the ‘left’ semiplane  $x < 0$  where the magnetic field is a constant  $B_0$ , the following profile is found

$$B(x) = \frac{B_0}{q_0^{(2)} - q_0^{(1)}} \left[ q_0^{(2)} e^{iq_0^{(1)}x} - q_0^{(1)} e^{iq_0^{(2)}x} \right], \quad (5.50)$$

where  $q_0^{(1,2)}$  are two solutions, of the possible four from Eq. (5.49), with a positive imaginary part (in order to vanish in  $x \rightarrow \infty$  limit).

The qualitative shape of the profile turns out to be highly dependent on the ratio between the two penetration depths. This is already clear from the expression under the square root in Eq. (5.49) (which can change sign), but we also have a physical interpretation. Begin with the straightforward case of a small shear penetration depth and large London length,  $q_s > 2q_L$ . The expression under the square root in Eq. (5.49) is positive and the magnetic field is governed by two functions with an exponential fall-off. In the limit when the shear length is much smaller than the London length,  $q_s \gg q_L$ , the two poles of the correlator Eq. (5.48) are approximately located at  $q_0^{(1)} \approx q_L$  and  $q_0^{(2)} \approx q_s$ . The term with  $q_0^{(1)}$  is dominant and the screening profile cannot be distinguished from that of a conventional BCS superconductor  $B(x) = B_0 \exp(-r/\lambda_L)$ . This can be understood in the following way: the screening of the magnetic field occurs at depths of order  $\lambda_L$ . However, at these scales, the medium has lost any knowledge about the shear rigidity and it behaves precisely as a ‘gaseous’ BCS superconductor. This limit, when the crystalline correlations are smaller than the screening lengths will be called ‘near-superfluid’ limit for this reason although in this case the shear penetration depth can still be quite large.

What is the behaviour of the screening in the opposite, ‘near-solid’ limit of the nematic phase? We anticipate unconventional effects, driven by the solid correlations. As soon as the shear length exceeds a half of the bare London depth, i.e. one crosses the disorder line  $q_s < 2q_L$ , the expression under the square root in Eq. (5.49) becomes negative, which causes the solutions in Eq. (5.49) to have both real- and imaginary part. The imaginary part was present before being responsible for the exponential screening. The novelty is the real part which leads to harmonic modulations of the magnetic field. Therefore, the total magnetic field decays in intensity, but its actual profile is a cosine function enveloped in a decaying exponential function. This overscreening effect is due to the residual solid correlations in the electron liquid. Recall that the magnetic screening in the charged superfluid takes lengths of order of the London length  $\lambda_L$  to be screened, while at the same

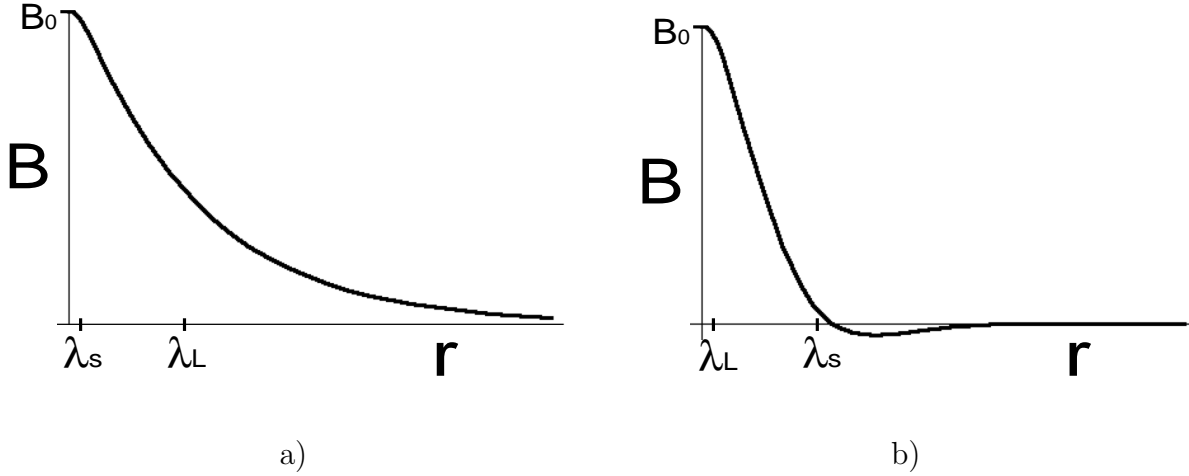


Figure 5.1: Static screening of external magnetic field in the isotropic nematic phase: a) small shear screening length  $\lambda_s \ll \lambda_L$ , i.e. ‘near-superfluid’ state, exhibits the standard ‘gaseous BCS like’ screening with the London penetration length  $\lambda_L$  as the characteristic length; b) above the disorder line  $\lambda_s > \lambda_L$ , the model has a remnant solid (shear) rigidity at scales of the London length. An attempt to screen the magnetic field at that scale ends in slight overscreening which causes the remainder of the (halfplane) system to repeat the scenario, now with a changed field sign. The ‘near-solid’ region of the nematic phase is thus characterized by the oscillating magnetic field pattern.

time the solid prevents this from happening. When exposed to an external magnetic field, the nematic phase will try to react by creating diamagnetic currents expelling the magnetic field. However, at the depth where the magnetic field is completely screened (first zero in Fig. 5.1b), due to the shear rigidity, which survives at lengths higher than the bare London length, a drag of the remaining layers will occur resulting in a slight overscreening of the external magnetic field. The remainder of the semiplane can now be treated recursively, as trying to screen the negative magnetic field experienced at the first intensity minimum. The next layer is, due to the reversed sign of the ‘external field’, paramagnetic, to be followed by a diamagnetic layer and so on. The result is naturally a decaying cosine. In the ‘near-solid’ limit,  $q_s \ll q_L$ , the solutions of Eq. (5.49) turn into the geometrical mean of the two screening lengths  $q_0 = \sqrt{q_s q_L} \exp(i(2k+1)\pi/4)$  [44]. Since the real part of the effective screening length cannot exceed the imaginary part (they are equal in the limit  $\lambda_s \gg \lambda_L$ ), the field intensity at the first dip is at bound by  $e^{-\pi \frac{\text{Im} q_0}{\text{Re} q_0}} \approx 0.043$  of the original field. The characteristic fall-off length in this limit is the geometric mean of two lengths  $\sqrt{\lambda_L \lambda_s}$ .

If the geometry of the problem was 2D instead of 1D, in other words, if we would consider a magnetic flux line penetrating a two-dimensional layer, matters change a little: the homogenous solutions of the equation for the magnetic field are now two Bessel functions  $K_0(q_0 r)$ , that behave asymptotically as  $\frac{e^{iq_0 r}}{\sqrt{r}}$ . This asymptotic behaviour is true even

when  $q_0$  acquires a real part except that this situation corresponds to the configuration of concentric rings of dia- and paramagnetic supercurrents. The 3D geometry has no physical importance since no magnetic monopoles exist (and our system is strictly 2D!), however, if it had been true, the profile of the magnetic field would be exactly the one given by the Yukawa potential  $B \propto \frac{e^{iq_0 r}}{r}$ . This expression is again applicable regardless on which sides of the disorder line the system finds itself.

Let us now turn to the static electric screening. Given the fact that the electric field is carried by the Coulomb photon, their propagators are proportional. The static electric field propagator follows directly from the propagator Eq. (5.46) in the limit  $\omega_n \rightarrow 0$ . This is just the static dielectric function the same result

$$G_{el.}^{-1}(q) = \varepsilon(q, \omega_n \rightarrow 0) = \frac{\mathcal{G}_\tau}{q^2} \Big|_{\omega_n \rightarrow 0} = 1 + \frac{1 + \lambda_g^2 q^2}{\lambda_f^2 q^2 + \lambda_c^2 \lambda_g^2 q^4}. \quad (5.51)$$

Next to the known ideal crystal electric field screening length  $\lambda_c$ , two other screening lengths are introduced:  $\lambda_f = c_K/\omega_p$  is the screening length corresponding to the electric screening in a liquid with a sound (compressional) velocity  $c_K$ , and  $\lambda_g = c_g/\Omega$  is the screening length associated with the dual longitudinal stress photons  $B_L^E$ . Since these are coding for the dislocation condensate degrees of freedom, this length has the physical meaning of correlation length of the dual condensate phase degree of freedom. In fact, due to the equality between the dislocation sound velocity  $c_d$  and the transversal phonon velocity  $c_T$ , this length is a half the shear screening length  $\lambda_g = \lambda_s$ .

Considering the solid ( $\lambda_g \rightarrow \infty$ ) and the liquid ( $\lambda_g \rightarrow 0$ ) limits, the standard electric field screening behaviour of the charged crystal and the fluid (with the characteristic length  $\lambda_f$ ) are recovered. When the correlation length  $\lambda_g$  is finite, the screening is determined by the poles of the propagator Eq. (5.51), given by

$$q_0 = \pm \frac{i}{\sqrt{2}\lambda_g\lambda_c} \left[ \lambda_g^2 + \lambda_f^2 \pm \sqrt{(\lambda_g^2 + \lambda_f^2)^2 - 4\lambda_g^2\lambda_c^2} \right]^{1/2}. \quad (5.52)$$

In analogy with the magnetic screening, the sign of the expression under the square root in Eq. (5.52) determines the nature of the screening. This expression can be rewritten in the following manner

$$\begin{aligned} (\lambda_g^2 + \lambda_f^2)^2 - 4\lambda_g^2\lambda_c^2 &= (\lambda_g^2 + \lambda_f^2 + 2\lambda_g\lambda_c)(\lambda_g^2 + \lambda_f^2 - 2\lambda_g\lambda_c) \\ &= ((\lambda_g + \lambda_c)^2 - \lambda_g^2 + \lambda_f^2)((\lambda_g - \lambda_c)^2 - \lambda_g^2 + \lambda_f^2) \\ &= (\lambda_g + \lambda_c + \lambda_T)(\lambda_g + \lambda_c - \lambda_T)(\lambda_g - \lambda_c + \lambda_T)(\lambda_g - \lambda_c - \lambda_T), \end{aligned} \quad (5.53)$$

introducing the transversal screening length  $\lambda_T = \sqrt{\lambda_c^2 - \lambda_f^2} = c_T/\omega_p$ , corresponding to the penetration depth of a medium with only shear rigidity. The right hand side of Eq. (5.53) defines two disorder lines for the electric screening:  $\lambda_g = \lambda_c \pm \lambda_T$ . In between these two lines, the poles Eq. (5.52) have both real and imaginary part corresponding to a damped oscillatory profile for the electric field. Outside this regime, we find the ‘near-solid’ and

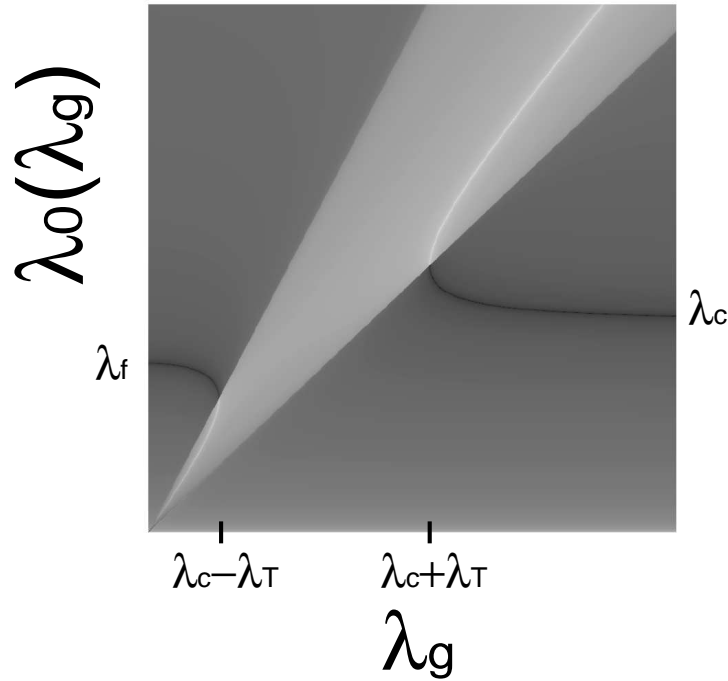


Figure 5.2: Imaginary poles of the static Coulomb propagator Eq. (5.51): Black and white points correspond to positive and negative strengths. In the ‘near-superfluid’ region on the left ( $\lambda_g < \lambda_c - \lambda_s$ ), the minute dislocation correlation length  $\lambda_g$  does not have a sufficient strength and does not ‘extend’ enough to cause the attractive effective Coulomb potential. On the opposite, ‘near-crystal’ side ( $\lambda_g > \lambda_c + \lambda_c$ ), the correlations in the dislocation condensate have longer range than the genuine Coulomb repulsion resulting in the change of the sign of the interaction at large distances. Between the two disorder lines ( $\lambda_c - \lambda_T < \lambda_g < \lambda_c + \lambda_T$ ) the screening develops oscillating patterns of over- and under-screened regions.

‘near-superfluid’ regimes with purely imaginary poles. These purely imaginary poles given by Eq. (5.52) are represented on Fig. 5.2. The pole strength is indicated by thickness and the sign by colour: black – positive, white – negative. These pole strengths will be necessary to demonstrate another unconventional feature: the overscreening of electric charge. This global effect is different from the overscreening in the regime between the two disorder lines with alternating over- and under-screening layers.

In spite of the three different regimes predicted by the theory, only one is of physical significance. This is a consequence of the microscopic electric screening lengths  $\lambda_{c,f}$  which are always of order of the lattice constant. On the other hand, in order to secure the validity of this dual elasticity framework, one needs to keep the shear/dislocation screening lengths large as compared to the lattice size. Hence, the physically relevant regime is the ‘near-solid’ limit  $\lambda_g \gg \lambda_{c,f}$ , which is at the same time the most interesting one due to its high level of correlations.

Let us imagine that an electric charge is inserted in the system. We are right now only interested in the behaviour of the electric field profile so we set the amount of charge to unity, although the units and constants in the 2D Maxwell theory are not properly defined. At the end of this discussion, an estimate for a 3D medium with 3D Coulomb forces will be presented. The substantial Maxwell equation with the spatio-temporal dispersion for the electric field in the nematic phase is in real space given by

$$\nabla_{\mathbf{x}} \cdot \int d\mathbf{x}' d\tau' \hat{\varepsilon}(\mathbf{x} - \mathbf{x}', \tau - \tau') \mathbf{E}(\mathbf{x}', \tau') = \rho_{el.}(\mathbf{x}, \tau), \quad (5.54)$$

where we used the Matsubara-Fourier transformed dielectric function Eq. (5.18).

For simplicity, we consider first the one-dimensional problem. A static unit charge at the coordinate origin  $\rho = \delta(x)$  implies that the electric field, as follows from the solution of Eq. (5.54), is in general given by

$$E(x) = A_1 e^{iq_0^{(1)}x} + A_2 e^{iq_0^{(2)}x}, \quad (5.55)$$

where  $A_{1,2}$  correspond to the pole strengths of poles  $q_0^{(1,2)}$  chosen in such way that the electric field Eq. (5.55) vanishes at infinity. In the physically relevant ‘near-solid’ limit,  $q_g \ll q_c$ , the poles and their strengths are approximately given by

$$\begin{aligned} q_0^{(1)} &= iq_g + O\left(\frac{q_g^2}{q_c}\right), & A_1 &= -\frac{q_g^3}{2q_T^2} + \dots, \\ q_0^{(2)} &= iq_c + O(g_g), & A_2 &= \frac{q_c}{2} + \dots \end{aligned} \quad (5.56)$$

The latter pole corresponds with the electric screening pole found in the ideal crystal. The former pole is more interesting because, it has a negative strength, while the solution following from it falls-off slower than the positive pole. This pole finds its origin in interaction of the dislocation condensate with the electric charge, which is clear from both its value and from the effect that it appears only in the nematic phase. Although the dislocations are electrically neutral, we already mentioned that their influence on the elastic medium causes a nonlocal coupling to the electric field, and vice versa. When an external electric charge is inserted in the system, it will interact with the charged medium, inducing, at the same time disturbances in the dislocation tangle. Because these inhomogeneities ‘extend’ up to the correlation length of the condensate, the electric influence of the charge finds a way to circumvent the crystalline screening and to act at much larger distances than possible in the ideal crystal. Apparently, the dislocation condensate does not only screen the electric field, it overscreens it according to the negative pole strength in Eq. (5.56). As a consequence, the electric field becomes attractive after a distance which is exactly equal to

$$x_0 = \frac{2\lambda_g\lambda_c}{\lambda_g - \lambda_c} \ln\left(\sqrt{\frac{2}{1-\nu}} \frac{\lambda_g}{\lambda_c}\right), \quad (5.57)$$

regardless the number of spatial dimensions. This effect, mediated by the condensate, has however a very weak strength and we may wonder if it has any true physical consequences. The minimum of the attractive potential can be analytically found in 1D case and it occurs at

$$x'_0 = \frac{4\lambda_g\lambda_c}{\lambda_g - \lambda_c} \ln\left(\sqrt[4]{\frac{2}{1-\nu}} \frac{\lambda_g}{\lambda_c}\right), \quad (5.58)$$

where the electric field has (negative) value of

$$E(x'_0) = \frac{e^{-\frac{x'_0}{\lambda_c}}}{2\lambda_c} \left(\frac{\lambda_c - \lambda_g}{\lambda_c}\right). \quad (5.59)$$

The leading expression is the strength of electric field that would be realized in the ideal crystal phase. The expression in the parentheses is negative and orders of magnitude larger than one. Hence, the overscreening effect does not only change the sign of the electric field, it also enhances its intensity by many orders of magnitude. Unfortunately for the effect, this minimum happens only after a significant distance, i.e. in the tail of the exponential fall-off, when, although much stronger than the original field, it is nevertheless much weaker than the relevant energy scale.

In order to make an estimate in real physical systems, we better consider what would happen in a real 3D system with the electric propagator given by Eq. (5.51). The electric field potential caused by a charge  $q_{el}$  inserted in this medium reads

$$A_\tau(r) \approx \frac{1}{4\pi\epsilon_0} \frac{q_{el}}{r} \left[ e^{-\frac{r}{\lambda_c}} - \frac{\lambda_T^2}{\lambda_g^2} e^{-r/\lambda_g} \right], \quad (5.60)$$

with the dielectric constant of the vacuum which is given as  $1/(4\pi\epsilon_0) = 14.4eV\text{\AA}/e^2$  in three dimensions. Now we need the bare electric screening length and the dislocation (shear) correlation length. The former is trivially defined and well known in the cuprates and it is a microscopic length of order of few Ångströms. It is not entirely clear where to look for the shear/dislocation length in the electron system of a cuprate. A scale that naturally arises in this system is the correlation length associated with the incommensurate spin fluctuations which is of order of few nanometers. Thus, the ratio between the two characteristic lengths is  $\lambda_g/\lambda_c \approx 10$ . The Poisson ratio is usually between 0 and 1, and we set it to  $\nu = 0.28$  in order to have rational phonon velocities ( $c_T = 0.6c_L$  and  $c_K = 0.8c_L$ ). In fact, quantitatively very little depends on the Poisson ratio, unless it is close to unity (liquid), when due to the similarity between the ideal crystal and the liquid, the effects of the fluctuating order become less apparent.

With the parameter estimates presented in the previous paragraph, the attractive minimum of the electric field can be numerically determined. In order to give the reader a feeling of the effect, the electric field is plotted in Fig. 5.3, zooming in on the region with the attractive Coulomb potential. The minimum of the potential is realized at  $r'_0 = 10.7\lambda_c$  and the depth of the potential is approximately  $10^{-4}/\lambda_L^2[\text{\AA}]$  corresponding to a tenth of a

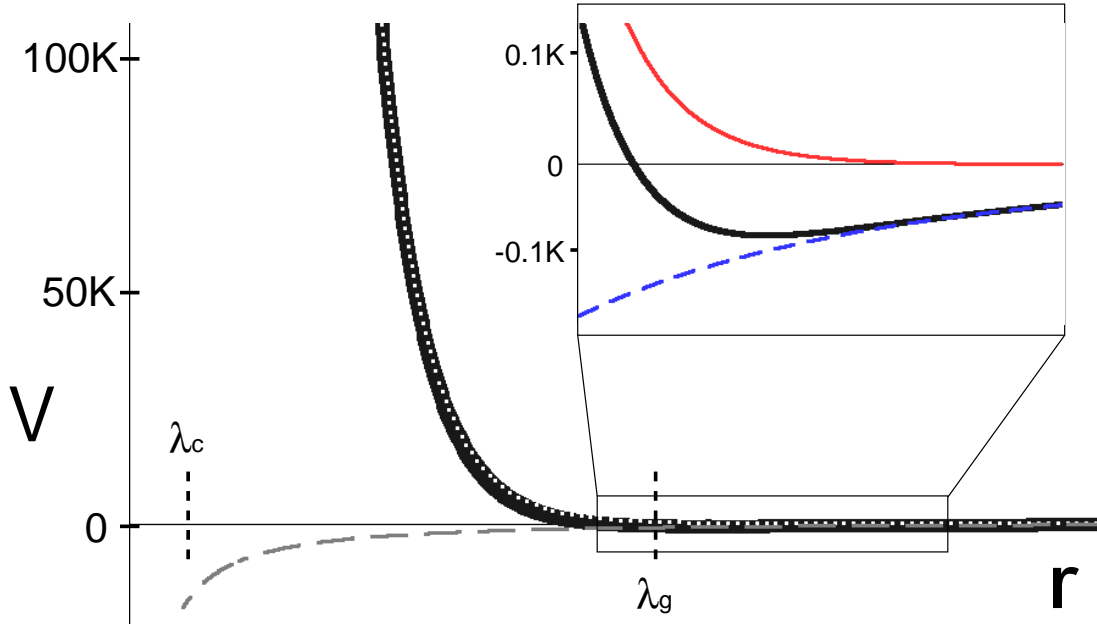


Figure 5.3: Overscreening of the Coulomb field in the isotropic nematic phase: The pole strength of the plasmon pole (dotted line in the main figure; thin solid line in the inset) is many orders of magnitude larger than the strength of the attractive pole. However, due to its larger penetration depth, the attractive potential (thin dashed line) eventually wins at larger distances causing a shallow attractive well. From the estimates in the text, the depth of this potential for two electrons should be of order of mili to a tenth of a Kelvin.

Kelvin. This whole estimate is of course quite rough. However, even if we overestimated the value by one or two orders of magnitude, the depth of the potential would have been of order of  $mK$ , which makes us speculate that this effect could be responsible for the charge separation effect, observed in cuprates.

Having addressed the static properties of the system, let us turn now to the dynamical EM response functions. We leave the longitudinal dielectric function for the end of this section, since it is experimentally the most relevant one and it will be discussed in detail. The EM response functions associated with the transversal elastic sector are the dynamical magnetic susceptibility  $\mu(\omega_n, \mathbf{q})$ , the transversal conductivity  $\varepsilon_T$  and the transversal optical conductivity  $\hat{\sigma}_T$ . These are not independent: determining one by an experiment the others directly follow as it can be seen from Eq. (5.23) or Eq. (5.28). As it turns out, the signals appearing within the nematic phase are visible only at finite wavelengths, whereas, the experiments measuring the listed observables are always limited to the zero-momentum. This is pure consequence of the enormous discrepancy between the velocities in the medium and the velocity of the EM photons, used to probe the system. Until now, this problem has not been overcome by any experimentalist. In the area of the semiconductor physics, a technique exists which makes it possible to scan the dispersion of surface polaritons.

This experiment involves a grating on the surface of the sample and in this manner the wavelength can be regulated. There are, however, many limiting factors to this technique: it allows control of the wavevector only parallel to the grating, the transversal field is not very well defined, and the wavelengths obtained in this manner are still much larger than the unit cell. Another drawback of this method, when applied to the particular case of YBCO, is that the roughness of the surface is always much higher than the desired grating. Given these limitations, our analysis of the transversal sector observables will be limited to the long-wavelength limit, hoping that an experiment, devised to probe large but finite wavelengths, may catch the fingerprints of the nematic phase.

Let us start out considering the optical conductivity  $\hat{\sigma}_T$ . It may be found from either the transversal EM photon propagator Eq. (5.47) or from the dual Kubo formula Eq. (5.43) and in the isotropic nematic phase it reads

$$\hat{\sigma}_T(\omega_n, q) = \frac{\omega_p^2}{\omega_n} \frac{\omega_n^2(\omega_n^2 + c_d^2 q^2) + \Omega^2(\omega_n^2 + c_g^2 q^2)}{(\omega_n^2 + c_T^2 q^2)(\omega_n^2 + c_d^2 q^2) + \Omega^2(\omega_n^2 + c_g^2 q^2)}. \quad (5.61)$$

In the long-wavelength limit ( $q \rightarrow 0$ ) this recovers the conductivity of the ideal conductor  $\hat{\sigma} = \omega_p^2/\omega_n$  which is not a surprise. Notice that here only the real part of the conductivity is considered. The imaginary part can be obtained either directly by Wick-rotation from the conductivity Eq. (5.61) or from the Kramers-Kronig relation.

What happens at finite wavelengths? The static pole  $\omega_n = 0$  is still present which is the hallmark of the superconductivity. Its strength, however, weakens according to

$$A_0 = \frac{\omega_p^2}{1 + \lambda_s^2 q^2}. \quad (5.62)$$

This can be interpreted as that, at shorter scales, where the translational order is restored, the superconductivity fades away. However, in order for the strength Eq. (5.62) to decrease significantly, one needs to examine the system at distances smaller than the shear penetration length. This offers a potential experimental detection of the fingerprint of the nematic conductivity, given the fact that the shear penetration length is much larger than the lattice constant. Even though that this weakening of the signal may not be easily detectable, one can focus instead on the signal from the other two poles which also contain this information due to the sum rules. As can be seen from the dual Kubo formula, these poles, reside at the same wavelengths as the neutral phonon poles. In the long-wavelength limit, the strengths of these two poles are similar and given by  $A_{1,2} = \omega_p^2 \lambda_s^2 q^2 / 4 + O(q^4)$ . Hence, by reducing the wavelengths probed in the optical conductivity experiment to the order of the shear penetration length, two additional poles in the real part of the conductivity should appear. The massless pole with the dispersion  $\omega \approx c_g q$  might be hard to detect due to its proximity to a much more intense ideal conductivity pole. The other pole is, however, gapped, and this might be crucial for the experimental detection. Based on earlier estimates of the screening lengths and the Poisson ratio and including the value for the plasmon gap  $\omega_p \approx 1eV$ , the shear Higgs gap follows to be of order of  $\Omega \approx 60meV$ . This is of course a crude estimate, but it actually falls not so far from the spin-gap value

( $10 - 50\text{meV}$ ), which might be thought of as a relevant energy gap in cuprates. Notice also that the shear Higgs gap is an order of magnitude lower than the plasmon gap. It has to be smaller, because otherwise the shear screening length would have been microscopic and our theory would no longer be applicable.

Another interesting feature of the medium related to the transversal EM response are the polaritons. It was already mentioned that the polariton dispersion follows from the transversal EM photon propagator, so we can directly use Eq. (5.47) to look for its poles. This yields a bicubic equation, and instead of the exact expression, we only present the long-wavelength approximate solutions. One polariton pole is located at  $\omega_1^2 = \omega_p^2 + O(q^2)$  and it has a nonvanishing strength in the long-wavelength limit  $A_1 \approx 1/(2\omega_p)$ . This is nothing else than the plasmon excitation of the electron liquid, which is robust to the presence of the dislocation condensate of the nematic phase. Recall the massless diffusion polariton pole of the ideal crystal. In the nematic phase an additional degree of freedom appears and combined with the diffusion polariton, two modes appear. One is gapped with the shear Higgs gap  $\omega_2 \approx \Omega$ , while the other has the same dispersion as the massless pole already encountered in the transversal sector. Hence, it appears as if the nematic superconductor can admit massless excitations which are, at least in the BCS superconductor, dangerous for the superconducting order since any supercurrent may decay into these excitations if not protected by the superconducting gap. A possible explanation for the coexistence of this massless degree and superconductivity may lie in fact that this superconductor does not acquire a gap according to the Abelian-Higgs or BCS mechanism. Therefore, it is the medium which acts as the carrier for the currents and accordingly, the supercurrents are nothing else than matter (superfluid) currents of the charged nematic phase. The supercurrent cannot decay into the massless mode propagating at the glide velocity because the supercurrent is already carried by that mode. It should also be clear that the presence of this massless mode does not mean that the medium is incompressible. The compressibility follows from the longitudinal dielectric function and in the remainder of the text, the analysis thereof will show that the charged nematic isotropic phase is incompressible electronic liquid.

The presence of the massless mode in the polariton spectrum implies, among other things, that light can be freely propagate through a nematic solid, although the propagation velocity is only  $c_g$  which results in a medium which is effectively totally reflective. Another circumstance that hinders the propagation of the massless polariton is its pole strength. While the strength of the plasmon pole is roughly a constant in the long-wavelength limit and the strength of the second polariton pole grows only proportionally to  $q^2$ , the massless polariton has a pole whose strength depends on the wave-number as  $q^3$  in the long-wavelength limit.

The final result regarding the EM response of the isotropic nematic phase is the longitudinal dielectric function 5.18. In the remainder of this section, we will study this response function in detail to arrive at experimental predictions that can be measured in principle although this requires a substantial upgrading of existing experimental methods. The standard experiment tailored to measure the longitudinal dielectric function is EELS [173], although there are other possibilities [174]. The outcome of our analysis will be that the

electron energy loss spectrum acquires an additional pole in the nematic phase. The origin of this pole may be traced back to the novel pole in the longitudinal elastic response of the neutral crystal: the excitation behind this pole is carried by the ‘dual shear superconductor’. However, as with other measurable electric responses, this fingerprint of the nematic order is absent in the long-wavelength limit and it is active only at finite wave-vectors which makes it hard to measure. This is a lucky circumstance for our theory: although we predict a feature no one has yet seen up to now, the fact is that experiments did not look into the right direction or did not push their limits into the required kinematical region. Given our predictions, we can tell precisely where to look and what to seek in order to (dis)prove the applicability of this theory for cuprates or any other candidate system and answer directly relevant questions for the cuprates such as the sense or nonsense of the fluctuating order.

Let us begin with the expression for the dynamical dielectric function. From the Coulomb propagator of the nematic phase Eq. (5.46) the dielectric function readily follows as

$$\hat{\epsilon} = 1 + \frac{\omega_p^2(\omega_n^2 + c_g^2 q^2 + \Omega^2)}{(\omega_n^2 + c_L^2 q^2)(\omega_n^2 + c_g^2 q^2) + \Omega^2(\omega_n^2 + c_K^2 q^2)}. \quad (5.63)$$

The ‘near-solid’ and ‘near-liquid’ limits are easily obtained

$$\hat{\epsilon}_{solid} = 1 + \frac{\omega_p^2}{\omega_n^2 + c_L^2 q^2}, \quad (5.64)$$

$$\hat{\epsilon}_{liquid} = 1 + \frac{\omega_p^2}{\omega_n^2 + c_K^2 q^2}, \quad (5.65)$$

with a single plasmon mode, with a plasmon gap  $\omega_p$  and having dispersion given either by the longitudinal ( $c_L$ ) or by the sound (compression) velocity ( $c_K$ ). Hence, deep in the solid or deep in the superconductor there is little new to be seen. However, when the competition is severe, a new feature appears in the longitudinal dielectric function which can be seen as the experimental signature of fluctuating order: the “electrical shear photon”.

Before we present a detailed analysis of the dielectric function, let us review the experimental significance. This is in first instance about EELS, but also soft X-ray inelastic scattering (RIXS). Let us focus on the EELS experiments and explain what do we expect to see in spectra of a nematic electron phase. The electron energy loss of a medium measured in a transmission EELS experiment is defined as

$$F_T(\omega, q) = \text{Im} \frac{1}{\hat{\epsilon}(i\omega - \delta, q)} \quad (5.66)$$

Recently, also experiments with low energy reflective EELS were performed where the loss function is given by

$$F_R(\omega, q) = \text{Im} \frac{1}{1 + \hat{\epsilon}(i\omega - \delta, q)}. \quad (5.67)$$

The difference between the two spectra, based on Eq. (5.63), results in an effective reduction of the plasmon frequency by factor of  $\sqrt{2}$ . In fact, the factor unity in Eq. (5.63) comes from the assumption that the background medium is featureless, having the dielectric function of the vacuum  $\hat{\epsilon} = 1$  which is not the case in cuprates. The oxygen atoms can polarize to such an extent to allow the dielectric functions  $\hat{\epsilon}_{eff}$  to be considerably larger than 1. The effective plasmon frequency with such a background is then renormalized to  $\omega_p = \sqrt{\frac{n_e(e^*)^2}{\rho\hat{\epsilon}_{eff}}}$ . The EELS formula Eq. (5.67) has the effect of only changing the effective permeability by one  $\hat{\epsilon}_{eff} \rightarrow 1 + \hat{\epsilon}_{eff}$  resulting in a small change of the measured plasmon gap.

Given the fact that we wish to obtain quantitative predictions to guide experimentalists, we have to estimate values for gaps and velocities specific to cuprates. These were already considered earlier so we continue to use these with one exception: In order to have a good illustration of the effect of the discrepancy between the shear and plasmon gap, their ratio is not fixed to 6/100, as it was the case in the previous part of this section, but we introduce instead a new parameter  $\xi = \Omega/\omega_p$  to analyse matters for arbitrary values of  $\xi$ . In the various plots we typically take  $\xi = 1/10$  as a representative example where the gaps are differing precisely one order of magnitude. In absolute numbers, the plasmon gap is kept at its approximate measured value of  $\omega_p = 1eV$ , while the shear Higgs gap is set to  $\Omega = 100meV$ . Since the shear penetration depth has to be large, this ratio cannot exceed unity. At the same time the glide velocity  $c_g$  is given in terms of the phonon velocity  $c_T$  significantly reducing the number of free parameters.

In Fig. 5.4 we represent two physically relevant cases of EELS spectra: a)  $\Omega = 0$ : no shear gap is present (the shear screening length is infinite). The system is in the ideal Wigner crystal phase showing one strong pole that is just the longitudinal phonon having acquired a plasmon gap; b)  $\Omega \ll \omega_p$ : the dual Higgs gap is present, meaning that this spectrum corresponds to the nematic phase. However, the dual mass has to be small compared to the plasmon gap in order for the theory to be applicable. The ‘electric’ shear photon is visible in the EELS spectrum, but its strength is much weaker than that of the robust plasmon pole. In order to assess their relative strengths, let us take the dielectric function Eq. (5.63) to analyse it in detail.

At this point we decided to introduce absolute dimensions in the problem, to express every physical length/frequency/etc. in their respective units. This is done purely for the purpose of illustrating the quantitative behavior of the EELS poles. As it turns out, the entire effect depends only on the gap ratio  $\xi$  and the Poisson ratio  $\nu$ , which we, at the end of the work, set to 1/10 and 0.28 respectively. The unit length we use is the electric screening length  $\lambda_c$ , so that the momentum is given by the dimensionless number  $k = q/q_c = \lambda_c q$ . With regard to the frequencies, the unit frequency is given by the plasmon gap so that we express the Matsubara frequencies by  $\varpi = \omega_n/\omega_p$ , while in these units the shear Higgs gap is just  $\xi$ . This choice of units implies that the longitudinal velocity becomes the unit velocity. Let us now use these units to rewrite the dielectric function Eq. (5.63)

$$\hat{\epsilon}(\varpi, k) = 1 + \frac{\varpi^2 + \frac{1-\nu}{4}k^2 + \xi^2}{(\varpi^2 + \frac{1-\nu}{4}k^2)(\varpi^2 + k^2) + \xi^2(\varpi^2 + \frac{1+\nu}{2}k^2)}. \quad (5.68)$$

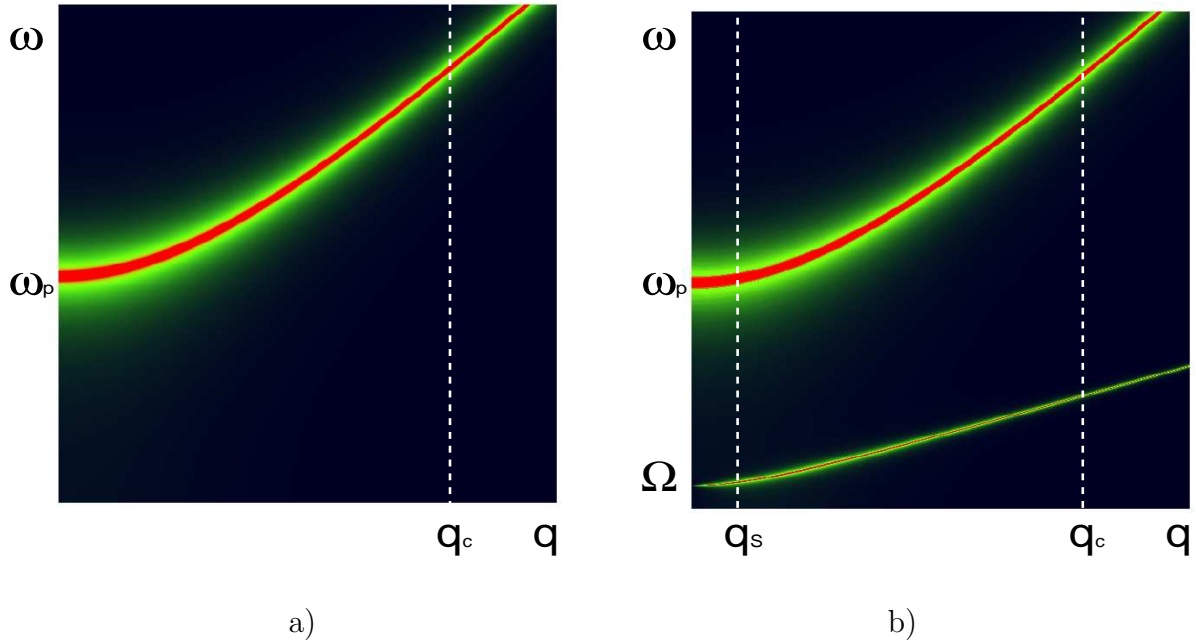


Figure 5.4: Electron energy loss spectroscopy (physically relevant gap values): the spectrum is found from the inverse dielectric function as  $\text{Im}(1/\varepsilon)$ : a) ideal Wigner crystal ( $\Omega = 0$ ), b) dominant plasmon gap ( $\omega_p \gg \Omega$ ). The ‘plasmon’ dispersion is barely changed and only few percent of its strength moved to the ‘electric shear photon’.

The dispersion of the two poles of the function Eq. (5.66) using the dielectric function Eq. (5.68) is given by

$$\varpi^2 = \frac{1 + \xi^2}{2} + k^2 \frac{5 - \nu}{8} \pm \sqrt{\left(\frac{1 - \xi^2}{2}\right)^2 + k^2 \frac{3 + \nu + \xi^2(1 - 5\nu)}{8} + k^4 \left(\frac{3 + \nu}{8}\right)^2}. \quad (5.69)$$

In the long-wavelength limit, the plasmon and the shear photons are both massive with dispersions, respectively,

$$\varpi_1 = 1 + \frac{k^2}{4} \left( (1 + \nu) + \frac{1 - \nu}{1 - \xi^2} \right) + O(k^4), \quad (5.70)$$

$$\varpi_2 = \xi + k^2 \frac{1 - \nu}{8} \frac{1 - 3\xi^2}{1 - \xi^2} + O(k^4). \quad (5.71)$$

As announced in the paragraph on polaritons, the dielectric function of the isotropic nematic Eq. (5.63) and its poles Eq. (5.71) demonstrate that the charged nematic isotropic phase is an incompressible phase of matter. Due to the hierarchy of the velocities, the modes do not cross and are therefore at short distances significantly smaller than any of the screening lengths. The model predicts two poles to behave as the crystalline longitudinal

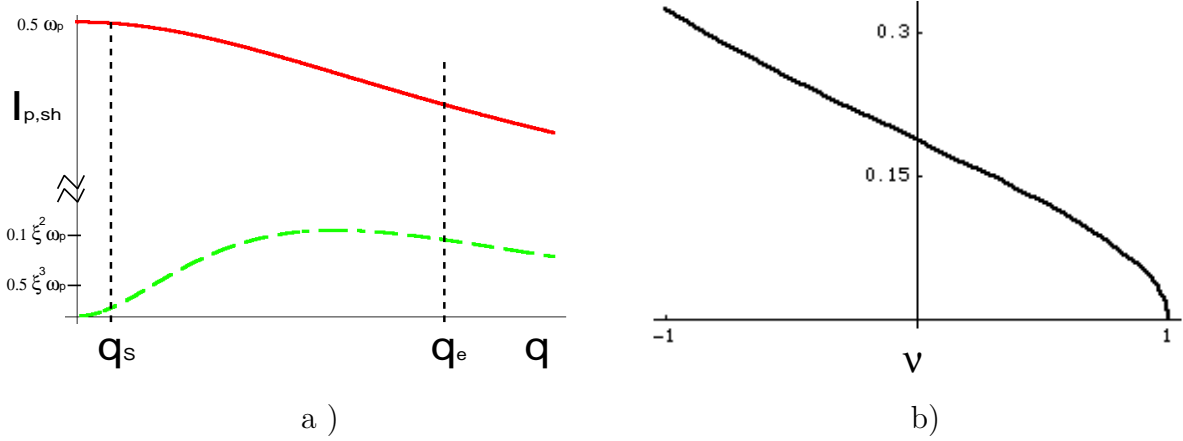


Figure 5.5: Pole strength of the ‘electric shear photon’: a) the strength of the plasmon pole (solid) is many orders of magnitude larger than that of the ‘electric shear photon (dashed). There are two wavelength regimes with a different behaviour: at intermediate wavelengths ( $q_S < q < q_e$ ) the pole develops the maximum strength (relative to the plasmon strength) of order of a tenth of  $\xi^2$ , i.e. 0.3% for the gap estimates in the text; in the potentially experimentally accessible long-wavelength regime ( $q < q_S$ ), the strength grows with square of the wavelength and reaches values of order of  $\xi^3$  or 0.1%. b) The prefactor in Eq. (5.73) as a function of the Poisson ratio  $\nu$ . At high Poisson ration ( $\nu \lesssim 1$ ), the strength is vanishing because the unmelted solid has a very weak shear rigidity in the first place. The ‘electric shear photon’ strength is naturally the most prominent when the entire crystalline rigidity rests on the shear (physically unlikely case  $\nu = -1$ ).

phonon  $\omega_1 = c_L q + O(1)$  and decoupled condensate of gliding dislocations  $\omega_2 = c_g q + O(1)$ . Naturally, due to the vanishing coupling, the shear pole becomes practically invisible.

We denote the strengths of the poles respectively as

$$A_{1,2}(q) = \lim_{\omega \rightarrow \omega_{1,2}(q)} [(\omega - \omega_{1,2}(q))F(\omega, q)] \quad (5.72)$$

and plot them in Fig. 5.5a. We do not show the lengthy expressions, to analyse Eq. (5.72) only in physically relevant cases. Already from looking at the figure, we can deduce that the plasmon mode is very robust to the presence of any charge and its strength does not change significantly from the ‘uncharged’ case where  $A_1 \propto 1/\sqrt{1+k^2}$ . The shear photon’s strength is many orders of magnitude smaller and it vanishes both in the short- and long-wavelength limit, with a maximum at intermediate distances.

At first instance, we may look for this minimum by expanding Eqs. (5.72) in  $\xi$ , knowing that this parameter is not larger than 0.1. The series up to a second order in  $\xi$  reproduce well short- and medium-wavelength regimes where the intensity maximum is located. We find its approximate position  $q_0 \approx q_c 2/\sqrt{3(3+\nu)}$  and the intensity

$$A_2(q_0) = \omega_p \left[ \frac{3\sqrt{3-3\nu}}{16\sqrt{3+\nu}} \xi^2 + O(\xi^4) \right]. \quad (5.73)$$

The prefactor in Eq. (5.73) is plotted in Fig. 5.5b as a function of the Poisson ratio  $\nu$ . It is clear that regardless the value of the Poisson ratio, the intensity maximum  $A_2$  cannot exceed a fraction of  $\xi^2$ . Having the strength of the plasmon pole close to  $\omega_p/2$ , the ratio of two pole strengths is limited to few parts per thousand relying on ‘optimistic’ estimate for the shear gap of 100meV.

From the estimate on the momentum where the shear photon has the maximum intensity, we do run into the problem of applicability of the model. With  $q_0$  being of the order of  $q_c$  and therefore microscopic, the reliability of the result Eq. (5.73) is questionable. In addition, existing EELS experiments can reach up to momenta which are much lower than the inverse microscopic lattice constant, i.e. the inverse electric screening depth  $q_c$ . Thus, in order to make reliable predictions, we need to analyse the strength  $A_2$  in the long-wavelength limit where the small  $\xi$  approximation is no longer valid. This is a consequence of another small number in the problem: at wavenumbers of order or shorter than the inverse shear screening length, the dimensionless momentum  $k$  is smaller than the gap ratio  $\xi$ , so that one has to expand first to small momenta. The series yield the long-wavelength pole strength

$$A_2(k) = \frac{\xi(1-\nu)}{4(1-\xi^2)^2}k^2 + O(k^4) \quad (5.74)$$

and at first sight it seems that instead of a square dependence of the strength in small  $\xi$  it is replaced by a linear one. Unfortunately, this is not true since the expansion Eq. (5.74) works only if  $k \lesssim \xi$  and the strength picks up therefore two additional powers of  $\xi$ . As a result, the total strength of the shear pole in the experimentally accessible and physically relevant regime of wavelengths longer than the shear penetration depth, acquires a weight that cannot exceed  $\lesssim \xi^3$ . The earlier estimate  $\xi = 1/10$  results in an expected strength ratio of some parts per thousand which we expect to be measurable in a dedicated experiments where the region with  $q \lesssim q_g \sim 0.1\text{\AA}^{-1}$  and  $\omega \lesssim \Omega \sim 100\text{meV}$  is investigated with high resolution EELS.

The message from this section and especially from the last paragraph should be clear: the ‘fluctuating order’ in the electronic liquid, as suggested in preceding works and as constructed here in terms of the dual elasticity theory, leaves its specific fingerprints on the EM response functions of the system. Although these require specific nonconventional experiments, which have to be pushed to their limits, once the measurements reach the desired kinematical regimes, the fluctuating order will reveal itself in terms of a unique experimental signal.

## 5.4 Charged ordered nematic

Having learned about the effects of the screened shear and the dynamical dislocation condensates in the isotropic nematic, the electric response functions of the *ordered* nematic phase of matter do not bring any real surprises. The effects seen in the charged isotropic phase are present here too, except that they are now modulated by the anisotropy. The

bottomline is that the ordered nematic phase screens only one of the two shear photons, and only in the appropriate ‘flavor’ direction, the system behaves as a liquid, while in the perpendicular direction it resembles a solid. In the neutral case, this naive perception has been demonstrated to be only of relevance to the static limit, whereas at any finite frequency a dynamical admixing of modes is found, associated with the spin-2 transformational properties of the screened shear mode. Such a behaviour is not an exception in charged system. We find that the order nematic behaves as a liquid in one and solid in the perpendicular direction only in the static limit. The dynamical response functions are found to transform, similarly as in the neutral system, according to spin-2 representation of the rotation group.

In this section, the anisotropic dual stress gauge field propagator (expressed in terms of the self-energy Eq. (4.90)) is used together with the effective Meissner term Eq. (5.37) to recover the EM response functions. Given that the dual stress gauge field propagator is quite complicated at arbitrary angles  $\eta$ , so is the Meissner term, containing also off-diagonal terms that couple the electric and magnetic properties. In order to avoid these uninteresting and lengthy technicalities, the EM properties are analysed, as for the electrically neutral case, for three specific angles  $\eta = 0, \pi/4, \pi/2$  where the sectors are decoupled. In order to demonstrate the significance of the anisotropy, and especially its effect on the electric-magnetic coupling, we address what happens at intermediate angles  $\eta$  using the EELS spectrum as a representative response function. However, we do this only in the long-wavelength limit which is relevant for the experiments. We find, next to the ‘electric shear photon’, an even weaker excitation, the light polariton, leaving its dynamical fingerprints in the EELS spectrum due to the coupling between electric and magnetic sectors.

Let us begin with the static properties of the ordered nematic phase. An advantage is that the coupling between the longitudinal and the transversal sector vanishes in the static limit, so the static Meissner term decouples into distinct magnetic and electric parts. In fact, the consequences of the static limit are much stronger. Consider the dual stress gauge field self-energy Eq. (4.90) and take the limit  $\omega_n \rightarrow 0$ . There is only a single term surviving, namely

$$-\Pi_H(\omega_n \rightarrow 0) = \frac{\Omega^2}{\mu} |B_{+1}^T|^2 \sin^2 \eta, \quad (5.75)$$

which restates the fact that, in the static limit, the dislocations have only one relevant ‘flavour’: the transversal one. The consequences for superconductivity are devastating as it appears that the ordered nematic phase has no ability to expel static magnetic fields. We will return to this issue after the effect of the ordered nematic on the electric screening is investigated. The static Meissner term following from the self-energy Eq. (5.75) acts only on the Coulomb photon and the total propagator for the EM Coulomb photon is identical to the propagator Eq. (5.51) found in the isotropic nematic phase with the anisotropy in the screening length given by

$$\lambda_g \rightarrow \frac{\lambda_g}{\sqrt{2} \sin \eta}. \quad (5.76)$$

Because the dislocation sound velocity  $c_d$  is the same in all directions, from the length anisotropy Eq. (5.76) it follows that the *static* shear Higgs gap has spin-1 anisotropy defined as  $\Omega(\eta) = \Omega \sin \eta / \sqrt{2}$  and it acts only in the electric (Coulomb) sector. The anisotropy of the gap could be conversely seen as that the isotropic nematic averages its Higgs gap to value  $\Omega$ . There is no need to analyse the behaviour of the electric field profile again, since the minimum shear penetration realized in the vicinity of angle  $\eta = \pi/2$  belongs to the ‘near-solid’ regime. Hence, the static Coulomb screening of the ordered nematic corresponds to a crystal screening in one direction and a ‘near-solid’ screening, presented in the previous section, in another direction. The overscreening of the electric field and the attractive Coulomb potential are exhibited in all directions, except that the effect is the strongest in directions almost perpendicular to the Burgers director and vanishes parallel to it.

There is however one exception to the behaviour presented in the previous paragraph. One might have noticed that the dual stress gauge field  $B_{+1}^T$  in the self-energy term Eq. (4.90) cannot develop the mass in the case of  $\eta = \pi/2$ , which is in contrast to the limit found in Eq. (5.75). This inconsistency follows from the fact that the Higgs term Eq. (4.90) is not uniformly convergent at the ( $\eta = \pi/2, \omega_n = 0$ ) point. Therefore, the static limit self-energy Eq. (5.75) is correct for all values of  $\eta$ , except  $\eta = \pi/2$ , representing the propagation exactly perpendicular to the Burgers director. In the opposite order of limits, by first taking  $\eta \rightarrow \pi/2$ , the dual Higgs self-energy Eq. (4.90) turns into a non-dynamical dual stress Meissner term, which implies a non-vanishing Meissner term for the EM photon  $A_T$ :

$$-\Pi_H = \frac{\Omega^2}{\mu} |B_{-1}^T|^2 \Rightarrow -\Pi_T = \omega_p^2 \frac{\omega_n^2 + \Omega^2}{\omega_n^2 + c_T^2 q^2 + \Omega^2}. \quad (5.77)$$

This implies that the superconductivity is recovered, of course only in this specific direction, while the Coulomb screening corresponds to that of the ideal crystal: there is a sharp discontinuity in the angular dependence of the EM response functions at this  $\eta$  value.

This extremely anisotropic superconductivity found in the ordered nematic phase does not correspond to the anisotropic superconductivity observed in YBCO [43], since it corresponds with the presence of the EM Meissner term only in a single direction. On the other hand, the isotropic phase has perfectly isotropic EM response, so one would like to see the phase with the EM properties that are somewhere in between in order to relate the theory to the superconductivity of cuprates. The solution to this problem can be found when one introduces the partially ordered nematic phase with the Burgers director order parameter given by

$$\hat{Q} = \begin{pmatrix} \cos 2\eta & \sin 2\eta \\ \sin 2\eta & -\cos 2\eta \end{pmatrix} = \frac{1+\epsilon}{2} (\cos \eta, \sin \eta)^{\otimes 2} + \frac{1-\epsilon}{2} (-\sin \eta, \cos \eta)^{\otimes 2}, \quad (5.78)$$

corresponding to a ground state that has an anisotropic dislocation condensate density. Two limiting cases of the Burgers director Eq. (5.78) are ordered- ( $\epsilon = 1$ ) and isotropic ( $\epsilon = 0$ ) nematic phase. The full calculation for that phase is not presented because it

would involve another chapter. However, the static case can easily be reproduced and here we just list the implications for the EM response functions. The magnetic and electric sectors are decoupled as expected due to the vanishing coupling in the static limit. The electric screening can again be expressed through an anisotropic screening length that varies between two directions as

$$\lambda_g^2 \rightarrow \frac{\lambda_g^2}{(1 - \epsilon) + 2\epsilon \sin^2 \eta}. \quad (5.79)$$

The properties of the isotropic and ordered nematic phases are easily recovered. Given that we already assumed the static limit when the screening length Eq. (5.79) was found, the nonuniform convergence of the Meissner term in the ordered nematic phase at  $\eta = \pi/2$  point is not apparent. Otherwise, the anisotropic gap Eq. (5.79) may be used for all  $\eta$  values. Although just a speculation at this moment, the anisotropy in the Coulomb force, caused by the anisotropic screening Eq. (5.79), might lead to the anisotropy in formation of Cooper pairs if one supposes that an electron liquid coexists with another charged nematic phase.

The effect of partial Burgers order is also relevant for the static screening of the magnetic field. The static Meissner term of the partially ordered nematic phase is equivalent to the corresponding term of the isotropic nematic Eq. (5.48) with the anisotropic shear screening length given by

$$\lambda_s \rightarrow \lambda_s \sqrt{\frac{\cos^2 \eta}{1 - \epsilon} + \frac{\sin^2 \eta}{1 + \epsilon}}. \quad (5.80)$$

The anisotropy effects diminish in the isotropic limit ( $\epsilon \rightarrow 0$ ) and become most prominent in the ordered limit ( $\epsilon \rightarrow 1$ ) when the first term in the parentheses of Eq. (5.80) diverges, meaning that the magnetic field cannot penetrate the phase. However, the nonuniform convergence is now manifest and one can convince oneself that the reversed order of limits (first  $\eta \rightarrow \pi/2$ , then  $\epsilon \rightarrow 1$ ) does yield a finite Meissner term.

This is surely relevant for the experimentally observed anisotropic superconductivity in cuprates [43]. In addition, the anisotropic screening length Eq. (5.80) may also give rise to the oscillatory screening of the magnetic field, predicted already for the isotropic nematic. There, however, the necessity of the first order transition to the isotropic superconductor led to the fact that the shear penetration depth  $\lambda_s$  could not overwhelm the bare London penetration depth  $\lambda_L$  which is known to be of order of thousands Ångströms. In the case of the partially ordered nematic state, one can circumvent this fact by a highly anisotropic, yet not completely ordered nematic state. The effective anisotropic shear screening lengths are given, parallel and perpendicular to the dominant Burgers direction by  $\lambda_{\parallel, \perp} = \lambda_s / \sqrt{1 \mp \epsilon}$ , and the proximity of  $\epsilon$  to the unity can result in one of these two lengths being larger than the bare London length. In that case, the magnetic field would be screened in the standard BCS-like exponential fashion in one direction, while in the other it would develop the oscillating screening pattern. This idea needs more thoughts since we do not know if this ‘almost ordered’ nematic state can be realized, either from the ideal Wigner crystal

in the first order phase transition or as the intermediate state in the ordered to isotropic nematic transition, whose order is unknown to us.

Having completed the analysis of the static properties, let us now turn to the dynamical EM response of the ordered nematic phase in the three particular ‘decoupled’ directions. The case of the perpendicular propagation  $\eta = \pi/2$  has been discussed before with the Meissner term given by self-energy Eq. (5.77). Since the longitudinal sector does not acquire any Higgs mass, the electric response functions (including the longitudinal dielectric function Eq. (5.18)) is the same as in the ideal crystal. The same is then true for the longitudinal conductivity which is equal to that of the ideal crystal (ideal conductor without pinning). The observable that is affected by the Meissner term Eq. (5.77) is the transversal optical conductivity

$$\hat{\sigma}_T = \frac{\omega_p^2}{\omega_n} \frac{\omega_n^2 + \Omega^2}{\omega_n^2 + c_T^2 q^2 + \Omega^2}. \quad (5.81)$$

Its pole at  $\omega_n = 0$  is the fingerprint of superconductivity with a strength that falls off in the same manner as in Eq. (5.62) except that the shear penetration depth acquires a factor of  $\sqrt{2}$ . The interpretation of this strength reduction is the same as it was in the isotropic case: at distances comparable to the shear penetration depth the medium recovers its solid nature and the superconducting pole weakens in favor of the ‘transversal plasmon’ mode with a dispersion given by  $\omega_n = \sqrt{\Omega^2 + c_T^2 q^2}$ . The polariton equation shows only two poles, as in the ideal crystal, with the difference that the massless diffusion mode acquired the shear Higgs gap. There are no massless modes in this direction and accordingly the medium behaves as a perfect mirror.

Considering a next representative propagation angle  $\eta = 0$  similar dynamical behaviors are found as in the perpendicular case  $\eta = \pi/2$ , since in both cases it is the ‘magnetic shear’ photon that is subjected to the Higgs mechanism. However, in the neutral case of chapter 4 it was clear that the constraints work differently in two cases, as well as that an additional degree of freedom enters: the condensate longitudinal photon  $B_L^\parallel \equiv B_L^L$ . Therefore, the effective Meissner term will be active only in the magnetic sector (EM transversal photon  $A_T$ ), but the prefactor will be different

$$\mathcal{L}_{Meiss.}(\eta = 0) = \frac{1}{2} \omega_p^2 \frac{\omega_n^2 (\omega_n^2 + c_d^2 q^2 + \Omega^2)}{(\omega_n^2 + c_T^2 q^2)(\omega_n^2 + c_d^2 q^2) + \omega_n^2 \Omega^2} |B_{-1}^T|^2, \quad (5.82)$$

having a vanishing value in the static limit. Hence, the medium is not superconducting in this direction. The lack of superconductivity is also apparent in the transversal conductivity which reads

$$\hat{\sigma}_T(\omega_n, q) = \omega_p^2 \frac{\omega_n (\omega_n^2 + c_d^2 q^2 + \Omega^2)}{(\omega_n^2 + c_T^2 q^2)(\omega_n^2 + c_d^2 q^2) + \omega_n^2 \Omega^2}, \quad (5.83)$$

with the  $\omega_n = 0$  pole missing.

The last representative case is  $\eta = \pi/4$ , and this does not require any special treatment. Propagating at this angle, the ‘electric shear photon’ is completely screened, while

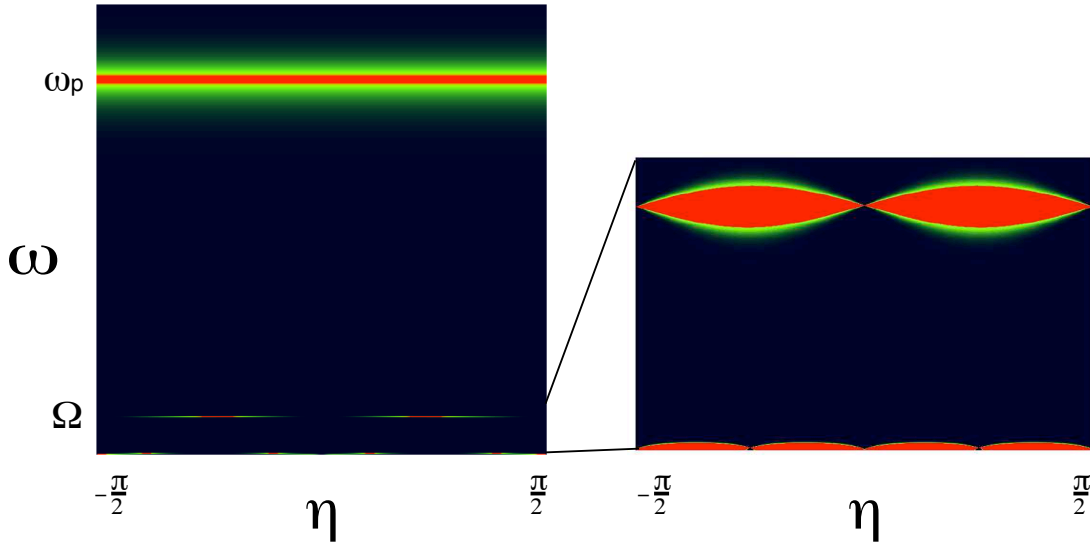


Figure 5.6: A predicted outcome of an EELS experiment (long but finite wavelength) on the ordered nematic: a) degenerate plasmon doublet has the dominant signal. The ‘electric shear photon’ is a faint feature, being the strongest at  $\eta = \pm\pi/4$  and vanishing perpendicular and parallel to the Burgers director. The weak diffusive polariton is visible at the bottom. b) when the low-energy region is zoomed in, the angular dependence of the pole strengths becomes manifest.

the transversal sector is unaffected. Similar as in the neutral nematic medium, the longitudinal sector for this direction is equivalent to the one of the isotropic nematic phase. Hence, at this specific angle the analysis of the EELS spectrum from the previous section applies. This means nothing else than that the ordered nematic phase should also leave its fingerprint in the EELS spectrum, except that the strength of the ‘electric shear photon’ will be anisotropic, given the fact that it is not present in the electron energy loss function at  $\eta = 0, \pi/2$ .

Beside the anisotropic ‘electric shear photon’, one should also expect that all dynamical excitations of the ordered nematic phase become visible as poles in the electron energy loss spectrum, given the fact that the longitudinal and transversal sector dynamically couple for general values of  $\eta$ . There are in total four such degrees of freedom: two phonon degrees of freedom, the condensate (longitudinal stress photon) degree of freedom and finally the EM transversal photon (light). In order to illustrate the angular dependence of the excitation poles in an EELS experiment, we plotted this spectral function in Fig. 5.6 for the case of the long but finite wavelength regime ( $q \approx q_e/100$ ) which should be experimentally accessible. In a charged medium both phonon degrees of freedom acquire a plasmon gap and a large pole strength. Because electron energy loss spectroscopy probes the longitudinal sector, it has only direct access to the gapped longitudinal (compressional) plasmon at the center of discussion in the previous section. The contribution from the transversal plasmon

exists only when the system is probed in some intermediate direction where the dynamical coupling between the two sectors switches on. Given that the longitudinal and transversal plasmon are degenerate in the long-wavelength limit, this contribution cannot be directly separated from the direct longitudinal plasmon signal in a real EELS experiment. These two plasmon poles represent the dominant signal in EELS spectrum, being many orders of magnitude stronger than the other poles. Next, there is a contribution from the ‘electric shear photon’ which was the most important feature of the isotropic phase with respect to experiment. This mode is fully visible, as discussed in the previous paragraph, at  $\eta = \pi/4$  and loses its strength as the angle deviates from that value. This is due to the fact that longitudinal plasmon couples to the ‘electric’ shear component, which has only a finite, angular dependent, overlap with the Higgs shear stress photon Eq. (4.81). Finally, there is the EM photon which turns into a polariton. From the long-wavelength limit of the dielectric function of the ordered nematic, we conclude that the dispersion of this polariton is still diffusive

$$\omega \approx c_T \lambda_L q^2 \sin 2\eta. \quad (5.84)$$

Thus, it seems as that light couples only to the softened transversal photon (plasmon) in the same way as it does in the ideal Wigner crystal. Because of the indirect coupling to the longitudinal plasmon (via the transversal plasmon), the strength of this polariton is the weakest in the EELS spectrum and it vanishes at the special ‘decoupling’ values of  $\eta$ . Unfortunately, there are fundamental experimental constraints prohibiting the detecting the polariton pole given by Eq. (5.84). In a spectrum measured in an EELS experiment, the main contribution to the signal comes from the elastic zero-momentum peak. Its strength overwhelms all other poles by many orders of magnitude. Although there are methods developed to subtract this signal, which is innate to the experiment and contains no information whatsoever about the probed system, the minute signal of the polariton will be overwhelmed by the noise of the elastic peak. In fact, given that the polariton has the weakest pole in the electron energy loss spectrum, and that earlier we argued that even the ‘electric shear photon’ is a faint feature, one easily concludes that the polariton would be hard to observe even if one could remove the contributions from the elastic peak.



# Chapter 6

## Conclusion

In this thesis a theory for electronic crystal melting has been presented, offering some quite surprising outcomes that one might expect to encounter in electron quantum liquid crystals characterised by fluctuating translational order. Of course, this was not possible without the use of the machinery of the duality where we relied on the notion that ‘order and disorder are relative matters’. This change in point of view can significantly simplify the theoretical description of the problem and we use this fact when describing the melted phase in terms of the dual theory developed initially by Kleinert [48]. The dual theory of melting of a bosonic quantum crystal is developed in this way and new liquid crystalline phases are identified. A surprise that follows is that the dual theory, being tailored to treat the melted phase as the ordered phase, yields the bare Meissner term Eq. (5.34) for the charged quantum liquid. Hence, this dual point of view does us yet another favour: the superconductivity comes for free and the normal metallic phase is viewed as a the one where the dual order, represented by the bare Meissner term, is destroyed by the fluctuations of the long-ranged dual stress fields.

The phase that we are a particularly interested in is the quantum nematic phase, characterized by the proliferation and condensation of dislocations, while disclinations are still massive. This phase, having the character of a liquid crystalline phase due to the presence of a partial order, is in between the ideal crystal (fully crystalline ordered phase) and superfluid phase (fully disordered). Accordingly, its properties are a mix of those of both worlds, showing massive shear and long-ranged compression at large length scales while the crystalline rigidities are recovering at short distances. The surprise is that under these circumstances a new propagating mode appears: the dual shear photon characterized by a Higgs mass expressing that at long distances shear rigidity has disappeared, while it resurfaces at shorter distances. This photon actually reflects the phase degree of freedom of the dual dislocation Bose condensate.

When the medium is also electric charged the theory predicts that the nematic phase turns into a true superconductor, which is not so hard to understand being aware the workings of the dual shear superconductor. However, the electromagnetic response functions of such a superconductor are now full of surprises. In contrast with the standard BCS theory, where the superconductivity arises as a ramification of the long-range off-diagonal

order of the constituent ‘gaseous’ bosons (Cooper pairs), the mechanism responsible for the superconductivity in the nematic charged phases is entirely different. The superfluid is, by means of the dual theory, the ordered state. It is characterized exclusively by compressional rigidity and it has to be an electromagnetic superconductor as well because of the well-known Wen-Zee theorem [159, 160, 161]. The nematic state is characterized by crystalline order at short distance. Nevertheless this order is transient and as such it cannot destroy the electromagnetic Meissner term. Because the transient order is present only at finite length- and time scales, all of its consequences on the Meissner term are apparent in the various response functions only at finite wavelengths and frequencies.

In this way, our theory for the electronic liquid crystalline states yields predictions which can be tested experimentally, although they require unconventional experiments. In principle, this amounts to a strategy to determine once and for ever if the notions of fluctuating order do apply to e.g. high- $T_c$  superconductivity. The feature that we find most promising in this regard is the novel ‘electric shear photon’ pole in the electron energy loss function and at this moment some experimental groups have already undertaken first steps to devise experiments that can probe the finite-wavelength regime and detect the pole’s weak signal. Other response functions like the optical (transversal) conductivity also feature excitations which are not of the kind found in conventional BCS superconductors. However, the existing experimental techniques are even more limited than EELS with regard to probing the relevant kinematical regimes. The transient order characterizing charged quantum liquid crystals also leaves its imprint through the static overscreening effects of electric and magnetic fields. Unfortunately, existing experimental techniques are designed to measure only the standard BCS London length and it would be interesting to see if experiments can be designed to search for the overscreening effects.

It would be unfair to not give the full credit to the pioneering work of Zaanen, Mukhin and Nussinov [44], where these ideas were employed for the first time. The theory presented here, should be seen as a follow up, removed a flaw associated with the dynamical (relativistic) treatment of the dislocation condensate. Apart from encountering a problem associated with the topological phase and identification of a new isotropic phase, we also did investigate the entire spectrum of EM properties of a charged liquid crystal. Somewhat as a sideline, we obtained results eventually of relevance to the construction of the dual theory in general. We refer to the interpretational issues associated with the dual gauge degrees of freedom as presented in section 2.3 and the glide principle derived in section 3.4. The former result clarifies the appearance of the additional degrees of freedom in the nematic phases and reveals the hidden connection between the dual shear photons and the dislocation degrees of freedom. The latter is a necessity for the understanding of the protection of the compressional properties of the superfluid.

Given the new theoretical results presented in this thesis, it is now up to the experimentalists to develop new experimental techniques, to measure the signatures of fluctuating order. One can wonder if our theoretical program is now completed or if there are still loose ends that need further attention. In our opinion, there are still a number of unresolved problems. One which does not require additional computations is related to the interpretation of the excitation spectra in the nematic and charged media. We are partic-

ularly puzzled about the presence of the diffusive poles, as found in the ordered nematic (Eq. (4.93)), as well as in the polariton spectrum of both the ideal crystal (Eq. (5.15)) and the ordered nematic (Eq. (5.84)). Although we presented some arguments referring to the loss of rigidity and second-order processes that could cause this diffusion, we find those explanations unsatisfactory and we would like to understand better what is the precise physical interpretation of these diffusive excitations. The other problem is more serious as it is related to the inconsistency encountered in the construction of the topological nematic state when the dual condensate is treated in its full relativistic glory. In section 4.6, the ‘inconsistent’ results previously obtained in section 4.5 were interpreted using a different disordering field. At that point we had to satisfy ourselves with the fact that we could explain only the isotropic nematic phase which, although showing quite unconventional features, is only a non-interacting approximation (in the Burgers sector) to the topological nematic phase. If the argument is correct, it implies that one needs to take into account the interactions coming from the expansion of the action Eq. (4.117). There is an open issue regarding the method one should use to treat these interaction effects. Apparently, the completely different mode content of the topological- and isotropic phase suggests that a perturbational approach might not work, although in principle it is possible that the mode content changes if the theory is excluded the Gaussian approximation.

All other issues may be considered as extensions of the original theory. One further generalization of the theory is to consider a less symmetric elasticity tensor than the isotropic one, Eq. (3.15), that we used throughout the thesis. Another possible extension is associated with the treating of the second-order gradient elasticity (Eq. (3.19)). However, after the hard work of the dualization and construction of the disorder theory has been accomplished, these generalization turn into a complicated but straightforward. In fact, we have some preliminary results where second-order gradient elasticity is included. However, because the dualization formalism for second-order gradient theories (see Ref. [48]) would require yet another chapter additional chapter to present, we decided to omit it. Let us just mention unexpected outcome that the additional terms in the elastic energy do not affect the shear Higgs mechanism, so that the phonon self-energies corresponding to the propagators Eq. (4.110) and (4.112) are still valid.

A different matter is the addressing of the fundamental limitations we had to impose onto our theory, which requires some further deep thoughts. These include the nontrivial statistics of the crystal constituents, the dimensionality of the medium and the issue of non-topological (interstitial) as well as the non-Abelian topological defects (disclinations). Most of these problems are actually ‘holy grails’ of modern physics with deep fundamental implications. Despite the lacking of a general formalism required to treat fermionic- or even anyonic crystals, we might still be able to speculate that in a medium melted by fermionic/anyonic dislocations the loss of shear rigidity is inevitable, resulting in a similar long-wavelength description as for the bosonic case, although the shear photon might have a different meaning, being associated with a dynamical Fermi- or anyon dislocation gas. Although we could leave the dimensionality issue related to the construction of a second-quantized theory of strings, to string theorists, we suspect that the Abelian-Higgs duality might be employed the other way round. In this manner, the condensation of

strings might be understood in terms of a type-II superconducting transition in higher dimensions, which could shed some light on this fundamental problem. The disorder field for disclinations, which is highly nontrivial because of its non-Abelian nature, is in a way similar to the problem of treating fermionic dislocations. However, due to their particular geometrical Berry phases associated with disclinations, it appears that the mathematical idea of quantum double symmetry groups has a real potential to make substantial progress on this deep problem. On the other hand, it appears that the treatment of non-topological defects in the theory (vacancies and interstitials), is a task which is relatively easy to accomplish. One should bear in mind that an interstitial is not just a bound pair of a dislocation and an antidislocation. These defects have the meaning of the classical wave function  $\Psi_0^{cl}$  amplitude fluctuations in a field theoretical description and it appears that a proper theory may be constructed using the knowledge of type-I superconductivity.

To conclude, let us mention a number of other interesting questions related to the dual theory of elasticity. One is concerned with the critical regime near the phase transitions in analogy with the Abelian-Higgs duality critical regime discussed in the section 2.4. There is still a number of open questions. The critical exponents that were used in section 2.4 were found for the case of a fully relativistic theory [63, 91]. The elastic action Eq. (3.24) does not satisfy this symmetry requirement and this can change the universality class of the transition and, accordingly, the values of the critical exponents. There is also an issue regarding the order of the transition: our theory with the disorder action Eq. (4.32) implicitly assumes that the transition from the ideal crystal to the nematic phase is of second order which is necessary in order to find a critical regime. The transition from the classical crystal to the nematic liquid crystal state is, however, of the first order, and the same is true for the transition from a normal state to the isotropic EM superconductor. We believe that the definite answer to these questions follows from the theory when the interstitial degrees of freedom are taken into account. This opens up a possibility that a new phase could emerge between the ideal crystal and the nematic phase.

The last important feature of the quantum nematic pertains to the problem of gravity. When we introduced elasticity in the introduction of chapter 3, we mentioned that the curvature and torsion induced by the elastic deformations and the topological defects can alternatively be treated using the language of differential geometry. There is no torsion in our universe and in an earlier work [146] it was demonstrated that in 2+1D the universe can be seen as a nematic phase of a ‘world-crystal’ which has lost its torsion through the proliferation of dislocations. The 3+1D version of this problem could possibly result in an theory for emerging gravity. As a curiosity, the transformational properties of shear degrees of freedom and gravitons match, because they are both spin-2 objects. There are, however, five shear degrees of freedom in an ideal crystal compared to two gravitons. Hence, the phase transition from the ideal ‘world crystal’ to the nematic ‘world’ phase should generate a Higgs mass for compression- and the three shear photons. This leaves us with two other shear photons having the highest helicity which should stay massless: these can be gravitons.

# Appendix A

## Mapping of a nonlocal interaction to $\Psi^4$ term

In chapter 2, we presented a mapping of action for a gas of random walkers onto the GLW action Eq. (2.35). The proof yielded quadratic contributions to the action in the long-wavelength limit, and  $\Psi^4$  term was added ‘by hand’, corresponding to short-range interaction between the particles. Then we promised to return to that issue in this appendix where mapping of inter-particle interactions onto the  $\Psi^4$  term of action Eq. (2.35) is demonstrated. The exact proof presented here is, however, based on a different mapping [49] and cannot be directly utilized for the description of the dislocation tangle. This will become clear after the details are presented and we will discuss the differences in the conclusion of this appendix. There are nevertheless two reasons that we include the mapping in the form presented in this appendix. First, it illustrates the origin of the  $\Psi^4$  term in Eq. (2.35) in a setup that is only slightly different from ours. Another reason is that the mapping, as presented by Kiometzis *et al.* [75], takes only local (short-range) interactions into account. The mapping given in this appendix uses the same idea as in Ref. [75]. However, we manage to incorporate any kind of potential, local or nonlocal, between the particles, which then acquires a corresponding  $\Psi^4$ -like term in Eq. (2.35). To the best of our knowledge, such a mapping, although a simple generalization of Ref. [75], has not been presented elsewhere. For us, it is of importance to stress that this mapping of arbitrary particle interactions can be further generalized to the case with a multitude of different particles. In this manner, the interaction term in Eq. (4.120) can be linked to the interaction between dislocations of different Burgers charges.

For the readers convenience we begin by repeating the ‘non-interacting’ part of the mapping as given in Ref. [75]. The only difference here is that the mapping can be generalized to an arbitrary dimension with the minute change of a single factor in the partition function. While the first part starts with the GLW complex theory and ends with a gas of free particles, the second part of the mapping, which incorporates the interaction, is performed ‘backwards’. The interaction is added to the particle action, and, by means of a Hubbard-Stratanovich auxiliary field, ‘pulled’ through the mapping so that it appears as a  $\Psi^4$  term in the complex field theory. At the end of the appendix, a brief discussion

regarding the differences between this mapping and that from chapter 2 is given.

Let us begin with the Hamiltonian of a free complex field theory

$$\hat{H} = \frac{1}{2} \int d^d x (|\nabla\Psi|^2 + m^2|\Psi|^2). \quad (\text{A.1})$$

This derivation is done for continuum theories, for discussions about the lattice derivation we refer the reader to Refs. [60, 176, 177]. The correlation function defined by Hamiltonian Eq. (A.1) is explicitly given by

$$G(\mathbf{x}) = \int \frac{d^d \mathbf{q}}{(2\pi)^d} \frac{e^{i\mathbf{q}\cdot\mathbf{x}}}{\mathbf{q}^2 + m^2}. \quad (\text{A.2})$$

This is written in the Schwinger proper-time representation [178] as an integral over the proper time  $s$

$$\begin{aligned} G(\mathbf{x}) &= \int_0^\infty ds e^{-sm^2} \int \frac{d^d \mathbf{q}}{(2\pi)^d} e^{i\mathbf{q}\cdot\mathbf{x}} e^{-s\mathbf{q}^2} \\ &= \int_0^\infty ds e^{-sm^2} \Gamma_d s^{-d/2} e^{-\frac{1}{4}\mathbf{x}^2/s}, \end{aligned} \quad (\text{A.3})$$

where we used the identity

$$\frac{1}{a} = \int_0^\infty ds e^{-sa}. \quad (\text{A.4})$$

The factor  $\Gamma_d$  is a constant which depends only on the number of dimensions  $d$  in the problem, and it follows after the momentum  $\mathbf{q}$  has been integrated out. For example,  $\Gamma_2 = 1/(4\pi)$  and  $\Gamma_3 = 1/(8\pi^{3/2})$ .

The right-hand side of Eq. (A.3) describes diffusion of a particle of mass  $1/2$ , i.e. it represents a sum over all real space paths starting at  $\mathbf{x}(s'=0) = 0$  and ending at  $\mathbf{x}(s'=s) = \mathbf{x}$  [179]

$$\Gamma_d s^{-d/2} e^{-\frac{1}{4}\mathbf{x}^2/s} = \int_{\mathbf{x}(s'=0)=0}^{\mathbf{x}(s'=s)=\mathbf{x}} \mathcal{D}\mathbf{x}(s') e^{-S[\mathbf{x}(s'), \dot{\mathbf{x}}(s')]}, \quad (\text{A.5})$$

with ‘free’ action

$$S[\mathbf{x}, \dot{\mathbf{x}}] = \frac{1}{4} \int_0^s ds' (\dot{\mathbf{x}}(s'))^2. \quad (\text{A.6})$$

The additional Boltzmann factor  $\exp(-sm^2)$  exponentially suppresses loops with large proper-time.

Having identified the Green’s function Eq. (A.2) with the diffusion problem Eq. (A.5), we may proceed to the partition function corresponding to Hamiltonian Eq. (A.1). Let us first integrate identity Eq. (A.4) to obtain

$$\ln a = - \int_0^\infty \frac{ds}{s} e^{-sa} + \text{const}. \quad (\text{A.7})$$

Denoting the integral over all momenta  $\mathbf{q}$  by a trace, we can write

$$\begin{aligned} \text{Tr} \ln(-\nabla^2 + m^2) &= - \int_0^\infty \frac{ds}{s} e^{-sm^2} \int \frac{d^d \mathbf{q}}{(2\pi)^d} e^{-s\mathbf{q}^2} \\ &= - \int_0^\infty \frac{ds}{s} e^{-sm^2} \oint \mathcal{D}\mathbf{x}(s') e^{-S}. \end{aligned} \quad (\text{A.8})$$

The closed path integral  $\oint \mathcal{D}\mathbf{x}$  runs over all closed loops. The ‘action’ is the same as in Eq. (A.6).

Using the famous identity

$$\text{Tr} \ln \hat{A} = \ln \det \hat{A}, \quad (\text{A.9})$$

where  $\hat{A}$  is an arbitrary matrix, one can write

$$[\det(-\nabla^2 + m^2)]^{-1} = e^{-W_0}, \quad (\text{A.10})$$

where we denoted the left-hand side of Eq. (A.8) by  $W_0$ . The exponential on the right-hand side of Eq. (A.10) can be expanded in a series as

$$e^{-W_0} = \sum_{N=0}^{\infty} \frac{1}{N!} \prod_{l=1}^N \left[ \int_0^\infty \frac{ds_l}{s_l} e^{-ms_l^2} \oint \mathcal{D}\mathbf{x}(s'_l) \right] \exp \left[ -\frac{1}{4} \sum_{l=1}^N \int_0^{s_l} ds'_l (\dot{\mathbf{x}}(s'_l))^2 \right]. \quad (\text{A.11})$$

This is precisely the partition function of a grand canonical ensemble of closed fluctuating loops that do not interact. On the other hand, the left-hand side of Eq. (A.10) can be viewed as an inverse functional determinant, which is the partition function of the free complex theory given by Hamiltonian Eq. (A.1). Hence, the identification of a gas of free loops with a free complex field theory.

Now we wish to add interactions to the problem. At this point we start to diverge from the course of exposition given in Ref. [75]. We begin with the grand canonical partition function Eq. (A.11) and add interaction terms so that it reads

$$\begin{aligned} Z &= \sum_{N=0}^{\infty} \frac{1}{N!} \prod_{l=1}^N \left[ \int_0^\infty \frac{ds_l}{s_l} e^{-m^2 s_l} \oint \mathcal{D}\mathbf{x}(s'_l) \right] \times \\ &\exp \left\{ -\frac{1}{4} \sum_{l=1}^N \int_0^{s_l} ds'_l [\dot{\mathbf{x}}(s'_l)]^2 - \sum_{l,k=1}^N \int_0^{s_l} ds'_l \int_0^{s'_k} ds'_k \frac{1}{2} V[\mathbf{x}(s'_l) - \mathbf{x}(s'_k)] \right\}. \end{aligned} \quad (\text{A.12})$$

The potential  $V(\mathbf{x}_2 - \mathbf{x}_1)$  may be arbitrary in contrast with the Ref. [75], where only the short-range potential  $V(\mathbf{x}) = \lambda \delta^{(d)}(\mathbf{x})$  is considered.

The interaction term in Eq. (A.12) poses a problem to the mapping we have just presented. However, it may be circumvented through the introduction of an auxiliary Hubbard-Stratanovich field. Let us first introduce Fourier transformed components of the interaction potential  $V$  by

$$V(\mathbf{x}) = \int \frac{d^d \mathbf{q}}{(2\pi)^d} \tilde{V}(\mathbf{q}) e^{-i\mathbf{q}\cdot\mathbf{x}}. \quad (\text{A.13})$$

The last term in the exponential in Eq. (A.12) becomes

$$\sum_{l,k=1}^N \int_0^{s_l} ds'_l \int_0^{s_k} ds'_k \int \frac{d^d \mathbf{q}}{(2\pi)^d} \frac{1}{2} \tilde{V}(\mathbf{q}) e^{-i\mathbf{q} \cdot [\mathbf{x}(s'_l) - \mathbf{x}(s'_k)]}. \quad (\text{A.14})$$

Now, the auxiliary field  $\sigma_{\mathbf{q}}$  is brought into the action via the identity

$$\begin{aligned} & \int \mathcal{D}\sigma_{\mathbf{q}} \exp \left[ - \int \frac{d^d \mathbf{q}}{(2\pi)^d} \sigma_{-\mathbf{q}} \frac{1}{2\tilde{V}(\mathbf{q})} \sigma_{\mathbf{q}} + i \int \frac{d^d \mathbf{q}}{(2\pi)^d} \int_0^s ds' \sigma_{-\mathbf{q}} e^{i\mathbf{q} \cdot \mathbf{x}(s')} \right] = \\ & \prod_{\mathbf{q}} \sqrt{2\pi \tilde{V}(\mathbf{q})} \times \exp \left[ -\frac{1}{2} \int \frac{d\mathbf{q}}{(2\pi)^3} \int_0^s ds' \int_0^s ds'' \tilde{V}(\mathbf{q}) e^{i\mathbf{q} \cdot [\mathbf{x}(s') - \mathbf{x}(s'')] } \right]. \end{aligned} \quad (\text{A.15})$$

The normalization constant (Jacobian of the HS transformation) comes from the Gaussian integrations and it will be cancelled at the end of the procedure.

The partition function Eq. (A.12) is rewritten, with help of Eq. (A.15), as

$$\begin{aligned} Z &= \prod_{\mathbf{q}} \frac{1}{\sqrt{2\pi \tilde{V}(\mathbf{q})}} \int \mathcal{D}\sigma_{\mathbf{q}} \exp \left[ - \int \frac{d^d \mathbf{q}}{(2\pi)^d} \sigma_{-\mathbf{q}} \frac{1}{2\tilde{V}(\mathbf{q})} \sigma_{\mathbf{q}} \right] \times \\ & \sum_{N=0}^{\infty} \frac{1}{N!} \prod_{l=1}^N \left[ \int_0^{\infty} \frac{ds_l}{s_l} e^{-m^2 s_l} \oint \mathcal{D}\mathbf{x}(s'_l) \right] \exp \left\{ - \sum_{l=1}^N \int_0^{s_l} ds'_l \left[ \frac{1}{4} [\dot{\mathbf{x}}(s'_l)]^2 - i\sigma[\mathbf{x}(s'_l)] \right] \right\}, \end{aligned} \quad (\text{A.16})$$

where  $\sigma[\mathbf{x}]$  represents the auxiliary field in real-space coordinates. After this step we resort to the relation between the inverse functional determinant and the loop gas partition function Eq. (A.10) and Eq. (A.11). The only difference with respect to the non-interacting case is that now we have an additional auxiliary field which enters the complex field action

$$\begin{aligned} Z &= \prod_{\mathbf{q}} \frac{1}{\sqrt{2\pi \tilde{V}(\mathbf{q})}} \int \mathcal{D}\sigma_{\mathbf{q}} [\det(-\nabla^2 + m^2 - i\sigma)]^{-1} \times \\ & \exp \left[ - \int \frac{d^d \mathbf{q}}{(2\pi)^d} \frac{\sigma_{-\mathbf{q}} \sigma_{\mathbf{q}}}{2\tilde{V}(\mathbf{q})} \right]. \end{aligned} \quad (\text{A.17})$$

The auxiliary field served the purpose of ‘smuggling’ the potential  $V$  through the mapping and now it can be integrated out. Together with the undesired Jacobian, this produces the  $\Psi^4$  term in the following way

$$\begin{aligned} & \prod_{\mathbf{q}} \frac{1}{\sqrt{2\pi \tilde{V}(\mathbf{q})}} \int \mathcal{D}\sigma_{\mathbf{q}} \exp \left[ - \int \frac{d\mathbf{q}}{(2\pi)^d} \frac{\sigma_{-\mathbf{q}} \sigma_{\mathbf{q}}}{2\tilde{V}(\mathbf{q})} + i \int d\mathbf{x} |\Psi(\mathbf{x})|^2 \sigma[\mathbf{x}] \right] \\ &= \prod_{\mathbf{q}} \frac{1}{\sqrt{2\pi \tilde{V}(\mathbf{q})}} \int \mathcal{D}\sigma_{\mathbf{q}} \exp \left[ - \int \frac{d\mathbf{q}}{(2\pi)^d} \left( \frac{\sigma_{-\mathbf{q}} \sigma_{\mathbf{q}}}{2\tilde{V}(\mathbf{q})} + i\sigma_{\mathbf{q}} \int d\mathbf{x} |\Psi(\mathbf{x})|^2 e^{-i\mathbf{q} \cdot \mathbf{x}} \right) \right] \\ &\rightarrow \exp \left\{ -\frac{1}{2} \int d\mathbf{x} d\mathbf{x}' |\Psi(\mathbf{x})|^2 \left[ \int \frac{d\mathbf{q}}{(2\pi)^d} \tilde{V}(\mathbf{q}) e^{i\mathbf{q} \cdot (\mathbf{x} - \mathbf{x}')} \right] |\Psi(\mathbf{x}')|^2 \right\} \\ &= \exp \left\{ -\frac{1}{2} \int d\mathbf{x} d\mathbf{x}' |\Psi(\mathbf{x})|^2 V(\mathbf{x} - \mathbf{x}') |\Psi(\mathbf{x}')|^2 \right\}. \end{aligned} \quad (\text{A.18})$$

Hence, the interaction between two loop segments maps onto  $\Psi^4$  term so that the total complex field action reads

$$S_{GLW} = \frac{1}{2} \int d^d \mathbf{x} \left[ |\nabla_{\mathbf{x}} \Psi(\mathbf{x})|^2 + m^2 |\Psi(\mathbf{x})|^2 + \int d^d \mathbf{x}' |\Psi(\mathbf{x})|^2 V(\mathbf{x} - \mathbf{x}') |\Psi(\mathbf{x}')|^2 \right], \quad (\text{A.19})$$

and this completes our derivation.

There is one technical detail we overlooked and now we return to it. Namely, the original proof of Ref. [75] considered the delta-function interaction for which all the Fourier coefficients are non-zero. On the other hand, a general potential  $V(\mathbf{x})$  that we wish to map may exhibit a vanishing Fourier coefficient for an arbitrary value of moment  $\mathbf{q}$  which compromises the Hubbard-Stratanovich identity Eq. (A.15). This problem is dealt with in a way similar to the implementation of the Ehrenfest constraint. This should not be a surprise given the fact that the duality presented in this thesis was a kind of Hubbard-Stratanovich transformation. What one should do in order to avoid the ‘singularity’ problem associated with the vanishing Fourier components  $\tilde{V}(q) = 0$  is to separate the momenta with zero Fourier components from the momenta with finite components. The latter can safely undergo the described treatment, while the components related to the former are absent in the course of mapping. In other words, one can assume that a constraint  $\sigma_{\mathbf{q}} \equiv 0$  is imposed for each  $\mathbf{q}$  with vanishing Fourier component of the interaction. In the last step in Eq. (A.18), the missing momenta do not contribute to the real-space potential  $V(\mathbf{x})$  as should be the case, and the original interaction potential is recovered.

Let us now mention the reason we cannot directly utilize the mapping presented in this appendix for the purpose of describing a tangle of defects (vortices or dislocations). It turns out, despite the fact that both describe a gas of loops, that the grand canonical ensemble of loops, with its partition function Eq. (A.11), has a different phase space as compared to the path integral Eq. (2.31). While in the original proof each loop is counted just once and weighted according to its length Eq. (2.19), the path integral in this appendix has a redundant counting, since each loop can be parameterized by the Schwinger proper-time in infinitely many ways. Each parameterization has a different weight as implied by action Eq. (A.6). At the moment we are not aware if there is a relation that would link the weight obtained in that way to the weight given by the loop action Eq. (2.19), and hence we are forced to use the mapping of section 2.2.



# Appendix B

## Defect current conservation laws

When the dislocation and disclination conservation laws Eq. (3.50 - 3.51) were presented, we had to resort to the identity Eq. (2.101) in order to derive these laws. There is yet another proof based on the connection between elasticity and differential geometry [48]. and gravity [123, 124, 125]. The disclination current conservation law obtained in this manner is published as part of the article on the glide constraint [50]. Deep inside, the assumptions of this proof are not any different from those behind the identity Eq. (2.101). Nevertheless, this proof appears more ‘elegant’ due to its origins.

The dynamical version of the disclination conservation law can be traced back to the material conservation. As an example consider a wedge disclination: the material added is proportional to the Frank vector (scalar in 2+1D) and it should not change over time. In this respect the disclination conservation law may be regarded as a generalization of the glide constraint for the general topological defects. The basic idea is that after the Volterra cutting procedure has been applied, no additional material should be introduced, which is the same as the requirement that all symmetrized strains and derivatives thereof are smooth everywhere, including the locus of the Volterra cut. This condition is hard wired into the proof of the generalized Weingarten theorem Eq. (3.44). As we will now show, the ramification of this principle for disclinations is a conservation law.

To make headway, it is convenient to first consider Euclidean Lorentz-invariant  $D + 1$  space time. The non-relativistic case will turn out to be a special case which directly follows from imposing the condition of the absence of time like displacements ( $u^\tau = 0$ ). What follows rests heavily on elastic analogs of identities in differential geometry which are discussed in detail in the last part of Kleinert’s book [48]. First, we introduce the tensor

$$R_{\mu\nu,\rho\sigma} = (\partial_\mu\partial_\nu - \partial_\nu\partial_\mu)\partial_\rho u^\sigma \quad (\text{B.1})$$

representing the Riemann-Christoffel curvature tensor in the geometrical formulation of the theory of elasticity (the  $u$ ’s are the usual displacements). The smoothness assumptions underlying the Weingarten theorem may be expressed as,

$$0 = (\partial_\mu\partial_\nu - \partial_\nu\partial_\mu)(\partial_\rho u^\sigma + \partial_\sigma u^\rho), \quad (\text{B.2})$$

$$0 = (\partial_\mu\partial_\nu - \partial_\nu\partial_\mu)\partial_\lambda(\partial_\rho u^\sigma + \partial_\sigma u^\rho), \quad (\text{B.3})$$

which in turn imply smoothness of the displacement second derivative

$$0 = (\partial_\mu \partial_\nu - \partial_\nu \partial_\mu) \partial_\lambda \partial_\rho u^\sigma. \quad (\text{B.4})$$

Cycling through the indices  $\mu$ ,  $\nu$ , and  $\lambda$  of the smoothness equation Eq. (B.4), we obtain the Bianchi identity for the displacement fields [180],

$$\partial_\mu R_{\nu\lambda,\rho\sigma} + \partial_\nu R_{\lambda\mu,\rho\sigma} + \partial_\lambda R_{\mu\nu,\rho\sigma} = 0. \quad (\text{B.5})$$

Starting from the other end, let us analyze a candidate for a disclination conservation law, corresponding to  $\partial_\mu T_{\mu\nu_1\nu_2\dots\nu_{D-2}}^{\alpha_1\alpha_2\dots\alpha_{D-1}}$ . This can be expressed in terms of the Riemann tensor where  $\{\alpha\}$  refers to a string of indices labeled by  $\alpha$ ,

$$\begin{aligned} \partial_\mu T_{\mu\{\nu\}}^{\{\alpha\}} &= \frac{1}{2} \epsilon_{\mu\{\nu\}\kappa\lambda} \epsilon_{\{\alpha\}\rho\sigma} \partial_\mu \partial_\kappa \partial_\lambda \partial_\rho u^\sigma \\ &= \frac{1}{2} \epsilon_{\mu\{\nu\}\kappa\lambda} \epsilon_{\{\alpha\}\rho\sigma} \partial_\mu (\partial_\kappa \partial_\lambda - \partial_\lambda \partial_\kappa + \partial_\lambda \partial_\kappa) \partial_\rho u^\sigma \\ &= \frac{1}{2} \epsilon_{\mu\{\nu\}\kappa\lambda} \epsilon_{\{\alpha\}\rho\sigma} \partial_\mu R_{\kappa\lambda,\rho\sigma} - \partial_\mu T_{\mu\{\nu\}}^{\{\alpha\}}. \end{aligned} \quad (\text{B.6})$$

The first term is zero as a consequence of the contraction of the Bianchi identity Eq. (B.5) and the Levi-Civita symbol  $\epsilon_{\mu\{\nu\}\kappa\lambda}$ . This implies that relativistic disclination currents are conserved. The non-relativistic case is just a special case: the vanishing of time like displacements means that all upper labels are space-like ( $\alpha \rightarrow a$ ) and it follows,

$$\partial_\mu T_{\mu\nu_1\nu_2\dots\nu_{D-2}}^{a_1a_2\dots a_{D-2}} = 0. \quad (\text{B.7})$$

Let us now try to envisage the physical consequences of this dynamical conservation law. In 2+1D, only wedge dislocations exist and the message of the conservation law Eq. (B.7) is clear: the Frank charge – the angle of an inserted wedge in the Volterra construction – behaves as a trivially conserved scalar component of a tensor. In higher dimensions, the disclination current similarly behaves as a conserved tensorial current. The defect density has information regarding both dislocations and disclinations. The disclination conservation law has separate ramifications for the defect density. The fundamental condition Eq. (B.4) can be directly rewritten into a conservation law for the defect density of a similar form as for the disclinations,

$$\partial_\mu \eta_{\mu\nu_1\dots\nu_{D-2}}^{\alpha_1\alpha_2\dots\alpha_{D-1}} = 0. \quad (\text{B.8})$$

This is not surprising as defect currents are proportional to disclination currents.

Together with the glide constraint, this completes the picture: the conservation of matter mandates that the ‘proper’ disclinations currents are also conserved. However, the ‘handicapped’ dislocation currents are not conserved a-priori (disclinations form their sources) but they have to pay the price that they can only glide.

# Appendix C

## Irreducible tensors of the symmetry group

The idea that one can make important statements about a system by mere analysis of symmetries is often attributed to Landau. In this very last part of the thesis we utilize this idea. By representing the field components of the physically relevant tensors (strains, stresses, dislocation currents and dual stress gauge fields) as irreducible tensors of the symmetry group in the problem, we can interpret these and give each component a precise physical meaning. The symmetry considerations presented here are simplified in the sense that they exclude the translational symmetries of the model. As it turns out, the rotational degrees of freedom combined with space and time reflections are sufficient for our needs and at the end of the section the specific degrees of freedom, be it strains, stresses, dual stress gauge fields or the defect currents, mentioned in the main part of the thesis, are associated with different irreducible representations of the symmetry group. The physical degrees of freedom, on the other hand, also have certain transformation properties and matching these with the properties of the (dual) degrees of freedom leads to the proper interpretation. As the example already encountered in the thesis, recall the glide constraint Eq. (3.61) and its relation to the compression. The compression is invariant under all possible (point group) transformations. The same is true for the glide constrained component of the dynamical dislocation currents. As a result, the suppression of the climb in the system is uniquely associated with the compressional rigidity. In the same manner, other degrees of freedom can be traced to their physical origins.

Let us start with the group of symmetries that the elastic action Eq. (3.24) has to obey. The Euclidian group  $E(2)$  is broken down to the product of the group of discrete lattice translations and the point group of the lattice. Since we are after the minimal model that is supposed to associate degrees of freedom with the irreducible representations of the symmetry group, the translations will be neglected in this short exposition. We concentrate on rotations, i.e. the point group which is in general determined through the symmetry group of the underlying crystalline lattice. Given the fact that the theory presented in this thesis is developed for the exclusive case of the isotropic elastic tensor Eq. (3.15) (although the generalization to an arbitrary tensor  $C_{ijab}$  is straightforward),

the point group symmetry explicitly analysed in this appendix will be the group of all (proper) rotations in two dimensions, denoted as  $C_\infty$ . This group does not exhaust all the symmetries of the crystalline lattice, in addition there is the spatial reflection symmetry  $\sigma_v$  which, together with proper rotations forms the group  $C_{\infty v}$ . Finally, we should add the time-inversion symmetry  $\sigma_\tau$  to cover the dynamics introduced in our action through term Eq. (3.23). The total point symmetry group is then  $C_{\infty v h}$ .

The next step is to determine the action of these symmetries on the single component vectors in the system, that is to find the vector representations of the symmetry group. Recalling from undergraduate physics courses in mechanics [167] as well as electromagnetism [165, 166], one should note that the space- and time-inversions act differently on different kinds of vectors. For example, the radius-vector  $\mathbf{r}$  perpendicular to the reflection axis, changes its orientation under the spatial reflection. The same is true for the force  $\mathbf{F}$ . On the other hand, their cross-product is the torque vector which is invariant under the same reflections. We shall refer to the former as polar-vectors, whereas the latter will be called axial-vectors. The same pattern is followed by the time-inversion symmetry: while the radius vector  $\mathbf{r}$  does not change under time-inversions, its first derivative, the velocity field, does. In order to draw the line between the two sorts, the former will be called true- and the later pseudo-vectors. Accordingly, there are four classes of vectors: true-polar-, true-axial-, pseudo-polar- and pseudo-axial-vectors. The examples are respectively radius vector, angular momentum, velocity and angular velocity. Let us add that in most of the cases, a distinction is not made between the spatial- and time-inversion with words ‘axial’ and ‘pseudo’ identified. We stress however the difference between the two symmetries.

Scalars exhibit different transformation properties, in the same manner as vectors. The same is true for tensors with more indices. It is even possible for a tensor to have different indices transforming differently under the same inversion. This will be the case, for example, when we analyse the dislocation currents. Let us just add that (proper) rotations are always represented in the same way independently from the type of scalar/vector/tensor. Therefore, the representations of the symmetry group will be determined by simple group multiplication of a proper rotation and the appropriate representations for the symmetries.

Although not of direct interest for our problem, we may begin with scalars. A scalar is invariant under proper rotations, i.e.  $D^{sc.[T|P][P|A]}(\mathcal{R}_\alpha) \equiv 1$ . The first choice of letters  $T$  and  $P$  stands for ‘true’ and ‘pseudo’, and the second letter can be  $P$  or  $A$  if the scalar is of ‘polar’ or ‘axial’ type. The space- and -time-reflections are represented in the following way:

$$D^{sc.TP}(\sigma_v) = 1, \quad D^{sc.TP}(\sigma_\tau) = 1, \quad (\text{C.1})$$

$$D^{sc.TA}(\sigma_v) = -1, \quad D^{sc.TP}(\sigma_\tau) = 1, \quad (\text{C.2})$$

$$D^{sc.PP}(\sigma_v) = 1, \quad D^{sc.TP}(\sigma_\tau) = -1, \quad (\text{C.3})$$

$$D^{sc.PA}(\sigma_v) = -1, \quad D^{sc.TP}(\sigma_\tau) = -1. \quad (\text{C.4})$$

If the scalar representations sounded boring because we could not apply them to the problems we presented in this thesis, now we turn to vectorial representation and their products, and as a first example, the strain field is decomposed into physically relevant

components. Let us suppose that a two-dimensional vector is represented by a column of length two (i.e.  $(a_x, a_y)^T$ ), and the 2+1-dimensional vector by a column with the first two elements corresponding to the spatial indices and the third one to the temporal index (i.e.  $(u_x, u_y, u_\tau)^T$ ). A proper 2D-rotation is represented by the matrix

$$D[\mathcal{R}(\alpha)] = \begin{pmatrix} \cos \alpha & -\sin \alpha & 0 \\ \sin \alpha & \cos \alpha & 0 \\ 0 & 0 & 1 \end{pmatrix}, \quad (\text{C.5})$$

when acting on a three-vector. The two-dimensional (spatial) representation  $\underline{D}$ , needed for ‘flavour’ representations is given by simple erasing of the last column/row. We also need to know how to represent reflections. The temporal inversion is represented by a unit matrix for representations of true-vectors and by a negative unit matrix for pseudo-vector representations. When defining spatial reflection representation, a certain axis has to be chosen, say  $x$ , to serve as the reflection axis. Then, the polar-vectors transform according to  $D^P[\sigma_v] = \text{diag}(-1, 1, 1)$ , and axial-vectors according to the unit matrix. Of course, the two-dimensional representation is again obtained by taking only the first two columns/rows.

For our first example, the strain field, we also need to determine the representation according to which the derivatives transform. This is a standard exercise in the general relativity which we repeat here. Begin with

$$\frac{\partial}{\partial x'^\mu} = \frac{\partial x^\nu}{\partial x'^\mu} \frac{\partial}{\partial x^\nu}. \quad (\text{C.6})$$

Then, express the old coordinate as  $x^\nu = [D^{-1}]^\nu_\mu x'^\mu$  and use the unitarity of the representation  $[D^{-1}]^\nu_\mu = D_\mu^\nu$ , to find that the derivative transforms under the representation  $D^T$  which is obtained by transposing representation  $D$ . Here and later in the text, unless stated otherwise, the plain letter  $D$  represents the representation under which the coordinates transform. That is the true-polar representation for spatial indices and pseudo-polar for the temporal index.

Knowing that the displacements transform the same way as a radial vector, that is as a true-polar-vector, we find that the strain transforms under the product of representations

$$\partial_{\mu'} u^{a'} = [D^T \otimes \underline{D}]_{\mu'a}^{\mu'a'} \partial_\mu u^a. \quad (\text{C.7})$$

This composite representation is decomposed into the Clebsch-Gordon series of the irreducible representations of the group of symmetries [181]. In the case of the  $C_{\infty v h}$  group, the series read

$$D \otimes \underline{D} = A_0^+ + B_0^+ + E_1^- + E_2^+. \quad (\text{C.8})$$

Let us first clarify the sub- and super-scripts of the representations. The subscript indicates the ‘spin’ of the representation. The super-scripts tell us whether the representation is invariant under the temporal reflection or not (+ means it is invariant).  $A_0$  is the representation invariant under rotations (spin-0), and also under spatial reflection, differently from

$B_0$  (also spin-0) that changes sign under  $\sigma_v$ . The spinful (two-dimensional) representations  $E_m$  always see the spatial inversion as a conjugation. A proper rotation is represented as  $e^{im\alpha\tau^z}$  with  $\tau^z$  being the Pauli matrix. The representation properties will help us identify strains components.

Through projection operators [181], the eigenvectors (irreducible representation vectors) are found:

$$|A_0^+\rangle = \partial_x u^x + \partial_y u^y = \partial_i u^i, \quad (\text{C.9})$$

$$|B_0^+\rangle = \partial_x u^y - \partial_y u^x = \epsilon_{ij} \partial_i u^j, \quad (\text{C.10})$$

$$|E_{\pm 1}^-, \pm\rangle = \frac{1}{\sqrt{2}} (\partial_\tau u^x \pm i \partial_\tau u^y) = \partial_\tau u^\pm, \quad (\text{C.11})$$

$$|E_{\pm 2}^+, \pm\rangle = \frac{1}{2} (\partial_x u^x - \partial_y u^y) \pm \frac{i}{2} (\partial_x u^y + \partial_y u^x) = \partial_\mp u^\pm. \quad (\text{C.12})$$

Note that the first two strains can also be expressed in holomorphic ( $\pm$ ) coordinates as  $\partial_+ u^+ \pm \partial_- u^-$ . Now we turn to the physical interpretation. The  $|A_0^+\rangle$  is clearly the compression strain. It is invariant to all the transformations of the symmetry group. The next is the rotation strain  $|B_0^+\rangle$  which sees only the spatial inversion. The spin-1 doublet  $|E_{\pm 1}^-\rangle$  consists of two velocities written in holomorphic fashion. These velocities change sign under the time reflection and acquire phase  $e^{\pm i\alpha}$  upon rotation. Spin two strains  $|E_{\pm 2}^+\rangle$  represent shear, and in this notation these may be viewed as a helical composition of the electric and magnetic shear.

Let us add for curiosity that these strains can be related to the vibrational degrees of freedom on a triangular lattice through the same analysis of the irreducible representations, now of the group  $C_{3vh}$ . The equivalence of the two is the reason behind the simple (isotropic) elastic tensor found in two-dimensional triangular lattice. Already in three spatial dimensions, the irreducible representations of the group of rotations  $O(3)$  differ from the irreducible representations associated with the vibrations of the simplest diamond lattice, which leads to the anisotropic elastic tensor as measured quite some time ago [182]. Talking about the vibrational microscopic degrees of freedom, we may also mention a similar classification of strains by Ahn *et al.* [183]. Their work is, however, focused on a square lattice which makes space for additional degrees of freedom.

After this interesting ‘dissection’ of the strain degrees of freedom we may find its implications on the form of the isotropic elastic tensor. When two irreducible tensor components are multiplied, their spins add up, while their parities (under each reflection separately) multiply. Since the only allowed terms in action must be invariant under all elements of the group representation, the only admitted terms must have total spin zero and contain an even number of ‘pseudo’ and an even number of ‘axial’ components. In the case of the linear elasticity, the most general action allowed by the  $C_{\infty vh}$  symmetry group has form

$$\mathcal{L}_{inv} = \frac{1}{2} [K_A (\partial_i u_i)^2 + K_B (\epsilon_{ij} \partial_i u^j)^2 + K_1 \partial_\tau u^+ \partial_\tau u^- + K_2 \partial_- u^+ \partial_+ u^-]. \quad (\text{C.13})$$

The coefficient  $K_A$  is clearly the compression modulus  $\kappa$ .  $K_2$  is the shear modulus  $\mu$  and  $K_1$  is the mass density  $\rho$ . This simplified approach cannot rule out the term with  $K_B$ . This is

a consequence of the fact that we use only linear (matrix multiplicative) representations in our approach whereas the true physical rotation, in addition, shifts the local rotation field by a constant. The same form of the linear elastic energy as that of Eq. (C.13) could have alternatively been obtained by demanding that only singlet components of the elasticity tensor Eq. (3.9) may appear in the action.

Given the fact that stress fields transform under the same representation as strain (Eq. (C.7)), everything said for the strains from the symmetry point of view, applies also to the stresses. There are compressional ( $\sigma_a^a$ ), rotational ( $\epsilon_{ab}\sigma_a^b$ ) and two shear stresses of spin-2 which were identified earlier in Eq. (4.79). The kinetic momenta densities form spin-1 stress fields  $\sigma_\tau^\pm$ . Notice that the Ehrenfest constraint has a precise meaning in terms of the symmetry: the stress component sensitive to the spatial reflection is not allowed. In analogy with the action Eq. (C.13) one can construct the minimal dual stress action allowed by symmetry. Contrasting its constants with the ‘inverse’ elasticity tensor it readily follows that  $K_A^\sigma = 1/(4\kappa)$ ,  $K_2^\sigma = 1/(4\mu)$  and  $K_1^\sigma = 1/\rho$ , illustrating how each coupling constant remains ‘confined’ to its own symmetry sector even after the dualization.

Finally, we arrive at most important and most interesting part of this appendix, the irreducible components of the dislocation currents. By identifying these, the appropriate gauge degrees of freedom are automatically recovered. One should, however, be careful since gauge fields do not have direct physical meaning and can be shifted by an arbitrary gauge transformation. Nevertheless, the experience from the chapter 4 taught us that after a definite gauge fixing has been chosen, one can correspond the dual stress gauge degrees of freedom with the physical degrees of freedom such as compression and shear.

We denote that representation with  $\mathcal{D}_J$  so that we have

$$J_{\mu'}^{a'} = [\mathcal{D}_J]_{\mu'\mu}^{a'a} J_\mu^a. \quad (\text{C.14})$$

The left-hand side can be expressed in the original strains

$$J_{\mu'}^{a'} = \epsilon_{\mu'\nu'\rho'} \partial_{\nu'} \partial_{\rho'} u^{a'} = \epsilon_{\mu'\nu'\rho'} D_{\nu'\nu}^T D_{\rho'\rho}^T \underline{D}^{a'a} \partial_\nu \partial_\rho u^a, \quad (\text{C.15})$$

as well as the right-hand side

$$[\mathcal{D}_J]_{\mu'\mu}^{a'a} J_\mu^a = [\mathcal{D}_J]_{\mu'\mu}^{a'a} \epsilon_{\mu\nu\rho} \partial_\nu \partial_\rho u^a. \quad (\text{C.16})$$

The identity that follows is contracted with tensor  $\epsilon_{\lambda\nu\rho}$  to find

$$[\mathcal{D}_J]_{\mu'\mu}^{a'a} = \frac{1}{2} \epsilon_{\mu'\nu'\rho'} \epsilon_{\mu\nu\rho} D_{\nu'\nu}^T D_{\rho'\rho}^T \underline{D}^{a'a}. \quad (\text{C.17})$$

This representation is decomposed into the Clebsch-Gordan series

$$\mathcal{D}_J = A_0^- + B_0^- + E_1^+ + E_2^-, \quad (\text{C.18})$$

which show one interesting difference compared to Eq. (C.8): the time-reflection status is here inverted. The static currents  $|E_1^+\rangle = J_\tau^\pm$  are time-inverse invariant as they represent the static dislocation charge. The dynamical currents are, on the other hand, sensitive to the time-inversion: the compression current  $|A_0^-\rangle = \epsilon_{ij} J_i^j$ , the rotation current  $|B_0^-\rangle = J_i^i$  and the doublet of shear currents  $|E_2^-\rangle = J_\pm^\mp$ . On this level, the glide constraint is exclusively associated with the dynamical singlet current  $|A_0^-\rangle$ .



# Bibliography

- [1] S. Sachdev, *Quantum Phase Transitions* (Cambridge University Press, 1999).
- [2] S. N. Bose, *Z. Phys* **26**, 178 (1924).
- [3] A. Einstein, *Sitz. Ber. Preuss. Akad. Wiss. (Berlin)* **22**, 261 (1924).
- [4] C. Monroe, W. S. H. Robinson, and C. Wieman, *Phys. Rev. Lett.* **65**, 1571 (1990).
- [5] M. Anderson, J. Ensher, M. Matthews, C. Wieman, and E. Cornell, *Science* **269**, 198 (1995).
- [6] W. Ketterle, K. Davis, M. Joffe, A. Martin, and D. Pritchard, *Phys. Rev. Lett.* **70**, 2253 (1993).
- [7] K. Davis *et al.*, *Phys. Rev. Lett.* **75**, 3969 (1995).
- [8] L. Landau, *Phys. Rev.* **60**, 356 (1941).
- [9] E. Wigner, *Phys. Rev.* **46**, 1002 (1934).
- [10] R. Jamei, S. Kivelson, and B. Spivak, *Phys. Rev. Lett.* **94**, 056805 (2005).
- [11] H. Onnes, *Commun. Phys. Lab.* **12**, 120 (1911).
- [12] W. Meissner and R. Oschenfeld, *Naturwiss.* **21**, 787 (1933).
- [13] F. London and H. London, *Proc. R. Soc. London* **A419**, 71 (1935).
- [14] V. Ginzburg and L. Landau, *Zh. Eksp. Teor. Fiz.* **20**, 1064 (1950).
- [15] E. Maxwell, *Phys. Rev.* **78**, 477 (1950).
- [16] C. Reynolds, B. Serin, W. Wright, and L. Nesbitt, *Phys. Rev.* **78**, 487 (1950).
- [17] J. Bardeen, L. Cooper, and J. Schrieffer, *Phys. Rev.* **108**, 1175 (1957).
- [18] G. Eliashberg, *Zh. Eksp. Teor. Fiz.* **38**, 966 (1960).
- [19] G. Eliashberg, *Sov. Phys. JETP* **11**, 696 (1960).

- [20] R. Laughlin, Phys. Rev. B **23**, 5632 (1981).
- [21] R. Laughlin, Phys. Rev. Lett. **50**, 1395 (1983).
- [22] K. von Klitzing, G. Dorda, and M. Pepper, Phys. Rev. Lett. **45**, 494 (1980).
- [23] D. Tsui, H. Stormer, and A. Gossard, Phys. Rev. Lett. **48**, 1559 (1982).
- [24] T. Ando, Y. Matsumoto, and Y. Uemura, J. Phys. Soc. Jpn. **39**, 279 (1975).
- [25] E. Fradkin and S. Kivelson, Phys. Rev. B **59**, 8065 (1999).
- [26] L. Balents, Europhys. Lett. **33**, 291 (1996).
- [27] J. Jain, Phys. Rev. Lett. **63**, 199 (1989).
- [28] J. Jain, Phys. Rev. B **41**, 7653 (1990).
- [29] M. Goerbig, P. Lederer, and C. Morais Smith, Phys. Rev. B **69**, 155324 (2004).
- [30] J. Bednorz and K. Mueller, Z. Phys **B64**, 189 (1986).
- [31] N. Bogoliubov, Zh. Eksp. Teor. Fiz. **34**, 58 (1958).
- [32] J. Zaanen and O. Gunnarson, Phys. Rev. B **40**, 7391 (1989).
- [33] H. Schultz, Phys. Rev. Lett. **64**, 1445 (1990).
- [34] V. Emery and S. Kivelson, Physica C **209**, 597 (1993).
- [35] J. Tranquada, B. Sternlieb, J. Axe, Y. Nakamura, and S. Uchida, Nature **375**, 561 (1995).
- [36] S. More, C. Chen, and S. Cheong, Nature **392**, 473 (1998).
- [37] S. Kivelson, E. Fradkin, and V. Emery, Nature **393**, 550 (1998).
- [38] P. Abbamonte *et al.*, Nature **431**, 1078 (2004).
- [39] Z. Nussinov and J. Zaanen, J. Phys. IV France **12**, 245 (2002), cond-mat/0209437.
- [40] Z. Nussinov and J. Zaanen, cond-mat/0209441.
- [41] H. Mook, P. Dai, , and R. Hunt, Nature **404**, 729 (2000).
- [42] J. Hoffmann *et al.*, Science **295**, 466 (2002).
- [43] V. Hinkov *et al.*, Nature **430**, 650 (2004).
- [44] J. Zaanen, Z. Nussinov, and S. Mukhin, Annals of Physics **310/1**, 181 (2004).

- [45] B. Halperin and D. Nelson, Phys. Rev. Lett. **41**, 121 (1978).
- [46] B. Halperin and D. Nelson, Phys. Rev. B **19**, 2457 (1979).
- [47] A. Young, Phys. Rev. B **19**, 1855 (1979).
- [48] H. Kleinert, *Gauge fields in Condensed Matter, Vol. II: Stresses and Defects, Differential Geometry, Crystal Defects* (World Scientific, Singapore, 1989).
- [49] M. K. H. Kleinert and A. Schakel, Phys. Rev. Lett. **73**, 1975 (1994).
- [50] V. Cvetkovic, Z. Nussinov, and J. Zaanen, cond-mat/0508664.
- [51] G. Mahan, *Many-particle Physics* (Plenum Press, New York, 1981).
- [52] A. Abrikosov, L. Gorkov, and I. Dzyaloshinski, *Methods of Quantum Field Theory in Statistical Physics* (Dover Publications, 1977).
- [53] R. Savit, Rev. Mod. Phys. **52**, 453 (1980).
- [54] H. Kramers and G. Wannier, Phys. Rev. **60**, 252 (1941).
- [55] J. Kogut, Rev. Mod. Phys. **51**, 659 (1979).
- [56] M. Halperin, Phys. Rev. D **19**, 517 (1979).
- [57] Z. Nussinov and E. Fradkin, Phys. Rev. B **71**, 195120 (2005).
- [58] D. Lee and M. Fisher, Phys. Rev. B **39**, 2756 (1989).
- [59] A. Zee, Physica A **281**, 442 (2000).
- [60] H. Kleinert, *Gauge fields in Condensed Matter, Vol. I: Superflow and Vortex Lines, Disorder Fields, Phase Transitions* (World Scientific, Singapore, 1989).
- [61] M. Fisher, P. Weichman, G. Grinstein, and D. Fisher, Phys. Rev. B **40**, 546 (1989).
- [62] V. Cvetkovic and J. Zaanen, cond-mat/0511586, submitted to Phys. Rev. B.
- [63] J. Hove and A. Sudbø, Phys. Rev. Lett. **84**, 3426 (2000).
- [64] K. Lee, PRD **48**, 2493 (1993).
- [65] R. Fazio and H. van der Zant, Phys. Rep. **355**, 235 (2001).
- [66] T. Banks, R. Myerson, and J. Kogut, Nucl. Phys. B **129**, 493 (1977).
- [67] A. Nguyen and A. Sudbø, Phys. Rev. B **60**, 15307 (1999).
- [68] J. Hove, S. Mo, and A. Sudbø, Phys. Rev. Lett. **85**, 2368 (2000).

- [69] V. Vaks and I. Larkin, JETP **49**, 975 (1965).
- [70] A. Polyakov, *Gauge Fields and Strings* (Harwood Academic Publishers, 1987).
- [71] J. Villain, J. Physique **36**, 591 (1975).
- [72] P. Anderson, Phys. Rev. **110**, 827 (1958).
- [73] P. Anderson, Phys. Rev. **130**, 439 (1963).
- [74] G. Parisi, *Statistical Field Theory* (Addison-Wesley, New York, 1988).
- [75] M. Kiometzis, H. Kleinert, and A. Schakel, Fortschr. Phys. **43**, 697 (1995).
- [76] V. Žigman, *Specijalna teorija relativnosti* (Studentski trg, Beograd, 1997).
- [77] N. Bogolyubov, N. Tolmachev, and D. Shirkov, *New Methods in the Theory of Superconductivity* (Academy of Sciences of the U.S.S.R., Moscow, 1958).
- [78] V. Galitskii, Sov. JETP **34**, 1011 (1958).
- [79] J. Bjorken and S. Drell, *Relativistic quantum fields* (McGraw-Hill, 1965).
- [80] D. Popović, *Teorija elektroslabih interakcija, SFIN 2* (Institut za fiziku, Zemun, 1995).
- [81] S. Elitzur, Phys. Rev. D **12**, 3978 (1975).
- [82] T. Hansson, V. Oganessian, and S. Sondhi, Annals of Physics **313**, 497 (2004).
- [83] X. Wen, Phys. Rev. B **65**, 165113 (2002).
- [84] H. Kleinert and J. Zaanen, Phys. Lett. A **324**, 361 (2004).
- [85] H. Kleinert, Br. J. of Phys. **35**, 359 (2005).
- [86] P. Higgs, Phys. Rev. Lett. **12**, 132 (1964).
- [87] P. Anderson, Phys. Rev. **112**, 1900 (1958).
- [88] P. Anderson, Phys. Rev. **130**, 439 (1963).
- [89] J. L. Guillou and J. Zinn-Justin, Phys. Rev. B **21**, 3976 (1980).
- [90] S. Shenoy, Phys. Rev. B **40**, 5056 (1989).
- [91] I. Herbut and Z. Tesanovic, Phys. Rev. Lett. **76**, 4588 (1996).
- [92] T. T. M. Hasenbusch, J. Phys. A: Math. Gen. **32**, 6361 (1999).
- [93] A. Gottlob and M. Hasenbusch, Physica A **201**, 593 (1993), cond-mat/9305020.

- [94] P. Olsson, *Europhys. Lett.* **58**, 705 (2002).
- [95] P. Olsson and S. Teitel, *Phys. Rev. Lett.* **80**, 1964 (1998).
- [96] D. Fisher, M. Fisher, and D. Huse, *Phys. Rev. B* **43**, 130 (1991).
- [97] K. Binder, *Phys. Rev. Lett.* **47**, 693 (1981).
- [98] K. Binder, M. Naunberg, V. Privman, and A. Young, *Phys. Rev. B* **31**, 1498 (1985).
- [99] Notice that the Josephson correlation length scales according to,

$$\xi_J = c/\rho_s \propto |\epsilon|^{-\nu(2-\eta_A)} \xrightarrow{\eta_A=1} |\epsilon|^{-\nu}. \quad (\text{C.19})$$

It is well known [184] that  $\xi_J$  is governed by the same exponent  $\nu$  in charge of the mass on the disordered side. According to the above equation, this can only be the case when  $\eta_A = 1$ , once again highlighting the remarkable consistency of the duality construction!

- [100] C. Dodson and P. Parker, *A User's Guide to Algebraic Topology* (Kluwer, Dordrecht, 1997).
- [101] E. Orowan, *Z. Phys.* **89**, 605 (1934).
- [102] E. Orowan, *Z. Phys.* **89**, 634 (1934).
- [103] M. Polanyi, *Z. Phys.* **89**, 660 (1934).
- [104] G. Taylor, *Proc. Roy. Soc.* **A145**, 362 (1934).
- [105] R. E. Peierls, *Phys. Rev.* **54**, 918 (1938).
- [106] L. Onsager, *Nuovo Cim. Suppl.* **6**, 249 (1949).
- [107] L. Onsager, *Ann. N.Y. Acad. Sci.* **51**, 627 (1949).
- [108] R. Stoops, editor, *L'Etat Solide, Proceeding of Neuvieme-Consail de Physique*, Brussels, 1952, Solvay Institut de Physique.
- [109] L. Burakovsky and D. Preston, *Solid State Comm.* **115**, 341 (2000).
- [110] J. Kosterlitz and D. Thouless, *J. Phys. C* **5**, L124 (1972).
- [111] J. Kosterlitz and D. Thouless, *J. Phys. C* **6**, 181 (1973).
- [112] C. Mott, *Proc. Roy. Soc.* **A215**, 1 (1952).
- [113] D. Fisher, B. Halperin, and R. Morf, *Phys. Rev. B* **20**, 4692 (1979).

- [114] Z. Nussinov, Phys. Rev. B **69**, 014208 (2004).
- [115] T. Kirkpatrick and P. Wolynes, Phys. Rev. A **35**, 3072 (1987).
- [116] T. Kirkpatrick and P. Wolynes, Phys. Rev. B **36**, 8552 (1987).
- [117] T. Kirkpatrick, D. Thirumalai, and P. Wolynes, Phys. Rev. A **40**, 1045 (1989).
- [118] T. Kirkpatrick and D. Thirumalai, Phys. Rev. Lett. **58**, 2091 (1987).
- [119] M. Lilly, K. Cooper, J. Eisenstein, L. Pfeiffer, and K. West, Phys. Rev. Lett. **82**, 394 (1999).
- [120] J.-X. Zhu *et al.*, Phys. Rev. Lett. **91**, 057004 (2003).
- [121] K. Ahn *et al.*, J. of Superconductivity **17**, 7 (2004).
- [122] K. Ahn, T. Lookman, and A. Bishop, Nature **428**, 401 (2004).
- [123] H. Kleinert, Ann. d. Physik **44**, 117 (1987).
- [124] H. Kleinert, *Proc. NATO Advanced Study Institute on Formation and Interaction of Topological Defects at the University of Cambridge* (Plenum Press, New York, 1995), cond-mat/9503030.
- [125] H. Kleinert, Gen. Rel. Grav. **32**, 769 (2000).
- [126] L. Landau and E. Lifshitz, *Theory of Elasticity* (Pergamon, New York, 1970).
- [127] W. Kleiner, L. Roth, and S. Autler, Phys. Rev. **A133**, 1226 (1964).
- [128] E. Kittinger, J. Tichý, and E. Bertagnolli, Phys. Rev. Lett. **47**, 712 (1981).
- [129] A. Ahsan, J. Rudnick, and R. Bruinsma, cond-mat/0512423.
- [130] P. Chaikin and T. Lubensky, *Principles of Condensed Matter Physics* (Cambridge University Press, 1995).
- [131] D. Nelson, *Defects and Geometry in Condensed Matter Physics* (Cambridge University Press, 2002).
- [132] J. Friedel, *Dislocations* (Pergamon Press, New York, 1954).
- [133] F. Nabarro, *Theory of Dislocations* (Clarendon, Oxford, 1967).
- [134] J. Hirth and J. Lothe, *Theory of Dislocations* (McGrawHill, New York, 1968).
- [135] G. Weingarten, Atti Accad. naz. Lincei Rc. [5] **10**, 57 (1901).
- [136] R. Bruinsma, B. Halperin, and A. Zippelius, Phys. Rev. B **25**, 579 (1982).

- [137] C. O'Hern and T. Lubensky, Phys. Rev. E **58**, 5948 (1998).
- [138] L. Golubović and M. Golubović, Phys. Rev. Lett. **80**, 4341 (1998).
- [139] C. O'Hern, T. Lubensky, and J. Toner, Phys. Rev. Lett. **83**, 2745 (1999).
- [140] E. Fradkin and S. Kivelson, Phys. Rev. B **59**, 8065 (1999).
- [141] A. MacDonald and M. Fisher, Phys. Rev. B **61**, 5724 (2000).
- [142] V. Emery, E. Fradkin, S. Kivelson, and T. Lubensky, Phys. Rev. Lett. **85**, 2160 (2000).
- [143] A. Vishwanath and D. Carpentier, Phys. Rev. Lett. **86**, 676 (2001).
- [144] B. Bernu and D. Ceperley, J. Phys.-Condens.Mat. **16**, 701 (2004).
- [145] F. Camino, W. Zhou, and V. Goldman, cond-mat/0502406.
- [146] H. Kleinert and J. Zaanen, Phys. Lett. A **324**, 361 (2004).
- [147] E. Witten, Nucl. Phys. B **373**, 187 (1992).
- [148] J. Klebanov and A. Polyakov, Mod. Phys. Lett. **A6**, 3273 (1991).
- [149] E. Witten and B. Zweibach, Nucl. Phys. B **377**, 55 (1992).
- [150] P. de Gennes and J. Prost, *The Physics of Liquid Crystals, 2nd Ed* (Clarendon Press, Oxford, 1993).
- [151] N. Muller, *Topological Interactions and Quantum Double Symmetries*, PhD thesis, Rijksuniversiteit Groningen, 2002.
- [152] P. Lammert, D. Rokhsar, and J. Toner, Phys. Rev. Lett. **70**, 1650 (1993).
- [153] P. Lammert, D. Rokhsar, and J. Toner, Phys. Rev. E **52**, 1778 (1995).
- [154] I. Low and A. Manohar, Phys. Rev. Lett. **88**, 101602 (2002).
- [155] N. Mermin and H. Wagner, Phys. Rev. Lett. **17**, 1307 (1966).
- [156] P. Hohenberg, Phys. Rev. **158**, 383 (1967).
- [157] E. Shender, Sov. Phys. JETP **56**, 178 (1982).
- [158] C. Henley, Phys. Rev. Lett. **62**, 2056 (1989).
- [159] X. Wen and A. Zee, Phys. Rev. B **41**, 240 (1990).
- [160] X. Wen and A. Zee, Int. J. Mod. Phys. B **4**, 437 (1990).

- [161] X. Wen and A. Zee, Phys. Rev. Lett. **69**, 1811 (1992).
- [162] H. Fröhlich, Phys. Rev. **79**, 845 (1950).
- [163] H. Fröhlich, Proc. R. Soc. A **223**, 296 (1954).
- [164] D. Lee, Phys. Rev. Lett. **88**, 227003 (2002).
- [165] L. Jackson, *Classical Electrodynamics* (Wiley, New York, 1963).
- [166] B. Milić, *Kurs klasične teorijske fizike II deo (Meksvelova elektrodinamika)* (Univerzitet u Beogradu, Beograd, 1996).
- [167] B. Milić, *Kurs klasične teorijske fizike I deo (Njutnova mehanika)* (Univerzitet u Beogradu, Beograd, 1995).
- [168] P. Martin, Phys. Rev. **161**, 143 (1967).
- [169] A. Rajagopal and K. Jain, Phys. Rev. A **5**, 1475 (1972).
- [170] D. Bohm and D. Pines, Phys. Rev. **82**, 625 (1951).
- [171] U. Fano, Phys. Rev. **103**, 1202 (1956).
- [172] J. Hopfield, Phys. Rev. **112**, 1555 (1958).
- [173] D. Penn, Phys. Rev. B **35**, 482 (1987).
- [174] J. van den Brink, cond-mat/0510140.
- [175] K. Schulte, *The interplay of Spectroscopy and Correlated Materials*, PhD thesis, Universiteit van Amsterdam, 1998.
- [176] J. Ambjørn, Fortschr. Phys. **36**, 595 (1988).
- [177] C. Itzykson and J. Drouffe, *Statistical Field Theory* (Cambridge Univ. Press, Cambridge, 1989).
- [178] J. Schwinger, Phys. Rev. **82**, 664 (1951).
- [179] R. Feynman, Rev. Mod. Phys. **20**, 367 (1948).
- [180] S. Weinberg, *Gravitation and Cosmology: Principles and Applications of the General Theory of Relativity* (Wiley, New York, 1972).
- [181] M. Damjanović, *O simetriji u kvantnoj nerelativističkoj fizici* (Fizički fakultet, Beograd, 2000).
- [182] H. McSkimin and W. Bond, Phys. Rev. **105**, 116 (1957).

[183] K. Ahn *et al.*, Phys. Rev. B **68**, 092101 (2003).

[184] M. Fisher, M. Barber, and D. Jasnow, Phys. Rev. A **8**, 1111 (1972).



# Samenvatting

Op macroscopische schaal bestaan objecten zoals bijvoorbeeld een stoel, een fles wijn of een glas water uit ontzettend veel atomen. Om precies te zijn is het aantal deeltjes typisch van de orde  $10^{23}$ . Afhankelijk van de randvoorwaarden, temperatuur bijvoorbeeld, kan het water in het zojuist genoemde glas verkeren in een gas, vloeibaar of vaste toestand. Deze eigenschappen op macroscopische schaal worden bepaald door processen op microscopische schaal. Typisch hebben de atomen waaruit de vaste stof is opgebouwd een kinetische energie en doordat ze met elkaar wisselwerken hebben ze ook een potentiële energie. Een van de belangrijke grootheden die de fase van het fysische systeem bepaald is de verhouding van deze potentiële en kinetische energie.

In de afwezigheid van interacties tussen de deeltjes gedraagt het systeem zich als een ideaal gas dat zich ofwel klassiek, zoals in het geval van waterdamp, ofwel bij lage temperaturen quantum mechanisch gedraagt. In het laatste geval blijkt dat de deeltjes zich op twee fundamenteel verschillende manieren gedragen, en beschreven worden door óf de Fermi-Dirac statistiek óf de Bose-Einstein statistiek.

Als we de interacties tussen de deeltjes meenemen dan blijkt dat we in de limiet van zwakke wisselwerking het gas kunnen beschrijven door een ideaal gas van ‘aangeklede’ of quasi-deeltjes. Het fysische beeld dat hierbij hoort is dat een deeltje dat door het gas heen vliegt de aanwezigheid van omringende deeltjes voelt en deze met zich meetrekt. Effectief vormt zich dan een deeltje plus wolk van deeltjes die collectief door het gas propageren. Van der Waals gassen, de conventionele BCS supergeleiders, Bose-Einstein condensaten, elektronen in metalen en neutronen in neutronensterren zijn slechts enkele voorbeelden van wisselwerkende veel-deeltjes systemen die zich gedragen volgens dit beeld.

Echter, er zijn systemen waarvoor de interactie-energie tussen de deeltjes domineert en de kinetische energie verwaarloosbaar is. Voor de beschrijving van deze systemen kunnen we het hierboven geschetste beeld van een gas van individuele quasi-deeltjes niet langer toepassen.

Gelukkig is er een manier om ook deze gevallen te behandelen. De fase waarin het systeem verkeert als de interactie energie veel groter is dan de kinetische energie kan worden beschouwd als een “ultiem gecorreleerde” toestand omdat elk deeltje sterk wisselwerkt met alle andere deeltjes. In het algemeen heeft de interactie tussen de deeltjes een localiserend effect en ordent het systeem zich volgens een roosterstructuur opdat de interactie energie wordt geminimaliseerd. Het Wigner kristal is hier een voorbeeld van. Voor de beschrijving van deze sterk gecorreleerde of geordende fase kunnen we niet langer gebruik maken van de

individuele deeltjes maar gebruiken we een nieuwe “duale” theorie. De collectieve excitaties van de sterk-gecorrleerde grondtoestand van de duale theorie nemen nu de rol van deeltjes op zich. Om dit punt toe te lichten kan men denken aan fononen, die geluid voortbrengen in de vaste stof fysika.

Door sterk-gecorrleerde systemen te beschrijven in termen van hun collectieve vrijheidsgraden is het mogelijk om het oorspronkelijke zeer gecompliceerde veel-deeltjes probleem sterk te vereenvoudigen. Bekende voorbeelden van dit soort systemen zijn de hoge-temperatuur supergeleiders die zijn waargenomen in de zogenaamde “cuprates”. Door onzuiverheden in de kristal-structuur te introduceren verandert de chemische structuur van deze materialen en wordt een overgang tussen twee verschillende grondtoestanden van de sterk-wisselwerkende electronen vloeistof geïnduceerd. De mate waarin onzuiverheden zijn toegevoegd wordt de doping genoemd. In de afwezigheid van onzuiverheden domineert de coulomb interactie en is het systeem een antiferromagnetische isolator. Zodra de doping toeneemt wordt de antiferromagnetische orde van de grondtoestand verwoest en vindt een overgang naar de supergeleidende fase plaats. Het blijkt dat er tussen de AF isolator en de supergeleidende fase nog een fase aanwezig is. In deze zogenaamde ‘stripe phase’ organiseren de gaten zich door de sterke interacties in lijn-achtige structuren. Deze ‘stripe phases’ is experimenteel waargenomen.

In de supergeleidende fase van de cuprates zijn Cooper-paren met een speciale  $d$ -golf symmetrie aanwezig. Echter, voor de beschrijving van de supergeleidende fase kunnen we geen gebruik maken van de BCS theorie voor de ‘klassieke’ supergeleiders. De reden hiervoor is dat de Cooper-paren in dit geval een hoge mate van correlatie vertonen. Er zijn experimentele aanwijzingen dat de electronen vloeistof in de hoge-temperatuur supergeleider op het punt staat om een overgang naar een sterk gecorrleerde toestand met kristalijne orde te ondergaan. Dit vormt mede een bron van inspiratie voor dit proefschrift.

In dit proefschrift wordt ingegaan op enkele aspecten van deze sterk gecorrleerde systemen. Een centraal thema hierbij is de zogenaamde “dualiteit”. In hoofdstuk 2 introduceren we dit concept en als voorbeeld beschouwen we de Abelse-Higgs dualiteit in  $2+1$  dimensies. Door gebruik te maken van zogenaamde duale ijkvelden kunnen zowel de geordende als de ongeordende fase van het systeem worden beschreven. Expliciet laten we zien dat een experiment dat de correlaties in geordende fase meet ook geschikt is om correlaties in de ongeordende fase te meten.

In hoofdstuk 3 introduceren we elasticiteit door middel van een veldentheorie en geven we een overzicht van zogenaamde topologische defecten. In het bijzonder beschouwen we een belangrijke topologische kinematische randvoorwaarde, de zogenaamde glide constraint van dislocaties.

Hoofdstuk 4 vormt de kern van dit proefschrift en richt zich op het gedeeltelijk verdwijnen van de kristalijne orde in de elektro-neutrale vaste stof. Om dit smeltproces te beschrijven maken we gebruik van soortgelijke technieken als in hoofdstuk 2. Het blijkt dat we de gesmolten fase kunnen voorstellen als een Bose-Einstein condensaat van dislocaties. Om preciezer te zijn kunnen we deze fase beschouwen als een intermediaire fase tussen de superfluide en kristalijne fase.

In hoofdstuk 5 kijken we naar een vaste stof die opgebouwd uit geladen deeltjes. In

het bijzonder is dit relevant voor de hoge-temperatuur supergeleiders. Wederom kunnen we de duale theorie opstellen voor dit systeem en het blijkt dat dit een totaal nieuwe manier is om naar supergeleiding te kijken. De gesmolten fase is een supergeleidende fase maar het onderliggende mechanisme is totaal verschillend van dat in conventionele BCS theorie. Bovendien leidt het nieuwe mechanisme tot voorspellingen van niet conventionele eigenschappen die gemeten zouden kunnen worden. In het bijzonder ligt het binnen de experimentele mogelijkheden om de theorie te toetsen door te kijken naar het electron energy loss spectrum. We voorspellen dat in dat spectrum een nieuwe excitatie zal verschijnen. Bovendien zal dit experiment uitsluitsel kunnen geven over de aanwezigheid van fluctuerende orde in de hoge-temperatuur supergeleiders.



# Curriculum vitæ

I was born in Jagodina, Serbia (at that time Yugoslavia), on February 26<sup>th</sup>, 1977. From 1992 to 1996 I attended the High School for Mathematics in Belgrade. During that time, but also during my primary education, I participated in various competitions in mathematics and in physics. The awarded prizes include an Honourable Mention Prize at the International Olympiad in Physics in Oslo in 1996, five first places on the national and republic levels of the competitions and one individual first prize and two (school) team victories in ‘friendly’ school competitions in Moscow in 1993 and 1994. In this pre-university period I conducted several research projects at Petnica Science Center, a science camp for gifted elementary/high-school students. One of the projects was awarded with an Honourable Mention at the “First Step to Nobel Prize” competition in Poland in 1995.

In 1996, I enrolled in studies of physics as an undergraduate student at the Department of Physics at University of Belgrade. I graduated in 2001 with GPA 9.93 out of 10. My diploma thesis work in the field of granular media physics was conducted under supervision of Prof. Dr. Sunčica Elezović-Hadžić. In 1999 and 2000 I had a 4-month traineeship at the Fraunhofer Institute for Optics and Mechanics in Jena (Germany) working on optical coating of polymers.

In 2001 I began my Ph.D. studies under supervision of Prof. Dr. Jan Zaanen at the Instituut-Lorentz for theoretical physics in Leiden. The main results of the research are contained within this thesis. In the last year of my graduate studies, I visited the Stanford University for six weeks. As a graduate student, I participated in four international and several local (Dutch) conferences and workshops. I also presented my work in Switzerland (Université de Fribourg), Serbia (University of Belgrade) and the United States (Stanford, Berkeley and Johns Hopkins University). As part of my position I taught several courses as a teaching assistant.

I will continue my career as a postdoctoral researcher in the Department for Physics and Astronomy of the Johns Hopkins University in Baltimore (United States).



# List of publications

- “Spin nematics revisited”, V. Cvetkovic, Z. Nussinov and J. Zaanen, J. Phys. IV **100**, 265 (2002).
- “Ordered limit of superconductivity”, V. Cvetkovic, J. Zaanen, Z. Nussinov and S. Mukhin, J. Phys. IV **131**, 81 (2005).
- “Topological kinematic constraints: dislocations and the glide principle”, V. Cvetkovic, Z. Nussinov and J. Zaanen, Phil. Mag. **86**, xxx (2006); cond-mat/0508664.
- “Vortex duality: watching the dual side with order propagators”, V. Cvetkovic and J. Zaanen, submitted to Phys. Rev. B; cond-mat/0511586.



# Acknowledgments

Obtaining a Ph.D. degree is not a solitary process. Through discussions with people in my surroundings I was able to gain new insights and ideas or overcome problems I had encountered in the course of my work. Sometimes the interactions were not exclusively work-related and in those times I enjoyed the company of these people.

In first place I owe special thanks to Zohar Nussinov for intensive collaboration and the support during hard times of the graduation process. The ‘stripe club’ was a strongly interactive group, mimicking its own subject, with few of its members that were specially helpful: Ian McCulloch, Sergei Mukhin, Jeroen van den Brink, Joseph Betouras and Darius Sadri. Among other people at the Lorentz Institute where the general atmosphere was always pleasant, I greatly benefited from discussions with Dániel Nógrádi, Alexander Morozov, Falk Bruckman and Ana Achúcarro. Finally, few of the people that were not directly involved in my work, but that I wish to explicitly mention include Dr. Dennis, Kepa, Jurke, Juan and of course Jelena.

